On effective field theory of dark matter

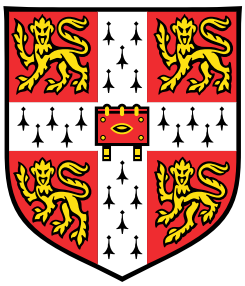

Ben Geytenbeek

Supervisor: Dr. Ben Gripaios

Cavendish Laboratory
University of Cambridge

This dissertation is submitted for the degree of
Doctor of Philosophy

Darwin College

July 2021

Declaration

I hereby declare that this thesis is the result of my own work and includes nothing which is the outcome of work done in collaboration except as declared in the preface and specified in the text and acknowledgements. It is not substantially the same work that has already been submitted before for any degree or other qualification except as declared in the preface and specified in the text. This dissertation does not exceed the prescribed word limit of 60,000 words for the Physics and Chemistry Degree Committee, including abstract, tables, footnotes and appendices but excluding table of contents, figure captions, list of figures, references and acknowledgements.

Ben Geytenbeek
July 2021

On effective field theory of dark matter

Ben Geytenbeek

We investigate the feasibility of dark matter particles existing in the Universe as a spin-$\frac{1}{2}$ fermion using effective field theories to parameterise the higher order physics. Our goal is to determine the requirements for exclusion of such particles by direct and indirect detection. In part I, based on ref. [1], we introduce a complete basis of operators up to dimension 5 for fermions that are part of singlet, doublet and triplet representation of the Standard Model $SU(2)$ electroweak symmetry group. Such particles correspond to the bino, higgsino and wino of supersymmetry models respectively. We determine the thermal relic density of particles interacting with each of our operators and show that viable thermal relics that evade experimental constraints can exist with masses as low as as 100 GeV and up to 10 TeV due to the mass splittings that arise at dimension 5. In part II, based on ref. [2] we further investigate the effect of fermionic dark matter that may interact through an electromagnetic dipole interaction at dimension 5 on energy transport in the Sun. In particular, we test whether the models can provide a solution to the solar abundance problem, a theoretical discrepancy between the observations of helioseismology and the theoretical Standard Solar Model. We introduce all of the necessary theoretical implementation and show that, although introducing dark matter may alleviate the tension of the solar abundance problem, the required interaction strengths are strongly ruled out by direct detection experiments.

Preface

The following portions of this thesis were completed in collaboration with others:

- The tabulation of α and κ coefficients in section 4.4.5 was completed by Pat Scott and Aaron Vincent using the derivation provided by the candidate.
- The calculation of the frequency separation ratios in section 5.3 was completed by Aldo Serenelli using data provided by the candidate.

Derivations of results from the literature are indicated in the text of this thesis.

Ben Geytenbeek
July 2021

Acknowledgements

The journey of a PhD is long and arduous one, and mine has been no different. This work would not have been able to be completed without the help and support of the High Energy Physics group at the Cavendish Laboratory, in particular my supervisor Dr Ben Gripaios and the SUSY working group; especially during the weekly group meetings and subsequent lunches. The occupants of the HEP Library, in particular Mr Herschel Chawdhry have been instrumental in supporting my progress and providing light hearted relief over the years.

I would also like to pay tribute to my former supervisors, collaborators and peers from the University of Adelaide who provided me with the inspiration to pursue a PhD in Cambridge, notably Prof Anthony Williams and A/Prof Martin White. The Physics Honours Class of 2015 in Adelaide has always encouraged and supported me both before and during my time in Cambridge when I have returned to visit, and have always made me feel welcome like I had never left, including Ryan Bignell, Tuong Cao, Joshua Charvetto, Raquel Hogben, Dona Kireta, Zach Matthews, Urwah Nawaz, Jason Oliver, Robert Perry, Andre Scaffidi, Kim Somfleth and the rest of the CoEPP and CSSM students and staff.

My attendance at Cambridge would not have been possible without the financial support of the Gates Cambridge Trust and the excellent work of the staff there to make everything as smooth as possible, in particular Jim Smith, Luisa Clarke, Celine Ophelders and Dr Jade Tran. The role of the Trust and Scholar's Council in helping to navigate the complexities of Cambridge cannot be understated, and I am thankful for everyone who I served with on Council or the Orientation Committee for their dedication and service, notably Margaret Comer, Emma Glennon, Marina Velickovic and Kevin Chew.

My time in Cambridge would not be complete without the support and friendships from the various communities I have become involved with. In particular, the broader Gates Community has been outstandingly welcoming to me, the Darwin College Cricket Club and Cavendish Laboratory Cricket Club have been excellent avenues for entertainment and the Cambridge University Real Tennis Club has been a wonderful community. From the latter, I particularly want to thank Kees Ludekens, Peter Paterson, Dr Victoria Harvey and Dr Christie Marrian for their support with both coaching and developing interesting projects off court.

Finally, I owe a great deal of appreciation for those friends and family not listed above who have aided, encouraged and supported me whilst providing excellent entertainment and friendship. In particular, I thank Annalise Higgins, Krittika D'Silva and Annika Pecchia-Bekkum for the various adventures and incidents over the course of my studies. Most notably, Jacqueline Siu, whose support for me has been unwavering and with whom I have shared many amazing adventures throughout my time in Cambridge. Lastly, the support of my family in Australia has been instrumental to my progress throughout my PhD.

Table of contents

List of figures

Chapter 1

Introduction

The problem of substantial amounts of unseen matter in the Universe was first identified by Fritz Zwicky in 1933 [3], and remains one of the biggest unsolved problems in theoretical physics. The search for an explanation has spanned many research fields and energy scales, including high energy particle colliders, nuclear recoil experiments, high energy gamma ray astronomy, galactic dynamics, large scale astronomical structure, astroparticle physics, gravitational lensing and galactic cluster dynamics, cosmology and particle physics beyond the Standard Model. While the astrophysical evidence for the existence of dark matter is relatively well understood, there is to date no understanding of dark matter on a fundamental level in terms of its nature, structure and interaction with the Standard Model. Indeed, various detection experiments have now all but ruled out many of the more appealing or straightforward scenarios for dark matter. As physicists look towards more sophisticated explanations, their models become increasingly complex with many parameters or complicated symmetry groups.

We instead seek to explore a model-independent description of a conceptually simple proposal for the particle nature of dark matter, namely, a fermion interacting with the Standard Model only via the weak interaction. We shall construct our fermions as gauge invariant quantities, and then model any higher order physics through a series of effective field theory operators. Given any particular model, we will subject the observable parameters to the exclusion constraints and require them to match the astrophysical and cosmological observations of dark matter. We shall also propose a relatively novel method that may illuminate more of the nature of dark matter, specifically a mechanism for energy transport in the Sun due to dark matter.

Before we begin constructing our models, we shall review the astrophysical evidence for and particle physics constraints on dark matter, including the relevant historical context. Understanding the requirements and limitations will be important for building a viable model. We shall also briefly review supersymmetry, of which we will discover features which closely map onto the models we will construct. Finally, we shall review the theoretical construction of effective field theories and how they allow us to incorporate higher energy physics in a model independent manner.

1.1 Early history of dark matter observations

Dark matter was first proposed by Zwicky [3] when estimating the mass of the Coma galaxy cluster. Assuming that the cluster is mechanically stable, the virial theorem relates the kinetic energy of a system of discrete particles, in this case galaxies, to the total gravitational potential energy. By measuring the kinetic energy from the relative redshifts of the galaxies in the cluster, which determines their relative velocities, calculating the gravitational potential energy gives an estimate for the mass of the system as a

whole. The expected mass of the system was inferred by taking the total luminosity of the cluster and assuming that the brightness is generated by stars of a similar mass and luminosity to the Sun. The result was a mass-luminosity ratio roughly 200 times greater than expected. Zwicky proposed that there was some additional dark matter keeping the structure bound. Zwicky [4] proposed using gravitational lensing predicted from general relativity by Einstein [5] as a means to accurately measure the cluster mass to determine the true mass and presence of dark matter, although both were sceptical that such lensing would be observed in practice [6], though it is now easily possible with modern technology and techniques. After the later discovery of a strong X-ray source from the Coma cluster [7], the presence of an inter-cluster gas emitting radiation via thermal bremsstrahlung appeared to be a viable explanation for the missing mass [8]. However, models of the inter-cluster gas as an isothermal sphere could not produce a sufficient mass of gas to account for a large percentage of the virial mass [9, 10]. The likeliest explanations would require new physics to extend the understanding of gravity, particle physics or astrophysics, or some combination thereof.

Meanwhile, Oort [11] calculated that there must be an amount of non-luminous matter in the region local to the Sun by measuring the kinematics of local stars relative to the galactic plane. Comparing to the luminosity of the given stars gave a mass measurement in the local region an order of magnitude above the visible mass, but instead concluded that the visible light was being largely obscured on its path between the source and the observer. Furthermore, Zwicky [12] also proposed that measurements of the orbital speeds of components of galaxies as a function of distance from the galactic centres would lead to a measurement of the amount of unseen matter within galaxies. The technique of Oort and the proposals of Zwicky eventually lead many years later to the measurements of galactic rotation curves by Rubin [13], the first definitive and widely accepted measurements of dark matter.

1.2 Galactic rotation curves

The first broad attention on the dark matter problem arose following improved measurements on the velocity distribution in the Andromeda Galaxy [14], the largest galaxy in the Local Group. The relation between the velocity distribution and the distance from the centre of a given galaxy is called the galactic rotation curve. If the only gravitational influence on the stars is due to the luminous material in the galaxy, then the stars at the outer edges of the galaxies are expected to move with slower velocities as they orbit relative to the inner stars. However, the observations showed a flat velocity distribution, which indicates additional non-luminous material beyond the visible regions of the galaxy [13].

Subsequent measurements were made of the rotation curves of other spiral galaxies using the redshift of the emission lines [15], which also showed evidence of non-luminous matter. Modelling of the visible components also improved [16], reducing uncertainties. For elliptical galaxies, which are devoid of thermal gasses, the motion of the constituent stars are not coherent as for spiral galaxies. Measurements of the galactic rotation curve of the Milky Way are more difficult due to difficulties calculating the distance to stars in the galactic neighbourhood. Examples have included measuring the spectra of emission from hydrogen [17] or carbon monoxide gasses [18], either in the inner galaxy or in Cephid variable stars [19], but all collate to a consistent result, albeit with greater uncertainties than the extragalactic measurements. Dwarf galaxies have proven especially of interest, as in general they have a high proportion of dark matter relative to their luminous matter [20].

The extra material is inferred to exist in a spherically symmetric halo extending well beyond the visible region of the galaxy [21]. Given measurements across multiple galaxies, the total mass of spiral galaxies is roughly a constant proportion to the amount of luminous matter [22]. The best fit model is a halo of matter modelled as an almost collisionless gas. The nature of the distribution is still not entirely

understood, especially in the inner cores of dark matter halos. In particular, a theoretical dilemma exists in the modelling of the dark matter halo in the form of the so-called cusp-core problem [23, 24]. Attempts to compute the formation of dark matter halos use N-body simulations of the dark matter in the galaxy, typically modelled as a collisionless gas. Numerous authors agreed that, for large radii, the density of dark matter falls off with the cube of the radius [23, 25–27]. The finding was in broad agreement in these regions with the observed density profile from surveys of large numbers of rotation curves [24, 28]. However, the inner regions near the centres of halos showed a discrepancy between the collisionless gas simulations and observations. Simulations suggest a so-called 'cuspy' profile, where the density is proportional to the radius of the halo, whereas the observations suggest a so-called 'core' profile, where the density in the inner regions is constant, independent of the radius within some scale distance of at least a few kiloparsecs. Higher resolution models continue to disagree with the observations [29–32]. The problem remains unresolved, though there have been several proposals to help alleviate the discrepancy. Solutions include removal of the assumption of spherical symmetry [33], addition of star formation and supernova feedback [34, 35] or clumps of dark matter undergoing dynamical friction [36–40]. The most relevant proposal for the detection of particle dark matter is that the dark matter be self-interacting [41–44]. Highly self-interacting models are ruled out as the halos become fluid-like and are unstable and prone to core collapse [45–47]. Self-interactions also heat the core and lead to evaporation, constraining the self-interaction such that the evaporation time is less than the age of the universe [43, 48–50]. Self-interactions remain a possible solution to the cusp-core problem [50–54], but at the very least are constrained by the simulations [55]. Overall, however, the halo is still an almost collisionless spherically symmetric distribution.

Various hypotheses for the description of the unseen material have been proposed, which have since been narrowed down to the current paradigm of particle dark matter. An early proposal was that the dark matter consisted of compact astrophysical objects like planets, brown dwarfs, comets and asteroids which do not emit substantial amounts of visible light. Such objects are colloquially known as MACHOs (MAssive Compact Halo Objects). Searches for MACHOs are conducted through gravitational microlensing, whereby if the MACHOs pass in front of a background star their gravitational field will focus light from the background star [56–58]. Such events cannot be easily forecast, and occur as isolated events, but can be limited statistically. Extensive searches using this technique suggest that the fraction of the halo consisting of MACHOs is at most approximately 20% [59], albeit with a wide confidence interval. Subsequent observations have ruled out a dark matter particles as mostly particles or halo objects with a mass range of $10^{-7} M_\odot$ to $10 M_\odot$ [60], that is, with masses greater than the Moon up to the largest red giant stars.

A similar hypothesis to MACHOs is that dark matter exists as a halo of so-called primordial black holes. Such black holes are hypothesised to have originated in the early universe [61]. They must be created sufficiently large to have survived the ongoing Hawking radiation [62] from the early universe to the present day to form the dark matter. Like MACHOs, constraints on the quantity of primordial black holes are also derived from lensing results, again excluding masses either less than a few solar masses and greater than the lunar mass [63]. Nonetheless, the prospect of primordial black hole dark matter remains on the fringe compared to the particle models, as there has been no definitive discovery of a primordial black hole itself. The majority of the remaining hypotheses is that dark matter exists in the form of some fundamental or composite particle as an extension to the Standard Model.

1.3 Colliding galaxy clusters

When interpreting the results of the galactic rotation curves, there are two distinct possibilities. Either there is a large amount of unseen material in the galaxies indicating the existence of a beyond the Standard Model dark matter particle or dark sector, or there is a deviation from the Newtonian gravitational dynamics at galactic scales. The possibility of the later arises because the galactic rotation curves only

measure the influence of dark matter, rather than observing it directly. The first direct evidence for particle dark matter arises in modern measurements of the masses of galaxy clusters.

Despite the pessimistic opinions on the likelihood on detecting gravitational lensing in galaxy clusters by Einstein and Zwicky [5, 6], modern techniques are able to detect lensing in two forms. Strong gravitational lensing occurs when the a galaxy is directly behind the galaxy cluster. The light from the background is bent around the cluster forming an arc of light, or in rare cases a full ring [64, 65]. However, though strong lensing gives a rather precise measurement of the mass of the cluster based on the radius of the arc. Instead, weak gravitational lensing occurs when the background galaxy is not directly in line with the galaxy cluster, but close enough to experience a sheer distortion to the observed shape of the galaxy. By averaging the sheer distortion of an array of background galaxies, it is possible to determine a map of the mass of the galaxy cluster [66, 67]. The resultant mass map may be compared with the luminous and X-ray sources [68–70]. Measurements consistently saw a direct overlap between the mass distributions and visible matter across the entire spectrum, albeit with a mass-to-light ratio on the order of one hundred times that of the Sun, and in rough agreement with the virial theorem estimates by Zwicky [3, 4, 6, 12].

The best evidence for the direct observation of particle dark matter arises when two large galaxy clusters collide perpendicular to the line of sight from the Earth. Large galaxy clusters consist of three major components: the visible galaxies that form the cluster, the intergalactic gasses which emit in the X-ray spectrum, and the dark matter component. When two such galaxies clusters collide, the dark matter and the visible galaxies act as a collisionless gas and pass through each other unimpeded, whereas the intergalactic gasses experience friction in the form of a bow shock and becomes spatially disconnected from the rest of the cluster. The masses of the respective elements can be measured using weak gravitational lensing measurements from the background galaxies, which shows a disconnect between the visible and X-ray spectrum and the mass contours [71]. The first successful observation which demonstrated the separation between the components was the Bullet Cluster [72–74]. The size of the separation between the centre of the galactic distribution and dark matter distribution also provides a constraint on the rough scale of the self-interaction of the dark matter components [75, 76]. Additional measurements have been made in other clusters which provide strong evidence for the existence of dark matter over models of modified gravity. Examples include observations of the Musket Ball Cluster [77], the Bullet Group [78], the Burst Cluster [79], the Train Wreck Cluster [80–82], Abell 2744 [83] and MACS J0025.4-1222 [84].

The prospect that dark matter does exist by a modification to the laws of general relativity has in recent times become more diminished following the detection of gravitational waves from colliding binary neutron star system by LIGO [85]. Such systems generate both gravitational waves and electromagnetic radiation that is detected through gamma ray [86], optical and radio sources as well as neutrinos [87]. The agreement in arrival times between the different sources indicates no discrepancy from the expectations from general relativity [88, 89]. Such a result rules out many models of modified relativistic gravity which seek to emulate dark matter. The prospect that dark matter consists of massive particles and not modified gravity appears very strong. The next step is to describe the nature of the proposed dark matter particle and determine the prospects for observing such particles.

1.4 Dark matter cosmological density

Beyond the well-established gravitational effects of dark matter, the additional properties such as its mass, composition and interactions are not well understood. A key question to probe is the energy density of dark matter, which also provides insights into potential particle models for dark matter. Evidence for the energy density comes from several sources, notably the cosmic microwave background (CMB) and big bang nucleosynthesis (BBN).

1.4.1 Cosmic microwave background

The cosmic microwave background (CMB) is a key probe into the physics of the early universe. After the big bang, the universe experienced a period of cooling. Initially, the temperature was sufficiently high such that nuclei were ionised and electrons were free, the primary interaction between them being Coulomb scattering. At this epoch, Photons are in thermal equilibrium with the electrons and nucleons and ionise any atoms which do happen to form. The photons are the dominant component of the energy density of the universe, leading to the epoch being known as the photon epoch.

As the universe cools below a temperature of ~ 4000 K, the electrons and the protons in the universe are finally able to combine to form atomic nuclei, mostly hydrogen atoms but also with some amounts of deuterium and helium and a trace amount of even heavier atoms. For historical reasons, this epoch is known as recombination [90]. After recombination, the photons in the universe can no longer undergo Thompson scattering from free ions. The process is known as photon decoupling. After decoupling, the photons have propagate until the present day with only around 10% undergoing further scattering [91]. As a result, the spectrum of the photons represent the nature of the universe at the moment that they were last scattered.

The photons as measured today follow a blackbody spectrum which has been heavily redshifted since the decoupling epoch. The measured wavelengths are now at microwave wavelengths [92, 93], representing a background spectrum to all microwave measurements. The spectrum is typically described as a series of spherical harmonics:

$$T(\theta, \phi) = \sum_{lm} a_{lm} Y_{lm}(\theta, \phi)\,. \tag{1.1}$$

The monopole, constant term, represents the mean temperature of the CMB, with a blackbody temperature of $T_{00} = 2.7255 \pm 0.0006K = 2\sqrt{\pi} a_{00}$ [94]. The temperature of the blackbody is related to the energy density of the photons at the present day by:

$$\rho_\gamma = \frac{\pi^2}{15} T_{00}^4 \simeq 0.260\,\text{eV cm}^{-3}\,. \tag{1.2}$$

The energy density is often expressed in terms of the density parameter Ω. Ω is defined in terms of the critical density ρ_c, the density at which the geometry of the universe flat:

$$\Omega \equiv \frac{\rho}{\rho_c} = \frac{8\pi G \rho}{3h^2}\,, \tag{1.3}$$

for Newton's gravitational constant G and Hubble parameter h. For the CMB photons, the cosmological density is $\Omega_\gamma \simeq 5.38 \times 10^{-5}$, much lower than the value required for a flat universe.

The dipole $l = 1$ component of the spectrum is dominated by a Doppler shift due to the motion of the solar system with respect to the local background radiation [95]. It may be verified by measurements of the radial velocities of local galaxies [96]. At spherical harmonics beyond $l \geq 2$, the anisotropies are intrinsic to the microwave background itself. The size of the anisotropies are remarkably small, first discovered at the order of magnitude of 10^{-5} by the COBE experiment [97]. As they are intrinsic, they give an insight into the nature of the early universe.

Sources of perturbation in the energy density as evident in the higher multipoles of the CMB can be caused by perturbations in the density of the early Universe. Notably, the scale of these perturbations can be predicted by models of gravity in the early universe, giving a theoretical prediction of the power spectrum - the 2-point function over the entire temperature field. The CMB has no preferred axis, as would be expected in a universe with no preferred frame, so the correlation between two points is dependent only on the l-component of the spherical harmonics which describes the angular separation, and not the m components which describe the orientation. To obtain the power spectrum, the power is summed over

all of the m modes for each l mode. The angular variation for a single harmonic Y_{lm} is approximately given by $\theta \sim \frac{\pi}{l}$.

There are a number of cosmological parameters which determine the Friedman-Robertson-Walker (FRW) cosmology [98], the theoretical model which is used to predict the power spectrum. The most relevant to the CMB are the baryon density $\Omega_b h^2$ and cold dark matter density $\Omega_c h^2$. The total mass density is also defined as $\Omega_m h^2 = \Omega_b h^2 + \Omega_c h^2$. There may also be a cosmological constant Λ with density Ω_Λ. The radiation component is fixed in the models by the $l = 0$ CMB measurement. Other parameters include the Hubble constant h, the optical depth of the decoupling surface τ, the spectral index n_s and a normalization amplitude A for the power spectrum [99]. The values of the energy densities a key in determining the size of the anisotropies - they determine the perturbations due to gravitational potentials. Separately, the baryonic number density is important in determining the power spectrum of the anisotropies due to variations in the Thompson scattering at decoupling. The Hubble constant, which describes the rate of expansion of the universe, impacts the propagation of CMB photons after decoupling, though it can be measured independently by the receding redshift of Cephid variable stars in nearby galaxies [100, 101].

Observations by the Wilkinson Microwave Anisotropy Probe (WMAP) [102–106] and later the Planck spacecraft [107–109] have consistently shown excellent agreement to the power law spectrum, leading to precise measurements of the above parameters. The inferred dark matter parameters from Planck are a baryonic density of $\Omega_b h^2 = 0.02212 \pm 0.00022$ and a dark matter density of $\Omega_c h^2 = 0.1206 \pm 0.0021$ [109]. Notably, the dark matter density makes up a sizeable majority of the overall matter density, a similar result to other predictions of the amount of dark matter in the universe. The result also implies that dark matter is expected to be non-baryonic, and not formed of particles that are not visible through conventional telescopes.

1.4.2 Big bang nucleosynthesis

The baryon density is independently measured via the primeval deuterium abundance. During a hot big bang, fusion between protons can create light nuclei including deuterium, ^{3}He and ^{4}He in a process called big bang nucleosynthesis. The abundances of deuterium are frozen out with the expansion of the universe, and the fraction remaining is sensitive to the energy density of matter at the freeze-out epoch [110]. Measurements of the deuterium abundance cannot occur in the solar neighbourhood due to burning by stars; instead the deuterium abundance is determined in high-redshift quasars, which have close to primordial abundances [111, 112].

Despite the large differences in the types of observations of the Hubble constant and baryon abundance, both show a consistent agreement with the ΛCDM model, an important double check on the validity of the ΛCDM results. Both models agree that the baryon density is $\Omega_b h^2 \sim 0.0193 \pm 0.0014$ [111], calibrated against the photon number density determined from measurements of the CMB. Again, the baryonic density is significantly lower than the overall matter energy density of the universe as determined by mass to light ratios and the cosmic microwave background.

The final major component of the energy density in the universe is the cosmological constant known as dark energy, which is independently verified by measurements of the redshift of Type-Ia Supernova [113–116], but beyond the scope of this work. The measurements together show that the energy density of the universe contains a majority proportion that cannot be explained through baryonic matter. Dark matter is an appealing the proposed solution, and dark matter particle candidates are expected to exist as particles beyond the Standard Model.

1.5 Dark matter candidates

Given the cosmological and astrophysical evidence for the existence of dark matter, there have been many proposed theoretical models for the nature of the dark matter objects themselves. We shall review a number of common theories of dark matter particles before a deeper analysis on the subset which corresponds to supersymmetric candidates.

1.5.1 Theoretical bounds on dark matter particles

In the ΛCDM cosmological model, there are two additional components beyond the vanilla baryonic elements. One is the presence of the cosmological constant Λ, or dark energy. The other is that there is dark matter in the Universe and that it is non-relativistic, also described as cold. The constraint that the dark matter is non-relativistic arises from calculating the Jean's mass of a gaseous body consisting primarily of particle dark matter, that is, the largest mass at which the body can be stable before it undergoes gravitational collapse and overcomes the gaseous pressure [117]. For relativistic dark matter particles, such as an eV scale fermion, the Jeans mass is several orders of magnitude greater than the typical mass of a galaxy. Such a scenario would dissipate any density perturbations due to the free streaming of the relativistic particles [118–121]. A similar result can be found for predicting the size of density fluctuations in the CMB in the very early universe [122]. The result is a requirement that any fermionic particular dark matter must be non-relativistic and have a mass greater than around $m_\chi \gtrsim 1\,\text{keV}$.

Given our present understanding of the Standard Model, it is a natural extension to assume that dark matter consists of some form of sub-atomic particle. There are several key requirements that particle dark matter must follow. First, it must interact gravitationally; that is, it must be massive. Second, it cannot interact via the strong or electromagnetic forces, at least at tree level with full electric charges [123, 124]. Third, it must be stable or very long lived, with an average lifetime at well beyond the present age of the universe.

The overall bounds for the potential mass of a dark matter particle are very wide. The lower mass limit for bosonic dark matter is $m_\chi \gtrsim 10^{-22}\,\text{eV}$, corresponding to the so-called fuzzy dark matter scenario [125]. Here, the very light mass means the particle has a very large de Broglie wavelength on the order of the size of a galaxy. The halo properties of the dark matter are then determined by the wave properties of the particle, with a very high occupation number since the particles are bosonic. For fermions, the lower bound is provided by the requirement for structure formation from the CMB, described above to be $m_\chi \gtrsim 1\,\text{keV}$. The upper bound derives from the limit from searches for MACHOs, determined to be $m_\chi \lesssim 10^{59}\,\text{eV}$ [60].

1.5.2 Weakly interacting massive particles

Despite there being potentially 81 orders of magnitude for the dark matter mass, the vast majority of the searches have focussed on the MeV to TeV range, the so-called 'WIMP' models, or the sub eV range, in particular axion models. Weakly Interacting Massive Particles (WIMPs) in general appear a well-motivated scenario for dark matter. Their abundance can be estimated through the process of dark matter freeze-out, leading to a so-called thermal relic [126–128]. In this scenario, it is assumed that dark matter exists in a particle form, and it can undergo $2 \to 2$ interactions with Standard Model particles in the early universe. Initially, these interactions are in thermal and chemical equilibrium with the Standard Model. However, with the expansion of the Universe, there reaches a point where the rate of collisions decreases exponentially; the particles are far enough apart that the likelihood of collisions

occurring is negligible. The relative density of dark matter is therefore fixed after this epoch. Such is a relatively simple and appealing mechanism for explaining the abundance of dark matter, as it implies a natural interaction with the Standard Model with a simple mechanism. The density fraction is known from the Planck data to be approximately 0.12, so we have a scale for the approximate annihilation cross section for the dark matter particles. It has long been noticed, that, given that $\langle \sigma v \rangle \approx \frac{\alpha^2}{m_\chi^2}$, an interaction strength on the order of the weak scale $\alpha \approx 0.01$ gives a dark matter particle mass of $m_\chi \approx 100$ GeV. Such masses are of a similar order of magnitude to similar scales in the Standard Model, such as the W, Z and Higgs boson masses, and so suggested a minimal degree of fine-tuning. The seeming coincidence that a weak scale interaction from a weak scale particle can correctly reproduce a thermal relic is known as the WIMP miracle. Such masses also arise naturally in many extensions to the Standard Model, especially supersymmetry, which gave candidate particles of an appropriate scale that interact weakly with the Standard Model. Finally, the prospect of building and running direct detection experiments to measure this mass scale is high, as there are a number of heavy nuclear elements of a similar scale for dark matter particles to recoil from. Collider experiments can also reach a similar scale threshold for production of 100 GeV particles. The overall focus of the vast majority of dark matter searches has thus been focused on the weak scale.

1.5.3 SuperWIMPs

An alternative model to weakly interacting massive particles as dark matter are so-called superweakly interacting massive particles, or superWIMPs. Such scenarios consist of particles with interaction strengths much lower than the weak scale. SuperWIMPs can be made to reproduce the dark matter density if they can be produced from WIMPs [129, 130]. The WIMPs are produced via the same thermal mechanism as outlined above, but decay on a timescale between the freeze-out epoch and the present day. The relic density of the superWIMPs is related to WIMPs by:

$$\Omega_{\mathrm{SWIMP}} = \frac{m_{\mathrm{SWIMP}}}{m_{\mathrm{WIMP}}} \Omega_{\mathrm{WIMP}} \,. \tag{1.4}$$

The superWIMP model means that the particle undergoing thermal freeze-out is not the same as the particle in the present day, and so is not subject to the same limitations. The result means that, for example, the thermal WIMP need not be electrically neutral and the superWIMP can be subject only to gravitational interactions.

Alternatively, superWIMPs can avoid thermal freeze-out all together if they are created directly during reheating post-inflation. During reheating, the inflation potential transfers energy to the Standard Model particles, which may have enough energy to produce superWIMPs, which then propagate to the present day [129, 130]. The scale of interactions is dependent on the cosmological parameters of inflation such as the reheating temperature [131], and the superWIMPs are never in thermal equilibrium with the Standard Model.

Common candidate superWIMPs include gravitinos [129, 130, 132–135] and axinos [136–139], the supersymmetric partners of the hypothetical gravitons and axions. For gravitons the original WIMP could be any heavier supersymmetric particle, with potential decay lifetimes from hours to months. Axinos may also exist simultaneously with axinos in a mixed component dark matter scenario [140].

1.5.4 Axions

At the lighter end of the allowed range of dark matter particles is a class of potential dark matter candidates called axions. Axions are originally proposed [141–143] as a solution to the so-called strong-CP

problem. The strong-CP arises due to the term

$$\mathcal{L} \supset \frac{g_3^2 \theta_3}{32\pi^2} \epsilon^{\mu\nu\rho\sigma} G^{\alpha}_{\mu\nu} G^{\alpha}_{\rho\sigma} \tag{1.5}$$

in the Standard Model Lagrangian, where $G^{\alpha}_{\mu\nu}$ is the gluon field with $SU(3)$ index α, g_3 is the coupling constant of the strong interaction and θ_3 is an angle parameter. The term is a total derivative, so does not contribute to the equations of motion, but is odd under CP, so will contribute to CP-violating interactions. The issue occurs as one such CP-violating interaction is the neutron electric dipole moment, which is predicted by this term to be approximately [144]:

$$d_n \simeq 3.6 \times 10^{-16} \theta_3 \; e\text{-cm}\,. \tag{1.6}$$

However, the experimental upper limit on the neutron electric dipole is $|d_n| < 3.0 \times 10^{-26}$ e-cm [145]. Although it may seem to be possible to rotate θ_3 to zero by symmetry, the presence of CP-violating weak interactions in the Standard Model provides another contribution to θ_3, so the bare parameter $\theta_3 < 10^{-10}$ implies a strong degree of fine tuning in the Standard Model.

The solution to the problem as proposed by Peccei and Quinn (PQ) [141] is to introduce a new global chiral $U(1)_{\mathrm{PQ}}$ symmetry with charges on the quarks Q_{PQ}, that is spontaneously broken by a complex scalar field φ with potential:

$$V(\varphi) = \lambda \left(|\varphi|^2 - \frac{f_a^2}{2} \right)^2 , \tag{1.7}$$

where the parameter f_a is known as the axion decay constant The vacuum expectation value of the field is then given by

$$\langle \varphi \rangle = \frac{f_a}{\sqrt{2}} e^{\frac{i\phi}{f_a}} \tag{1.8}$$

where ϕ is a Goldstone boson, and it is this Goldstone boson which is identified as the axion.

It is the presence of the charges under the $U(1)_{\mathrm{PQ}}$ symmetry which alleviates the strong CP problem via colour anomalies contributing to eq. (1.5). The axion field is free to be shifted by a constant to absorb θ_3 into ϕ via a field redefinition, with the CP violation now parametrised by $\frac{\phi}{f_a}$. The full consequences on the strong CP problem are beyond the scope of this work, but can be found in reviews on the topic (e.g. ref. [146]).

Of interest here is that axions are proposed as a candidate particle for dark matter. The axion mass m_a is determined by the axion decay constant f_a by:

$$m_a = \frac{\sqrt{m_u m_d}}{m_u + m_d} m_\pi \frac{f_\pi}{f_a} \simeq 6\,\mu\mathrm{eV} \left(\frac{10^{12}\ \mathrm{GeV}}{f_a} \right) , \tag{1.9}$$

where m_u, m_d and m_π are the up quark, down quark and pion masses and f_π is the pion decay constant. Notably, the axion can interact at the loop level with photons through the coupling:

$$\mathcal{L} \supset -g_\gamma \frac{\alpha}{\pi} \frac{\pi}{f_a} \vec{E} \cdot \vec{B}\,, \tag{1.10}$$

where α is the fine structure constant and g_γ is a model-dependent parameter at $\mathcal{O}(1)$ [147–150]. Such an interaction gives a method of decay for the axion. Importantly for axion dark matter, the mass is limited by constraints on the decay constant. The simplest constraint requires that the lifetime of axions must be greater than the age of the Universe in order to be stable as dark matter, hence requiring $m_a \lesssim 20\,\mathrm{eV}$. More stringent constraints come from the neutrino signal on the supernova SN 1987A at $m_a \lesssim 10\,\mathrm{meV}$ [151].

Although the most appealing production mechanism is thermal freeze-out, it cannot produce the requisite quantity of dark matter for two reasons. Firstly, the required axion mass would make it relativistic and hence hot dark matter, chiding with the requirement that dark matter be non-relativistic. Second, the required axion mass for a thermal relic is $m_a \simeq 80\,\text{eV}$, much higher than the requirement on the lifetime of axions to be present in the universe at the present day. Alternative proposals utilise the phenomenology of axions and the PQ theory, but they do not account for the full amount of dark matter in the universe [152, 153].

Given that axions are significantly lighter than weakly interacting massive particles, the direct detection constraints arise from different experimental searches which involve dark matter axions scattering from a background magnetic field. The strongest constraints arise from the ADMX experiment [154], with a particular focus on the μeV mass range.

1.5.5 Sterile Neutrinos

In the theory of weak interactions in the Standard Model, the only neutrinos present are left handed, which couple to left handed electrons. In the Standard Model, the mass terms provide for a mixing between the left and right handed states, but no such neutrino states are present. Therefore, under the Standard Model, neutrinos are expected to be massless. However, the observation of neutrino oscillations in atmospheric neutrinos by Super-Kamiokande [155] and solar neutrinos by SNO [156] suggests that neutrinos have non-zero mass, in contravention to the Standard Model prediction.

An appealing resolution to the neutrino mass problem is to introduce a right-handed neutrino into the model. Necessarily, the right handed neutrino will be a singlet under the gauge transformations of the Standard Model, namely, no electromagnetic charge, no color charge and no weak interactions. The only manner by which these particles may interact with the Standard Model is via mixing with the left-handed neutrinos via the Yukawa coupling [157]:

$$\mathcal{L} \supset \lambda_{i\beta}\overline{\nu}^{i}_{L}\nu_{R}H^{\beta} - \frac{1}{2}M_{\alpha\beta}\overline{\nu}^{\alpha}_{R}\nu^{\beta}_{R}\,. \tag{1.11}$$

where there are $i = 1, 2, 3$ left-handed neutrinos and $\alpha, \beta = 1, \ldots N$ right-handed neutrinos with Yukawa coupling $\lambda_{i\beta}$ to Higgs boson H and right-handed mass term $M_{\alpha\beta}$. The level of mixing is determined by the neutrino mass matrix

$$m_{\nu} = \begin{pmatrix} 0 & \lambda_{i\beta}v \\ \lambda^{*}_{i\beta}v & M_{\alpha\beta} \end{pmatrix} \tag{1.12}$$

where v is the Higgs vev. Of the different mass eigenstates, three of them must correspond very closely to the left handed neutrinos of the Standard Model, albeit now with a very small mass, and are called active neutrinos. The remainder will therefore correspond to the right handed neutrinos and are called sterile neutrinos. Limits on mixing of the active neutrinos to the sterile neutrinos implies that the sterile neutrinos should have a mass larger than their active counterparts. However, as the masses of active neutrinos can be very small, it is still possible to have a light sterile neutrino As the sterile neutrinos are inert, massive particles, they are a potential candidate for dark matter [158].

Due to their inert nature, sterile neutrinos cannot produced in a thermal freeze-out, but instead may be produced by oscillations where the temperature of the universe is approximately $T \sim 100$ MeV [158]. Due to their necessarily light masses, sterile neutrinos are also subject to the constraints on warm dark matter from structure limits from the Lyman-alpha forest [159]. Alternatively, sterile neutrinos may be produced by some other hypothesised heavier particle [160]. Searches for sterile neutrino dark matter utilise the fact that they are expected to undergo a loop-level decay to a photon and an active neutrino [161]. Constraints arise from searches in the X-ray spectrum, with an unidentified emission line at 3.5 keV in

some measurements of galaxies and galaxy clusters [162, 163]. However, the lack of detection in dwarf galaxies casts doubt to the origin of the signal as sterile neutrino dark matter [164, 165].

1.5.6 Hidden dark matter

It is, of course, also possible that there could be any number of dark matter particles which have interactions independent of the gauge interactions of the Standard Model. There is plenty of choice to introduce a whole catalogue of new particles, with new gauge interactions and symmetries so long as the only interaction to the Standard Model is gravitational. Hypothesised examples include 'mirrored' or 'hidden' models, which suggest additional matter particles and forces that replicate the Standard Model [166, 167].

Such models are typically difficult to test experimentally, as they do not generally have a connection to other phenomenological issues nor do they generate any non-gravitational signal. Potential experiments involve searches for so-called connector particles at particle colliders, which have interactions with both the Standard Model and hidden sectors [168].

1.6 Direct detection searches

There are several methods of generalised and specialised experimental and observational searches for particle dark matter, in particular, dark matter at the weak scale. One of the main categories of such searches is so-called direct detection. In general, direct detection searches are conducted in deep underground laboratories, which shields the detector from the background radiation due to cosmic ray particle showers using the depth of rock. The detector searches for a scattering interaction between an ion in the target material and a dark matter particle. The resultant energy deposit is measured via the scintillation of the scattered nucleus, the light from which is measured in photomultiplier tubes, or through phonon production creating small temperature pulses [169, 170]. Such a set-up is ideal for WIMP candidates with a mass on the order from a few GeV up to the TeV scale, which corresponds to particles with a similar mass to the corresponding detection nuclei.

1.6.1 Spin independent dark matter searches

There are generally two classes of interaction between dark matter particles and Standard Model nuclei. The first is spin independent scattering, also known as scalar scattering, the cross section is strongly dependent on the mass of the target nuclei. Searches generally use targets with larger atomic nuclei to increase detection rates. The second class is spin dependent scattering, also known as axial-vector scattering. Here, the scattering rates are proportional to the spin of the target nuclei $J(J+1)$, which favours target nuclei with higher spin quantum numbers.

Early direct detection experiments for spin independent scattering were built using crystal detectors of sodium iodide (NaI) [171–173] or germanium [174–176]. Such isotopes were favoured as they are relatively heavy with masses ~ 100 GeV, which maximises the potential recoil energy from dark matter particles with similar, also relatively heavy masses. For dark matter particles which undergo a vector coupling, the cross section is approximately proportional to the number of nucleons in the target nuclei, also favouring heavier nuclei. For particles undergoing an axial coupling with the Standard Model, such as Majorana neutralinos, the cross sections are dependent on the spin properties of the target nuclei, favouring nuclei not just with larger spin values, but how the spin is distributed among the constituent quarks and nucleons [177].

Direct detection experiments using the crystal detectors were set up in deep underground laboratories, including the DAMA/NaI experiment at Gran Sasso National Laboratory [178] and the CDMS-I experiment at Stanford University, later moved to the Soudan Mine [179]. Although the DAMA/NaI experiment initially showed no direct evidence for a dark matter signal [178], it was later reported that there was a seasonal modulation in the energy deposits in the DAMA/NaI detector [180]. An annual modulation in the signal may be due to the motion of the Earth with respect to the galactic background during its orbit, peaking in late spring in the northern hemisphere [181]. Follow up studies over a seven year period have repeatedly shown evidence for the annual modulation at DAMA/NaI [182, 183], continuing into its successor experiment DAMA/LIBRA for a further seven years [184–186]. The result is interpreted as evidence for a dark matter particle with mass of approximately $30 - 200$ GeV with a spin-independent cross section of approximately $10^{-42} - 10^{-41}$ cm^2.

However, the apparent success of the dark matter searches in the sodium-iodine experiments was not replicated in then-contemporary germanium, silicon or tungsten-based scintillation detectors. Almost immediately, the CDMS experiment appeared to exclude most of the DAMA signal region [179, 187, 188]. After the move to the Soudan Underground Laboratory, the upgraded CDMS-II completely excluded the DAMA signal region [189, 190], with cross-sections excluded down to 10^{-42} cm^2 for masses in the order of tens of GeV. Further experiments have increased the detector size and exposure time and technological improvements have slowly increased the exclusion region to around 10^{-44} cm^2 [191–198]. Additionally, there has been focus on improving the sensitivity in the low mass ~ 10 GeV region with the CDMSlite experiment [197, 199–201].

Notably, the CDMS experiment has not detected any annual modulation in the nuclear recoil rate, also in contradiction to the DAMA results [202, 203]. The DAMA result is now highly disputed, with no other experiment able to replicate the results [204, 205]. The SABRE experiment is a proposed southern hemisphere experiment designed to measure whether the DAMA modulation is a seasonal effect or an in-phase modulation [206]. Nevertheless, there have still been numerous attempts to reconcile the DAMA signal with other experiments by invoking various models such as a mixed-coupling of dark matter [207], inelastic dark matter [208], dark matter interacting via electrons [209] or light dark matter [210].

In more recent years, however, stronger bounds have been placed on the dark matter cross section in a series of experiments with xenon as the target nuclei. Such experiments are searching for a scintillation or ionisation signal following the interaction of a nuclei with a dark matter particle. The early proof-of-concept experiments used a fiducial volume of approximately 10 kg of liquid xenon, namely the ZEPLIN-I [211] and XENON10 [212] experiments. Since then, subsequent experiments have increased the fiducial volume increased by an order of magnitude for the ZEPLIN-II [213], ZEPLIN-III [214], LUX [215, 216], PandaX-I [217], PandaX-II [218, 219] and XENON100 [220–222] experiments. No xenon-based experiment has shown a hint of a signal for dark matter. The current generation of experiments seeks to expand by an order of magnitude with approximately one ton of fiducial volume, namely the XENON1T [223, 224] and LZ [225] experiments. The early results from the XENON1T experiment represent the strongest bounds yet on the dark matter cross section at the weak scale.

There exists a theoretical limit on the sensitivity of the current technology of direct detection experiments which arises from a strong background signal from neutrino recoil. There are numerous processes in the Sun that can produce neutrinos. Although most are emitted through the fusion of protons via $p + p \rightarrow d + e^+ + \nu_e$, some are also emitted through higher-order processes with slightly heavier elements. There are trace amounts of ^{8}B produced by helium fusion in the Sun which decay by the process $^8\mathrm{B} \rightarrow {}^8\mathrm{Be} + \mathrm{e}^+ + \nu_\mathrm{e}$. These neutrinos are predicted to scatter elastically from the target nuclei in direct detection experiments at extremely low but not insignificant cross sections [226, 227]. Other potential neutrino sources include neutrinos produced in the upper atmosphere by interactions between cosmic rays and atmospheric gasses [228] and neutrinos produced by nuclear processes in supernovae [229, 230]. Both

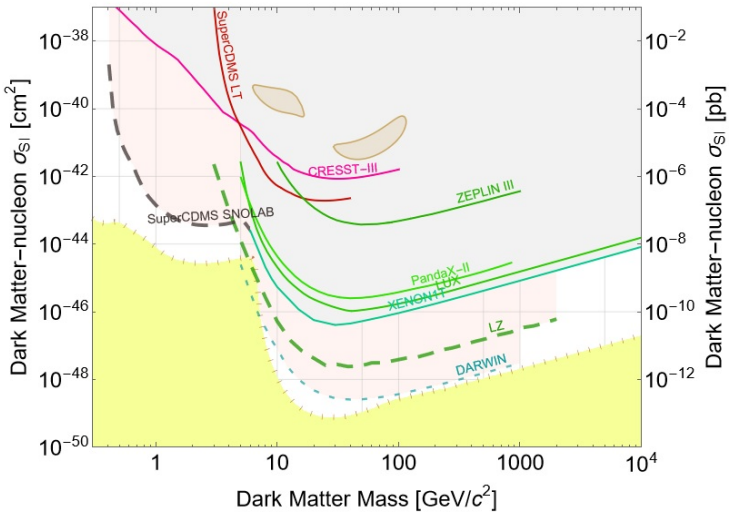

Figure 1.1: A selection of current spin independent direct detection dark matter constraints from current generation xenon-based detectors (green, solid line) [214, 216, 218, 224], low-threshold germanium and silicon detectors (red, solid line) [199, 240, 241], and projections of next-generation exclusion limits (dashed line) [225, 242]. The shaded yellow region shows the projected neutrino floor [238]. The brown contours show the DAMA/Libra annual modulation signal [204].

are expected to produce neutrinos with significantly higher energies than the solar neutrinos, albeit with a significantly lower event rate [231]. Estimates of the nucleon-neutrino cross section are in the order of 10^{-45} cm^2, though the value is dependent on the nature of the target nucleus. If the dark matter detector is sensitive to cross sections of such a magnitude as is expected for the ton-scale experiments, it is expected that there will be a significant additional background to the experimental data [232]. Given the low event rates expected from dark matter-nucleon cross sections, it will be very difficult to differentiate any signal from the background noise. The first detection of elastic neutrino-nucleon scattering has been observed by COHERENT [233], allowing for more accurate calculations about the expected height of the neutrino floor [234]. However, there are still numerous proposals of methods and techniques to overcome the neutrino background, some or all of which would need to be employed in future to push searches below the neutrino floor. Examples include: measuring an annual modulation in the modern experiments, analogous to the DAMA results [232, 235]; employing a directional detector, which would allow backgrounds neutrinos from solar sources to be excluded [236, 237]; combining limits from experiments with different target materials [238]; or building a detector with sufficiently fine energy resolution so as to distinguish neutrino events from dark matter events [239].

The current exclusion limits on the dark matter mass and cross section are shown, along with the neutrino floor, in figure 1.1[1]. The strongest limits derive from the xenon-based experiments and extend to approximately 10^{-46} cm^2 in the mass region of $10 - 100$ GeV. Lighter dark matter particles are less likely to trigger an scintillation event above the detectors threshold. The best constraints for lower-mass particles are found from crystal-based experiments with germanium or silicon as such experiments are searching for a phonon in the ionisation of a crystal, which allows a lower threshold than scintillation.

The direct detection experiments provide some of the strongest bounds against the detection of particle dark matter interacting through the weak force. Despite suggested hints of a signal from DAMA, the required interaction strength has now been strongly excluded by other experiments. However, as the experimental sensitivities approach the neutrino floor, alternate methods, approaches or techniques will be required to further the search for dark matter.

[1]Plot generated by the SuperCDMS Dark Matter Limit Plotter, available at: https://supercdms.slac.stanford.edu/dark-matter-limit-plotter

1.6.2 Spin dependent dark matter searches

There is a class of dark matter scattering interactions with Standard Model nuclei which depends on the spin quantum numbers $J(J+1)$ of the target nuclei, so-called spin-dependent interactions. Thus, the interaction strength is determined by the nucleon composition of the target nucleus: where the number of protons in the nucleus is odd then the dark matter to proton interactions dominate the cross section, whereas if the number of neutrons in the nuclei is odd then the dark matter to neutron interaction dominates. Notably, if the nuclei has even numbers of protons and neutrons then the interaction rates are highly suppressed. Candidate target nuclei include Na, I, Cs and F which all have odd numbers of protons. Meanwhile, Xe and Ge have stable isotopes with odd numbers of neutrons.

In general, target nuclei with higher masses do not necessarily improve detection rates as such experiments are not optimised for spin dependent constraints. As such, the constraints on spin dependent cross sections of dark matter can be several orders of magnitude weaker than the spin independent constraints in direct detection experiments. An example of an early constraint from heavy nuclei experiments on spin dependent dark matter scattering neutrons from in Xe was provided by ZEPLIN-II [243] at $\sim 10^{-37}$ cm^2 for a dark matter particle with mass around ~ 100 GeV. Modern constraints from LUX [244] and PandaX-II [245] can now reach as low as $\sim 10^{-39}$ cm^2.

Meanwhile, experiments that directly interrogate spin dependent cross sections choose target nuclei which have a favourable combination of nucleons. Of those, ^{19}Fe has been shown to be particularly favourable [246] for scattering from protons. Experiments such as PICASSO [247] and COUPP [248] use superheated fluorocarbons as the active material. The early bound on the scattering cross section of dark matter from protons was $\sim 10^{-36}$ cm^2 for a particle with a mass between $10-100$ GeV [247]. The modern constraints now reach as low as $\sim 10^{-41}$ cm^2 with results from PICO-60 [249]. The sensitivity of the fluorocarbon based experiments provides the tightest constraints on GeV-scale spin dependent dark matter detection.

Experiments using iodine crystals are also particularly good at spin dependent detection due to the nuclei's relatively larger nuclear spin value [250]. Constraints arise from crystal scintillation experiments, typically using either NaI like NAIAD [251] and [252] or CeI like KIMS [253]. Indeed, the metal ions also provide an additional source for spin-dependent scattering. Crystal experiments can also search for sub-GeV particles using Li-based target crystals in experiments such as CRESST [254]. The constraints on a particle of 1 GeV is $\sim 10^{-30}$ cm^2 for proton scattering, the tightest constraints at the low mass regions.

The fact that the spin dependent constraints are significantly weaker than the spin independent constraints briefly gave rise to a suggestion that a spin dependent interaction could alleviate the tension between the annual modulation in the DAMA observations and null results from other experiments [255,256]. The idea is reinforced by the fact that DAMA is a NaI crystal detector. The annual modulation favours a relatively light ~ 10 GeV dark matter particle and allows a small spin dependent dark matter to proton interaction of 10^{-37} cm^2, although the expected interaction with a neutron could be as high as 10^{-35} cm^2 [257]. However, these cross sections do remain in tension with other experiments [253].

A selection of current exclusion limits on spin dependent dark matter for both scattering of a dark matter particle from protons and neutrons is shown in figure 1.2[1]. The different sensitivities of the different target nuclei in each of the experiments in different areas of the parameter space can be seen across both the proton and neutron scattering. The fluorocarbon experiments provide the strongest constraints, down to the xenon neutrino floor, but only for scattering via protons. Meanwhile, the lithium based experiments provide the best constraints at the GeV scale.

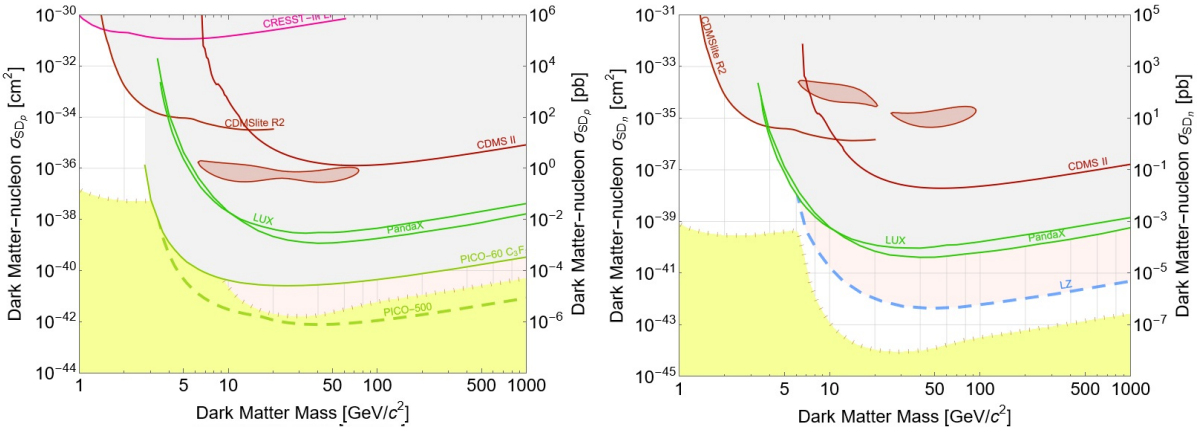

Figure 1.2: A selection of current spin dependent direct detection dark matter constraints for scattering from protons (left) and neutrons (right) from current generation xenon-based detectors (green, solid line) [214, 224, 244, 245], low-threshold lithium and iodine detectors (red, solid line) [193, 201, 241], fluorocarbon bubble chambers [249] and projections of next-generation exclusion limits (dashed line) [249]. The shaded yellow region shows the projected neutrino floor for xenon-based detectors [238]. The red contours show the DAMA/Libra annual modulation signal [204].

1.7 Indirect Detection Searches and Solar Neutrinos

Another class of dark matter constraints are the so-called indirect detection searches. In general, these searches aim to measure annihilation rates from dark matter to the Standard Model in galactic and extragalactic regions. Annihilation of dark matter in some models may be expected to produce gamma-ray photons by a direct annihilation via one-loop interactions such as $\chi\chi \to \gamma\gamma$ or $\chi\chi \to Z\gamma$ [258–261], or by emission of a photon during an annihilation process to other Standard Model particles in a so-called internal bremsstrahlung [259, 260, 262, 263]. The former generates the observed particles in the 2-body final state and is expected to appear as a sharp line in the photon spectrum, whereas the latter may emit a photon from a virtual charged state or from an external leg as final state radiation resulting in a diffuse contribution to the spectrum. In any case, such photons are expected to appear as otherwise unaccounted-for gamma-ray sources coincident with expected dark matter distributions. Additionally, dark matter annihilations may be a source of neutrino production [264, 265], which may be seen by a neutrino telescope.

There are two major sources of expected dark matter annihilation that have been the subject of searches by gamma-ray and neutrino telescopes. The Milky Way galactic centre is expected to be the highest local concentration of dark matter, and is therefore expected to be a strong source of dark matter annihilation [266–269]. However, there are large uncertainties associated with the galactic centre constraints due to the concentration of alternative gamma-ray and neutrino sources nearby [270] and due to the difficulties in modelling the dark matter distribution in the central region of galaxies, the so-called cusp-core problem [23–32]. Dwarf galaxies offer an alternative source of dark matter annihilation without the large background uncertainties [271–278] as they are highly concentrated in dark matter [279–282]. However, the associated signal strength is expected to be significantly lower due to the decreased resolution of the more distant galaxies. Other potential sources include galaxy clusters [283–291], and galactic and extragalactic diffuse dark matter [292–298], but all suffer similar problems of either large uncertainties or small signal strength or both.

There are multiple techniques and experiments which are searching for dark matter through annihilation into gamma rays. The HESS [299], MAGIC [300] and VERITAS [301] telescopes are ground-based atmospheric cherenkov gamma ray telescopes. Gamma ray photons from outer space enter the upper atmosphere of the Earth and collide with a nuclei, depositing energy and momentum into the molecule,

which in turn may collide with another nuclei and so on. The result is a cascade of particles which spreads to the ground with a small flash of cherenkov light that can be observed through a ground-based optical telescope. By reconstructing the shower from multiple angles, the original direction and energy of the incoming gamma ray can be determined. Contrastingly, the Fermi Large Area Telescope [302] is a satellite-based gamma-ray telescope. Since the telescope is located above the atmosphere, it may detect gamma rays directly without requiring reconstruction of a particle shower. Gamma rays interact with metal sheets and undergo electron-positron pair production, creating a small electric charge that can be measured in a semiconductor. Both the ground-based and satellite-based detectors have provided bounds on the rate of dark matter annihilation.

The galactic centre in particular has been the subject of searches by FermiLAT and HESS. One constraint is derived spectrum lines through direct annihilation of $\chi\chi \to \gamma Z$ and $\to \gamma\gamma$ [294,303–307]. The constraints on the dark matter from the line emission spectrum reach to $\langle \sigma v \rangle \sim 10^{-29}$ cm^3 s^{-1} for masses in the GeV to TeV regime, subject to the choice of dark matter density profile. Claims of an excess in the gamma ray spectrum in the FermiLAT signal from the galactic centre appear to have now come to nothing [308]. Alternatively, there is a constraint from the across the entire gamma ray spectrum, which measures processes like $\chi\chi \to W^+W^-$ and $\chi\chi \to \tau^+\tau^-$ or $\chi\chi \to bb$ [266, 267, 309]. The constraints are strongest for dark matter masses on the order of 1 TeV, with cross sections as low as $\langle \sigma v \rangle \sim 10^{-26}$ cm^3 s^{-1}. Similar constraints can be derived from the background gamma ray spectrum across the entire galaxy, not just the centre [294, 310–312]. Such an observation is less prone to the uncertainty in the dark matter profile due to the cusp-core problem and potential alternate gamma ray sources [309, 313], but the lower densities result in a weaker constraint of around $\langle \sigma v \rangle \sim 10^{-24}$ cm^3 s^{-1}, which is due to the spectrum constraint. Such masses and cross sections approximately correspond to the expected values that would be seen in a thermal relic which primarily interacts via the weak force, making the indirect detection searches a valuable tool to interrogate models of weakly interacting massive particles.

Dwarf galaxy measurements have also placed strong bounds on the searches for dark matter via annihilation as they do not suffer the same levels of uncertainty as the galactic centre observation. There is also more data available which allows for greater statistics, even if the expected signal strength is smaller. Early searches only considered a limited number of well-known dwarf galaxies, with limited constraints [274, 277, 278, 314–316] Modern analyses combine the constraints from observations of approximately 45 known or candidate dwarf galaxy systems. The constraints on the spectrum emission from Milky Way dwarf satellite galaxies with FermiLAT has been steadily tightening to around $\langle \sigma v \rangle \sim 10^{-26}$ cm^3 s^{-1} for masses on the order of 1 TeV [272, 317–320]. Results from ground-based cherenkov telescopes are weaker due to less observation time, with results from VERITAS and MAGIC at $\langle \sigma v \rangle \sim 10^{-23}$ cm^3 s^{-1} [321–323]. The HESS telescope has also searched for gamma ray line emission in a small number of dwarf galaxies, with a constraint less than the galactic centre of around $\langle \sigma v \rangle \sim 10^{-25}$ cm^3 s^{-1} [324].

Indirect detection experiments have also calculated dark matter constraints from a number of other astrophysical sources of dark matter. HESS has observed a couple of globular clusters in the galactic halo, albeit with a relatively weak bound of $\langle \sigma v \rangle \sim 10^{-23}$ cm^3 s^{-1} [325]. Limits from annihilation in galaxy clusters are even weaker at $\langle \sigma v \rangle \sim 10^{-21}$ cm^3 s^{-1} due to the very low rates of the expected signals [284, 290, 326].

In addition to the galactic-scale objects, there have also been attempts to constrain dark matter based on compact objects using gamma ray astronomy. HESS has published limits based on the predict small dark matter halos around black holes [274], but there is sizeable uncertainty in the modelling of the black holes themselves. A more promising scenario is dark matter annihilation based on accumulation in the Sun. As a massive object, the Sun can gravitationally capture dark matter from the galaxy after interactions with atoms in the atmosphere [327, 328]. Alternatively, a small dark matter self-interaction allows additional capture by scattering from dark matter particles already bound by the Sun [329].

Searches for gamma-ray emission are problematic as the photons struggle to escape the Sun without interacting with the stellar atmosphere. However, there are still constraints available from models which allow emission of a dark matter particle after a long-lived mediator escapes the Sun, or from a dark matter halo with radius greater than the solar radius [330].

An alternate indirect detection constraint from solar dark matter arises where the by products of the annihilation are neutrinos, which can transport beyond the stellar atmosphere without a collision with any nuclei. Constraints from neutrinos from the Sun have been provided by the ANTARES experiment [331,332] in the Mediterranean Sea, and the IceCube experiment [333–335] at the South Pole, at three to five orders of magnitude weaker than nuclear recoil direct detection experiments. A similar principle applies to capture and annihilation by dark matter captured in the Earth, with a similar order of magnitude on the constraints [336, 337].

Similarly, neutrino telescopes can be used to search for neutrinos from annihilations in the galactic centre as per the gamma ray searches. The principles are similar, except that the annihilation products decay to neutrinos rather than gamma rays, resulting in an expected emission spectrum. Searches from the Milky Way centre have provided limits of approximately$\langle \sigma v \rangle \sim 10^{-23}$ cm^3 s^{-1} at masses 1 TeV, although it is highly dependent on the choice of dark matter density profile [338–340]. Similar bounds arise in neutrino telescope observations from dwarf galaxies and galaxy clusters [341]. The neutrino bounds are stronger than the gamma ray bounds for smaller masses (i.e. < 100 GeV) as the bounds are only weakly dependent on the cross section. Neutrinos from annihilations in the galactic centre provide the strongest bounds on very heavy masses above 1000 TeV [342].

Indirect searches for dark matter have searched for dark matter annihilations in a number of astrophysical sources, including the galactic centre, dwarf galaxies, galaxy clusters, the Sun and the Earth. Annihilation processes can decay directly to neutrinos or photons, or to another on-shell particle which decays into neutrinos or photons. Along with direct detection experiments, they are the best tools available to probe different scenarios of particle dark matter that exist in the Universe. We are now ready to apply these constraints to specific proposals for models of dark matter.

1.8 Supersymmetry and neutralinos

The WIMP miracle has provided guidance to searches for dark matter to expect a weakly interacting particle with a mass in the scale of GeV to TeV. However, no such particle has yet been discovered in direct or indirect detection experiments, and no heavy beyond the Standard Model particles have been detected at particle colliders. Concurrently with the continuous improvement of experimental constraints on dark matter, there has been a development of theoretical candidates for dark matter particles which can subvert the constraints. One of the most popular classes of candidate models for many years has been supersymmetric dark matter. Supersymmetry is a relatively straightforward extension to the Standard Model that provides natural dark matter candidates that satisfy the criteria to be a WIMP. Parts of the theory of supersymmetric dark matter particles are equivalent to more generalised models of beyond the Standard Model physics and vice versa, so we shall recap the simplest models of supersymmetry, the motivations and the candidate dark matter particles.

1.8.1 Supersymmetry fundamentals

Supersymmetry introduces a new transformation into the Standard Model whereby fermionic particles transform into a bosonic state and vice versa; all other quantum numbers remain invariant [343]. The result is a shift in the spin angular momentum quantum number by a factor of $\frac{1}{2}$. Supersymmetry provides one

of the few ways of expanding the set of symmetries of the Standard Model [344], as most other non-trivial symmetries are forbidden under the so-called Coleman-Mandula "no-go" theorem [345]. In its simplest forms, the new supersymmetric transformations introduce an additional boson into the model for every fermion in the Standard Model, and an additional fermion into the model for every boson in the Standard Model in order to maintain the overall symmetry of the Lagrangian. Apart from the change to the spin of the particle, the quantum numbers and gauge structures of the new particles are identical to their Standard Model counterparts, though notably their masses are not bound by this constraint. The particle catalogue in supersymmetry models is at least double in size to the Standard Model, though additional beyond the Standard Model particles such as axions will increase this number further. The scenario where the superpartners are the only additions to the catalogue is known as the Minimal Supersymmetric Standard Model (MSSM).

Each of the quarks and leptons in the Standard Model obtains a bosonic superpartner. As the left and right-handed leptons behave differently under the weak transformation, we should expect them to produce different superpartners. Recall that the neutrinos do not have a right-handed component in the Standard Model, so there are no superpartners to consider. Additionally, the Higgs sector is expanded from the known 125 GeV Higgs boson [346, 347] two an expanded sector with five physical Higgs bosons, three neutral and two charged, which equates to two $SU(2)$ doublets. Without the extra Higgs fields in a supersymmetric theory, there would be no mechanism to cancel out chiral anomalies in triangular fermionic loops as the sum of the hypercharges of the fermionic particles is non-zero [348]. Additionally, it is not possible to construct a supersymmetric theory using conjugate fields, however the generation of masses from the Higgs mechanism requires using the conjugate fields for generating masses of particles with opposite isospin (for a detailed explanation, see ref. [349] and references therein). Including a second Higgs doublet with opposite hypercharge resolves both tensions. Finally, when considering the electroweak gauge bosons, we consider the superpartners of the particles in the interaction basis W^0 and B, not the mass basis Z boson and photon. A summary of the Standard Model fields and their supersymmetric counterparts in the MSSM including their naming conventions is shown in table 1.1.

1.8.2 Spontaneous symmetry breaking in supersymmetry

Constructing supersymmetric Lagrangians in an exercise in writing down generalised interaction terms which satisfy the supersymmetry transformations. For a set of scalar fields ϕ_i and left-handed fermions ψ_i, the possible terms are written in a generalised manner as:

$$\mathcal{L} \supset \left(-\frac{1}{2} W^{ij} \psi_i \psi_j + W^i F_i + x^{ij} F_i F_j \right) + \text{c.c.} - U \,, \tag{1.13}$$

where W^{ij}, W^i, x^{ij} and U are polynomials of the scalar fields and F_i are the so-called auxiliary terms which have no kinetic term but allows the free fields to be invariant under supersymmetry transformations. It is possible to show that the W^{ij} and W^i terms can be written in terms of a superpotential:

$$W = L^i \phi_i + \frac{1}{2} M^{ij} \phi_i \phi_j + \frac{1}{6} y^{ijk} \phi_i \phi_j \phi_k \,, \tag{1.14}$$

with

$$W^{ij} = \frac{\delta^2}{\delta \phi_i \delta \phi_j} W \tag{1.15}$$

$$W^i = \frac{\delta W}{\delta \phi_i} \tag{1.16}$$

SM name	SM symbol	SM spin	$SU(3)_C \times SU(2)_L \times U(1)_Y$ representation	SUSY name	SUSY symbol	SUSY spin
Leptons				**Sleptons**		
electron/electron neutrino	$(\nu_e,\, e_L)$	1/2	$(\mathbf{1}, \mathbf{2}, -\frac{1}{2})$	selectron/selectron sneutrino	$(\tilde{\nu}_e,\, \tilde{e}_L)$	0
electron	$e_R^\dagger$	1/2	$(\mathbf{1}, \mathbf{1}, 1)$	selectron	$\tilde{e}_R^*$	0
muon/muon neutrino	$(\nu_\mu,\, \mu_L)$	1/2	$(\mathbf{1}, \mathbf{2}, -\frac{1}{2})$	smuon/smuon sneutrino	$(\tilde{\nu}_\mu,\, \tilde{\mu}_L)$	0
muon	$\mu_R^\dagger$	1/2	$(\mathbf{1}, \mathbf{1}, 1)$	smuon	$\tilde{\mu}_R^*$	0
tau/tau neutrino	$(\nu_\tau,\, \tau_L)$	1/2	$(\mathbf{1}, \mathbf{2}, -\frac{1}{2})$	stau/stau sneutrino	$(\tilde{\nu}_\tau,\, \tilde{\tau}_L)$	0
tau	$\tau_R^\dagger$	1/2	$(\mathbf{1}, \mathbf{1}, 1)$	stau	$\tilde{\tau}_R^*$	0
Quarks				**Squarks**		
up/down	$(u_L,\, d_L)$	1/2	$(\mathbf{3}, \mathbf{2}, \frac{1}{6})$	sup/sdown	$(\tilde{u}_L,\, \tilde{d}_L)$	0
up	$u_R^\dagger$	1/2	$(\overline{\mathbf{3}}, \mathbf{1}, -\frac{2}{3})$	sup	$\tilde{u}_R^*$	0
down	$d_R^\dagger$	1/2	$(\overline{\mathbf{3}}, \mathbf{1}, \frac{1}{3})$	sdown	$\tilde{d}_R^*$	0
charm/strange	$(c_L,\, s_L)$	1/2	$(\mathbf{3}, \mathbf{2}, \frac{1}{6})$	scharm/sstrange	$(\tilde{c}_L,\, \tilde{s}_L)$	0
charm	$c_R^\dagger$	1/2	$(\overline{\mathbf{3}}, \mathbf{1}, -\frac{2}{3})$	scharm	$\tilde{c}_R^*$	0
strange	$s_R^\dagger$	1/2	$(\overline{\mathbf{3}}, \mathbf{1}, \frac{1}{3})$	sstrange	$\tilde{s}_R^*$	0
top/bottom	$(t_L,\, b_L)$	1/2	$(\mathbf{3}, \mathbf{2}, \frac{1}{6})$	stop/sbottom	$(\tilde{t}_L,\, \tilde{b}_L)$	0
top	$t_R^\dagger$	1/2	$(\overline{\mathbf{3}}, \mathbf{1}, -\frac{2}{3})$	stop	$\tilde{t}_R^*$	0
bottom	$b_R^\dagger$	1/2	$(\overline{\mathbf{3}}, \mathbf{1}, \frac{1}{3})$	sbottom	$\tilde{b}_R^*$	0
Scalar Bosons				**Higgsinos**		
Higgs boson (u)	$(H_u^+,\, H_u^0)$	0	$(\mathbf{1}, \mathbf{2}, +\frac{1}{2})$	Higgsino (u)	$(\tilde{H}_u^+,\, \tilde{H}_u^0)$	1/2
Higgs boson (d)	$(H_d^0,\, H_d^-)$	0	$(\mathbf{1}, \mathbf{2}, -\frac{1}{2})$	Higgsino (d)	$(\tilde{H}_d^0,\, \tilde{H}_d^-)$	1/2
Gauge Bosons				**Gauginos**		
gluon	g	1	$(\overline{\mathbf{8}}, \mathbf{1}, 0)$	gluino	$\tilde{g}$	1/2
charged W boson	$W^\pm$	1	$(\overline{\mathbf{1}}, \mathbf{3}, 0)$	charged wino	$\tilde{W}^\pm$	1/2
neutral W boson (EWSB: Z and γ)	W^0	1	$(\overline{\mathbf{1}}, \mathbf{3}, 0)$	neutral wino	$\tilde{W}^0$	1/2
B boson (EWSB: Z and γ)	B^0	1	$(\overline{\mathbf{1}}, \mathbf{1}, 0)$	bino	$\tilde{B}^0$	1/2

Table 1.1: List of Standard Model particles and their SUSY partners in terms of their chiral multiplets. Note that the neutral W boson and the B boson obtain masses via spontaneous symmetry breaking; their mass eigenstates are the Z boson and the photon.

Indeed, the terms in the superpotential can contribute to the mass terms of the Standard Model scalar bosons, namely the Higgs boson. The Lagrangian terms for the gauginos λ^a also follow directly from taking the terms for the gauge bosons in the covariant derivatives and mandating that they must follow supersymmetry. There are many more complications to these derivations, but they are beyond the scope of this work.

Because supersymmetry is not observed at low energy scales, it is expected that supersymmetry will be broken. Any interactions in the theory which break supersymmetry are expected to be soft, that is, have positive mass dimension so as to maintain a mass hierarchy between the electroweak and Planck scales. The soft supersymmetry breaking terms allowable in the Lagrangian are:

$$\mathcal{L} \supset -\left(\frac{1}{2}M_a\lambda^a\lambda^a + \frac{1}{6}a^{ijk}\phi_i\phi_j\phi_k + \frac{1}{2}b^{ij}\phi_i\phi_j + t^i\phi_i\right) + \text{c.c.} - \left(m^2\right)^i_{\ j}\,\phi^{j*}\phi_i\,, \tag{1.17}$$

for gauginos λ^a and scalar fields ϕ_i. Notably for our models, this includes mass terms for the gauginos. Even though our models in this work are not explicitly supersymmetric, we borrow the standard notation that the gaugino masses are labelled M_1 and M_2. The parameters of the supersymmetry breaking are free parameters, albeit subject to observational constraints. Meanwhile, the other possible soft supersymmetry breaking terms involve the scalar bosons in the theory, which for the MSSM is the pair of Higgs doublets. The result of adding these terms is a modification to the Higgs spectrum through the b term.

One of the consequences of having two Higgs doublets in the model is that there is a modification to the electroweak symmetry breaking procedure in the model. In such models, the Higgs fields posses two complex $SU(2)$ doublets, which corresponds to 8 real degrees of freedom, two for each complex number for each of the two components of the two doublets.

As a reminder, for the case of a single complex scalar $SU(2)$ doublet, the Higgs mechanism gives masses to three gauge bosons by breaking electroweak symmetry. Consider a scalar particle $\Phi = \begin{pmatrix}\phi^+\\ \phi^0\end{pmatrix}$ with mass μ and a potential added to the Lagrangian given by:

$$V(\Phi) = |\mu|^2\Phi\Phi^\dagger - \lambda\left(|\Phi\Phi^\dagger|\right)^2\,, \tag{1.18}$$

for some $\lambda > 0$. Such a model is known as the Weinberg-Salam model [350]. For the case that $|\mu|^2 > 0$, the potential preserves the symmetries of the Lagrangian since it is invariant under the transformations of the theory. However, where $|\mu|^2 < 0$, the state for minimum energy is no longer at $\phi^0 = 0$. Instead, we expand the potential about the minimum value, the so-called vacuum expectation value commonly referred to as a vev. In such a model, the vev is given by $\frac{v}{\sqrt{2}} \equiv \sqrt{-\frac{\mu^2}{2\lambda}}$, the value of the field at the minimum value. There are many possible parametrisations of the field at the vev, since the minimum energy is only dependent on the combination $\Phi^\dagger\Phi$. A popular choice is given by:

$$\langle\Phi\rangle \equiv \frac{1}{\sqrt{2}}\begin{pmatrix}0\\ v\end{pmatrix}\,. \tag{1.19}$$

The complex scalar may now be expanded in terms of real scalar fields $h(x)$ and $\eta_i(x)$ as:

$$\Phi(x) = \begin{pmatrix}\eta_1(x) + i\eta_2(x)\\ \frac{v}{\sqrt{2}} + h(x) + i\eta_3(x)\end{pmatrix}\,. \tag{1.20}$$

Our theory has now acquired three Nambu-Goldstone bosons [351], $\eta_i(x)$. Each of these bosons can be removed from the theory completely by a clever choice of gauge for any of the massless gauge bosons in the theory. By choosing the unitary gauge for the $W^\pm$ and B^0, these bosons are said to have eaten the Nambu-Goldstone bosons. The only remaining factor is $h(x)$, which becomes the Higgs boson. The

side-effect of the process that the gauge bosons attain a mass term. Given that the Lagrangian for the field is:

$$\mathcal{L} \supset |D_\mu \Phi|^2 - V(\Phi)\,, \tag{1.21}$$

where

$$D_\mu = \partial_\mu + igW_i + i\frac{g'}{2}B_\mu \tag{1.22}$$

is the covariant derivative for the $SU(2)\times U(1)$ model and Φ has hypercharge $\frac{1}{2}$, there will be an interaction with the second component of Φ and the gauge bosons packed inside D_μ. In particular, since v is just a real number, there are mass terms for the gauge bosons of the form:

$$\mathcal{L} \supset \frac{1}{2}\begin{pmatrix}0 & v\end{pmatrix}\left(\partial_\mu + igW_i + i\frac{g'}{2}B_\mu\right)^2\begin{pmatrix}0\\ v\end{pmatrix}. \tag{1.23}$$

So the initial 4 degrees of freedom in the doublet field have become three mass terms of the gauge bosons and one physical real scalar boson, the Higgs boson. Such a theory also fixes the masses of the gauge bosons to the coupling parameters and the vev:

$$m_W = \frac{gv}{2}\,; \tag{1.24}$$

$$m_Z = \frac{v}{2}\sqrt{g^2+g'^2}\,; \tag{1.25}$$

$$m_A = 0\,. \tag{1.26}$$

A similar modification is made to the Yukawa terms in the coupling which gives masses to the Standard Model fermions except the neutrino, as the lack of right handed neutrino prevents a Yukawa coupling from being written down.

Now consider the case where there are two $SU(2)$ doublets $H_u = \begin{pmatrix}H_u^+\\ H_u^0\end{pmatrix}$ and $H_d = \begin{pmatrix}H_d^0\\ H_d^-\end{pmatrix}$. In such a scenario, the scalar potential for the fields is given by:

$$\begin{aligned} V = {} & \left(|\mu|^2 + m_{H_u}^2\right)\left(|H_u^0|^2 + |H_u^+|^2\right) + \left(|\mu|^2 + m_{H_d}^2\right)\left(|H_d^0|^2 + |H_d^-|^2\right) + \left[b\left(H_u^+ H_d^- - H_u^0 H_d^0\right) + \text{c.c.}\right] \\ & + \frac{1}{8}\left(g^2+g'^2\right)\left(|H_u^0|^2 + |H_u^+|^2 - |H_d^0|^2 - |H_d^-|^2\right)^2 + \frac{1}{2}g^2|H_u^+ H_d^{0*} + H_u^0 H_d^{0*}|^2\,. \end{aligned} \tag{1.27}$$

The terms proportional to $m_{H_u}^2$, $m_{H_d}^2$ and b arise from the soft breaking of the MSSM, while the remaining terms arise from the auxiliary fields in the superpotential. By a similar argument to above, there is choice about where the fields may be expanded around, which for simplicity is chosen such that at the minimum energy $H_u^+ = 0$ and $H_d^- = 0$. Therefore, the minimum of the potential permits electromagnetism to be unbroken as the charged components will not have vevs. Next, the potential must be bounded from below, that is, a minimum of the potential must exist. Equivalently, the quadratic components of the scalar potential must be positive, so:

$$2b < 2|\mu|^2 + m_{H_u}^2 + m_{H_d}^2\,. \tag{1.28}$$

Similarly, for the symmetry to be broken, $H_u = H_d = 0$ must not be a stable minimum of the potential, so:

$$b^2 > \left(|\mu|^2 + m_{H_u}^2\right)\left(|\mu|^2 + m_{H_d}^2\right). \tag{1.29}$$

Notably, if $m_{H_u}^2 = m_{H_d}^2$, both constraints can not simultaneously be satisfied.

Given the constraints, the phenomenology of the model follows in a similar manner to the case above. However, we now have two vevs:

$$v_u \equiv \langle H_u^0 \rangle \,; \tag{1.30}$$

$$v_d \equiv \langle H_d^0 \rangle \,. \tag{1.31}$$

By convention, the parameter $\tan\beta$ is defined by the ratio of the two vevs:

$$\tan\beta \equiv \frac{v_u}{v_d} \,. \tag{1.32}$$

From here, expressions for the masses fall out of the equations:

$$v_u^2 + v_d^2 = v^2 = \frac{2m_Z^2}{g^2 + g'^2} \,; \tag{1.33}$$

$$m_{H_u}^2 + |\mu|^2 - b\cot\beta - \frac{1}{2}m_Z^2\cos(2\beta) = 0 \,; \tag{1.34}$$

$$m_{H_d}^2 + |\mu|^2 - b\tan\beta + \frac{1}{2}m_Z^2\cos(2\beta) = 0 \,, \tag{1.35}$$

which is unconstrained as there are four unknown parameters: $|\mu|^2$, b, $m_{H_u}^2$ and $m_{H_d}^2$. Note here that as $|\mu|^2$ respects supersymmetry while b, $m_{H_u}^2$ and $m_{H_d}^2$ break supersymmetry, but all four combine to give the Z boson mass. It is expected that there may be a mechanism to resolve the so-called μ problem by aligning all four parameters at the same scale [352].

Now we can return to the effect of introducing both doublets on the number of degrees of freedom before and after electroweak symmetry breaking. Initially, there were 8 degrees of freedom: two doublets each contain two elements which are complex, giving two additional parameters. As with the one doublet case, three of the degrees of freedom are lost eaten as the Nambu-Goldstone bosons are eaten by the gauge bosons - they become the masses of the gauge bosons in the theory. There are still five remaining degrees of freedom in the model, corresponding to five mass eigenstates of the Higgs scalar. First, there are two CP-even neutral scalars h^0 and H^0. Conventionally, these are chosen such that h^0 is lighter than H^0. Additionally, there is one CP-odd neutral eigenstate A^0. The remaining two degrees of freedom are in two charged scalars $H^\pm$ with $+1$ and -1 charge. These eigenstates are chosen such that they diagonalise the scalar potential. The mass states are given by:

$$m_{A^0}^2 = \frac{2b}{\sin(2\beta)} = 2|\mu|^2 + m_{H_u}^2 + m_{H_d}^2 \,; \tag{1.36}$$

$$m_{h^0,H^0}^2 = \frac{1}{2}\left(m_{A^0}^2 + m_Z^2 \mp \sqrt{\left(m_{A_0}^2 - m_Z^2\right)^2 + 4m_Z^2 m_{A^0}^2\sin^2(2\beta)}\right) \,; \tag{1.37}$$

$$m_{H^\pm}^2 = m_{A^0}^2 + m_W^2 \,. \tag{1.38}$$

Although the masses of A^0, H^0 and $H^\pm$ can be arbitrarily large, m_{h^0} is bounded such that

$$m_{h^0}^2 < m_Z|\cos(2\beta)| \,, \tag{1.39}$$

which may appear to conflict with observations of the observed Higgs mass. However, such a mass is subject to sizeable loop corrections from other supersymmetric particles. The precise details of such corrections and the viability of the MSSM as a result is beyond the scope of this work Overall, the presence of the two Higgs doublets results in five mass eigenstates arising from the Higgs mechanism.

1.8.3 Supersymmetric dark matter candidates

Given that supersymmetry has introduced a new collection of particles, we seek to identify potential dark matter candidates There are several requirements that a candidate must pass. Firstly, any dark matter candidate must be a singlet under $SU(3)$, otherwise it would undergo the strong interaction, ruling out all of the squarks and the gluino. Next, it must be electrically neutral, otherwise it would interact with the Standard Model strongly through photons, which rules out the charged wino and all three generations of the selectrons. The remaining candidates are the sneutrinos, the higgsinos, the wino and the bino. The left handed sneutrinos may seem like a potential candidate as they are an electrically neutral color singlet with arbitrary mass [353, 354], but are generally not considered viable due to their sizeable coupling with the Z boson. Right handed sneutrinos do remain a viable dark matter candidate [355], assuming that right handed neutrinos exist in an expanded Standard Model. There are then strong limits from early direct detection experiments [356] and double beta decay experiments [357, 358], which have ruled out the possibility that the sneutrinos can be a thermal relic [359]. There is a minor modern interest in heavy right-handed sneutrino dark matter [360], but that is beyond the scope of this work as we will generally be focussed on dark matter candidates that are fermionic.

Much of the attention in the literature has been on the supersymmetric partners of the Higgs boson and the electroweak gauge bosons [361]. Apart from the gluino, which is a color triplet, the remainder of the gauginos and higgsinos are color singlets, making them candidate dark matter particles, including four which are also electrically neutral. As all four neutral particles have the same quantum numbers, they are expected to mix to form four different mass eigenstates [362]. Such eigenstates are typically labelled χ_1, χ_2, χ_3 and χ_4, ordered from lightest to heaviest called neutralinos. The lightest such particle, or perhaps the two lightest particles if they are near-degenerate, are the dark matter candidates. There is a corresponding mixing matrix $\mathcal{M}$ defined for the basis $\left(\tilde{B} \quad \tilde{W}^0 \quad \tilde{H}_d^0 \quad \tilde{H}_u^0\right)$:

$$\mathcal{M} = \begin{pmatrix} M_1 & 0 & \frac{-g'v_d}{\sqrt{2}} & \frac{g'v_u}{\sqrt{2}} \\ 0 & M_2 & \frac{gv_d}{\sqrt{2}} & \frac{-gv_u}{\sqrt{2}} \\ \frac{-g'v_d}{\sqrt{2}} & \frac{gv_d}{\sqrt{2}} & 0 & -\mu \\ \frac{g'v_u}{\sqrt{2}} & \frac{-gv_u}{\sqrt{2}} & -\mu & 0 \end{pmatrix}, \tag{1.40}$$

where M_1, M_2 and μ are the mass parameters of the bino, wino and higgsino, v_u and v_d are the vacuum expectation values from the two Higgs doublets and g and g' are the weak coupling parameters, where we have not included modifications due to loop corrections. There are several scales in the mass matrix, namely the mass scales M_1, M_2 and μ and the two vacuum expectation values. The former two scales are unconstrained, the latter plays a role in the scalar Higgs potential in the Standard Model [363]. If one of the mass parameters is an order of magnitude smaller than the others, then the lightest supersymmetric particle will dominated by one (or in the case of the higgsino, two) interaction eigenstates, in a similar manner to the mixing due the CKM matrix in the Standard Model sector. Such models are referred to as, for example, higgsino-like or wino-like dark matter. Such models have been well-studied in the literature (for reviews, see ref. [364, 365]). Earlier works considered that these particles would have masses at or around the GeV scale, however such ideas are now often discounted as they are constrained by the measurements of the width of the decay of the Z boson at LEP [366, 367].

It is an important requirement for any viable model of dark matter to be able to reproduce the observed dark matter density from the early universe, particularly as a thermal relic. Considering only models with a dominant component of a neutralino as dark matter, there are a handful of cases which produce thermal relics. For example, for bino-like dark matter it is not possible to construct a thermal relic without mixing with another state as the particle is inert to the Standard Model. For wino-like and higgsino-like dark matter, the single parameter in the theory means that, so long as the remainder of the physics is at a

higher scale, the mass at the thermal relic density is precisely determined. The details of the calculation are subject to the so-called Sommerfeld enhancement, where non-perturbative interactions provide an attractive or repulsive force prior to the annihilation event which increases the cross section [368–370]. Due to the differences in the strength of the Sommerfeld enhancement, wino-like thermal relic dark matter occurs at a mass of 3 TeV [371] and higgsino-like thermal relic dark matter occurs at a mass of 1 TeV [372]. However, such models are subject to rather strong constraints from indirect detection searches. In particular, wino-like thermal relic dark matter has already been excluded [373–378], while higgsino-like is under tension from the same experiments [379].

An important question is the stability of the dark matter candidates, as they should be sufficiently long lived to remain in significant quantities in the Universe to the present day without decaying. It is expected that a heavier particle in the supersymmetric sector should be able to decay into other supersymmetric particles, so a dark matter candidate would be the lightest mass particle in the sector, but there needs to be a mechanism preventing decay into the lighter Standard Model sector. A commonly invoked resolution is a new global symmetry called R-parity, which is conserved under the spontaneous breaking of supersymmetry. Such a symmetry is introduced to preserve fermion number in supersymmetric theories [380]. Otherwise, supersymmetry would allow operators which appear to violate baryon and lepton number conservation, which is heavily bound by limits on the decay of the proton [381]. The imposition of R-parity assigns a new, positive quantum number to the Standard Model particles and a negative number to the introduced supersymmetric particles [382, 383]. The direct result of theories which preserve R-parity is that odd particles (i.e. supersymmetric particles) cannot decay into even particles (i.e. Standard Model particles) and vice versa. Hence, any supersymmetric particle decay must result in other supersymmetric particles, with the lightest such particle being stable. Any such particle is therefore a strong dark matter candidate.

It is increasingly apparent that the simplest models of neutralino thermal relic dark matter are unlikely to be the true description of dark matter. We must instead turn to more complex descriptions of the dark matter in order to attempt to describe or fully exclude neutralino dark matter. However, more complex models are difficult to describe and are often dependent on the precise description of the higher order supersymmetry or other theory. We need a model independent approach to describe any other additional physics that affects these models of neutralinos.

1.9 Effective field theories

A perennial problem with the perturbation theory for particle physics is the presence of UV divergent integrals in the action term of a given interaction due to the loop contributions at higher orders in the perturbation theory [384]. The UV divergences generally correspond to short distance, high momentum interactions. The common solution to these divergences is to introduce a prescription of renormalisation to redefine the bare mass parameters in terms of physical mass parameters that account for the self interactions from the higher order terms in the perturbation theory [385–388]. A common renormalisation regime is to impose a momentum cut-off Λ such that $p^2 \lesssim \Lambda^2$ on the action for the interaction [389]. The result is to remove the high momentum interactions which cause the UV divergence. The exact result is returned in the limit $\Lambda \to \infty$. The computation of the coupling parameters where the regulating parameter is finite means that the coupling parameters themselves are dependent on the regularisation parameter. Where the regularisation parameter is greater than the mass scales involved in the interaction, the physical parameters of the theory, that is those which incorporate the regularisation, are very good approximations for the fully perturbative parameters. The reason the approximations are so effective is that the interactions that are incorporated into the regularisation parameter occur at higher energy scales.

When we construct Lagrangians to describe a quantum field theory, we generally consider terms of up to dimension 4, that is, some combination of operators $\mathcal{O}^{(d)}$ with dimension d and coupling parameters λ_i and c_i:

$$\mathcal{L} = \sum_i \lambda_i^2 \mathcal{O}_i^{(2)} + \sum_j \lambda_j \mathcal{O}_j^{(3)} + \sum_k c_k \mathcal{O}_k^{(4)} \,, \tag{1.41}$$

where the λ_i have dimension 1 and c_i are dimensionless. Together, these terms describe the theory in terms of 2-point interactions (mass terms), kinetic terms, 3-point interactions and 4-point interactions. Their relative strengths are given by the coupling parameters, which after renormalisation describes the physical masses and interactions of the theory. In most descriptions, it is not possible to write down any renormalisable $\mathcal{O}^{(5)}$ terms without reference to the regularisation scheme, and fully renormalisable quantum field theories are truncated at dimension 4.

The requirement that we know all of the higher order physics when constructing our regularisation schemes for our interactions up to dimension 4 means that to describe any low energy interaction, we would have to specify all of the higher order physics. For complicated higher order physics such as supersymmetry, or in cases where we do not know the nature of the higher order physics be it supersymmetry or otherwise, computation would prove nearly impossible. However, an alternative is to consider constructing a so-called effective field theory for the theory. In an effective field theory, the Feynman diagrams which include higher order physics are approximated by a series of regularised operators with dimensions 5 or above. Such operators may describe additional 3-point or 4-point interactions of the lower scale particles, decoupled from the fields at the higher scale. Where the higher scale physics is known, such interactions can be matched to the effective field theory operators at lower energies [390]. The result is a series of Lagrangian terms:

$$\mathcal{L}_{\text{EFT}} = \sum_i \frac{c_i}{\Lambda} \mathcal{O}_i^{(5)} + \sum_j \frac{c_j}{\Lambda^2} \mathcal{O}_j^{(6)} + \dots \,, \tag{1.42}$$

for a series of operators $\mathcal{O}^{(d)}$ with dimension d, dimensionless coupling parameters c and regularisation scales Λ. The effective field theory Lagrangian $\mathcal{L}_{\text{EFT}}$ essentially describes the difference between the full Lagrangian and the dimension-4 Lagrangian describing only the lower order physics. The brilliance of the effective field theory approach is that so long as the set of operators $\mathcal{O}^{(d)}$ spans the space of operators at dimension d, the specifics of the higher order physics does not need to be written explicitly, allowing calculation of the physical parameters at low energies to be model independent. Once a physical description for the parameter has been determined, it can then be matched back to the higher order theory.

That effective field theory can describe the low energy behaviour of a particle without reference to the higher energy theory makes it an appealing framework for studying the behaviour of dark matter. Since dark matter is stable, non-relativistic and interacts only weakly with the Standard Model, it is reasonable to assume that dark matter particle masses are at a sufficiently low energy scale and form part of some larger dark sector of new physics. The goal for some proposed dark matter is to consider not only the required dimension 4 interactions but any and all possible dimension 5 Lagrangian terms.

The precise implementation of effective field theories to dark matter theories is dependent on the precise description of the particle nature of the proposed dark matter. Examples that we will consider here include electromagnetic dipole interactions and interactions with the Higgs Boson. The higher order interaction that corresponds to an otherwise neutral particle possessing an electromagnetic dipole moment is a modification to the two-point self interaction through a loop with positive and negative charged components [2, 391–404]. The interaction with the Higgs Bosons parametrise mass splittings between fermionic dark matter particles [405, 406].

In part I, we shall develop our understanding of the effective field theory couplings up to dimension 5 for an arbitrary fermion added to the Standard Model, including the constraints on and limitations of

such models, with the ultimate goal of determining the regions of the parameter space which correspond to viable thermal relics. In particular, in chapter 2, we construct the Lagrangians for models where dark matter is a $SU(2)$ singlet, doublet or triplet, incorporating all potential Lagrangian terms at each order in the theory. We consider the effect of each additional term on the mass spectrum of the theory, and notice that some dimension 5 terms can induce mass splittings between the otherwise degenerate neutral and charged components. In chapter 3, we consider the effect of such particles, in particular the mass splittings, on the thermal relic density of dark matter. We recap the theories of relic density via the Boltzmann equations and introduce the experimental constraints on the model, including the modification to the annihilation rates due to the Sommerfeld enhancement. Finally, we compute the relic density and show that the introduction of dimension 5 operators greatly expands the range of viable masses for thermal relic dark matter by orders of magnitude in both directions.

In part II, we delve deeper into a subset of operators at dimension 5 which correspond to electromagnetic dipole moments and have momentum and velocity dependent cross sections. Such cross sections have been hypothesised to partially resolve a tension between observations and models in the Sun known as the solar abundance problem. In chapter 4, we introduce the solar abundance problem and its relationship to helioseismology and the sound speed profile of the Sun. We introduce the mathematical preliminaries required for injecting electromagnetic dipole dark matter into the Sun, including calculations of the cross section for scattering electromagnetically from a nucleus. We use the cross sections to introduce the relevant physical processes affected by dark matter in the Sun, namely the capture of dark matter particles by the Sun and energy transport due to dark matter particles within the Sun. In chapter 4 we examine the effect of the dark matter on a number of solar observables representing a range of regions within the Sun, with the goal of fitting the best points in the dark matter parameter space based on the uncertainties in each measurement. Finally, in chapter 6, we summarise our results for each chapter, noting the limitations and future directions of each result.

Part I

Neutralino thermal relics with effective field theory operators

Based on Geytenbeek & Gripaios (2021) *Effective field theory analysis of composite higgsino-like and wino-like thermal relic dark matter*, published in Journal of Cosmology and Astroparticle Physics, volume 2021, page 060 [1]

Chapter 2

Effective field theory model building

Starting from the set of particles in the conventional Standard Model, we seek to explore the minimum addition of new fields and interactions to the Standard Model which still accounts for a dark matter candidate. By completely exploring these scenarios, we hope to identify how to construct more complicated models. In particular, focus is given to interaction strengths and masses around the weak scale, as these give rise to the so-called 'WIMP miracle' of a thermally produced relic abundance for the dark matter (see section 1.4).

To begin, consider adding a new fermion to the Standard Model. What are the requirements to be considered a dark matter candidate? Immediately, the new fermion must be a $\mathrm{SU}(3)_C$ singlet, as any gauge-field interaction with gluons would result in a strongly-interacting dark matter candidate which doesn't fit with any observations of dark matter. By a similar argument, we expect the candidate to be electrically neutral. Although dark matter models with microcharges do exist (e.g. ref. [407]), we do not seek to modify the Standard Model gauge fields in such a generalised model. Thus, a constraint is imposed on the weak hypercharge of the fermion.

The only remaining group theory variable from the Standard Model is the structure of the $\mathrm{SU}(2)_L$ representation. There are several choices here: a singlet representation $\tilde{B}$, a doublet representation $\tilde{H}$ or a triplet representation $\tilde{W}$. These three representations are most commonly represented in the literature as a bino, higgsino or wino respectively, as they each naturally arise in supersymmetric models (see Table 1.1). However, when used in the context of supersymmetry, these three particle families are also associated with a number of other interactions with supersymmetric particles with strengths determined by other supersymmetric parameters. To maintain generality, we consider the bino, higgsino and wino from supersymmetry to be a subset in the family of the singlet, doublet and triplet fermions, and will borrow the relevant nomenclature from supersymmetry to describe these multiplets. As such, we refer to these multiplets as bino-like, higgsino-like and wino-like. Furthermore, it is entirely reasonable to consider fermion multiplets of higher order [408], but we do not do so for two reasons. Firstly, due to the analogies with supersymmetric models, the singlet, doublet and triplet fermions have seen significantly more focus in the literature, so are more relevant to many models of modern theoretical physics. Secondly, all three multiplets are already found in nature in the Standard Model, so reasonable extensions to a new sector are not a great expansion to the theoretical conceptions.

The singlet model brings a single new particle to the particle catalogue. As a singlet, definitionally there is no overall weak isospin. So by the weak hypercharge formula:

$$Y_W = Q - T_3, \tag{2.1}$$

for weak hypercharge Y_W, charge Q and third-component of weak isospin T_3, the requirement of no overall charge gives that we must have zero weak hypercharge. The doublet and triplet models are more complicated: in addition to electrically neutral components which form the dark matter candidate, there will also be some electrically charged components of the multiplet. For the doublet, the overall weak isospin is $T = \frac{1}{2}$ with two components with weak isospin $T_3 = \pm\frac{1}{2}$. To obtain an overall electric charge of zero for at least one particle, there are then two options for the weak hypercharge: $Y_W = \pm\frac{1}{2}$, we shall require both such particles in the model in order to write down a mixed mass term that satisfies the $U(1)$ symmetry. Similarly for the triplet, with weak isospin $T = 1$ there are three components with weak isospin $T_3 = 0, \pm 1$. Conventionally, the weak hypercharge is chosen as $Y_W = 0$ by analogy with the wino and W-boson; other choices for the weak hypercharge result in fermions with a double charge, which we do not consider further in this work.

First, we will review the familiar terms of the singlet, doublet and triplet models at dimensions 3 and 4 in sections 2.1 and 2.2 respectively; these correspond to the mass and kinetic terms of the model respectively. In doing so, we will discover the structure of the mixing matrices of the particles and the free mass and interaction parameters. Next, we introduce a basis of relevant new terms for the effective field theory at dimension 5 in section 2.3. We shall explore the implications of the new terms on the mixing matrices and free parameters, in particular the new mass splittings that are generated between the previously degenerate states in section 2.4. Finally, we summarise the analogy between the new parameters and electromagnetic dipole moments in section 2.5, including a brief look at the anapole moment at dimension 6.

2.1 Dimension 3 - Mass terms

Given these three models, we now seek to develop the minimal number of appropriate terms to be added to the Standard Model Lagrangian. We start with the mass terms, these are at dimension 3 (each of the fields is dimension $\frac{3}{2}$), and contain one dimension 1 parameter - the mass parameter. The mass parameters are not necessarily fundamental parameters; they may be the result of the relevant Higgs mechanism or another mass generation process. However, in our model they are free parameters; we do not prescribe the physics which generates these mass terms. We shall construct the particles with Majorana mass terms, with the Dirac structure if any arising naturally from the combinations of particle-antiparticle pairs in the Mass terms.

2.1.1 Singlet

The singlet $\tilde{B}$ is simply represented as a single particle with zero electric charge $\tilde{B}^0$. We therefore obtain a simple mass term with a mass parameter M_1, which may in principle be complex:

$$\mathcal{L} \supset -\frac{1}{2} M_1 \tilde{B}^0 \tilde{B}^0 \,, \tag{2.2}$$

where the factor $-\frac{1}{2}$ is by convention. M_1 is a free parameter, though we do not specify whether it is a fundamental parameter of the theory (as in the MSSM) or a low-energy integration of a higher order theory. As a singlet, there is no additional gauge structure, so is sterile.

2.1.2 Doublet

As there are two values for the weak hypercharge, in order to write down a consistent model we expect to introduce the two doublets to the Standard Model in a pair. We represent the doublet higgsinos as a pair

of two-component spinors:

$$\widetilde{H}_u = \begin{pmatrix} \widetilde{H}_u^+ \\ \widetilde{H}_u^0 \end{pmatrix} ; \tag{2.3}$$

and

$$\widetilde{H}_d = \begin{pmatrix} \widetilde{H}_d^0 \\ \widetilde{H}_d^- \end{pmatrix} , \tag{2.4}$$

where we have used the round brackets for the representation of the gauge group. The mass parameter is labelled μ. The mass term will therefore be familiar from supersymmetry:

$$\mathcal{L} \supset -\mu\epsilon^{ij}(\widetilde{H}_u)_i(\widetilde{H}_d)_j + \text{h.c.}\,, \tag{2.5}$$

for the antisymmetric tensor ϵ^{ij} such that $\epsilon^{12} = -\epsilon^{21} = +1$, where the indices ij to indicate the gauge components. The use of the antisymmetric tensor ensures that each term of the Lagrangian is electrically neutral.

It will be convenient later to reconfigure the two-component Weyl spinors into a four-component Dirac spinor. In the chiral basis we can construct the four-component spinors as $\widetilde{H}^0 = \begin{bmatrix} \widetilde{H}_u^0 \\ \widetilde{H}_d^{0\dagger} \end{bmatrix}$ and $\widetilde{H}^+ = \begin{bmatrix} \widetilde{H}_u^+ \\ \widetilde{H}_d^{-\dagger} \end{bmatrix}$ where the square brackets indicate spinor components. To determine the mass terms, we expand the index components of eq. (2.5):

$$\begin{aligned} \mathcal{L} \supset & -\mu\left((\widetilde{H}_u)_1(\widetilde{H}_d)_2 - (\widetilde{H}_u)_2(\widetilde{H}_d)_1 + (\widetilde{H}_d)_2^\dagger(\widetilde{H}_u)_1^\dagger - (\widetilde{H}_d)_1^\dagger(\widetilde{H}_u)_2^\dagger\right) \\ = & -\mu\left(\widetilde{H}_u^+\widetilde{H}_d^- - \widetilde{H}_u^0\widetilde{H}_d^0 + (\widetilde{H}_d^-)^\dagger(\widetilde{H}_u^+)^\dagger - (\widetilde{H}_d^0)^\dagger(\widetilde{H}_u^0)^\dagger\right) \end{aligned} . \tag{2.6}$$

Factoring:

$$\mathcal{L} \supset -\mu\overline{\widetilde{H}^0}\widetilde{H}^0 + \mu\overline{\widetilde{H}^+}\widetilde{H}^+ . \tag{2.7}$$

assuming $\mu = \mu^\dagger$. It is now possible to factor the Dirac spinors into a single $SU(2)$ doublet $\widetilde{H} = \begin{pmatrix} \widetilde{H}^+ \\ \widetilde{H}^0 \end{pmatrix}$, The model therefore also represents a single $SU(2)$ doublet being added to the Standard Model. The mass is given by:

$$\mathcal{L} \supset -\mu\overline{\widetilde{H}_i}\widetilde{H}_i\,. \tag{2.8}$$

The choice of the antisymmetric tensor in eq. (2.5) is now clear as it allows a seamless analogy between the Weyl spinors that are useful for formulating SUSY models and simplifying the $SU(2)$ components and the Dirac spinors which allows a simple description of the weak interactions in terms of the gauge field representations.

Note here that the neutral component of the mass of the higgsino can be written in the form of a mixing matrix:

$$\mathcal{L} \supset \widetilde{H}_i^0\mathcal{M}_{ij}^{(1)}\widetilde{H}_j^0 = -\frac{1}{2}\begin{pmatrix} \widetilde{H}_u & \widetilde{H}_d \end{pmatrix}\begin{pmatrix} 0 & -\mu \\ -\mu & 0 \end{pmatrix}\begin{pmatrix} \widetilde{H}_u \\ \widetilde{H}_d \end{pmatrix} . \tag{2.9}$$

The two doublets are equally mixed and hence indistinguishable. As the eigenvalues of $\mathcal{M}_{ij}$ are $\pm\mu$, the higgsinos create two particles of equal mass.

2.1.3 Triplet

Finally, the $SU(2)$ triplet model introduces a weakly-interacting Majorana particle $\widetilde{W}$ with zero weak hypercharge. The triplet includes two charged components $\widetilde{W}^{\pm}$ and a neutral component $\widetilde{W}^0$, which can be packed into a triplet as:

$$\widetilde{W}_i = \begin{pmatrix} \widetilde{W}^+ \\ \widetilde{W}^0 \\ \widetilde{W}^- \end{pmatrix} . \tag{2.10}$$

So as to maintain analogy to supersymmetry, the mass parameter is labelled M_2, and the mass term is:

$$\mathcal{L} \supset -\frac{1}{2} M_2 \widetilde{W}_i \widetilde{W}_i \, ; \tag{2.11}$$

again where the factor of $\frac{1}{2}$ is introduced as a manner of convention. Here, the charged and neutral components have equal mass; there is no splitting between them.

2.1.4 Mixed models

In models like supersymmetry, it is not uncommon for two or more of the three mass parameters described above (μ, M_1 and M_2) to be mixed. It is particularly useful for the singlet models, as these would otherwise be sterile and not interact with the Standard Model. The two configurations that we consider are a combination of the singlet and triplet models, which corresponds to the supersymmetric partners of the $SU(2)$ gauge bosons, and a combination of all three models. In the former case, we construct a mixing matrix for the neutral components based on a two-component vector of Weyl spinors $\psi = \begin{pmatrix} \widetilde{B}^0 & \widetilde{W}^0 \end{pmatrix}$ such that:

$$\mathcal{L} \supset -\frac{1}{2} \psi_i \mathcal{M}^{(2)}_{ij} \psi_j = -\frac{1}{2} \begin{pmatrix} \widetilde{B}^0 & \widetilde{W}^0 \end{pmatrix} \begin{pmatrix} M_1 & 0 \\ 0 & M_2 \end{pmatrix} \begin{pmatrix} \widetilde{B}^0 \\ \widetilde{W}^0 \end{pmatrix} . \tag{2.12}$$

Presently, as the mixing matrix is diagonal, there will be no mixing between the two states until the terms at dimension 4 and 5 are added. The only charged component comes from the triplet. For the case that all three are mixed, we obtain a vector $\psi = \begin{pmatrix} \widetilde{B}^0 & \widetilde{W}^0 & \widetilde{H}^0_u & \widetilde{H}^0_d \end{pmatrix}$, and therefore a mixing matrix of:

$$\mathcal{L} \supset -\frac{1}{2} \psi_i \mathcal{M}^{(3)}_{ij} \psi_j = -\frac{1}{2} \begin{pmatrix} \widetilde{B}^0 & \widetilde{W}^0 & \widetilde{H}^0_u & \widetilde{H}^0_d \end{pmatrix} \begin{pmatrix} M_1 & 0 & 0 & 0 \\ 0 & M_2 & 0 & 0 \\ 0 & 0 & 0 & -\mu \\ 0 & 0 & -\mu & 0 \end{pmatrix} \begin{pmatrix} \widetilde{B}^0 \\ \widetilde{W}^0 \\ \widetilde{H}^0_u \\ \widetilde{H}^0_d \end{pmatrix} . \tag{2.13}$$

2.2 Dimension 4 - Kinetic terms

The dimension 4 terms in the theory arise primarily due as kinetic terms for the fermions. By dimensional analysis, to reach dimension 4, we can either have two fermions (dimension $\frac{3}{2}$) and a derivative $\gamma^\mu \partial_\mu$ (dimension 1) or two fermions and a gauge boson (dimension 1). The two terms will be linked by the requirement that the derivative term is gauge invariant, leading to boson terms determined by the gauge structure of the multiplets.

2.2.1 Singlet

The singlet model is invariant under the $SU(3) \otimes SU(2) \otimes U(1)$ transformations of the Standard Model, that is the singlet model exists in the trivial representation of $SU(2)$. The singlet has zero weak hypercharge, so there will not even be a contribution from the $U(1)$ electromagnetic group. We therefore do not expect

any modifications to the kinetic term, which will be given by:

$$\mathcal{L} \supset i\overline{\widetilde{B}_i^0}\gamma^\mu \partial_\mu \widetilde{B}_i^0 \,. \tag{2.14}$$

The result is that the singlet is sterile in the Standard Model.

2.2.2 Doublet

The doublet model lives in the fundamental representation of $SU(2)$, so we expect that the higgsinos will interact with the $SU(2)$ gauge bosons. Additionally, the higgsinos have hypercharge $\pm\frac{1}{2}$, so there will also be an interaction with the $U(1)$ gauge bosons. The expansion of the covariant derivative of the doublet term in the Lagrangian appears as:

$$\mathcal{L} \supset i\overline{\widetilde{H}_i}\gamma^\mu \left(\partial_\mu - igA_\mu^a \frac{\tau_{ij}^a}{2} - ig'YB_\mu\delta_{ij}\right)\widetilde{H}_j \,, \tag{2.15}$$

where we have used the Dirac fermions $\widetilde{H}_i$ from eq. (2.8), A_μ^a and B_μ are, respectively, the $SU(2)$ and $U(1)$ Standard Model gauge bosons in the interaction basis, g and g' are the Standard Model gauge couplings, $Y = \pm\frac{1}{2}$ is the weak hypercharge of the doublet, and τ_{ij}^a are the generators of the $SU(2)$, that is, the Pauli matrices:

$$\tau_1 = \begin{pmatrix} 0 & 1 \\ 1 & 0 \end{pmatrix}, \quad \tau_2 = \begin{pmatrix} 0 & -i \\ i & 0 \end{pmatrix}, \quad \tau_3 = \begin{pmatrix} 1 & 0 \\ 0 & -1 \end{pmatrix}. \tag{2.16}$$

When the Higgs Boson undergoes spontaneous symmetry breaking, the gauge bosons from the fundamental representation transform into the mass basis in the usual way:

$$W_\mu^\pm \equiv \frac{1}{\sqrt{2}}(A_\mu^1 \mp iA_\mu^2)\,, \tag{2.17}$$

$$Z_\mu \equiv \frac{-gB_\mu + gA_\mu^3}{\sqrt{g^2+g'^2}}\,, \tag{2.18}$$

$$A_\mu^\gamma \equiv \frac{gB_\mu + g'A_\mu^3}{\sqrt{g^2+g'^2}}\,. \tag{2.19}$$

Combined with the mass in eq. (2.8), we have now discovered the usual interactions between an $SU(2)$ fermionic doublet and the gauge bosons. There are no additional new gauge invariant Yukawa terms in the theory because the only scalar particle in the model is the Higgs boson.

2.2.3 Triplet

For the triplet model, the weak hypercharge is zero, so we do not expect there to be an interaction with the $U(1)$ boson. Meanwhile, the triplet lives in the adjoint representation of $SU(2)$, so we can construct the covariant derivative for the kinetic term for the Weyl spinors as:

$$\mathcal{L} \supset i\widetilde{W}_i\overline{\sigma}^\mu \left(\delta_{ij}\partial_\mu - igA_\mu^a \frac{T_{ij}^a}{2}\right)\widetilde{W}_j + \text{h.c.}\,, \tag{2.20}$$

where T_{ij}^a are the three-dimensional representations of the generators of $SU(2)$ given by:

$$T^1 = \frac{1}{\sqrt{2}}\begin{pmatrix} 0 & 1 & 0 \\ 1 & 0 & 1 \\ 0 & 1 & 0 \end{pmatrix}, \quad T^2 = \frac{1}{\sqrt{2}}\begin{pmatrix} 0 & -i & 0 \\ i & 0 & -i \\ 0 & i & 0 \end{pmatrix}, \quad T^3 = \begin{pmatrix} 1 & 0 & 0 \\ 0 & 1 & 0 \\ 0 & 0 & 1 \end{pmatrix}, \tag{2.21}$$

and σ^μ is the four-vector extension to the Pauli matrices:

$$\sigma^0 = \overline{\sigma}^0 = \begin{pmatrix} 1 & 0 \\ 0 & 1 \end{pmatrix}, \quad \sigma^1 = -\overline{\sigma}^1 = \begin{pmatrix} 0 & 1 \\ 1 & 0 \end{pmatrix}, \quad \sigma^2 = -\overline{\sigma}^2 = \begin{pmatrix} 0 & -i \\ i & 0 \end{pmatrix}, \quad \sigma^3 = -\overline{\sigma}^3 = \begin{pmatrix} 1 & 0 \\ 0 & -1 \end{pmatrix}. \tag{2.22}$$

The interaction between the neutral particle and the gauge bosons permits annihilation of the dark matter candidate, producing a thermal relic with a mass of 3 TeV, which is consequently ruled out by indirect detection [373–378].

2.2.4 Mixed models - Yukawa terms

In addition to the dimension 4 terms which arise from the kinetic terms and the expansions to the covariant derivative, it is also possible to construct dimension 4 terms via a Yukawa coupling, that is two fermions (dimension $\frac{3}{2}$) and a scalar boson (dimension 1). In the Standard Model, the only scalar boson is the Higgs Boson. In order for the term to be gauge invariant, we construct the terms of the form $\psi^a(\varphi_i^\dagger \mathcal{T}^a_{ij}\phi_j)$, for fermions ψ and φ, scalar boson ϕ and some gauge representation $\mathcal{T}^a_{ij}$. For the Higgs boson, we have two options for ϕ, corresponding to both positive and negative choices of the weak hypercharge for the scalar boson:

$$H_u = \begin{pmatrix} H_u^+ \\ H_u^0 \end{pmatrix}; \tag{2.23}$$

and

$$H_d = \begin{pmatrix} H_d^0 \\ H_d^- \end{pmatrix}. \tag{2.24}$$

.

To make a gauge invariant quantity, we must combine the Higgs boson and higgsino with a sum of fermion from an equivalent representation. Therefore, consider the representation product for $SU(2)$ representations $\overline{\mathbf{2}} \otimes \mathbf{2} = \mathbf{3} \oplus \mathbf{1}$. Fortunately, $\mathbf{3} \oplus \mathbf{1}$ is the direct sum of the $SU(2)$ representations of $\widetilde{W}_i$ and $\widetilde{B}^0$. So we can use the adjoint and trivial representations for $\mathcal{T}^a_{ij}$, giving us the Lagrangian terms:

$$\mathcal{L} \supset \left(g'\widetilde{B}^0\delta_{ij} + g\widetilde{W}_a T^a_{ij}\right)\left(\overline{\widetilde{H}_u}^i H_u^j + \overline{\widetilde{H}_d}^i H_d^j\right). \tag{2.25}$$

Crucially, our terms now have an interaction with the Higgs boson, which undergoes spontaneous symmetry breaking and obtains a vacuum expectation value. As we have two Higgs boson fields, we will have two vevs, defined by:

$$(H_u)_0 = \begin{pmatrix} 0 \\ v_u \end{pmatrix}; \tag{2.26}$$

and

$$(H_d)_0 = \begin{pmatrix} v_d \\ 0 \end{pmatrix}. \tag{2.27}$$

We therefore obtain modifications to the mass mixing matrix in eq. (2.13):

$$\mathcal{L} \supset -\frac{1}{2}\psi_i \mathcal{M}^{(3)}_{ij}\psi_j = -\frac{1}{2}\begin{pmatrix}\widetilde{B}^0 & \widetilde{W}^0 & \widetilde{H}^0_u & \widetilde{H}^0_d\end{pmatrix}\begin{pmatrix} M_1 & 0 & \frac{-g'v_d}{\sqrt{2}} & \frac{g'v_u}{\sqrt{2}} \\ 0 & M_2 & \frac{gv_d}{\sqrt{2}} & \frac{-gv_u}{\sqrt{2}} \\ \frac{-g'v_d}{\sqrt{2}} & \frac{gv_d}{\sqrt{2}} & 0 & -\mu \\ \frac{g'v_u}{\sqrt{2}} & \frac{-gv_u}{\sqrt{2}} & -\mu & 0 \end{pmatrix}\begin{pmatrix}\widetilde{B}^0 \\ \widetilde{W}^0 \\ \widetilde{H}^0_u \\ \widetilde{H}^0_d\end{pmatrix}. \tag{2.28}$$

Now, unlike before, there is mixing for the bino and wino states to and from the higgsino state. The result is the bino is no longer strictly sterile, so long as it mixes with the other neutral states. For it to be a viable dark matter model, there must be another neutralino present of a similar mass scale. For the case that the second particle is a wino, the model particles are referred to as gauginos. Meanwhile, if the second particle is a higgsino, the model is referred to as a well-tempered neutralino. These terms, however, are not expected to have a significant impact on direct detection as their interaction with the Standard Model involves a Higgs Boson as an intermediate product.

2.3 Dimension 5 - Effective field theory operators

We now turn to the novel features of our model: the dimension 5 terms. Although dimension 5 is not renormalisable, the effective field theory allows us to consider these terms as a valid approximation for higher order physics, up to some cut-off scale Λ. In general, the scales of the model should be smaller than Λ for the model to have any physical interpretation. We seek to construct all valid dimension 5 operators for the models described above.

2.3.1 Singlet

The inclusion of operators of dimension 5 and higher is an approximation for particles and vertices at a higher scale when measured at the lower scale. We do not specify whether the particle is composite, whether it belongs to a supersymmetric theory or any other specification of the higher scale physics. Notably, supersymmetry is a possible but far from the only possible UV completion. If it were supersymmetric, examples of higher order terms which integrate to dimension 5 terms include the top-stop-higgsino Yukawa coupling - which is dependent on the mass scale of the stop squark - or the effects of other weakly-interacting neutral fermions at higher mass scales, such as higher scale winos and binos for lower scale higgsinos or vice versa.

At dimension 5 we have more options for constructing higher order operators using dimensional analysis. Fermions ψ at dimension $\frac{3}{2}$ may still only exist in pairs, forming three-fifths of the operator. The other two dimensions can be produced by a pair of bosons ϕ, giving operators of the form $\psi\psi\phi\phi$. Crucially, each of the pairs of particles, either $\psi\psi$ and $\phi\phi$ or both $\psi\phi$ terms, can be made to be gauge invariant individually allowing easy construction of all operators. The ϕ in each case can be either gauge bosons or scalar bosons. For the singlet case, there is no gauge structure within the singlet, so we can combine directly with an invariant coupling of the scalar bosons:

$$\mathcal{O}^B_1 = (H^\dagger)^i (H)_i \tilde{B}^2 \,. \tag{2.29}$$

Such an operator represents the only interaction for the singlet model with the Standard Model. Although annihilation products are still possible, the scattering cross section for such a model will be highly suppressed as the only available diagram would involve both a loop and a dimension 5 operator. However, eq. (2.29) does provide a modification to the mass of the particle after the spontaneous symmetry breaking of the Higgs boson.

Turning to combinations between the singlet fermions and the Standard Model gauge bosons. As the singlets have no gauge structure, we can only connect to the other gauge bosons with no gauge structure, namely the $U(1)$ gauge boson. We could try to write down dimension 5 operators like:

$$\mathcal{O}_1^B = \overline{\tilde{B}}\sigma^{\mu\nu}B_{\mu\nu}\tilde{B}\,, \tag{2.30}$$

$$\mathcal{O}_2^B = \overline{\tilde{B}}\sigma^{\mu\nu}B^*_{\mu\nu}\tilde{B}\,, \tag{2.31}$$

where $B_{\mu\nu}$ and $\sigma^{\mu\nu}$ will be defined in eqs.(2.40)-(2.44), however these terms will vanish as for them to be gauge invariant, we must multiply by the weak hypercharge of the bino, which is zero. Additionally, we will later discover in section 2.5.1 that even if the weak hypercharge were non-zero, such a term is forbidden as a Majorana particle cannot posses these electromagnetic terms.

2.3.2 Doublet

For the doublet model, we are combining the $SU(2)$ doublet from the Higgs boson in eqs.(2.23)-(2.24) with the $SU(2)$ doublet from the higgsino. The naïve approach is to unite the scalar doublet and the fermion doublet separately to produce gauge invariant quantities, for example, we would generate a term like:

$$\mathcal{O} = \epsilon^{ij}\epsilon^{kl}(H)_i(H)_j(\widetilde{H}_d)_k(\widetilde{H}_d)_l\,, \tag{2.32}$$

however these terms are forbidden [405]. Recall that the Higgs bosons H are symmetric by their boson nature, so when combined with the antisymmetric tensor ϵ^{ij} to make the gauge invariant quantity above, there is an exact cancellation, so combinations $\phi\phi$ and $\psi\psi$ are not possible as gauge invariant quantities for this combination of particles. Instead, we need to combine the fermionic and bosonic components together directly to make a gauge invariant quantity. Thus, we should either expect the fermion and boson to be in the same gauge representation, or that the combination of the fermion and boson be in a representation which balances the representation of the second fermion and second boson. For the case of the doublet model coupling to the Higgs boson, we shall see that these two cases are the equivalent. Later, for the triplet case, only the latter case is valid.

Consider the gauge invariant quantity of combining a Higgs boson H with a higgsino. There are two possible combinations depending on which of the two hypercharges the doublet has: $(H^\dagger)^i(\widetilde{H}_u)_i$ and $\epsilon^{ij}(H)_i(\widetilde{H}_d)_j$. These can be combined in four different ways:

$$\mathcal{O}_1^H = (H^\dagger)^i(\widetilde{H}_u)_i(H^\dagger)^j(\widetilde{H}_u)_j\,, \tag{2.33}$$

$$\mathcal{O}_2^H = \epsilon^{ij}\epsilon^{kl}(H)_i(\widetilde{H}_d)_j(H)_k(\widetilde{H}_d)_l\,, \tag{2.34}$$

$$\mathcal{O}_3^H = \epsilon^{jk}(H^\dagger)^i(\widetilde{H}_u)_i(H)_j(\widetilde{H}_d)_k\,, \text{ and} \tag{2.35}$$

$$\mathcal{O}_4^H = \epsilon^{jk}(H^\dagger)^i(\widetilde{H}_d)_i(H)_j(\widetilde{H}_u)_k\,. \tag{2.36}$$

Possible integrations for these terms include taking the gauginos out of the MSSM. These terms naturally modify the higgsino masses after the spontaneous symmetry breaking of the Higgs Boson as we shall see shortly. Physically, a mass modification represents a mixing between the masses of the higgsino-like particle and a particle of significantly higher mass.

Now consider the alternative: the direct product of the representations of the fermionic and bosonic component. This gives a factor of $(H^\dagger)_i\tau^a_{ij}(\widetilde{H}_u)_j$, which can combine to give an operator like:

$$\mathcal{O}' = \left[(H^\dagger)_i\tau^a_{ij}(\widetilde{H}_u)_j\right]\left[(H^\dagger)_k\tau^a_{kl}(\widetilde{H}_u)_l\right]\,. \tag{2.37}$$

However, the $SU(2)$ generators τ^a_{ij} are subject to the Fierz identity [409]:

$$\tau^a_{ij}\tau^a_{kl} = 2\delta_{il}\delta_{jk} - \delta_{ij}\delta_{kl}\,. \tag{2.38}$$

Eq. (2.37) then becomes:

$$\begin{aligned}
\mathcal{O}' =& \left[2\delta_{il}\delta_{jk} - \delta_{ij}\delta_{kl}\right]\left[(H^\dagger)_i(\widetilde{H}_u)_j(H^\dagger)_k(\widetilde{H}_u)_l\right] \\
=& 2\delta_{il}\delta_{jk}\left[(H^\dagger)_i(\widetilde{H}_u)_j(H^\dagger)_k(\widetilde{H}_u)_l\right] - \delta_{ij}\delta_{kl}\left[(H^\dagger)_i(\widetilde{H}_u)_j(H^\dagger)_k(\widetilde{H}_u)_l\right] \\
=& 2\left[(H^\dagger)_i(\widetilde{H}_u)_i(H^\dagger)_j(\widetilde{H}_u)_j\right] - \left[(H^\dagger)_i(\widetilde{H}_u)_i(H^\dagger)_j(\widetilde{H}_u)_j\right] \\
=& (H^\dagger)_i(\widetilde{H}_u)_i(H^\dagger)_j(\widetilde{H}_u)_j \\
=& \mathcal{O}_1^H\,.
\end{aligned} \tag{2.39}$$

from eq. (2.33). The remaining permutations of $\widetilde{H}_u$ and $\widetilde{H}_d$ in eq. (2.37) can be transformed into a linear combinations of eqs. (2.33)-(2.36) in a similar manner, thus eqs. (2.33)-(2.36) are a sufficient set of operators to span dimension 5.

Now consider constructing operators with an interaction between the doublet fermions and the Standard Model gauge bosons. Here, we are coupling to the field strength tensors for the $U(1)$ and $SU(2)$ gauge bosons; we label these $B_{\mu\nu}$ and $W^a_{\mu\nu}$ respectively. The field strength tensors are defined as:

$$B_{\mu\nu} = \partial_\mu B_\nu - \partial_\nu B_\mu\,, \tag{2.40}$$

$$W^a_{\mu\nu} = \partial_\mu A^a_\nu - \partial_\nu A^a_\mu + f^{abc}A^b_\mu A^c_\mu\,, \tag{2.41}$$

where f^{abc} are the structure constants for $SU(2)$. The field strength tensors have dimension 2, so we can combine with 2 fermions to give our dimension 5 operators. Additionally, we can also define the dual of the field strength tensors as:

$$B^*_{\mu\nu} = \epsilon_{\mu\nu\sigma\rho}B^{\sigma\rho}\,, \tag{2.42}$$

$$(W^a_{\mu\nu})^* = \epsilon_{\mu\nu\sigma\rho}(W^a)^{\sigma\rho}\,. \tag{2.43}$$

The field strength tensor and its dual span the space of the operators constructed from the gauge fields at dimension 2. To make the field strength tensor Lorentz invariant, we balance with the $\sigma^{\mu\nu}$ matrices, defined here as:

$$\sigma^{\mu\nu} = \frac{i}{2}\left(\gamma^\mu\gamma^\nu - \gamma^\nu\gamma^\mu\right)\,. \tag{2.44}$$

The introduction of Dirac indices is then balanced by the pair of fermions, allowing for the construction of the relevant bilinears. We are now ready to construct the appropriate dimension 5 terms to be gauge invariant. The field strength tensor of the $U(1)$ gauge boson is a singlet under $SU(2)$, so we can easily construct an interaction with the doublet field. For the $SU(2)$ gauge field, we need to use a representation which is compatible with the $SU(2)$ representations of the doublet. Along with the dual fields, we obtain another four operators which together we label the as the electric and magnetic dipole terms:

$$\mathcal{O}_5^H = \overline{\widetilde{H}_i}\sigma^{\mu\nu}B_{\mu\nu}\widetilde{H}_i\,, \tag{2.45}$$

$$\mathcal{O}_6^H = \overline{\widetilde{H}_i}\tau^a_{ij}\sigma^{\mu\nu}W^a_{\mu\nu}\widetilde{H}_j\,, \tag{2.46}$$

$$\mathcal{O}_7^H = \overline{\widetilde{H}_i}\sigma^{\mu\nu}B^*_{\mu\nu}\widetilde{H}_i\,, \text{ and} \tag{2.47}$$

$$\mathcal{O}_8^H = \overline{\widetilde{H}_i}\tau^a_{ij}\sigma^{\mu\nu}(W^a)^*_{\mu\nu}\widetilde{H}_j\,, \tag{2.48}$$

where we have used the combined $SU(2)$ generator to bind the $\bar{\mathbf{2}} \otimes \mathbf{2}$ representation of the higgsino doublets to the $\mathbf{3} \oplus \mathbf{1}$ representation of the field strength tensor. The $\mathbf{1}$ component in the $\mathbf{3} \oplus \mathbf{1}$ addition of representations in eq. (2.46) is cancelled by a careful linear combination of eq. (2.45) and (2.46). Here, the presence of the $SU(2)$ generator component τ^a_{ij} in eq. (2.46) and (2.48) mixes the two states of the doublet. Given that the neutral states are mixed, any mass splitting between the two neutral states results means any associated annihilation or scattering must be inelastic [410]. The collection of operators in eqs. (2.33-2.48) represent the complete set of gauge-invariant operators at dimension 5 up to the usual redundancies in effective field theory, as dimensional analysis and symmetry restrict us to operators involving two fermions and two bosons.

2.3.3 Triplet

For the triplet case, we no longer posses the same gauge structure as the Higgs Boson, which limits the number of new operators that we can construct. Consider coupling the triplet model to a doublet scalar boson. We cannot couple the triplet fermion directly to the boson in a gauge invariant way, so we must construct each component to be gauge invariant. Thus, we can construct a pair of scalar bilinear of the $\widetilde{W}$ and H components, giving a single term linking the Higgs boson to the triplet:

$$\mathcal{O}_1^W = (H^\dagger)^i (H)_i \widetilde{W}^2 \,. \tag{2.49}$$

As for the higgsino case, possible integrations for the wino case include other fermion multiplets at a higher mass scale, such as the higgsinos or binos from the MSSM. Eq. (2.49) also induces a shift in the masses of the doublets due to the spontaneous symmetry breaking of the Higgs boson, but it will not produce a mass splitting between the charged and neutral states.

Now consider the interaction between triplet fermions and gauge bosons. We can write down terms coupling the wino to the Abelian $B_{\mu\nu}$ field strength tensor, and the non-Abelian $W^a_{\mu\nu}$ field strength tensor from eqs. (2.42)-(2.43) and their duals $B^*_{\mu\nu}$ and $(W^a)^*_{\mu\nu}$, which are CP-violating terms. For the $SU(2)$ gauge bosons, these terms are constructed with the $SU(2)$ tensor generator T^a_{ij}:

$$\mathcal{O}_2^W = \widetilde{W}_i T^a_{ij} \sigma^{\mu\nu} W^a_{\mu\nu} \widetilde{W}_j \,, \text{ and} \tag{2.50}$$

$$\mathcal{O}_3^W = \widetilde{W}_i T^a_{ij} \sigma^{\mu\nu} (W^a_{\mu\nu})^* \widetilde{W}_j \,. \tag{2.51}$$

Again, these terms will correspond to electromagnetic dipole moments as we will shortly discover. Because of this fact, we cannot introduce operators which directly join the tensor indices of the doublet using $\widetilde{W}_i \sigma^{\mu\nu} B_{\mu\nu} \widetilde{W}_i$ or $\widetilde{W}_i \sigma^{\mu\nu} B^*_{\mu\nu} \widetilde{W}_i$ as though they are Lorentz and gauge invariant, they vanish identically via the antisymmetry of the fermionic components, as these components would have corresponded to an electric dipole operator which is forbidden for Majorana particles under a CPT-invariant theory [411, 412]. However, the terms in eqs. (2.50)-(2.51) avoid this by the presence of the generator T^a_{ij}, which contains both symmetric and antisymmetric components so avoids the constraints for CPT-invariant theorems.

However, by introducing a gauge field with matrix components, it is possible to form a Lorentz invariant via a coupling between the antisymmetric components of T^a_{ij} and the antisymmetric combination $\widetilde{W}_i \widetilde{W}_j$. Hence the terms in eqs. (2.35) and (2.36) can avoid the constraints on magnetic dipoles in CPT-invariant theories.

2.3.4 Mixed models

Finally, we turn to terms which arise from models that contain multiple multiplet fermions of a similar scale. Such a model can resolve the issue for the triplet case coupling to the Higgs boson via a lack of

gauge invariant representations. We consider a product of two dimension 2 $SU(2)$ via $\bar{\mathbf{2}} \otimes \mathbf{2} = \mathbf{3} \oplus \mathbf{1}$. Fortunately, $\mathbf{3} \oplus \mathbf{1}$ is the direct sum of the $SU(2)$ representations of $\tilde{W}^a$ and $\tilde{B}$. In order for proper dimensional analysis, we must add an additional singlet $\tilde{B}$. Eq. (2.52) shows the $\mathbf{3}$ component of the direct sum; the $\mathbf{1}$ component is equal to and mixed with eq. (2.29). Hence, we can account for the extra component by a redefinition of the coefficient of $\mathcal{O}_3^W$. Hence, we can admit a new operator for a model which contains both a triplet and a singlet:

$$\mathcal{O}_1^{BW} = ((H^\dagger)^i T^a_{ij} (H)^j) \tilde{W}^a \tilde{B}\,; \tag{2.52}$$

Such a term provides a mixing between the neutral component of the triplet and the singlet via the spontaneous symmetry braking of the Higgs boson. Further, there are no additional terms in the mixed models that correspond to interactions between some combination of fermions and gauge bosons.

2.4 Mass splittings from spontaneous symmetry breaking

To examine the properties of these operators developed in section 2.3, we must first collate the dimension-5 terms into the effective Lagrangian. Each of these terms will possess a coupling constant, which is bound to be less than order one to ensure a perturbative solution, as for the familiar coupling constants from the Standard Model. Further, each operator is subject to some UV cut-off scale Λ (with units of dimension 1). For the effective field theory to be valid, all relevant mass scales in the operator should be less than the cut-off scale. The choice of the cut-off scale is arbitrary. In order to ensure that the relevant physics is independent of the choice of cut-off scale, any change to the cut-off scale is compensated by an equivalent change in the coupling constant, so long as the requirement that it be less than order one is still observed.

For the singlet model, the Lagrangian is compiled as:

$$\mathcal{L} \supset \sum_{i=1}^{8} \frac{b_i}{\Lambda} \mathcal{O}_i^B + \text{h.c.}\,, \tag{2.53}$$

for coupling parameter b_i. For the doublet model, the Lagrangian is compiled as:

$$\mathcal{L} \supset \sum_{i=1}^{8} \frac{c_i}{\Lambda} \mathcal{O}_i^H + \text{h.c.}\,, \tag{2.54}$$

for some coupling coefficients c_i. Similarly for the triplet model, we construct the Lagrangian as:

$$\mathcal{L} \supset \sum_{i=1}^{3} \frac{d_i}{\Lambda} \mathcal{O}_i^W + \text{h.c.}\,, \tag{2.55}$$

for coupling parameters d_i. Finally, for the mixed models, we construct the Lagrangian as:

$$\mathcal{L} \supset \sum_{i=1}^{1} \frac{e_i}{\Lambda} \mathcal{O}_i^{WB} + \text{h.c.}\,. \tag{2.56}$$

In principle, the parameters c_i, d_i and e_i can be complex. However, in this work, we consider them to be real. In most circumstances in this work, we are not considering circumstances where we are combining multiple operators, so the complex phase of the operator is not relevant. However, we do allow for the case where the operator is negative.

One of the key consequences of the dimension 5 operators is that they provide a coupling between the fermions and the Higgs boson, which will undergo spontaneous symmetry breaking and create new

mass terms in the Lagrangian via the Higgs mechanism [405]. The relevant terms for the higgsino-like models are eqs. (2.33)-(2.34), the relevant term for the wino-like models is eq. (2.49) and the relevant term for mixed models is eq. (2.52). In particular, we have new operators which provide mixing between the neutral wino and bino as is the case of $\mathcal{O}_1^{WB}$, or new diagonal terms in the mixing matrix for the higgsinos in $\mathcal{O}_1^H$ and $\mathcal{O}_2^H$, which means that the eigenvalues of the mass matrix are no longer equal. The latter creates a mass splitting between the two neutral states. Some terms will only add to the neutral components on the diagonal such as $\mathcal{O}_3^H$ and others will add only to the charged states such as $\mathcal{O}_4^H$. To determine the magnitude of the new mass terms, we consider the vacuum state of the Higgs boson to be determined by eqs. (2.26)-(2.27). For the higgsino models in eqs. (2.33)-(2.34), we construct a mixing matrix building from $\mathcal{M}_{ij}^{(1)}$ in eq. (2.9) for the neutral mass terms as:

$$\mathcal{L} \supset \widetilde{H}_i^0 \mathcal{M}_{ij}^{(1)} \widetilde{H}_j^0 = -\frac{1}{2} \begin{pmatrix} \widetilde{H}_u & \widetilde{H}_d \end{pmatrix} \begin{pmatrix} \frac{v^2 c_1}{\Lambda} & -\mu + \frac{v^2 c_3}{2\Lambda} \\ -\mu + \frac{v^2 c_3}{2\Lambda} & \frac{v^2 c_2}{\Lambda} \end{pmatrix} \begin{pmatrix} \widetilde{H}_u \\ \widetilde{H}_d \end{pmatrix} . \tag{2.57}$$

To determine the physical masses of the two neutral particles, we must diagonalise the matrix $\mathcal{M}_{ij}^{(1)}$ to obtain the eigenvalues in the mass basis. We follow the Takagi diagonalisation method for complex matrices [413]. Here, any complex symmetric matrix of the form:

$$\mathcal{M} = \begin{pmatrix} a & c \\ c & b \end{pmatrix} , \tag{2.58}$$

can be diagonalised by an $n \times n$ unitary matrix U such that:

$$U^T \mathcal{M} U = \text{diag}\left(m_1, m_2, ..., m_n\right) , \tag{2.59}$$

for real, non-negative m_i, which are the so-called singular values of M, not the eigenvalues; defined as the non-negative roots of the eigenvalues of $\mathcal{M}^\dagger \mathcal{M}$. For the 2×2 case, the matrix U can be parametrised by:

$$U = VP = \begin{pmatrix} \cos\theta & e^{i\phi}\sin\theta \\ -e^{i\phi}\sin\theta & \cos\theta \end{pmatrix} \begin{pmatrix} e^{-i\alpha} & 0 \\ 0 & e^{-i\beta} \end{pmatrix} , \tag{2.60}$$

where $0 \leq \theta \leq \frac{\pi}{4}$ and $0 \leq \alpha, \beta, \phi < \pi$. Eq. (2.59) is then evaluated as:

$$\begin{pmatrix} a & c \\ c & b \end{pmatrix} V = V^* \begin{pmatrix} \sigma_1 & 0 \\ 0 & \sigma_2 \end{pmatrix} . \tag{2.61}$$

where $\sigma_1 = m_1 e^{2i\alpha}$ and $\sigma_2 = m_2 e^{2i\beta}$. Expanding gives:

$$\sigma_1 = a - ce^{-i\phi}\tan\theta = be^{-2i\phi} - \frac{ce^{-i\phi}}{\tan\theta} , \tag{2.62}$$

$$\sigma_2 = b + ce^{i\phi}\tan\theta = ae^{2i\phi} + \frac{ce^{i\phi}}{\tan\theta} , \tag{2.63}$$

where

$$e^{i\phi} = \frac{bc^* + a^*c}{|bc^* + a^*c|} , \tag{2.64}$$

and

$$\tan(2\theta) = \frac{2\,|bc^* + a^*c|}{|b|^2 - |a|^2} . \tag{2.65}$$

We then obtain expressions for the singular values of: $\mathcal{M}$

$$m_i^2 = |\sigma_i|^2 = \frac{1}{2}\left[|a|^2 + |b|^2 + 2|c|^2 \mp \sqrt{\left(|b|^2 - |a|^2\right)^2 + 4\,|bc^* + a^*c|^2}\right] . \tag{2.66}$$

Expanding for the mass matrix in eq. (2.57), we obtain equations for the masses in the higgsino model:

$$m_{1,2}^2 = \frac{1}{2}\left(2|\bar{\mu}|^2 + \frac{v^4(|c_1|^2+|c_2|^2)}{\Lambda^2} \pm \sqrt{\frac{v^8(|c_1|^2-|c_2|^2)^2}{\Lambda^4} + 4\frac{v^4|c_2\bar{\mu}^* + c_1^*\bar{\mu}|^2}{\Lambda^2}}\right). \tag{2.67}$$

Here, we consider the limit whereby the parameters are real, though more generally, we can consider complex phases to be equal. The neutral particle masses are then given by:

$$m_1 = \left|\widetilde{\mu} - \frac{c_1+c_2}{2\Lambda}v^2\right| \tag{2.68}$$

and

$$m_2 = \left|\widetilde{\mu} + \frac{c_1+c_2}{2\Lambda}v^2\right|, \tag{2.69}$$

with the charged mass given by

$$m_\pm = \left|\mu + \frac{c_4}{2\Lambda}v^2\right|. \tag{2.70}$$

Here we have defined:

$$\widetilde{\mu} = \frac{1}{2}\sqrt{\frac{(c_1-c_2)^2}{\Lambda^2}v^4 + 4\bar{\mu}^2}, \tag{2.71}$$

and

$$\bar{\mu} = \mu - \frac{c_3}{2\Lambda}v^2, \tag{2.72}$$

where $v \simeq 246$ GeV is the Higgs vacuum expectation value. Note that in the limit where $c_1 \simeq c_2$ as we consider later in this work, then $\widetilde{\mu} \simeq \bar{\mu}$. Finally, note that the θ parameter in eq. (2.60) with:

$$\tan\theta \simeq 1 + \frac{c_2-c_1}{2\mu\Lambda}v^2. \tag{2.73}$$

Consider the masses for the neutral particle, that is, the dark matter candidate, in eqs. (2.68) and (2.69). There are two parameters here: $\tilde{\mu}$ and $c_1 + c_2$. The relative scales of these two parameters determines the scale of the mass of the dark matter candidate. In the main, one of the two parameters will dominate the dark matter mass, however an interesting phenomenon occurs when $\widetilde{\mu} \sim \frac{v^2}{\Lambda}$. Here, the two parameters approximately cancel each other, resulting in a dark matter mass orders of magnitude smaller than the other mass scales in the model, including the chargino, which would still have a mass of $\mathcal{O}(\mu)$. The presence of a large mass difference between the charged and neutral components has a significant effect on the relic density as coannihilations are no longer as relevant for the annihilation calculation. We will show that the region where this cancellation occurs is capable of producing a feasible thermal relic dark matter with a mass significantly lower than the canonical thermal relic dark matter mass.

Now, we move on to a similar feature of the triplet models. Here, we only have one operator that contributes as a mass term after spontaneous symmetry breaking of the Higgs boson. Eq. (2.49) provides a modification to the mass term for the triplet model in eq. (2.11), though unlike the doublet case where the masses occur on the anti-diagonal of the mixing matrix, the mass modification affects all particles in the model equally. Here, the charged and neutral components will have equal masses regardless of the

scale of the coupling. The mass component of the Lagrangian then becomes:

$$\mathcal{L} \supset \widetilde{W}^i \left(M_2 + \frac{d_1 v^2}{\Lambda} \right) \widetilde{W}^i \,. \tag{2.74}$$

Hence, we do not expect to see any splitting of the masses so do not expect any modification to the physics of the dark matter, although the underlying mathematics of the relative sizes of M_2 and d_1 is altered, the physical masses will be unchanged. Similarly for the singlet model, the mass component of the Lagrangian becomes:

$$\mathcal{L} \supset \widetilde{B} \left(M_1 + \frac{b_1 v^2}{\Lambda} \right) \widetilde{B} \,. \tag{2.75}$$

The situation is different when we move to models which combine the triplet and the singlet models. As discussed in section 2.1.4, these models represent the two gauginos from supersymmetric models, albeit at two separate scales M_1 and M_2. Although unlike the doublet case, the unmodified mixing matrix possess parameters on the main diagonal, rather than the anti-diagonal. Therefore, in order to generate a model with a mass splitting between the neutral and the charged state, the new components in the mixing matrix need to be off the diagonal, i.e. they will mix the two components. Fortunately, such an operator exists in the form of eq. (2.52). In addition to the diagonal components in eq. (2.49) and eq. (2.29), which as we have seen simply shift the values of M_1 and M_2, we obtain a modification to the mixing matrix in eq. (2.12):

$$\mathcal{L} \supset \psi_i \mathcal{M}^{(2)}_{ij} \psi_j = \begin{pmatrix} \tilde{B} & \tilde{W}^0 \end{pmatrix} \begin{pmatrix} M_1 + \frac{d_3 v^2}{\Lambda} & \frac{d_1 v^2}{2\Lambda} \\ \frac{d_1 v^2}{2\Lambda} & M_2 + \frac{d_2 v^2}{\Lambda} \end{pmatrix} \begin{pmatrix} \tilde{B} \\ \tilde{W}^0 \end{pmatrix} . \tag{2.76}$$

As before in the doublet model, we seek to obtain the physical masses from the mixing matrix using Takagi diagonalisation outlined in eqs. (2.58)-(2.66). Here, we obtain the two masses for the neutral components as:

$$m_1 = \frac{1}{2} \left(M_T - \sqrt{\Delta M^2 + \frac{d_1^2 v^4}{\Lambda^2}} \right) ; \tag{2.77}$$

and

$$m_2 = \frac{1}{2} \left(M_T + \sqrt{\Delta M^2 + \frac{d_1^2 v^4}{\Lambda^2}} \right) , \tag{2.78}$$

where

$$M_T = M_1 + M_2 + \frac{(d_2 + d_3) v^2}{\Lambda} \,, \tag{2.79}$$

and

$$\Delta M = M_1 - M_2 + \frac{(d_2 - d_3) v^2}{\Lambda} \,. \tag{2.80}$$

Furthermore, the mass of the charged component is also modified:

$$m_\pm = M_2 + \frac{d_2 v^2}{\Lambda} \,. \tag{2.81}$$

Once again, the mass of the lightest neutral particle is the dark matter candidate, and there is a nexus between two mass scales in the problem. Consider the case where $M_T \sim \sqrt{\Delta M^2 + \frac{d_1^2 v^4}{\Lambda^2}}$, here the cancellation reduces the mass of the neutral component while leaving the mass of the charged component

unchanged - a mass splitting. As for the doublet case, this nexus causes an increased relic density for these lower masses due to the decreased coannihilation rates.

It is possible to combine the doublet mixing matrix from eq. (2.57) and the singlet-triplet combined mixing matrix in eq. (2.76) into a single, combined mixing matrix for all four neutral particle. Indeed, this mirrors the four neutralinos that appear in supersymmetry models. Using the form of eq. (2.28), we obtain a full mixing matrix of:

$$\begin{aligned}\mathcal{L} \supset & -\frac{1}{2}\psi_i \mathcal{M}^{(3)}_{ij}\psi_j \\ = & -\frac{1}{2}\begin{pmatrix}\widetilde{B}^0 & \widetilde{W}^0 & \widetilde{H}^0_u & \widetilde{H}^0_d\end{pmatrix}\begin{pmatrix} M_1 + \frac{d_3 v^2}{\Lambda} & \frac{d_1 v^2}{2\Lambda} & \frac{-g' v}{\sqrt{2}} & \frac{g' v}{\sqrt{2}} \\ \frac{d_1 v^2}{2\Lambda} & M_2 + \frac{d_2 v^2}{\Lambda} & \frac{gv}{\sqrt{2}} & \frac{-gv}{\sqrt{2}} \\ \frac{-g' v_d}{\sqrt{2}} & \frac{gv}{\sqrt{2}} & \frac{v^2 c_1}{\Lambda} & -\mu + \frac{v^2 c_3}{2\Lambda} \\ \frac{g' v_u}{\sqrt{2}} & \frac{-gv}{\sqrt{2}} & -\mu + \frac{v^2 c_3}{2\Lambda} & \frac{v^2 c_2}{\Lambda} \end{pmatrix}\begin{pmatrix}\widetilde{B}^0 \\ \widetilde{W}^0 \\ \widetilde{H}^0_u \\ \widetilde{H}^0_d\end{pmatrix}.\end{aligned} \tag{2.82}$$

Such a mixing matrix combines all four neutral states with terms from the dimension 3, dimension 4 and dimension 5 operators. We do not seek to diagonalise this matrix, and shall not be considering this model further. Such a model is relevant in this work only when all three natural mass scales M_1, M_2 and μ are roughly equal. Where one or more of the mass scales is an order of magnitude higher than the others, we consider that neutral component to be included in the effective field theory approximation, that is, its interactions are integrated into the remaining dimension 5 operators.

We have now introduced all dimension-5 terms of the singlet, doublet, triplet and mixed models introduced separately into the theory. These terms account quite generally for the leading effects of physics at higher scales. The new terms provide both electric and magnetic dipole-like interactions, and couplings to the Higgs provide mass terms. There is a regime for the doublet and mixed singlet-triplet models where if the effective field theory couplings is sufficiently balanced against the raw mass parameters in the theory, the masses may split, cancel or dominate, which is relevant to the coannihilation rates in the relic density calculations.

2.5 Electromagnetic dipole terms

We now turn our attention from the new dimension 5 terms which couple to the Standard Model Higgs Boson to the new dimension 5 terms which couple to the gauge bosons, which we have been referring to as electromagnetic dipole interactions. We now explore the relationship between these operators and electromagnetic dipoles. Although we do not expect any change to the mass spectrum of the model, such operators now allow for new scattering processes from Standard Model particles, specifically the exchange of a long-range photon in scattering from charged particles. We will derive an analytic expression for the scattering cross section which we will later use to calculate direct detection rates as well as the thermal conduction of dark matter in the solar interior.

2.5.1 Correspondence between operators and dipole moments

When developing our dimension 5 terms, we have introduced the field strength tensors $B_{\mu\nu}$ and $W^a_{\mu\nu}$ in eqs. (2.40) and (2.41), with the Dirac components determined by the sigma matrices $\sigma^{\mu\nu}$ in eq. (2.44). Such a composition can be represented in bra-ket notation for some Dirac or Majorana ψ as:

$$\langle\psi^\dagger|\, H_M\, |\psi\rangle = \frac{c}{\Lambda}\langle\psi|\, \sigma^{\mu\nu} F_{\mu\nu}\, |\psi\rangle\ , \tag{2.83}$$

for Hamiltonian H_M, operator coupling constant c with cut-off scale Λ and arbitrary field strength tensor $F_{\mu\nu}$. Recall that the Hamiltonian operator has an eigenvalue of energy E_M, representing the potential energy generated by a particle possessing such an operator. For the dual field strength tensors $B^*_{\mu\nu}$ and $(W^a_{\mu\nu})^*$, consider the identity:

$$\frac{i}{2}\sigma^{\sigma\rho}\epsilon_{\mu\nu\rho\sigma} = \sigma^{\mu\nu}\gamma^5 \,. \tag{2.84}$$

Here, we see that the effect of considering the dual field strength tensors, that is, multiplying the field strength tensor with the antisymmetric tensor $\epsilon_{\mu\nu\rho\sigma}$ is equivalent to considering the operator as corresponding to a Dirac pseudotensor due to the γ^5 component. The Hamiltonian H_E then becomes:

$$\langle\psi^\dagger|\, H_E \,|\psi\rangle = \frac{c}{\Lambda}\,\langle\psi|\, \sigma^{\mu\nu}F^*_{\mu\nu}\,|\psi\rangle = -2i\frac{c}{\Lambda}\,\langle\psi|\, \sigma^{\mu\nu}F_{\mu\nu}\gamma^5\,|\psi\rangle \ . \tag{2.85}$$

To see the relationship between the coupling to the field strength tensors and the electromagnetic dipole moments, consider the electromagnetic field strength tensor:

$$F_{\mu\nu} = \partial_\mu A^\gamma_\nu - \partial_\nu A^\gamma_\mu \,, \tag{2.86}$$

where A^γ_μ is defined in eq. (2.19) as a linear combination of the B_μ and A^a_μ fields after electroweak symmetry breaking, that is, $F_{\mu\nu}$ is a linear combination of $B_{\mu\nu}$ and $W^a_{\mu\nu}$ which represents the massless Standard Model photon. Classically, A^γ_μ is the electromagnetic four-potential:

$$A^\gamma_\mu = \left(V, \vec{A}\right) \,, \tag{2.87}$$

for electric potential V and magnetic potential $\vec{A}$, with the field strength tensor:

$$F_{\mu\nu} = \begin{pmatrix} 0 & E_x & E_y & E_z \\ -E_x & 0 & -B_z & B_y \\ -E_y & B_z & 0 & -B_x \\ -E_z & -B_y & B_x & 0 \end{pmatrix} \,, \tag{2.88}$$

where $\vec{B} = \vec{\nabla}\times\vec{A}$ and $\vec{E} = -\vec{\nabla}V - \frac{\partial\vec{A}}{\partial t}$ are defined from Maxwell's equations. The field strength tensor may also be written as:

$$\begin{aligned} F_{0i} = -F_{i0} &= E_i \,, \\ F_{ij} &= -\epsilon_{ijk}B^k \,, \end{aligned} \tag{2.89}$$

where Latin indices indicate the 3 spatial dimensions, ϵ_{ijk} is the Levi-Civita symbol, and $F_{00} = 0$. Now consider the factor of $\sigma^{\mu\nu}$ in the chiral basis. Here, the γ-matrices are defined in terms of its 2×2 spinor components as:

$$\gamma^0 = \begin{pmatrix} 0 & \mathbb{I} \\ \mathbb{I} & 0 \end{pmatrix} \,, \quad \gamma^i = \begin{pmatrix} 0 & \sigma^i \\ -\sigma^i & 0 \end{pmatrix} \,, \quad \gamma^5 = \begin{pmatrix} -\mathbb{I} & 0 \\ 0 & \mathbb{I} \end{pmatrix} \,, \tag{2.90}$$

where $\mathbb{I}$ is the 2×2 identity matrix and σ^i are the Pauli spin matrices. We therefore construct $\sigma^{\mu\nu}$ using eq. (2.44) giving:

$$\sigma^{00} = 0 \tag{2.91}$$

$$\sigma^{0i} = -\sigma^{i0} = i\begin{pmatrix} -\sigma^i & 0 \\ 0 & \sigma^i \end{pmatrix} \tag{2.92}$$

$$\sigma^{ij} = \begin{pmatrix} \epsilon_{ijk}\sigma_k & 0 \\ 0 & \epsilon_{ijk}\sigma_k \end{pmatrix} \,, \tag{2.93}$$

where we have used the Pauli matrix identity:

$$\sigma_i\sigma_j = \delta_{ij}\mathbb{I} + i\epsilon_{ijk}\sigma_k\,. \tag{2.94}$$

Finally, we can construct the Lorentz invariant $\sigma^{\mu\nu}F_{\mu\nu}$ as:

$$\sigma^{\mu\nu}F_{\mu\nu} = \sigma^{00}F_{00} + \sigma^{0i}F_{0i} + \sigma^{i0}F_{i0} + \sigma^{ij}F_{ij}\,. \tag{2.95}$$

As the two components in eq. (2.92) have opposite signs, when we insert such a term into the bilinear for a Dirac fermion, the left handed and right handed components will have opposite signs, so assuming there is no bias in the ratio of left to right handed components, there will not be a contribution to the Hamiltonian in eq. (2.83). The result is that the only contribution to H_M arises from the $\sigma^{ij}F_{ij}$ which gives a Hamiltonian operator:

$$H_M = \frac{c}{\Lambda}\begin{pmatrix}\vec{\sigma}\cdot\vec{B} & 0\\ 0 & \vec{\sigma}\cdot\vec{B}\end{pmatrix}\,, \tag{2.96}$$

that is, the potential energy of the operator is given by:

$$E_M = \frac{c}{\Lambda}\vec{S}\cdot\vec{B}\,, \tag{2.97}$$

where $\vec{S}$ is the spin of $|\psi\rangle$. Eq. (2.97) can be readily identified as the potential energy of a magnetic dipole $U = -\vec{m}\cdot\vec{B}$ for magnetic moment $\vec{m}$ defined as:

$$\vec{m} = -\frac{c}{\Lambda}\vec{S}\,. \tag{2.98}$$

We can therefore associate the coupling constant and cut-off scale combination as representing the magnetic moment of $|\psi\rangle$, as such we will introduce the label:

$$\mu_\chi = \frac{c}{\Lambda}\,, \tag{2.99}$$

as for similar magnetic moments for familiar Standard Model particles such as the electron, proton and neutron. It is common to express the units of the magnetic moment not by the cut-off scale Λ in GeV^{-1}, but in units of the Bohr magneton $\mu_B = \frac{1}{2m_e} = \frac{e\hbar}{2m_e c}$ where m_e is the rest mass of the electron. Hence we shall be referring to the operators $\mathcal{O}_5^H$ and $\mathcal{O}_6^H$ in eqs. (2.45)-(2.46) and $\mathcal{O}_2^W$ in eq. (2.50) as the magnetic dipole operators.

For the dual field strength tensor operators, we construct the Hamiltonian H_E in a similar way. However whereas we previously considered a cancellation to the potential due to opposite signed terms in eq. (2.92), the presence of the γ^5 component means that the opposite sign now occurs in the σ^{ij} component. We therefore obtain the Hamiltonian operator as:

$$H_E = \frac{c}{\Lambda}\begin{pmatrix}\vec{\sigma}\cdot\vec{E} & 0\\ 0 & \vec{\sigma}\cdot\vec{E}\end{pmatrix}\,, \tag{2.100}$$

with the potential energy of the operator given by:

$$E_E = \frac{c}{\Lambda}\vec{S}\cdot\vec{E} \tag{2.101}$$

As before, we see that eq. (2.101) is identified as the potential energy of an electric dipole $U = -\vec{p}\cdot\vec{E}$ where the dipole moment $\vec{p}$ is defined as:

$$\vec{p} = -\frac{c}{\Lambda}\vec{S}\,. \tag{2.102}$$

Thus for the dual field strength tensor case, the coupling constant and cut-off scale represents the electric dipole moment of $|\psi\rangle$. We therefore introduce the label:

$$\mathcal{D} = \frac{c}{\Lambda}\,, \tag{2.103}$$

where the units of $\mathcal{D}$ are usually expressed as e - cm - electron centimetres.

Electric and magnetic dipole dark matter has been studied in the literature in the context of electromagnetic $U(1)$ interactions [2, 391–404]. The model received particular attention as a potential resolution for the DAMA annual modulation [184], where the strongest limits from null result direct detection experiments have been applied at mass scales of a few to a few hundred GeV. In particular, there were suggestions that inelastic magnetic dipole models could both reproduce DAMA and satisfy the relic abundance criteria [394], though less consideration has been given to these models following the increased tension between the DAMA result and other direct detection experiments.

A key feature of the electromagnetic dipole operators is their behaviour under CPT transformations. Ideally, new operators introduced to a theory should be CPT invariant, so our new operators should be even under CPT. However, recall that $\vec{\sigma}$, an angular momentum variable, is odd under time reversal but even under charge conjugation and parity. In order to be an CPT invariant operator, the remaining components in the operator must also be CPT odd. However, both the electric field $\vec{E}$ and the magnetic field $\vec{B}$ are CPT even: $\vec{B}$ is odd under both time reversal and charge conjugation and $\vec{E}$ is odd under both parity and charge conjugation. Where the operator acts on a Majorana particle, that is, a self-conjugate particle, it will not be possible to maintain a CPT consistent theory [411, 412]. As the multiplets we consider are Majorana, it would appear that all electromagnetic dipole moments are forbidden. However this is not so. For the doublet model, where the two neutral states have equal mass, the accounting trick of combining both doublets into one Dirac fermion in eq. (2.8) alleviates the restrictions. Similarly, where the dipole is inelastic, either by a split in the masses caused by the operators like $\mathcal{O}_1^H$ and $\mathcal{O}_2^H$ or through an interaction between the neutral and charged eigenstates, the restrictions are also void. There is no such resolution for the singlet case in eq. (2.2) which is therefore banned from future consideration. Finally, we note that the nature of the electric field means that the electric dipole moment operators are CP-violating.

2.5.2 Anapole moments

There is another electromagnetic term which is often considered alongside the electric and magnetic dipole models which can subvert the restrictions on Majorana particles, namely the anapole moment and arises as a result of parity violating interactions [414]. The anapole moment, a special case of the toroidal moment where the interaction is elastic [415], is a purely electrodynamic phenomenon, it does not appear in electrostatic multipole expansions. It appears classically as an induced current in a solenoidal shape, with the current $\vec{J}$ taking the role of the dipole field instead of $\vec{E}$ or $\vec{B}$. Anapole moments have been measured in caesium [416] and are hypothesised for neutrinos [417]. Anapole dark matter is often studied alongside other electromagnetic dipole dark matter and has been generally considered as a feasible model [391, 395, 400, 401, 411, 418, 419]. To construct an operator for the anapole moment, we begin with the potential energy of the operator:

$$E_A = \frac{c}{\Lambda^2}\vec{S}\cdot\vec{J}, \tag{2.104}$$

for electromagnetic current

$$J_\mu = \left(\rho, \vec{J}\right)\,. \tag{2.105}$$

By analogy with the electric and magnetic dipoles above, we construct a Hamiltonian operator as:

$$H_A = \frac{c}{\Lambda^2}\begin{pmatrix} 0 & \vec{\sigma}\cdot\vec{J} \\ \vec{\sigma}\cdot\vec{J} & 0 \end{pmatrix} . \tag{2.106}$$

The Dirac structure here is different to the electric and magnetic dipole cases as we are now coupling to a single 4-vector rather than a tensor, although the resultant eigenvalues are equivalent. From here, we note that:

$$\gamma^i\gamma^5 = \begin{pmatrix} 0 & \sigma^i \\ \sigma^i & 0 \end{pmatrix} , \tag{2.107}$$

$$\gamma^0\gamma^5 = \begin{pmatrix} 0 & \mathbb{I} \\ -\mathbb{I} & 0 \end{pmatrix} . \tag{2.108}$$

We see that the γ-matrix component for the anapole moment will then be $\gamma^\mu\gamma^5$, as the potential due to the time-like component will be cancelled as per the examples above. To transform $\vec{J}$ into a more familiar form, consider the inhomogeneous Maxwell equation:

$$\partial^\nu F_{\mu\nu} = J_\mu \, . \tag{2.109}$$

which allows us to construct a Hamiltonian for the anapole moment as:

$$\langle\psi| H_A |\psi\rangle = \frac{c}{\Lambda^2}\langle\psi|\gamma^\mu\gamma^5\partial^\nu F_{\mu\nu}|\psi\rangle \ . \tag{2.110}$$

Note here that the additional derivative ∂^ν compared to the electric and magnetic dipoles increases the operator to dimension 6, and is compensated by an additional factor of the cut-off scale Λ. Although we do not seek to develop a full catalogue of dimension 6 operators, we do consider the anapole in limited circumstances here due to its consideration in connection with the other electromagnetic dipole moments.

Chapter 3

Relic density

The criteria for a dark matter candidate to be considered a viable theoretical model is determined by a number of key observables of the Universe. Although the forefront of experimental constraints on such models arise form direct and indirect detection searches, there are a number of key fundamental questions that must first be asked about a candidate particle or model, namely, can the model explain the astrophysical and cosmological observations of dark matter? In chapter 1, we discovered that any dark matter particle should exist in the universe in halos around large gravitational objects such as galaxies and galaxy clusters. It should be non-relativistic and non-baryonic as determined by the universe expansion rate and cosmic microwave background – the so-called ΛCDM model. In chapter 2, we developed a model based on a set of particle physics constraints. A dark matter candidate particle should be stable and long-lived, at least on the time scales of the age of the Universe, and its interactions with the Standard Model limited to the weak and gravitational sectors, or at least a suppressed coupling to the electromagnetic sector. Now, we seek to expand our selection of model constraints to another key theoretical question. Any viable dark matter model needs to explain why dark matter occurs in the Universe with an abundance on a similar order of magnitude to the abundance of baryonic matter.

An appealing scenario for the production of dark matter in the Universe and its stability through to the present day occurs where the dark matter particles may exist in thermal equilibrium with the Standard Model in the early Universe [126–128]. At some point in the early Universe prior to Big Bang Nucleosynthesis, the dark matter particles thermally decoupled from the Standard Model particles, freezing their relative abundance. After decoupling, their abundance depletes via annihilation, which is counteracted by the concurrent expansion of the Universe. Eventually, the expansion is sufficiently large such that annihilation events are exceedingly rare, fixing the dark matter cosmic density, the so-called relic abundance of dark matter.

Such a concept is particularly appealing for models which maintain a weak interaction with the Standard Model for both cosmological and phenomonological reasons. In the thermal relic scenario, the freeze out is expected to occur prior to Big Bang Nucleosynthesis as the relative densities at that epoch can be calculated from the primodial deuterium abundance [110], which favours masses closer to the weak scale or above. Phenomologically, the combination of a typical weak scale interaction with a typical a weak scale correctly produces the relic abundance, the so-called WIMP miracle [364]. Freeze out mechanisms are also present in familiar Standard Model cosmological processes such as photon decoupling during recombination and neutrino decoupling, leading to the cosmic microwave background radiation and cosmic neutrino background respectively [420].

Although thermal freeze out is an appealing mechanism, there are some notable exceptions to such a process. If there are multiple non-baryonic particles with similar masses, the relic abundance is affected

by the annihilations of the slightly larger particle into the smaller one [421, 422]. Such processes will be important for our investigation as we consider in particular similar mass higgsinos, or combined neutral and charged fermion multiplets. Other exceptions include where the light dark matter annihilates into a heavier state in so-called forbidden dark matter models [422, 423], as well as a suite of non thermal production mechanisms, either by decay of particles already out of thermal equilibrium or primordial black holes [424], but we do not consider these further.

For our models of higgsino and wino-like dark matter, for the canonical renormalisable dimension 4 couplings there is only a single parameter that determines the relic abundance after thermal freeze out, namely the mass parameters μ, M_1 and M_2, depending on the model chosen. The only diagrams which contribute to annihilation of dark matter in the early universe are interactions with the gauge bosons, with operator terms arising from the covariant derivative in the Lagrangian. The diagrams include s-channel annihilation to a number of Standard Model particles via a Z boson, or t-channel annihilation to a pair of W bosons. As the coupling strength for these interactions is fixed by the Standard Model electroweak coupling parameters g and g', only the mass parameter at dimension 3 is free which directly corresponds to a predicted value of the relic density.

The annihilation cross section is indirectly proportional to the relic density of the dark matter particles, since for an increased annihilation cross section, the dark matter particles deplete more efficiently resulting in less overall dark matter after freeze out. If we assume that the dark matter consists of a single category of particle which freezes out at a single abundance, then the observed relic abundance constrains the annihilation cross section within the error on the measurement of the observed abundance. However, such assumptions can not necessarily be justified without a laboratory based measurement of dark matter particles, so the relic abundance instead becomes a bound on the cross section, absent other non-thermal processes that influence the dark matter cosmic density. Since the annihilation cross section is set directly by the dimension 4 parameters, the assumption that the relic abundance is the only thermal process for dark matter suggests a specific particle mass for each model. For higgsino-like dark matter, the constrained mass is 1 TeV. For wino-like matter, the lack of coannihilations with a second neutral state gives a constrained mass of 3 TeV. Consequently, searches for dark matter have focussed on the TeV-scale mass region. Notably, the 3 TeV wino thermal relic has been ruled out by indirect detection experiments [378, 425], while the higgsino model maintains viability as it possesses mass splittings between its two neutral states.

We seek to investigate the effect of introducing the dimension 5 operators on the relic density. In section 3.1, we will sketch the calculation of the relic density from the Boltzmann equations. We then introduce the selection of experimental constraints that we apply to our parameter spaces in section 3.2, followed by an introduction to modifications to the annihilation rate due to the Sommerfeld enhancement in section 3.3. From there, we will examine each of our operators and consider where the combinations of parameters which produce thermal relics and whether or not they are viable in section 3.4. We shall see that the electromagnetic dipole models can provide additional annihilation at high masses to provide thermal relics greater than their canonical counterparts, while the Higgs couplings produce thermal relics at low masses due to the cancellation in the mass terms.

3.1 Relic density Boltzmann equations

We now review the Boltzmann equation which describes the evolution of the dark matter density in the early Universe. We will sketch the justification for the historically conventional reasoning behind nominating weakly interacting massive particles as a candidate for dark matter. We will identify the confluence of energy scales which leads to the so-called WIMP miracle that motivates the energy scales

of direct detection of dark matter, and briefly introduce coannihilations as a key component in the relic density calculation for dark matter with degenerate or near degenerate mass states. Our derivations here closely follows the work of refs. [422, 426].

We seek to construct the differential equation describing the evolution of the local dark matter number density n with time in the early Universe. In general, if there are multiple species of dark matter, they may be described by multiple number densities n_i, though we continue here for a single species. There are several factors at play which can affect the dark matter number density. One key process is the expansion of the universe as described by the Hubble parameter $H(t)$. Such an expansion does not affect the total number of dark matter particles, but decreases the local density due to the increase in space. Additionally, there may be a net creation or destruction of dark matter particles through annihilation and creation processes with particles in the Standard Model. The strength of the interaction is parameterised by the thermalised annihilation cross section $\langle\sigma v\rangle$. The annihilation rate is dependent on the densities of dark matter in the universe and given by n^2 - the square is present since there are two particles involved in the interaction. Similarly, the creation rates are dependent on the Standard Model number densities, which is in thermal equilibrium with the dark matter, with a separate annihilation rate. In such an equilibrium, the principle of detailed balance means that the annihilation rate for the Standard Model into dark matter particles is identical to the annihilation rate for dark matter into the Standard Model subject to the equilibrium conditions. We can therefore construct the Boltzmann equation as:

$$\frac{dn}{dt} + 3H(t)n = \langle\sigma v\rangle \left(n_{\text{eq}}^2 - n^2\right) . \tag{3.1}$$

It is useful to express eq. (3.1) in terms of scale and dimension independent quantities. To do so, we define parameters $Y = \frac{n}{s}$ for s the total entropy density of the Universe. The entropy density in equilibrium is given by

$$s = \frac{2\pi^2}{45} g_* T^3 , \tag{3.2}$$

where g_* is the number of degrees of freedom in the Standard Model and T is the temperature scale of the universe. Since the entropy scales with the cube of the temperature, it also scales with the cube of the scale factor $a(t)$. The result is that the parameter $Y(t)$ is independent of the expansion scale. Similarly, it useful to describe the time scale in terms of the temperature of the Universe since the temperature is a monotonically decreasing parameter in the expansion of the Universe. The temperature can be made model independent relative to the mass scale m_χ of the dark matter by a parameter x such that $x = \frac{m_\chi}{T}$. The relationship between the time scale and x is given by $\frac{dx}{dt} = H(x)x$. The Boltzmann equation is then rewritten as:

$$\frac{dY}{dx} = -\frac{xs(x)\langle\sigma v\rangle}{H(x)} \left(Y^2 - Y_{\text{eq}}^2\right) , \tag{3.3}$$

which is often written in terms of a parameter λ:

$$\frac{dY}{dx} = -\frac{\lambda}{x^2} \left(Y^2 - Y_{\text{eq}}^2\right) \tag{3.4}$$

where

$$\lambda \equiv \frac{2\pi^2}{45} \frac{M_P}{1.66} \frac{g_{*s}}{g_*^{\frac{1}{2}}} m_\chi \langle\sigma v\rangle , \tag{3.5}$$

which follows from the definition of s in eq. (3.2) and where the Hubble parameter in a radiation dominated universe is given by

$$H = 1.66 g_*^{\frac{1}{2}} \frac{m_\chi^2}{M_P} , \tag{3.6}$$

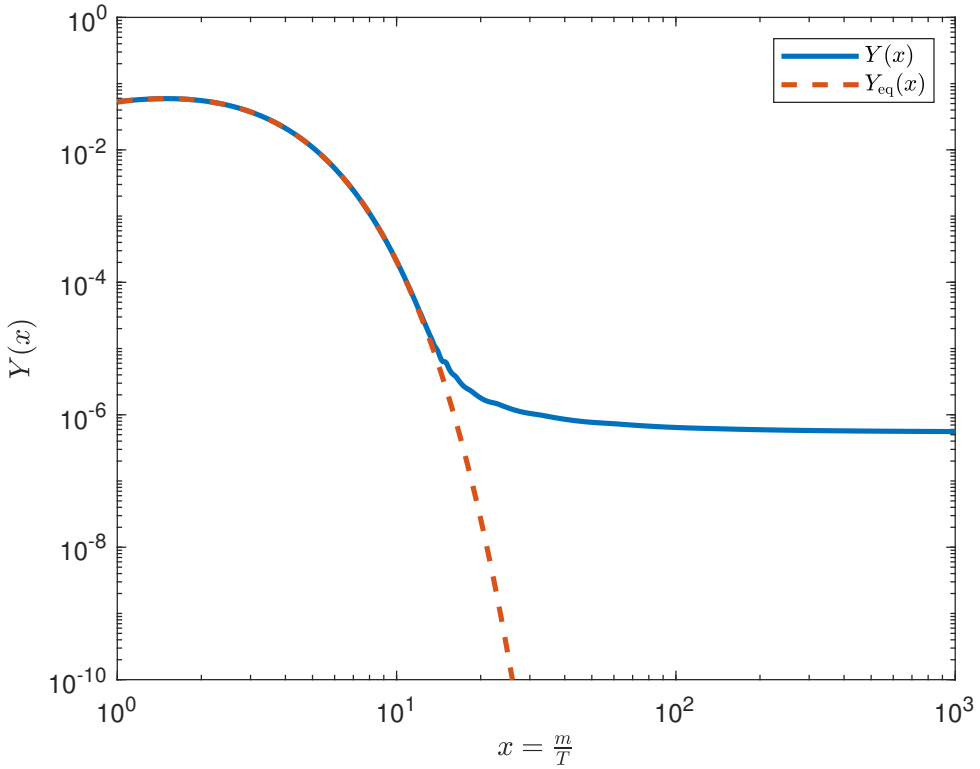

Figure 3.1: Sketch of evolution of co-moving density Y and equilibrium density $Y_{\rm eq}$ for a 100 GeV dark matter particle with interaction strength $\langle \sigma v \rangle = 10^{-30}$ cm^2 s^{-1}

and where M_P is the Planck mass, and the dependence on the dark matter mass and the factor of 1.66 have arisen from the definition of the Hubble parameter

$$H = \left(\frac{8}{3}\pi G\rho\right)^{\frac{1}{2}} \tag{3.7}$$

and energy density

$$\rho = g_* \frac{\pi^2}{30} T^4 \,. \tag{3.8}$$

There is not an analytic solution for Y in terms of x for the equation above. When implemented in full calculations, the Boltzmann equation is calculated fully numerically for Y. The equilibrium number density $Y_{\rm eq}$ can be approximated non-relativistically via [422]:

$$n_{\rm eq} \simeq g_* \left(\frac{m_\chi T}{2\pi}\right)^{\frac{3}{2}} e^{-\frac{m_\chi}{T}} \,, \tag{3.9}$$

or in terms of $Y_{\rm eq}$ as:

$$Y_{\rm eq} \simeq \frac{45}{2^{\frac{5}{2}}\pi^{\frac{7}{2}}} x^{\frac{3}{2}} e^{-x} \,. \tag{3.10}$$

An example of the equilibrium number density $Y_{\rm eq}$ and the dark matter co-moving density Y for sample mass and cross section for this model is shown in Figure 3.1. Note that as the universe evolves, the equilibrium number density decreases exponentially as it cools past the point $x = 1$, that is, $m_\chi = T$. Beyond this point, the Standard Model particles present which may annihilate to create the dark matter particles do not, on average, posses enough kinetic energy for the interaction to proceed. However, the congruent annihilation process may still go ahead, resulting in an overall depletion of dark matter in the Universe. If not for the expansion of the Universe, under the thermal model there would not be any dark matter present in the Universe today.

However, a second threshold is reached when the interaction rate $\Gamma = n\langle\sigma v\rangle$ reaches the same order of magnitude as the Hubble constant $H(x)$. Prior to this epoch, the large number density n of dark matter particles means that $\Gamma(x) \gg H(x)$, so there are always available particles for annihilation to occur and the dark matter is in thermal equilibrium $Y(x) \simeq Y_{\rm eq}(x)$. Any perturbation away from equilibrium is restored as the right hand side of eq. (3.3) is negative, that is, the equilibrium is maintained so long as the coefficient $\frac{\lambda\langle\sigma v\rangle}{x^2}$ from eq. (3.3) is sufficiently large to counteract the perturbation.

As the number density depletes for $x > 1$, the dark matter will soon reach the so-called freeze-out epoch x_f, whereby $\Gamma(x) \simeq H(x)$. After the freeze-out epoch, the coefficient $\frac{\lambda\langle\sigma v\rangle}{x^2}$ of eq. (3.3) can no longer restore the density to the equilibrium density, so the dark matter co-moving density is roughly fixed at the value at the freeze-out epoch. Physically, this corresponds to the expansion of the Universe reaching a point where dark matter particles can no longer annihilate as the mean free paths of such interactions become prohibitively large. The result is that an amount of dark matter survives to the present day, although the local density n still decreases as the entropy of the Universe increases.

Here, we shall sketch an approximate solution to the Boltzmann equation to highlight the relevant physics and provide a rough approximation for the scales of masses and interaction strengths which correspond to the observed value of the dark matter density in the Universe at the present day. In the large x limit, i.e. $\Gamma(x) \ll H(x)$, the dark matter is not in thermal equilibrium so the co-moving number density $Y(x)$ is much larger than the equilibrium density, $Y(x) \simeq Y_{\rm eq}(x_f) \gg Y_{\rm eq}(x)$, where $Y_{\rm eq}(x_f)$ is the equilibrium density at the freeze-out epoch. Under these conditions, the Boltzmann equation can then approximated as:

$$\frac{dY}{dx} \simeq -\frac{\lambda Y^2}{x^2}\,, \tag{3.11}$$

using the definition of λ in eq. (3.5). We assume, for the sake of the example here, that $\langle\sigma v\rangle$, and hence λ is independent of x, although in the general case there may be an energy dependence of the interaction, especially as we are considering a thermally averaged cross section. We may now integrate to obtain an expression for Y as:

$$\frac{1}{Y(x=\infty)} - \frac{1}{Y(x=x_f)} = \frac{\lambda}{x_f}\,, \tag{3.12}$$

where as $x \to \infty$, $T \to 0$. We also assume for simplicity that $Y(x = x_f) \gg Y(x = \infty)$ as is common in the literature [427], however such an assumption significantly weakens the approximations made. The result is a good rule-of-thumb approximation for the present day co-moving number density:

$$Y(x=\infty) \simeq \frac{x_f}{\lambda}\,. \tag{3.13}$$

Here, the number of dark matter particles in the present day (i.e. $x = \infty$) is determined by the epoch of freeze-out, cosmological parameters at $T \simeq m_\chi$ and the cross section of annihilation. The epoch of freeze-out is determined by equating $\Gamma \simeq H(x_f)$, which gives an empirical determination that $x_f \sim \mathcal{O}(10)$ as demonstrated in Figure 3.1. However, a full computation of the relic abundance should consider carefully the calculation of the freeze-out epoch, as it is highly dependent on the phenomenological parameters of the dark matter. If the interaction strength between the dark matter and Standard Model is stronger, the freeze-out epoch is delayed as more annihilations can take place in a slightly more expanded universe, resulting in a lower overall present day number density. Conversely, a weaker interaction will result in a higher present day number density. Hence, we may use the present day co-moving number density to calculate the fraction of the critical density of dark matter at the present day:

$$\Omega_\chi h^2 = \frac{m_\chi s(x=\infty) Y(x=\infty)}{\rho_c} \simeq \frac{10^{-26}\ \mathrm{cm}^3\ \mathrm{s}^{-1}}{\langle\sigma v\rangle}\,, \tag{3.14}$$

where $\rho_c = \frac{3H^2}{8\pi G}$ is the critical density of the universe. The fraction of the critical density is the commonly reported measurable property which describes the observed quantity of dark matter in the Universe, and is measured to be $\Omega h^2 = 0.1188 \pm 0.0010$ [108]. Here the effect of the annihilation cross section on the dark matter density is clear. We therefore obtain an order of magnitude approximation to the predicted scale of the annihilation interactions between dark matter and Standard Model particles to be approximately 10^{-27} cm^3 s^{-1}. By coincidence, the required rate ia approximately equal to the rate that would be expected for a particle with a mass approximately at the weak scale m_W interacting via a coupling approximately equal to the weak coupling α_W. The resultant interaction strength for such a particle is approximately $\frac{\alpha_W}{m_W}$. It is important to stress that there is no objective reason to expect such an agreement of scales; at no point in the calculation have we specified that the dark matter particle is weakly interacting. The congruence of the scales is popularly known as the WIMP miracle and has motivated the scale and scope of many dark matter searches, particularly direct detection. However, the failure of such direct detection experiments to discover dark matter has necessitated a re-evaluation of the simple thermal relic model [428].

By introducing the new operators at dimension 5 to the model, we can alter the scenario in two ways. First, we can introduce new diagrams that provide additional avenues for dark matter annihilation. Such scenarios can reduce overabundant relic densities to levels that are viable. Second, modifications to the masses of the dark matter particles may alter the annihilation cross section relative to the bare mass parameters.

Additionally, the models we consider differ from the simple calculation presented above as there are multiple annihilation products with near-degenerate masses. Such scenarios mean that there are multiple annihilation rates to consider, including the rate of annihilation from heavier Standard Model particles into both of the near-degenerate particles. The marginally heavier of the two will later decay into the lightest. The overall process is called coannihilation [422]. In such scenarios, the inelastic scattering of dark matter particles can also affect the number density of each species. Other common modifications include forbidden channel annihilation, where the dark matter has sufficient energy to annihilate into a marginally heavier Standard Model particle, and circumstances where the annihilation rate is near a pole in cross section [422]. Such modifications are not significant in the regions of interest in the parameter space of interest in our models, as they require the dark matter mass to be of a similar scale to at least the weak bosons in the Standard Model; our models are most interesting at scales tens to hundreds of times more massive.

The coannihilation rates are important as higgsino-like models have both two near-degenerate neutral particles as well as a near-degenerate charged state. Similarly, the wino-like models have a degeneracy between the charged and neutral states. The coannihilation rates become most significant where the difference between the masses is of a similar scale to the temperature of the Universe at freeze-out. Such a requirement ensures that the higher mass particle is kinematically accessible for the annihilation processes that are taking place. The Boltzmann equation is therefore expanded to become a coupled equation for a particle i with density n_i

$$\frac{dn_i}{dt} + 3H(t)n_i = -\sum_{j,X} \left[\langle \sigma_{ij} v \rangle \left(n_i n_j - n_i^{\mathrm{eq}} n_j^{\mathrm{eq}} \right) - \left(\langle \sigma'_{ij} v \rangle n_i n_X - \langle \sigma'_{ji} v \rangle n_j n'_X \right) - \Gamma_{ij} \left(n_i - n_i^{\mathrm{eq}} \right) \right] , \quad (3.15)$$

where the three terms describe the annihilation, inelastic scattering and decay with annihilation cross section $\langle \sigma_{ij} v \rangle$, scattering cross section $\langle \sigma'_{ij} v \rangle$ and decay rate Γ_{ij} against a Standard Model particle X respectively.

The quantity of interest is $n = \sum_{i=1}^{N} n_i$, the total number of dark matter particles after freeze out as any higher mass particles present at the freeze out epoch will decay to the lightest state by the present

day. Resultantly, the Boltzmann equation sums to

$$\frac{dn}{dt} = -3H(t)n - \sum_{i,j=1}^{N} \langle \sigma_{ij} v \rangle \left(n_i n_j - n_i^{\mathrm{eq}} n_j^{\mathrm{eq}} \right) . \tag{3.16}$$

The incorporation of such additional interactions can provide a significant alteration to the calculated relic abundance for a given model [422]. Indeed, for our models, the coannihilation pathways $i \neq j$ are dominant over the direct annihilation pathways $i = j$. The above differential equation is solved numerically in our simulations. Such a calculation is done via the codes outlined in section 3.4.

3.2 Experimental constraints on physical models

Before we calculate the relic abundance for each of our points in parameter space, we must consider the experimental constraints that must be applied on each of our models. There are three broad categories of constraint, namely direct detection experiments, indirect detection experiments and collider experiments, which can exclude parameter points for the models we consider. We now consider each family in turn.

The direct detection bounds on thermal relic higgsino-like and wino-like dark matter are relatively weak. The strongest such bounds on these models occur for masses well below that required to produce a thermal relic, as the nuclear recoil as measured in these experiments is most efficient when the nuclear mass is on a similar order of magnitude to the dark matter mass. However, as the typical relic abundance for these models of dark matter are at the TeV scale, bounds from recoil from GeV scale nuclei are not strong. Additionally, our models possess characteristics that differ from minimal supersymmetry models which also depress the bounds that can be inferred from direct detection. At tree level, the t-channel scattering for the higgsino-like models is suppressed since there is a cancellation in the vertex describing the interaction with the Z boson where there are neutral components of near degenerate mass. Similarly, there is reduced s-channel scattering compared to minimal supersymmetric model since there are no heavy squarks to act as intermediate states [429, 430]. The result is a scattering cross section that is smaller than the fundamental limit of the neutrino floor for direct detection experiments, well below any of the current limits of modern experiments. Meanwhile, in a model without other supersymmetry components to provide off shell states, there are no tree level diagrams which permit elastic scattering as there is no interaction to the Z boson. Therefore, direct detection bounds do not rule out significant regions of the parameter space under the usual conditions of a small mass splitting between the neutral and charged states [410, 431]. However, there is one notable exception. There are regions of the parameter space where the lightest stable dark matter candidate is the charged component of the doublet or triplet. Such scenarios are strongly excluded as dark matter due to several experimental limits on dark matter, one example of which is measurements of the abundance of superheavy isotopes of hydrogen in sea water [432].

The strongest constraints on dark matter at the thermal relic scale arise from indirect detection searches. Here, the by products of annihilation events in high concentration dark matter locations such as the galactic centre [294] or galaxy clusters [319] are the subject of searches in gamma ray astronomy with ground based and satellite based telescopes. The lack of observation of such annihilation events provides an upper bound on the annihilation cross section of the dark matter particles for any given set of parameters. We impose constraints on our models based on the satellite based Fermi-LAT observations of a selection of dwarf spheriod galaxies [319] and the ground based HESS observations of the galactic centre [266]. The Fermi-LAT observations provide stronger constraints for dark matter masses at approximately 100 GeV, while the HESS constraints provide the stronger constraints for dark matter masses at approximately 1 TeV. The indirect detection constraints rule out the canonical wino-like dark matter before the imposition of dimension 5 operators [378]. Here, the strongest bound is for annihilation into a W^+W^- channel, as such

processes are directly produced by the the electric and magnetic dipole interactions. Here, we compute the cross section for a range of annihilation processes using the `micrOMEGAs` code [433–435]. We calculate the modification to the raw annihilation rate by the Sommerfeld enhancement [436–438] as detailed in section 3.3. The strongest constraints occur at a resonance near the W boson mass due to the W^+W^- annihilation channel.

Above the thermal relic scale there is a fundamental upper bound on dark matter which has previously been in thermal equilibrium with the early Universe. The requirement that the S matrix for annihilation of dark matter in the early Universe be unitary places an upper limit on the dark matter cross section, and via the freeze-out density, the mass [439]. The upper limit on the mass is $m_\chi \sim 340$ TeV. such a limit forms the upper bound of the regions we investigate.

The final set of constraints arise from collider experiments. If the dark matter mass is less than the mass of the Z boson, decays of on shell Z bosons to the dark matter particle are possible if there is a coupling between the dark matter particle and the Z boson, then decays to dark matter are possible and will contribute some component of the decay width of the Z boson. As such decays are not detectable by the collider, they form part of the so-called invisible width of the Z boson. The limits on the invisible width are provided by decays measured by LEP [366, 440–444], and limit the mass of the charged component of the fermion to no less than 37 GeV [443], as smaller mass particles are more probable decay products. No such constraint is placed on the neutral component of the higgsino-like fermion as there is no direct coupling to the Z boson.

We have now covered all aspects of the constraints on dark matter, including direct and direct detection and collider constraints, all of which apply in some capacity to our models. In order to implement them correctly, we must first consider modifications to the annihilation cross section for indirect detection due to the Sommerfeld enhancement.

3.3 Sommerfeld enhancement

The calculation of the annihilation cross section for indirect detection and to a lesser extent the relic abundance is subject to the so-called Sommerfeld enhancement [445]. Here, the non-perturbative contributions from a light force carrier become significant in the calculation of indirect dark matter searches [446–449].

The Sommerfeld enhancement occurs in annihilation processes where there is exchange of a force carriers prior to the annihilation interaction in a so-called ladder diagram, an example of which is shown in figure 3.2. Equivalently, in non-relativistic quantum mechanics, the Sommerfeld enhancement can be seen as a potential $\mathcal{V}(r)$ in the Schrödinger equation which can attract or repel an incoming particle. Consequently, the resultant wavefunction undergoes a modification compared to the unperturbed case, which is described as a factor known as the Sommerfeld factor $S = \frac{|\psi(\infty)|^2}{|\psi(0)|^2}$, that is, an enhancement of the wavefunction at the bare scattering case by a modification to the wavefunction as it propagates from infinity to the centre of the potential.

In general, the Sommerfeld enhancement arises when the Compton wavelength of the force carrier is longer than $(\alpha m_\chi)^{-1}$ which allows the dark matter to form a bound state [449]. Where the force carrier is a W or Z boson, as in our theories, the mass scale for the Sommerfeld enhancement to be relevant is on the order of a few TeV [446, 447], the same scale of the masses which generate the correct relic density. The calculation of the Sommerfeld enhancement therefore becomes an important factor in computing the indirect detection limits where annihilation occurs. However, where the particles are relativistic or near-relativistic, the effects of the enhancement are reduced as it is not possible to form a bound state. We therefore would not expect to see a significant modification to the relic density calculations, as such annihilation happens at higher temperatures in the early universe.

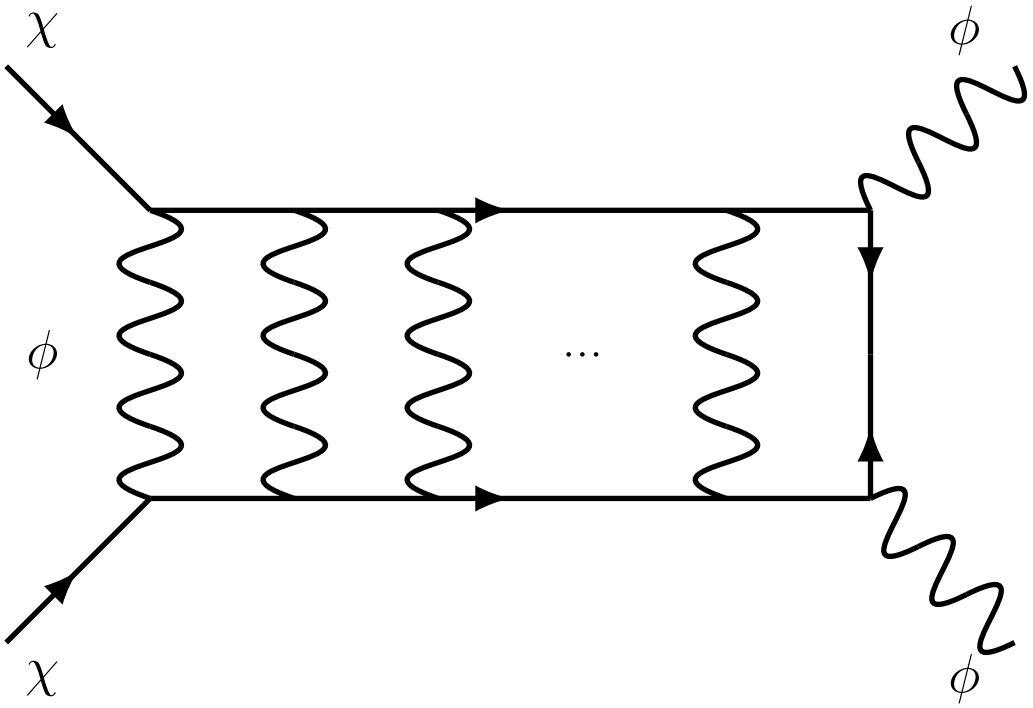

Figure 3.2: Ladder diagram for Sommerfeld enhancement of dark matter annihilation

The attractive force carrier leads to modification to the thermally averaged cross section by the Sommerfeld factor S:

$$\langle \sigma_{\rm an} v_{\rm rel} \rangle = \langle \sigma_{\rm an} v_{\rm rel} \rangle_0 S(v_{\rm rel}) \,, \tag{3.17}$$

for perturbative cross section $\langle \sigma_{\rm an} v_{\rm rel} \rangle_0$ and relative velocity $v_{\rm rel}$. For a massless force carrier ϕ with fine structure constant α, the Sommerfeld factor is given by:

$$S = \frac{\frac{\pi\alpha}{v_{\rm rel}}}{1 - e^{-\frac{\pi\alpha}{v_{\rm rel}}}} \,. \tag{3.18}$$

However, in our models of wino-like and higgsino-like dark matter, the force carrier is the massive W boson through the dimension-4 coupling in eqs. (2.15) and (2.20). The model will then produce resonant effects as bound states can form with the weak bosons at the TeV scale and above, making them key for determining the viability of the dark matter model [437, 450]. In general, multiple such resonances occur at integer multiples of the Compton wavelength of the W boson. The full calculation of the Sommerfeld enhancement for annihilation where the intermediate particle is an excited state follows from the potential due to the weak boson and is outlined below following the procedure in ref. [436]. The Sommerfeld factor for our two-state (lightest neutralino and lightest chargino) system is calculated from the radial component of the spherically symmetric Schrödinger equation [436] for scattering in the presence of the Yukawa potential $\mathcal{V}(r)$ generated by the interacting W bosons as:

$$\frac{d}{dr}\left(r^2 \frac{d\vec{R}_l(r)}{dr}\right) - m_\chi r^2 \left(\mathcal{V}(r) - m_\chi v_{\rm rel}^2\right) \vec{R}_l(r) = l(l+1)\vec{R}_l(r) \,, \tag{3.19}$$

for dark matter mass m_χ, partial wave l, and where the attractive potential is given for a two-state wavefunction as [449]:

$$\mathcal{V}(r) = \begin{pmatrix} 0 & V(r) \\ V(r) & 2\delta \end{pmatrix} \,, \tag{3.20}$$

where $V(r)$ is the Yukawa potential

$$V(r) = -\alpha \frac{e^{-m_\phi r}}{r} = -\frac{e^{-r\epsilon_\phi}}{r}\,. \tag{3.21}$$

From here, it is possible to transform the wavefunction under a change of variables $R_l(r) = \frac{\psi(r)}{r}$ since the lowest-l partial wave dominates for the short range interactions. Further, we transform to the dimensionless parameters $\epsilon_v = \frac{v}{\alpha}$, $\epsilon_\delta = \sqrt{\frac{2\delta}{m_\chi}}$ and $\epsilon_\phi = \frac{m_\phi}{m_\chi \alpha}$ where δ is the mass difference between the lightest chargino and lightest neutralino and α is the structure constant for the force carrier ϕ with mass m_ϕ. We thus obtain the vectorised Schrödinger equation

$$\psi''(r) = \begin{pmatrix} \frac{l(l+1)}{r^2} - \epsilon_v^2 & V(r) \\ V(r) & \frac{l(l+1)}{r^2} + \epsilon_\delta^2 - \epsilon_v^2 \end{pmatrix} \psi(r) \equiv M\psi(r)\,. \tag{3.22}$$

To solve for the Sommerfeld factor, we must solve for the wavefunction at the limits of 0 and ∞. To perform the calculation, we first compute the eigenvalues of M to obtain expressions for the wavefunction. The eigenvalues of M follow as:

$$\lambda_\pm = -\epsilon_v^2 + \frac{l(l+1)}{r^2} + \frac{\epsilon_\delta^2}{2} \pm \sqrt{\frac{\epsilon_\delta^4}{4} + V(r)^2}\,. \tag{3.23}$$

with eigenvectors

$$\psi_\pm = \frac{1}{\sqrt{2}} \begin{pmatrix} \mp\sqrt{1 \mp \left(1 + \frac{4V(r)^2}{\epsilon_\delta^4}\right)^{-\frac{1}{2}}} \\ \sqrt{1 \pm \left(1 + \frac{4V(r)^2}{\epsilon_\delta^4}\right)^{-\frac{1}{2}}} \end{pmatrix}\,. \tag{3.24}$$

The key factor in these expressions is the Yukawa potential $V(r)$, which is not straightforward to compute analytically. Instead, to find a solution for the Schrödinger equation, the Yukawa potential is split into a small-r and a large-r approximations, following ref. [436]. In the small-r region, the exponent term in the Yukawa potential approaches zero, so the potential is well approximated by a massless Coulomb potential $V_C(r) \simeq \frac{1}{r}$. In this region, the mass of the W boson is small compared to the distance between the two particles, and essentially behaves as a massless boson. The particles here have formed their bound state. For the large-r region, we approximate the Yukawa potential with an exactly-solvable exponential potential $V_E(r) \simeq V_0 e^{-\mu r}$ for some selection of parameters μ and r. Such an approximation reflects the fact that bosons are indeed massive and cannot interact strongly at long distances. Compared to a massless boson, there is not an attractive force that can draw the two particles together. The transition between these regimes is shown in figure 3.3. Between the two regimes, the wavefunction is approximated using the WKB approximation [451–453], up to a matching radius r_M chosen such that $V(r_M) = \max(\epsilon_\delta^2/2, \epsilon_\phi^2)$. The matching condition allows the parameters of the exponential potential to be determined, namely, the exponent is given by:

$$\frac{1}{\epsilon_\phi} = \frac{1}{\mu}\left(r_M + \frac{1}{\mu}\right)\,. \tag{3.25}$$

The Schrödinger equation in the large-r scenario is given by substituting $V \to V_E$ in eq. (3.22). We therefore obtain a new set of eigenvalues $\lambda_\pm^E$:

$$\lambda_\pm^E = -\epsilon_v^2 + \frac{\epsilon_\delta^2}{2} \pm \sqrt{\frac{\epsilon_\delta^2}{4} + V_E(r)^2}\,. \tag{3.26}$$

Although the details of the derivation are beyond the scope of this work, the exact solution to the Schrödinger equation can now be calculated for each of the potentials as they now have analytic solutions. Such calculations have been completed in ref. [436], which contains further details of such a derivation.

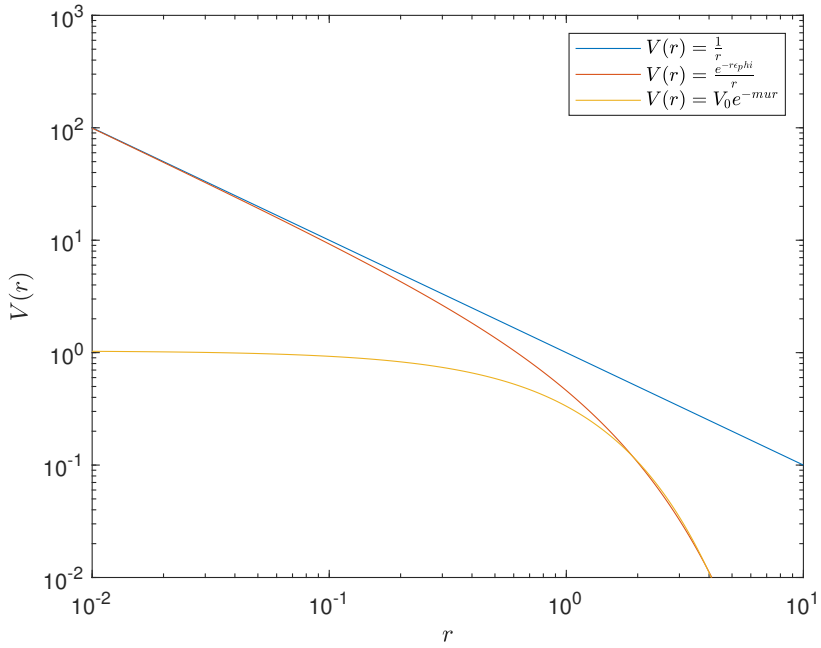

Figure 3.3: Transition between potential (blue) and exponential (orange) regimes for a Yukawa potential (red) for a dark matter particle of mass 3 TeV with a W-boson force carrier.

For a wavefunction is given by $\psi(r) = \begin{pmatrix} \psi_1(r) \\ \psi_2(r) \end{pmatrix}$, the exact solution is:

$$\begin{aligned}\psi_1(r) = \eta e^{ir\epsilon_v}{}_0F_3\left[\{\}, \left\{1 - \frac{i\epsilon_v}{\mu}, \frac{1}{2} - \frac{i\epsilon_v}{2\mu} - \frac{i\sqrt{\epsilon_v^2 - \epsilon_\delta^2}}{2\mu}, \frac{1}{2} - \frac{i\epsilon_v}{2\mu} + \frac{i\sqrt{\epsilon_v^2 - \epsilon_\delta^2}}{2\mu}\right\}, z\right] \\ - \frac{\sqrt{z}\zeta e^{ir\sqrt{\epsilon_v^2 - \epsilon_\delta^2}}{}_0F_3\left[\{\}, \left\{\frac{3}{2} - \frac{i\epsilon_v}{2\mu} - \frac{i\sqrt{\epsilon_v^2 - \epsilon_\delta^2}}{2\mu}, \frac{3}{2} - \frac{i\epsilon_v}{2\mu} + \frac{i\sqrt{i\sqrt{\epsilon_v^2 - \epsilon_\delta^2}}}{2\mu}, 1 - \frac{i\epsilon_v}{\mu}\right\}, z\right]}{\frac{\epsilon_v^2}{4\mu^2} + \left(\frac{1}{2} - i\frac{\sqrt{\epsilon_v^2 - \epsilon_\delta^2}}{2\mu}\right)^2}\end{aligned} \tag{3.27}$$

and:

$$\begin{aligned}\psi_2(r) = - \frac{\sqrt{z}\eta e^{ir\epsilon_v}{}_0F_3\left[\{\}, \left\{\frac{3}{2} - \frac{i\epsilon_v}{2\mu} - \frac{i\sqrt{\epsilon_v^2 - \epsilon_\delta^2}}{2\mu}, \frac{3}{2} - \frac{i\epsilon_v}{2\mu} + \frac{i\sqrt{i\sqrt{\epsilon_v^2 - \epsilon_\delta^2}}}{2\mu}, 1 - \frac{i\epsilon_v}{\mu}\right\}, z\right]}{\left(\frac{1}{2} - \frac{i\epsilon_v}{2\mu}\right)^2 + \frac{(\epsilon_v^2 - \epsilon_\delta^2)}{4\mu^2}} \\ + \zeta e^{ir\sqrt{\epsilon_v^2 - \epsilon_\delta^2}}{}_0F_3\left[\{\}, \left\{1 - \frac{i\epsilon_v}{\mu}, \frac{1}{2} - \frac{i\epsilon_v}{2\mu} - \frac{i\sqrt{\epsilon_v^2 - \epsilon_\delta^2}}{2\mu}, \frac{1}{2} - \frac{i\epsilon_v}{2\mu} + \frac{i\sqrt{\epsilon_v^2 - \epsilon_\delta^2}}{2\mu}\right\}, z\right]\end{aligned} ; \tag{3.28}$$

where

$$z = V_0^2 \frac{e^{-\mu r}}{16\mu^4}, \tag{3.29}$$

and ${}_pF_q$ are the generalised hypergeometric functions defined as the power series for a function z as:

$${}_pF_q(a_1, \ldots, a_p; b_q, \ldots, a_q; z) = \sum_{n=0}^{\infty} \frac{(a_1)_n \ldots (a_p)_n}{(b_1)_n \ldots (b_q)_n} \frac{z^n}{n!}, \tag{3.30}$$

where the rising factorial $(a)_n$ is defined as

$$(a)_n = \begin{cases} 1, & n = 0; \\ a(a+1)(a+2)\ldots(a+n-1), & n \geq 1. \end{cases} \tag{3.31}$$

The empty brackets in eq. (3.27)-(3.28) indicate that there are no coefficients of $(a_i)_n$ to be applied in eq. (3.30). The boundary conditions of the wavefunctions are defined by the parameters η and η as the coefficients of each of the terms of the two wavefunctions. Since the calculation of the Sommerfeld factor S is defined as the wavefunction on the boundary, both of these factors need to be computer. Ref. [436] performs the calculation by evaluating the generalised hypergeometric functions in terms of the Gamma functions $\Gamma[z] = \int_0^\infty x^{z-1}e^{-x}dx$. The parameters η and ζ are defined thus by the boundary conditions to be:

$$\eta = \frac{-2\sqrt{2}\pi^2 e^{\frac{\epsilon_v \pi}{\mu}}\left(ie^{\frac{i\epsilon_\Delta \pi}{\mu}+i\theta_-}\phi_-(0) - e^{\theta_+}\phi_+(0) + e^{\frac{2i\epsilon_\Delta \pi}{\mu}+2i\theta_- +\theta_+}\phi_+(0)\right)}{\sqrt{\mu}\left(e^{\frac{\epsilon_v \pi}{\mu}}+e^{\frac{i\epsilon_\Delta \pi}{\mu}}\right)\left(e^{\epsilon_v \pi+i\epsilon_\Delta \pi+2\mu i\theta_-}\mu - 1\right)\Gamma\left[1-\frac{i\epsilon_v}{\mu}\right]\Gamma\left[\frac{1}{2}+\frac{\epsilon_\Delta}{2\mu}-\frac{i\epsilon_v}{2\mu}\right]\Gamma\left[\frac{1}{2}-\frac{\epsilon_\Delta}{2\mu}-\frac{i\epsilon_v}{2\mu}\right]}\,; \tag{3.32}$$

and

$$\zeta \simeq 0\,, \tag{3.33}$$

for $\epsilon_v < \epsilon_\delta$, and

$$\eta = \frac{-2\sqrt{2}\pi^2 e^{\frac{\epsilon_v \pi}{\mu}}\left(i\phi_-(0)e^{\frac{\epsilon_\Delta \pi}{\mu}+i\theta_-} + \frac{4\phi_+(0)e^{\theta_+}\left(e^{2\left(\frac{\epsilon_\Delta \pi}{\mu}+2i\theta_-\right)}-1\right)}{2-e^{2(\theta_T-\theta_Y)}+2e^{2(\theta^*+\theta_T-\theta_Y)}+e^{-2\theta^*}}\right)}{\sqrt{\mu}\,\Gamma\left[1-\frac{i\epsilon_v}{\mu}\right]\Gamma\left[\frac{1}{2}-i\frac{\epsilon_v+\epsilon_\Delta}{2\mu}\right]\Gamma\left[\frac{1}{2}-i\frac{\epsilon_v-\epsilon_\Delta}{2\mu}\right]\left(e^{\frac{\epsilon_v \pi}{\mu}}+e^{\frac{\epsilon_\Delta \pi}{\mu}}\right)\left(e^{\frac{\epsilon_v \pi+\epsilon_\Delta \pi+2\mu i\theta_-}{\mu}}-1\right)}\,; \tag{3.34}$$

and

$$\zeta = \frac{-2\sqrt{2}\pi^2 e^{\frac{\epsilon_\Delta \pi}{\mu}}\left(i\phi_-(0)e^{\frac{\epsilon_v \pi}{\mu}+i\theta_-} - \frac{4\phi_+(0)e^{\theta_+}\left(e^{2\left(\frac{\epsilon_v \pi}{\mu}+2i\theta_-\right)}-1\right)}{2-e^{2(\theta_T-\theta_Y)}+2e^{2(\theta^*+\theta_T-\theta_Y)}+e^{-2\theta^*}}\right)}{\sqrt{\mu}\,\Gamma\left[1-\frac{i\epsilon_\Delta}{\mu}\right]\Gamma\left[\frac{1}{2}-i\frac{\epsilon_v+\epsilon_\Delta}{2\mu}\right]\Gamma\left[\frac{1}{2}-i\frac{\epsilon_\Delta-\epsilon_v}{2\mu}\right]\left(e^{\frac{\epsilon_v \pi}{\mu}}+e^{\frac{\epsilon_\Delta \pi}{\mu}}\right)\left(e^{\frac{\epsilon_v \pi+\epsilon_\Delta \pi+2\mu i\theta_-}{\mu}}-1\right)}\,, \tag{3.35}$$

for initial conditions $\phi_+(0)$ and $\phi_-(0)$ with the dimensionless parameter ϵ_Δ defined by:

$$\epsilon_\Delta = \sqrt{|\epsilon_\delta^2 - \epsilon_v^2|}\,, \tag{3.36}$$

and with phases defined as:

$$i\theta_- = \int_{r_S}^{r_M}\sqrt{\lambda_-^E}dr - 4iz_S^{\frac{1}{4}} - \int_0^{r_M}\sqrt{\lambda_-}dr\,; \tag{3.37}$$

$$\theta_+ = \int_{r_S}^{r_M}\sqrt{\lambda_+^E}dr - 4z_S^{\frac{1}{4}} - \int_0^{r_M}\sqrt{\lambda_+}dr\,; \tag{3.38}$$

$$\theta_T = \int_{r^\dagger}^{r_M}\sqrt{\lambda_+^E}dr\,; \tag{3.39}$$

$$\theta^* = \int_0^{r^*}\sqrt{\lambda_+}dr\,; \tag{3.40}$$

and

$$\theta_Y = \int_0^{r_M}\sqrt{\lambda_+}dr\,, \tag{3.41}$$

with r_S and $z_S = z(r_S)$ as psuedo-parameters defined as:

$$V_0 e^{-\mu r_S} \gg \left\{\epsilon_v^2, \epsilon_\delta^2\right\}\,, \tag{3.42}$$

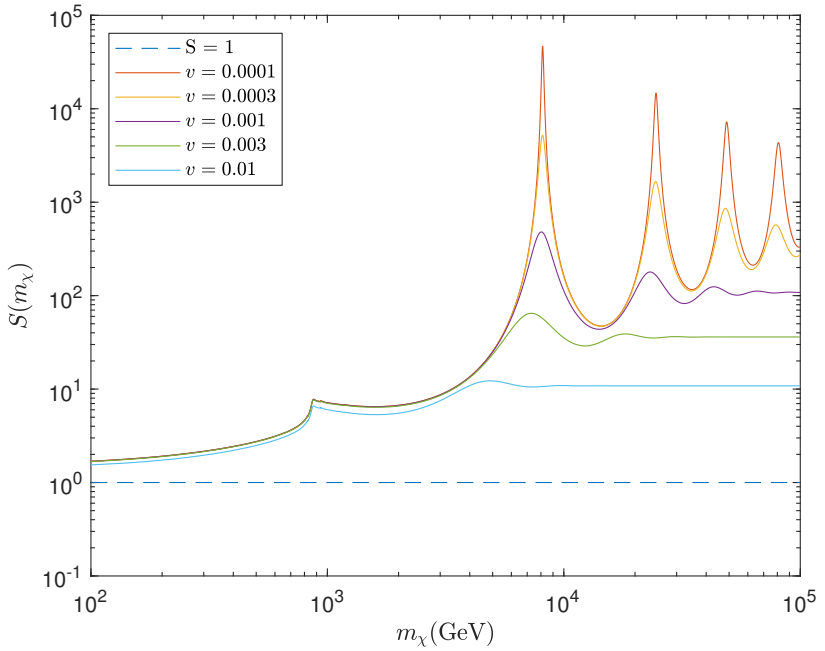

Figure 3.4: S-factor dependence on dark matter mass for range of velocities $\frac{v}{c} = \{0.0001, 0.0003, 0.001, 0.003, 0.01\}$ in natural units and $\delta = 0$. The case for no enhancement ($S = 1$) is shown as a horizontal dashed line.

and $r^\dagger$ defined such that

$$V_E(r^\dagger) = \epsilon_v \sqrt{\epsilon_v^2 - \epsilon_\delta^2}\,. \tag{3.43}$$

The Sommerfeld enhancement for s-wave annihilation for a particle in the ground state, in our case, the neutral state, is given by:

$$S = |\psi(\infty)|^2\,, \tag{3.44}$$

with initial conditions $\psi(0) = \begin{pmatrix} 1 \\ 1 \end{pmatrix}$, i.e. $\phi(0) = \begin{pmatrix} 0 \\ \sqrt{2} \end{pmatrix}$. Simplifying eq. (3.27), the Sommerfeld factor becomes [436]

$$S = \frac{2\pi}{\epsilon_v} \sinh\left(\frac{\epsilon_v \pi}{\mu}\right) \begin{cases} \frac{1}{\cosh\left(\frac{\epsilon_v \pi}{\mu}\right) - \cos\left(\sqrt{\epsilon_\delta^2 - \epsilon_v^2}\,\frac{\pi}{\mu} + 2\theta_-\right)} & \epsilon_v < \epsilon_\delta\,; \\ \frac{\cosh\left(\left(\epsilon_v + \sqrt{\epsilon_v^2 - \epsilon_\delta^2}\right)\frac{\pi}{2\mu}\right)\operatorname{sech}\left(\left(\epsilon_v - \sqrt{\epsilon_v^2 + \epsilon_\delta^2}\right)\frac{\pi}{2\mu}\right)}{\cosh\left(\left(\epsilon_v + \sqrt{\epsilon_v^2 - \epsilon_\delta^2}\right)\frac{\pi}{\mu}\right) - \cos(2\theta_-)} & \epsilon_v > \epsilon_\delta\,. \end{cases} \tag{3.45}$$

We have now sketched the derivation for the Sommerfeld enhancement factor for our models of dark matter. We can now examine the effect of the Sommerfeld enhancement on our models. Figure 3.4 shows the magnitude of the S-factor as a function of the dark matter mass for a range of relative velocities and for the scenario of no mass splitting. The dipole moment interactions in eqs. (2.45-2.48) and (2.50) as well as the Higgs-higgsino interaction in eqs. (2.35-2.36) do not see a mass splitting as detailed in section 2.3.

Where the dark matter particle mass is at the GeV scale, the S-factor is of order $S \sim 1$, that is, there may be a small enhancement to the annihilation cross section, but it is not significant enough to alter the signature for indirect detection. In such scenarios, the particle mass is too light to form a bound state with a heavy force carrier, and so the only interaction between the two incoming particles is the annihilation interaction itself. As the mass increases to the TeV scale, the mass of the dark matter particle is much larger than the mass of the force-carrier, so the latter appears similar to a massless force-carrier, making it possible to form a bound state as the non-perturbative interactions become more significant. The Coloumbic potential starts to approximate the Yukawa potential in the WKB approximation for larger radii, essentially increasing the effective cross section for two interacting particles.

At the mass which corresponds to a dark matter particle with the correct relic density in the canonical models, that is, between 1 TeV and 3 TeV, the enhancement reaches an order of magnitude above the underlying cross section. The result is a minor increase to the bounds provided on models by indirect detection in this region, which leads to the exclusion of wino-like dark matter as a viable dark matter model [378].

At the 10 TeV scale, the Sommerfeld enhancement reaches a resonance, with further resonances at higher masses. Here, rather than simply being attracted into the Coulombic potential well, full bound states are formed between the particles at integer multiples of the Compton wavelength. The size of the resonances as well as the baseline of the resonances is larger for decreasing relative velocities. The size of the resonances dependent on the relative velocity of the incoming particles. For non-relativistic particles, as is typical in galactic halos, especially dwarf spheriodal galaxies where indirect detection bounds are stronger, the resonances are large - up to 4 or 5 orders of magnitude compared to the bare cross sections. The effect of the Sommerfeld enhancement on the cross section for measurements of annihilation, particularly indirect detection, at such velocities is expected to be very significant [454]. For indirect detection, the typical relative velocity is determined by the thermalised galactic rotational velocity, approximately $v \sim 0.001$, which we use in further calculations of the Sommerfeld enhancement in this work.

For relativistic and near-relativistic relative velocities, the resonances due to the Sommerfeld enhancement are suppressed, resulting in an overall reduction in S factor to an order of magnitude or less. The suppression arises as the relativistic particles have significantly more kinetic energy making it more difficult to bind into a potential well. However, there is still a residual enhancement, which may have a minor effect in cases of annihilation of such relativistic velocities, notably in the thermal freeze-out [455, 456].

In some of our models, namely the interaction between higgsinos and higgs bosons, a mass splitting is generated between the neutral and charged particles or between the two otherwise degenerate neutral particles. Such mass splittings are important for measuring annihilation as the annihilation processes are inelastic. Taking the masses from eqs. (2.68) and (2.70), the mass difference between the neutral and charged components is:

$$\delta = \left| \left| \mu + \frac{c_4}{2\Lambda} v^2 \right| - \left| \widetilde{\mu} - \frac{c_1 + c_2}{2\Lambda} v^2 \right| \right| . \tag{3.46}$$

By way of demonstration, we assume that the mass and coupling parameters are real, that the cut-off scale is equal for all parameters, and $c_1 = c_2$, avoiding any complex phases that would serve to reduce the overall mass splitting. The latter assumption can be generalised by shifting the neutral component but not the charged component. Under these assumptions, the modified mass parameter $\widetilde{\mu}$ in eq. (2.71) reduces to $\bar{\mu}$ in eq. (2.72). The mass difference can therefore be approximated as:

$$\delta \sim \left| \frac{c_1 + c_2 + c_3 - c_4}{2\Lambda} v^2 \right| . \tag{3.47}$$

The coupling parameters c_i can then be chosen relative to the cut-off scale such that the largest parameter is $\mathcal{O}(1)$, giving an approximation for the mass difference simply as:

$$\delta \sim \frac{v^2}{\Lambda} . \tag{3.48}$$

That is, for increasing values of the cut-off parameter Λ, the mass difference will be decreasingly small, whereas for stronger dimension 5 interactions, the mass difference will increase.

At very large Λ, the mass difference will be on the order of a few MeV. Here, there is a small effect on the Sommerfeld enhancement, shifting by a few percent or so. When Λ reduces to approximately 100 TeV, the mass splittings are now on the order of a few GeV. Here, there is now a substantial reduction of the

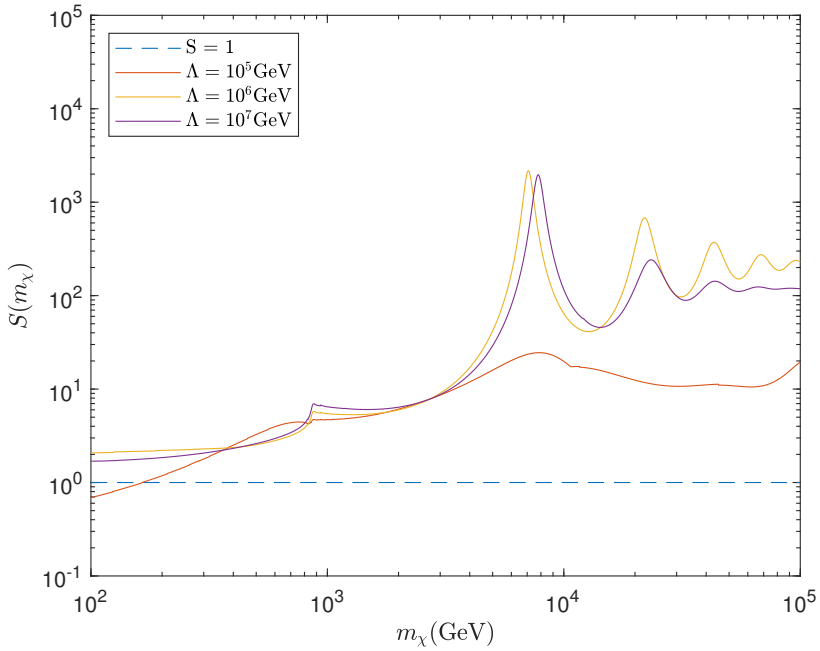

Figure 3.5: S-factor dependence on mass splitting higgsino- dark matter for range of cut-off parameters Λ. The case for no enhancement ($S = 1$) is shown as a horizontal dashed line.

Sommerfeld enhancement. The resonances that were previously present are now no longer possible as it is not possible to form a bound state in an interaction which requires a large mass difference in the inelastic interaction between the incoming and outgoing legs of the diagrams. In such cases, only the bare interaction cross section is applicable to the annihilation.

The calculation of the Sommerfeld enhancement is an important part of the calculation of the annihilation cross section for the indirect detection rates of our models of dark matter. There is an order of magnitude enhancement to the annihilation cross section due to non-perturbative terms in the regions of interest at the TeV scale. Where there is a small mass splitting, the Sommerfeld enhancement is reduced at very high masses. At larger mass differences, the assumptions in this calculation break down as the non-perturbative contributions are no longer comparable to a particle and its excited state.

3.4 Relic density calculations

We can now calculate the relic abundance for models of dark matter which include each of the additional dimension 5 operators introduced in section 2. These include the eight dimension 5 operators for higgsino-like dark matter in eqs. (2.33-2.48), the five dimension 5 operators for wino-like dark matter in eqs. (2.49), (2.50) and (2.51) and the one dimension 5 operator for bino-like dark matter in eq. (2.52). We will investigate modifications to the canonical relic density spectrum caused by modifications to the higgsino-like masses in eqs. (2.68) and (2.69) and to the wino and bino-like particle masses in eqs. (2.77) and (2.78). We compute the relic densities and corresponding direct and indirection limits with the `micrOMEGAs` computer code [433–435], utilising the inbuilt `CalcHEP` [457] and `LanHEP` [458] functionality to generate the required Feynman diagrams and calculate the associated squared matrix elements.

We consider each operator and its effect on the physics separately. For some operators, the effect of two operators is equivalent, so they are combined for simplicity of explanation. Adjustments to the relative size of such operators typically result in a shift to the relevant physics by a rescaling of the relevant parameter. There are two parameters which determine the physics for each operator. The first is the bare mass parameter, μ or $M_{1,2}$ for higgsino-like and wino or bino-like dark matter respectively. The

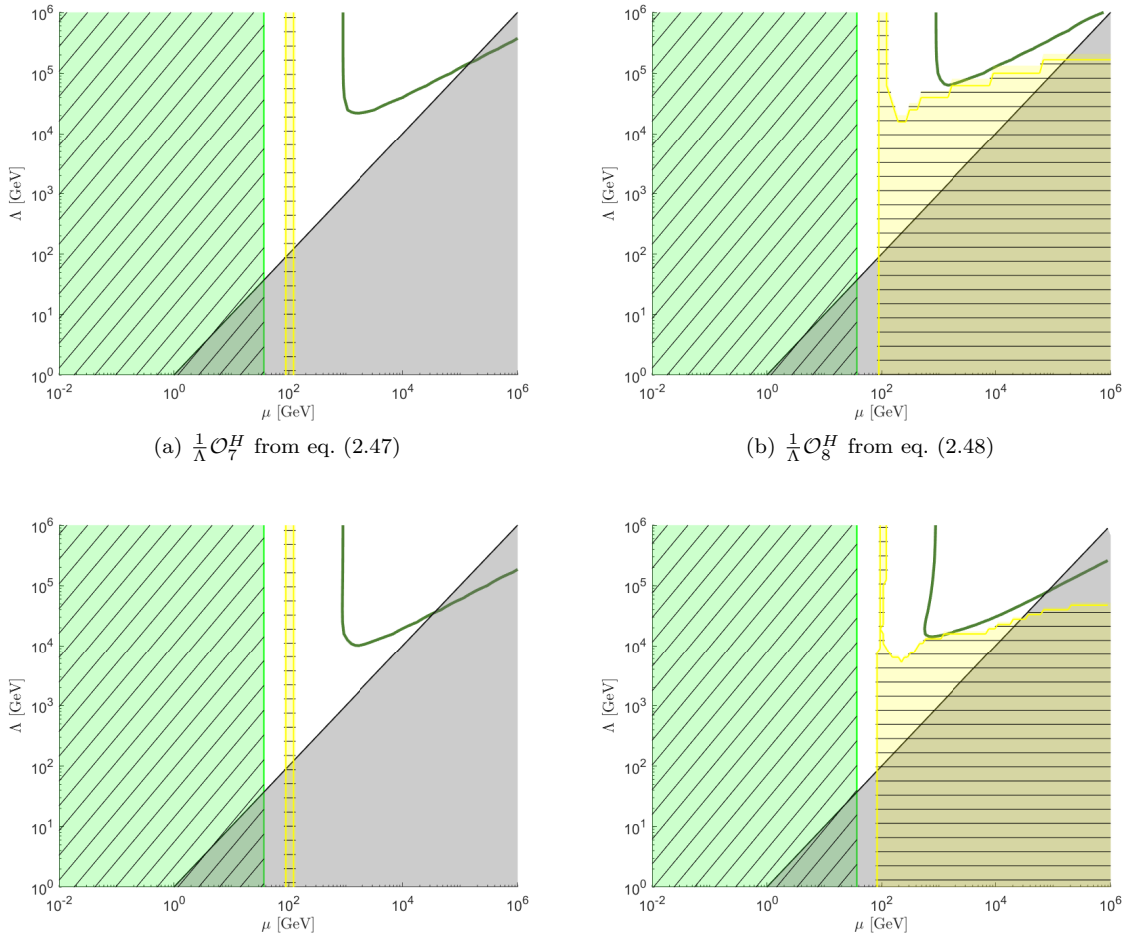

(a) $\frac{1}{\Lambda}\mathcal{O}_7^H$ from eq. (2.47)

(b) $\frac{1}{\Lambda}\mathcal{O}_8^H$ from eq. (2.48)

(c) $\frac{1}{\Lambda}\mathcal{O}_5^H$ from eq. (2.45)

(d) $\frac{1}{\Lambda}\mathcal{O}_6^H$ from eq. (2.46)

Figure 3.6: Parameter space for electric (top) and magnetic (bottom) dipole operators. The horizontal axes show the mass parameter μ and the vertical axes UV-cutoff allowed for the parameter point, determined with the numerical coefficients $c_i = 1$. The contours of parameter values which satisfy the relic abundance are shown as a solid green line. The regions where the EFT is not valid are shaded grey. The regions excluded by indirect detection are shaded yellow with horizontal hatching. The regions excluded by LEP are shaded and green with upwards diagonal hatching (for charginos).

second is the combination of the coupling parameter b_i, c_i, d_i and e_i defined in eq. (2.53)-(2.56) and the associated UV cut off scale Λ. Although we technically have a free choice for the relative scales between the parameters and the cut-off scale, in all cases we set the coupling parameters equal to one, representing the largest possible coupling allowed for a given cut-off scale. Such a choice maximises the region of parameter space whereby the effective field theory is valid, that is, the UV cutoff scale is greater than all of the physical masses in the theory. Where the effective field theory is not valid and the higher scale physics becomes, we highlight it as an excluded region in our plots.

We calibrate each model to the observed value of the relic density to highlight which sets of parameters produce viable thermal relics and which sets of parameters produce overabundances of dark matter. We compare each model to the observed relic density from Planck satellite observations, which show the density of dark matter in the Universe as $\Omega h^2 = 0.1188 \pm 0.0010$ [108]. In all plots, we show the viable relic density regions as a thick green line.

3.4.1 Higgsino electromagnetic dipole interactions

We now begin analysing the parameter space for each of our dimension 5 operators, the relevant constraints and the required relic abundances. The parameter space for the magnetic dipole interaction of higgsino-like dark matter is shown in figures 3.6c-3.6d and the electric dipole interaction in figures 3.6a-3.6b for the operators in eqs. (2.45)-(2.46) and eqs.(2.47)-(2.48) respectively. Such operators provide annihilation processes from two higgsinos to two gauge bosons as well as momentum dependent annihilations to a single gauge boson. The strongest interactions occur for the smallest values of Λ. The annihilation cross section in the region of the parameter space $\Lambda < 10$ TeV and $\mu > m_W$ is dominated by the magnetic dipole interactions. Such interactions deplete the overabundant dark matter, which can decrease the dark matter density to the observed relic abundance. The model allows thermal relic dark matter with masses of up to 70 TeV, corresponding to a magnetic dipole with a strength of 10^{-3} to 10^{-4} times the proton magnetic moment.

However, the operators also produce annihilation by products that can be detected by indirect detection experiments. Specifically,he operator $\mathcal{O}_6^H$ annihilates directly to the a pair of W bosons, while the $\mathcal{O}_5^H$ operator only annihilates into a combination of Z bosons and photons. The latter channels are channels that are easily detected by indirect detection because of the large spectrum of the massless photon, while the former channel are more straightforward to detect from the decay of the on-shell W boson. The indirect detection bounds are shown here for the W^+W^- channel only [319]. The reduced relic abundance due to the annihilation channel also reduces the total annihilation that can be measured by direct detection.

3.4.2 Higgs-higgsino interaction with neutralino mass splitting

Next, we consider the category of operators corresponding to dimension 5 couplings between the Higgs boson and the higgsino. Such operators provide additional mass terms to the dark matter candidate after the Higgs boson undergoes spontaneous symmetry breaking. We divide such operators into two categories. The first category are the operators which correspond to a splitting of the masses of the two neutralinos, while the second category do not split the masses of the two neutralinos. For the first category, the masses of the two higgsinos and the chargino also become non-degenerate. There are two such operators $\frac{c_{1,2}}{\Lambda}(\mathcal{O}_1^H + \mathcal{O}_2^H)$, defined in eqs. (2.33) and (2.34). We combine these operators in a linear combination of the two coupling parameters c_1 and c_2. Such a linear combination sets both coupling constants as equal, essentially removing the offset to $\bar{\mu}$ in the equation for $\tilde{\mu}$ in eq. (2.71) as it is dependent on the difference between the two coefficients. Such an offset does not alter the underlying physics in a general sense, only shifts the relative sum of the two operators. The mass of the chargino is unaffected by these operators and so is completely determined by μ.

We show the mass contours of the doublet model in figure 3.7a for positive and negative values of the coupling parameter. Since the chargino masses are unchanged for these operators, the mass contours are vertical lines equal to the μ parameter. However, for the neutral masses, the result is slightly more complicated. Where $\mu \gg \frac{v^2}{\Lambda}$, that is, μ and Λ are both large, the component of the mass due to the mass parameter μ dominates the mass terms and so the mass of the neutral particle is approximately equal to the mass of the charged particle. Meanwhile, for $\mu \ll \frac{v^2}{\Lambda}$, that is, μ and Λ are both small, the contribution due to the dimension 5 term after symmetry breaking dominates the mass of the neutral component. As the chargino mass remains at μ, the lightest stable particle in the model is indeed the chargino μ. Such models are clearly not viable a they interact with the Standard Model through the electric charge and is shown as ruled out by direct detection experiments. There is a different behaviour however, in the regime where $\mu \sim \frac{v^2}{\Lambda}$. Here, the opposite signs of the contributions to the mass in eq. (2.68), or the presence of

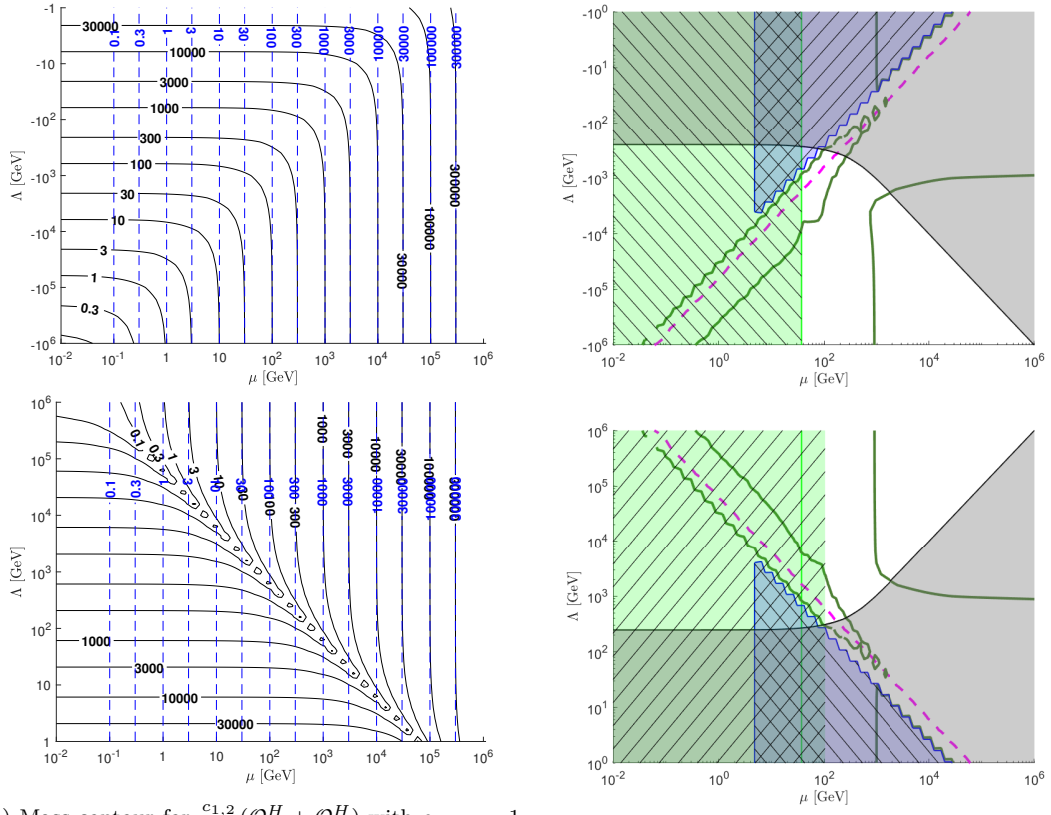

(a) Mass contour for $\frac{c_{1,2}}{\Lambda}(\mathcal{O}_1^H + \mathcal{O}_2^H)$ with $c_{1,2} = -1$ (top) and $c_{1,2} = +1$ (bottom)

(b) $\frac{c_{1,2}}{\Lambda}(\mathcal{O}_1^H + \mathcal{O}_2^H)$ from eqs. (2.33-2.34) with $c_{1,2} = -1$ (top) and $c_{1,2} = +1$ (bottom)

Figure 3.7: Mass contour plots (left) and parameter space (right) for Higgs-higgsino operators. Mass contour shows the lightest neutralino mass in black and the lightest chargino mass in blue as a function of the input parameters. The top graphs show negative values of the coupling constant and the bottom graphs show the positive values. The region where $\mu \simeq \frac{v^2}{\Lambda}$ is marked as a dashed magenta line. The regions excluded by direct detection are shaded blue with downwards diagonal hatching. For a description of the parameter space plots, see the caption of fig. 3.6.

a negative coupling constant in eq. (2.69), mean that there is a cancellation in the mass of the lightest particles, much smaller than the previously degenerate chargino mass, which remains at μ.

We show the constraints and relic density for a range of parameters for the mass splitting models in figure 3.7b. We show the region of interest where the mass splitting is large, that is, $\mu \sim \frac{v^2}{\Lambda}$ as a dashed magenta line. When such an approximate equality is an exact equality, the mass of the lightest particle is exactly zero. However, without some specific relation in the higher order theory such a model would be highly fine tuned and improbable. Indeed, we are not suggesting that such a fine tuning occurs, only that the two quantities are of a similar order. In such a regime, where the mass degeneracy is no longer held, there is a distinct effect on the relic abundance. For mass degenerate models, the coannihilation modes for annihilation between the near-degenerate higgsinos and charginos annihilate via a W boson dominate. Where the two neutral cases are exactly equal, there is no annihilation component between the neutral bosons [459]. Such cases correspond in supersymmetry to cases where the wino and bino are not present, or are at least at scales many orders of magnitude above the higgsino mass scale. The lack of such annihilation is due to cancellation in the higgsino-higgsino-Z boson terms in the Lagrangian, leaving the coannihilation as the primary annihilation mode [460]. By removing the degeneracy, there are no longer valid modes of annihilation, leaving to a Universe overabundant in dark matter. From the extreme case where the cancellation is exact, there is a continuous transition to the case where the masses are degenerate and coannihilations permitted. Along the variation, there is an arbitrary, non fine

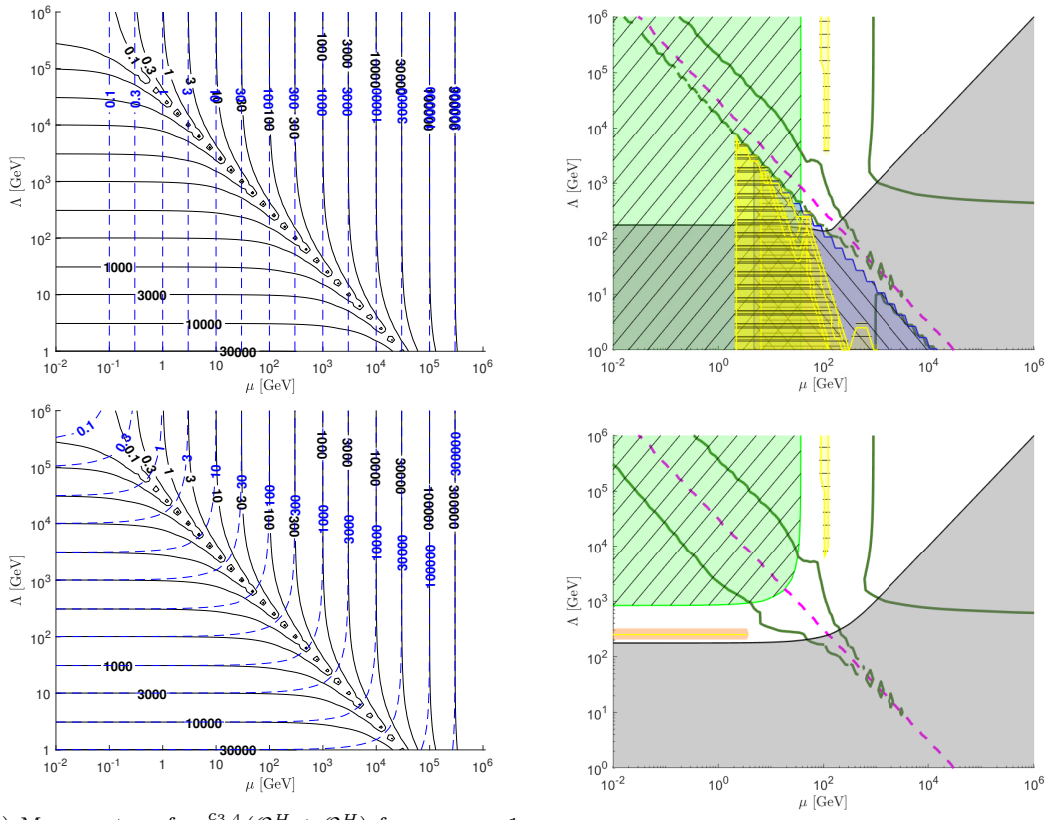

(a) Mass contour for $\frac{c_{3,4}}{\Lambda}(\mathcal{O}_3^H + \mathcal{O}_4^H)$ for $c_{3,4} = -1$ (top) and $c_{3,4} = +1$ (bottom)

(b) $\frac{c_{3,4}}{\Lambda}(\mathcal{O}_3^H + \mathcal{O}_4^H)$ from eqs. (2.35-2.36) for $c_{3,4} = -1$ (top) and $c_{3,4} = +1$ (bottom)

Figure 3.8: Mass contour plots (left) and parameter space (right) for Higgs-higgsino operators. Mass contour shows the lightest neutralino mass in black and the lightest chargino mass in blue as a function of the input parameters. The regions excluded by direct detection are shaded blue with downwards diagonal hatching. For a description of the parameter space plots, see the caption of fig. 3.6.

tuned point where there is sufficient annihilation to generate a dark matter density that corresponds to the observed relic density. Such a contour generates viable dark matter with masses from a range from $m_\chi \sim 50$ GeV to $m_\chi \sim 100$ GeV, with the lower bound provided by the LEP constraints. Finally, as for the electromagnetic dipole cases, the direct annihilation through the higgsino-higgs interaction also provides additional contributions to the annihilation cross section for large mass particles, however, the required interaction strength is not a valid effective field theory.

3.4.3 Higgs-higgsino interaction without neutralino mass splitting

We now turn to the remaining operators which couple a higgsino-like particle to a higgs boson, those which do not provide a mass splitting between the neutralino masses. There are two such operators, namely $\frac{c_{3,4}}{\Lambda}(\mathcal{O}_3^H + \mathcal{O}_4^H)$ from eqs. (2.35)-(2.36). Again considering a linear combination of the two operators only provides a shift in the location of the relevant physics, but no change to the underlying physics itself. The parameters space covers a similar range to the mass splitting components above, but the Lagrangian terms now have different effects on the mass spectrum. The c_3 component corresponds only to an overall shift in the neutral components, while the c_4 component generates a splitting between the charged and neutral components in eq. (2.70), disconnected from the modified mass parameter in eq. (2.72). The mass spectrum for these models is shown in figure 3.8a.

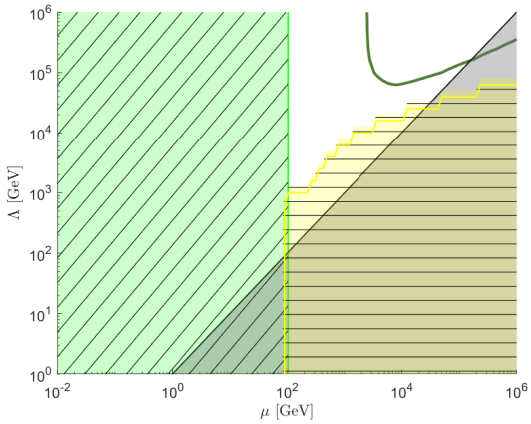

(a) $\frac{1}{\Lambda}\mathcal{O}_2^W$ from eq. (2.50)

Figure 3.9: Parameter space for wino magnetic dipole operator. For a description, see the caption of fig. 3.6

For our models, we once again have a dichotomy between the two components of the mass terms in the Lagrangian. When $\mu \gg \frac{v^2}{2\Lambda}$, that is, both μ and Λ are large, the masses of all particles is roughly degenerate and equal to μ, with no change to the overall mass spectrum. Conversely, where $\mu \ll \frac{v^2}{2\Lambda}$, that is, both μ and Λ are small, the masses of the higgsinos are again both large and approximately degenerate, with $m_1 = m_2 = \frac{v^2 c_3}{2\Lambda}$ and $m_\pm = \frac{v^2 c_4}{2\Lambda}$, noting here that we have set $c_3 = c_4$. Like the mass splitting case, there is an interesting cancellation where $\mu \sim \frac{v^2}{2\Lambda}$. Note here that the mass spectrum is symmetric about the line $\mu = \frac{v^2}{2\Lambda}$. The relevant parameter space is shown in figure 3.8b. However, along the line, at least for the positive coupling parameter case, the masses of the neutral components cancel while the charged components increase by at most a factor of two. As before, since the annihilation processes that contribute to the relic density are the coannhilations between the neutral and charged components, a cancellation between the terms means the coannihilations are no longer efficient, reducing the amount of annihilation overall. Again as the mass splitting case, there is a continuous variation away from the highly fine tuned scenario and the degenerate scenario, with the relic density reaching the observed value at an arbitrary point along the variation. The result is a viable dark matter thermal relic with masses between $m_\chi = 80$ GeV and $m_\chi = 120$ GeV. The cancellation also affects the neighbourhood of the canonical 1 TeV thermal relic, reducing the amount of viable annihilations and expanding the viable region to a lower bound of approximately $m_\chi = 500$ GeV. Once again, the direct annihilation also contributes to the annihilation cross section, albeit at masses close to the limits of the effective field theory.

Where the coupling parameter is negative, there is a mass cancellation in the chargino and a doubling of the mass for the higgsino as seen in eq. (2.70). The result is that along the line $\mu \sim \frac{v^2}{\Lambda}$, although the coannihilations are suppressed, there is not a regime with a viable neutralino relic density, with the parameter space restricted by the constraints on chargino dark matter. Finally, if the linear combination of the coupling parameters is complex, or the coupling parameters themselves are complex, there is a constant transition between the negative and positive scenarios varying with the overall phase from 0 to π, with the inflection point at $\frac{\pi}{2}$ corresponding to a shift of the lightest particle from the neutral to the charged component.

3.4.4 Wino inelastic magnetic dipole

We now turn to the relic density and constraints on wino-like dark matter due to the dimension 5 operators. First, we consider the interaction due to the magnetic dipole in eq. (2.50). The parameter space for the inelastic magnetic dipole is presented in figure 3.9a. The masses of such a model are determined only by

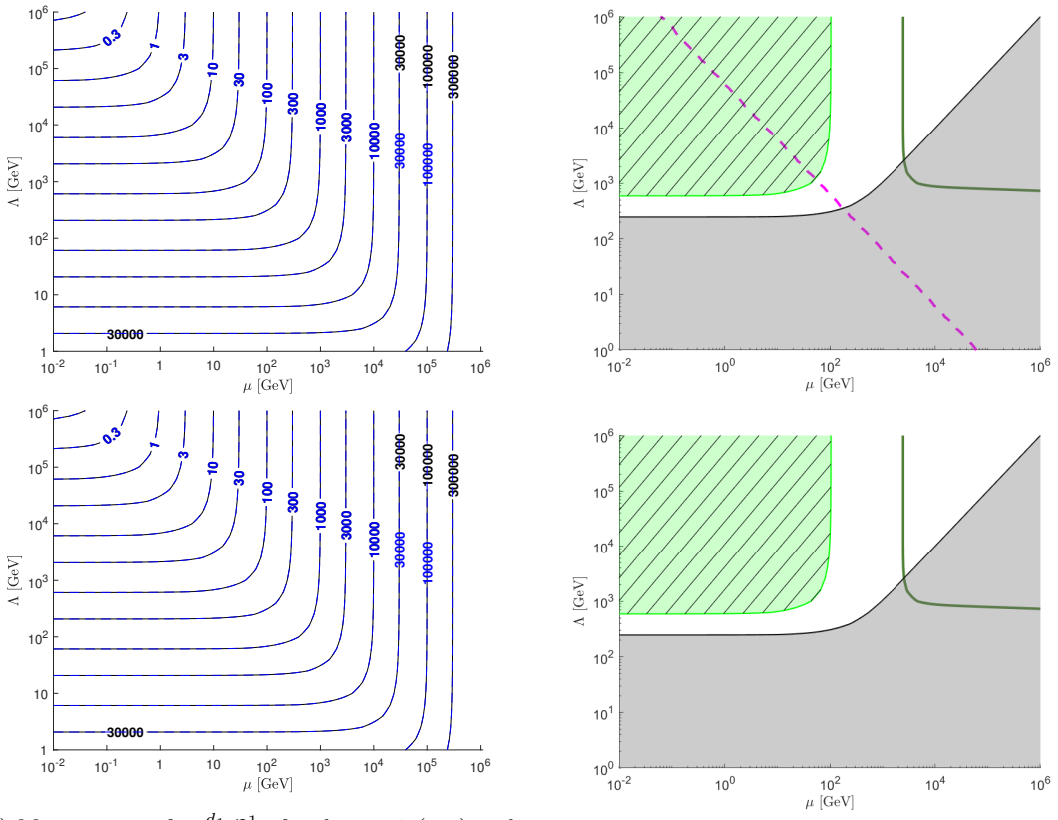

(a) Mass contour for $\frac{d_1}{\Lambda}\mathcal{O}_W^1$ for $d_1 = -1$ (top) and $d_1 = +1$ (bottom)

(b) $\frac{d_1}{\Lambda}\mathcal{O}_W^1$ from eq. (2.49) for $d_1 = -1$ (top) and $d_1 = +1$ (bottom)

Figure 3.10: Mass contour plots (left) and parameter space (right) for wino-Higgs operators. For a description of the mass contour plots, see the caption of fig. 3.7. For a description of the parameter space plots, see the caption of fig. 3.6.

the mass parameter M_2. The effect of such physics on the parameter space are similar to the higgsino-like dark matter particles. Where the interaction is weak, the dipole component has a negligible effect on the relic density, which corresponds to the canonical 3 TeV thermal relic. Such thermal relics are excluded by indirect detection experiments, with the cross section magnified due to the Sommerfeld enhancement. For a larger interaction strength, that is, a lower cut-off, the direct annihilation due to the magnetic dipole operator becomes significant, reducing the overabundance of dark matter for larger masses. Introducing the additional annihilation allows thermal relics for masses in the range 3 TeV $\lesssim m_\chi \lesssim$ 100 TeV for the case $d_3 = 1$. However, the annihilation that produces the relic densities can also be detected through indirect detection techniques. Such techniques are generally not quite as effective at higher masses, meaning that the increased mass some thermal relics are viable, while at masses closer to 3 TeV, the thermal relics are either ruled out or on the boundary of current experiments.

3.4.5 Wino-Higgs interaction

As with the interaction between the higgsino and the Higgs boson, the interaction between the wino and the Higgs boson produces alterations to the mass spectrum. The mass spectrum is shown in figure 3.10a. However, there are no opportunities for cancellations between two opposing sign mass terms in the Lagrangian. There are also no changes to the relative degeneracy between the charged and neutral components. Where $\frac{d_1 v^2}{\Lambda} < M_2$, the mass parameter M_2 dominates the mass of the wino components. However, where $\frac{d_1 v^2}{\Lambda} > M_2$, the contribution from the dimension 5 component after spontaneous symmetry breaking dominates. The resultant parameter space is shown in figure 3.10b. Since

there are no modifications to the degeneracies in the mass spectrum, the relic density represents a mapping following the contours of the mass spectrum, with the 3 TeV thermal relic following the 3 TeV mass contour. The exception occurs when direct annihilation through the dimension 5 operator is significant, which results in an increased overall annihilation cross section and reduced relic density.

3.5 Discussion

The effective field theories of doublet and triplet dark matter represent two major forms of interaction with the Standard Model, namely coupling via a Higgs boson and coupling via an electromagnetic dipole. Both have distinct effects on the parameter space of dark matter and its relic density. We have now computed the relic density and consequential experimental bounds due to direct and indirect experiments and collider bounds from the LEP experiment.

For each of the operators we consider, if the strength of the relevant interaction is sufficiently large then direct annihilation through the dimension 5 operators dominates the annihilation cross section. Such operators can provide thermal relics through sufficient annihilation of early universe dark matter. The operators which produce direct annihilation to two Higgs bosons require large coupling strengths to provide enough annihilation to produce a relic abundance, which occur at a scale beyond the UV cutoff of the theory. For the interactions with an electromagnetic dipole moment, the process of annihilation due to the dimension 5 operators produces viable thermal relics due to inelastic magnetic dipoles with strengths as low as $\mathcal{O}(10^{-3})$ times the proton magnetic moment while still avoiding the UV cutoff. In models where these theories are valid, there is a substantial increase in the spectrum of viable thermal relic dark matter, up to $m_\chi = 100$ TeV. Descriptions of higher mass or sufficiently strongly interacting operators must be dealt with as part of a more descriptive theory, with higher scale components made explicit. The viable regions may be detectable via an indirect detection experiment with an increase in sensitivity of a factor of $\mathcal{O}(10)$.

For the operators that provide new couplings between the dark matter and the Higgs boson, the fact that the Higgs boson undergoes spontaneous symmetry breaking provides new mass terms for the particles. Such operators produce mass splittings either between the neutral and charged components, or in the case of the higgsinos, the two neutral components. We have seen that where the neutral components split, one component of the neutral mass may approach zero. In these regions, the decoupling of the masses results in a loss of efficiency of coannihilation processes. The result is a region of parameter space with a thermal relic well below the canonical mass, at or around 100 GeV. Such regions are only bounded by the LEP constraints on the invisible Z width, within range of near future experiments. The operators required to produce such results require coupling parameters too strong to be produced by the conventional MSSM, but could be produced by a different higher scale theory, which could be some flavour of supersymmetry.

Here, we have assumed that the coupling parameters of the dimension 5 operators are real, though in principle, such parameters may be complex. Where these parameters are complex, there is no overall change to the direct annihilation components for larger masses, though there are modifications to the mass splittings in, for example, the last term in eq. (2.67). Where the relative combination of terms is not parallel or anti-parallel, the sum of the oblique or orthogonal components results in masses somewhere between the exact cancellation and the exact superposition. In general, at least where the masses are not strictly orthogonal, there is still a decoupling of the mass parameters and the resultant physics due to the reduction in coannihilation components still applies.

We have only considered most of the relevant operators in isolation, except where such operators provide a similar function on the parameter space to each other. In general, however, combinations of higher order operators do not exist in isolation, and would appear in higher order theories in linear

combinations. Where such operators are combined, the result is additional modes of annihilation, resulting in a reduction in the scale of interaction required to produce a viable thermal relic. Including the additional interactions will still result in cancellations in the masses between the raw mass parameter μ and the coupling parameter, the average of c_1 and c_2 in the regime where coannihilations are suppressed.

We have only considered models that correspond to higgsino-like or combined gaugino-like dark matter, the latter being the combination of wino-like and bino-like dark matter, with any other components relegated to a significantly higher scale. Many other combinations of neutral particles exist which include multiple neutral states, such as the so-called "well-tempered neutralino" which combines a neutral higgsino with a bino, or a fully mixed higgsino, wino and bino combination. Unless the mass parameters of each of these models is the same scale, the effective field theory approach encompasses these scenarios by integrating out the heavier mass particles. If they are at the same scale, our models do not apply due to the Yukawa terms which mix the different neutralinos, meaning that the mass terms for the mass basis particles will be significantly altered.

Introducing the effective field theory approach has simplified the analysis of fermionic models of dark matter without specifying the higher order theories, supersymmetry or otherwise. Allowing such higher dimensional operators has increased the range of values permitted for thermal relic dark matter from a single, deterministic value to a wide spectrum ranging from a few hundred GeV to a few hundred TeV. Such regimes may be constrained in the near future by new experiments, but the results show that higgsinos remain viable candidates for dark matter particles.

Part II

Electromagnetic dipole dark matter detection in solar energy transport

Based on Geytenbeek et. al. (2017) *Effect of electromagnetic dipole dark matter on energy transport in the solar interior*, published in Journal of Cosmology and Astroparticle Physics, volume 2017, page 029 [2]

Chapter 4

Theory of dark matter in the Sun

Dark matter, regardless of whether it is a thermal relic or otherwise, has never been observed in direct or indirect detection experiments [184, 197, 200, 216, 218, 221, 248, 461–464]. While developments in direct detection experiments continue to improve detection thresholds, new methods of identifying and testing dark matter models are an appealing option to shed light on the true nature of dark matter. One appealing class of observation features modelling the effect of dark matter on solar physics, which provides an indirect method of constraining certain parameters of dark matter. The scale of the physical size of the Sun can counteract the weakly interacting nature of the dark matter, increasing the concentration of dark matter particles in a nearby locale and meaning high precision measurements could observe very small modifications to the solar interior.

In this chapter, we introduce one of the key sets of observations in the Sun that can be affected by dark matter, namely the solar abundance problem and helioseismology, and the mathematical preliminaries required to describe such effects. In section 4.1, we introduce the solar abundance problem and the measurements made by helioseismology, and outline how dark matter can be a potential solution. We begin the mathematical preliminaries in section 4.2 by deriving the cross sections of electromagnetic dipole dark matter scattering via an electric current from nuclei in the Sun, and consider the form factors which describe the interaction of photons within the nucleus. In section 4.3, we compute the rate equation for the population of dark matter particles within the Sun including the saturation of the capture rate of dark matter. In section 4.4 we consider the Boltzmann collision equation which describes the processes of transporting energy within the Sun due to the dark matter, and define and calculate the thermal conductivities and diffusivities for each of our models of dark matter and how such quantities influence the energy transport. We also introduce the Knusden transport for when the interaction is no longer in thermal equilibrium.

4.1 Solar abundance problem

The theoretical framework for solar dark matter arose in the literature as part of a catalogue of potential solutions to the solar neutrino problem [465–474]. The solar neutrino problem was a theoretical dilema whereby the observed flux of neutrinos from ^{8}B decay in the Sun was measured as significantly lower than the theoretical flux predicted by then-contemporary solar models [475, 476]. Although the later discoveries of neutrino oscillations in atmospheric neutrinos by Super-Kamiokande [155] and later in solar neutrinos by SNO [477] alleviated the solar neutrino problem by allowing the neutrinos to oscillate to other states while in transit between the Sun and the Earth, it had been proposed that the reduced neutrino rate was due to a lower than expected core temperature inside the Sun [478]. By cooling the core, the expected

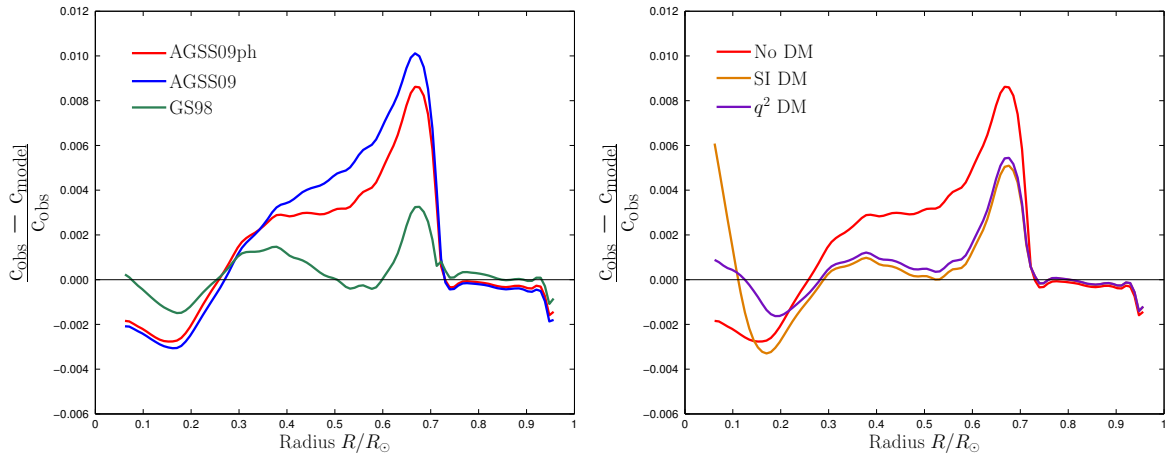

Figure 4.1: Relative error in the speed of sound profile of various Standard Solar Models. Left: Comparison of models before revision of solar abundances (Green, GS98 [490]) to after (Blue, AGSS09 [491]); (Red, AGSS09ph [492]). Right: Comparison of best-fit models Solar Models with constant cross section, spin independent dark matter (Orange [493]), momentum dependent (q^2) dark matter (Purple [494, 495]), and no dark matter (Red [492])

rate of production of ^{8}B from the fusion of helium isotopes is reduced, which also reduces the flux of neutrinos from their associated decays. Introducing interactions between the elements in the Sun and dark matter provides a mechanism for the heat transport out of the solar core [465–467].

Although the original motivations for solar dark matter were realised by other mechanisms, the theoretical framework that was developed remains valid. Several key processes were identified and calculated. First, the dark matter needs to be captured by the Sun from the galactic halo [328]. Here, the dark matter scatters from the nuclei in the Sun to below the escape velocity of the Sun, moving into a gravitational orbit and a stellar halo. Next, the dark matter can thermalise through self-interactions or further scatterings, resulting in some degree of evaporation from the Sun [327, 479]. When inside the galactic halo, scattering within the Sun can cause thermal transport to occur, typically from the core to the radiative or convection zones [480, 481]. Finally, given sufficient concentration of dark matter within the gravitational influence of the Sun, there is predicted to be a degree of annihilation between dark matter particles, which can produce a neutrino spectrum [468, 482]. The Sun then becomes a good laboratory for testing the scattering properties of dark matter, especially off lighter elements such as hydrogen and helium.

The modern description of the solar interior derives not from neutrinos, but from helioseismology, which studies propagation of pressure waves in the Sun. Such waves induce surface oscillations, which are detected via Doppler radar techniques [483]. Such surface oscillations are identified as modes of a series of spherical harmonics Y_{lm} which propagate acoustically with a range of low to high angular degrees l [484–486]. The identification of a large number of modes allows for mapping of the acoustic properties of the solar interior. The rate of propagation as a function of the radius of the Sun is termed the sound speed profile, and is mapped directly from the oscillation modes [487]. The sound speed is directly determined from the temperature profile of the Sun, which is predicted by the theoretical modelling of the Sun [488, 489].

Early attempts to theoretically model the speed sound profile of the Sun suffered from a lack of oscillation modes to make reliable predictions, with large errors on the inversions especially around the solar core ($R < 0.2R_\odot$). The first high precision mapping of the solar profile which included the solar core was provided by the Global Oscillation Network Group (GONG) project [496] and the Global Oscillations at Low Frequencies (GOLF) experiment on the Solar and Heliospheric Observatory (SOHO) spacecraft [497], which included a large number of low degree modes mapping the solar core [498–501].

These new observations showed a slight discrepancy near the border of the radiative zone and the convective zone ($R \sim 0.6R_{\odot}$), the transition between non-thermal and thermal energy transfer [490, 502, 503]. Here, the observed speed of sound is greater than the models predicted, indicating that the models are too cold. The discrepancy is shown in figure 4.1 as the GS98 model.

The next development caused a significant discrepancy in the theoretical understanding of the solar models, leading to a phenomenon called the solar abundance problem. Updated spectroscopy data from the Sun revised the solar metal content downwards by a factor of 2 [491, 504–513]. The change in the solar abundance is due to two reasons. First, the refinement of the modelling due to the new three-dimensional hydrodynamic models of the photosphere has increased the accuracy of the models. Second, and more significantly, there were major improvements in the treatments of how the models depart from the local thermal equilibrium at the atomic level which generated the absorption lines [514–517]. The resultant absorption lines are refined through spectroscopy, with improvements to the measurements of atomic data, line selection and equivalent widths. Suggested improvements based on alternate 3D models [518] and measurements of the solar wind [519]. Such alterations do not hold up to scrutiny based on spectroscopic fundamentals [511–513] and the neglected fractionation effects [520] respectively.

The result was worsened helioseismology fits, as the sound speed profile is dependent on the description of the elemental abundances at different depths of the Sun [521–525]. The result of the changes to the metallicity was that the Standard Solar Models could not reproduce the sound speed profile from helioseismological observations. The discrepancy at the convective zone boundary was exacerbated, shown as the AGSS09 model in figure 4.1. Subsequent updates to the metallicity has reduced the discrepancy slightly [491, 492, 526] as shown as model AGSS09ph in figure 4.1, although the error is still statistically significant. Additionally, the metallicity observations has caused significant tension with other solar observations, namely the radius of the convection zone R_{cz} [521] and the surface helium abundance Y_s [492, 526, 527].

An appealing solution to resolve the solar abundance problem is to introduce dark matter into the processes modelling the sound speed profile of the Sun. The goal is to introduce a mechanism that can transport energy from the core to the outer regions. Consider a dark matter particle which interacts sufficiently weakly with the stellar material such that it satisfies other solar observables such as the neutrino flux. There are then two mechanisms for energy transfer: local thermal equilibrium and Knusden transport. In local thermal equilibrium, the dark matter interacts with the local solar matter sufficiently strongly so that the dark matter maintains a thermal equilibrium with the surrounding material, allowing for short distance energy transport within the Sun [480]. As the strength of the dark matter to Standard Model interaction increases, the interaction becomes increasingly short distance, reducing the amount of energy that can be transported. However, the number of interactions increases meaning the dark matter can pick up energy from the surrounding material more easily. Conversely in the Knusden limit, the interactions are much weaker, leading to a mean free path between interactions to be of a size similar to the size of the Sun itself [481]. In this regime, interactions are rarer, but transport energy easily over longer distances allowing the dark matter to easily take energy from the solar core to the outer regions.

Initial investigations into the effect of dark matter on solar energy transport did not show any measurable improvements to the solar abundance problem [528]. Such investigations typically focussed on intermediate mass dark matter particles close to the then threshold of dark matter direct detection experiments (30 GeV − 100 GeV). The largest effects occurred where the cross section approaches the transition between the local thermal equilibrium and Knusden energy transport regimes, where the luminosity of energy transported is maximised [529, 530]. Later investigations have considered lighter dark matter particles (1 GeV − 10 GeV) where the mass more closely matches the masses of common nuclei in the Sun such as hydrogen and helium [493, 531]. Such models are shown as the SI DM models in figure 4.1. The result is an improved measurement of the sound speed profile at the border of the

convective and radiative zones, but also results in a significant reduction in the core temperature of the Sun. Problems arise with such models due to the strong constraints on the temperature of the inner core from measurements of neutrino fluxes.

A proposed solution to the drastic reductions in core temperature is to consider models of dark matter where the cross section is momentum or velocity dependent [494, 495, 532, 533]. Here, the cross section is different at different layers of the Sun, as the thermalised dark matter in the hot core can interact at a different cross section to the cooler outer regions. The most promising such model, where the cross section depends on the momentum squared of the dark matter and is shown as the q^2 DM model in figure 4.1. Such models can accomplish a warming in the outer regions of the Sun without causing a collapse in the core temperature due to the dualism of the cross section.

We now seek to develop models which contain such momentum and velocity dependent cross sections from a theoretical perspective. We will see that the electromagnetic dipole models which we developed in chapter 2 contain such momentum and velocity dependent cross sections, namely the electric dipole, magnetic dipole and anapole models. Each of these three models provides different momentum and velocity dependent cross sections with slightly different functional forms to that considered previously in the literature. The operators are momentum dependant because the mediating particle, the photon, is a massless rather than a massive boson, so the denominator of the propagator is q^2 instead of $q^2 + m^2 \simeq m^2$. We will review and develop the theoretical formalisms for modelling the effects of these models on helioseismology. Two of our models possess linear and non-linear combinations of momentum and velocity dependent cross sections that require novel mathematical approaches. We will construct all relevant physical quantities in order to implement these models for simulations of relevant helioseismology in the `DarkStec` package [495].

4.2 Electromagnetic scattering cross sections

We shall now develop further the scattering cross sections and theoretical constraints on dipole moment dark matter that we introduced in chapter 2. As we are only looking at the interaction term of the neutral components with electromagnetic photons, we do not specify the gauge structure of the fermion that we are considering. We have already seen that the doublet, higgsino-like neutral fermion can be structured in terms of a Dirac fermion, while the triplet, wino-like neutral fermion must be structured as a Majorana fermion. In section 2.5.1, we discovered that electric and magnetic dipoles are forbidden for Majorana fermions, with only the anapole moment being permitted. Nonetheless, here we consider the dark matter particle to be any generic Dirac fermion χ for the electric and magnetic dipole moment models, and any generic Dirac or Majorana fermion χ for the anapole model. Further, in chapter 2 we defined the operators in terms of the unbroken gauge field strength tensors $B_{\mu\nu}$ and $W^a_{\mu\nu}$. Now we consider only the components that correspond to the pure electromagnetic gauge fields after spontaneous symmetry breaking in eq. (2.19), with field strength tensor $F_{\mu\nu}$.

We now construct the generalised electromagnetic Lagrangian terms. For the electric dipole moment, we generalise $\mathcal{O}_7^H$ and $\mathcal{O}_8^H$ in eqs. (2.47)-(2.48) for the doublet and $\mathcal{O}_3^W$ in eq. (2.51) [394]:

$$\mathcal{L}_{\rm ED} = -\frac{i}{2}\mathcal{D}\overline{\chi}\sigma^{\mu\nu}\gamma^5\chi F_{\mu\nu}\,; \tag{4.1}$$

where we have used the identity in eq. (2.84) to rewrite the dual field strength tensor in terms of the a Dirac psuedo-tensor with the inclusion of the γ^5 component. The electric dipole moment $\mathcal{D}$ is defined in terms of the higgsino coupling parameters as a linear combination of the coefficients of the operators $\mathcal{O}_7^H$

and $\mathcal{O}_8^H$ for:

$$\mathcal{D} = \frac{gc_7 + g'c_8}{\Lambda\sqrt{g^2+g'^2}}\,, \tag{4.2}$$

and for the wino coupling parameters as:

$$\mathcal{D} = \frac{g'd_3}{\Lambda\sqrt{g^2+g'^2}}\,. \tag{4.3}$$

For the magnetic dipole, we generalise the $\mathcal{O}_5^H$ and $\mathcal{O}_6^H$ operators from eqs. (2.45)-(2.46) for the doublet models and $\mathcal{O}_2^W$ from eq. (2.50) as [394]:

$$\mathcal{L}_{\rm MD} = \frac{1}{2}\mu_\chi \overline{\chi}\sigma^{\mu\nu}\chi F_{\mu\nu}\,; \tag{4.4}$$

where the magnetic dipole moment μ_χ is again defined as a linear combination of operators $\mathcal{O}_5^H$ and $\mathcal{O}_6^H$ for the doublet model as:

$$\mu_\chi = 2\frac{gc_5 + g'c_6}{\Lambda\sqrt{g^2+g'^2}}\,, \tag{4.5}$$

and similarly for the triplet coupling parameters:

$$\mu_\chi = 2\frac{g'd_2}{\Lambda\sqrt{g^2+g'^2}}\,. \tag{4.6}$$

Finally, for the anapole, the analogous operators appear at dimension 6, unlike the magnetic and electric dipoles where the analogous operators appeared at dimension 5. We introduced the anapole operator in section 2.5.2. Building from the effective Hamiltonian in eq. (2.110), the anapole Lagrangian is written as:

$$\mathcal{L}_{\rm AN} = \frac{g}{2\Lambda^2}\overline{\chi}\gamma^\mu\gamma^5\chi\partial^\nu F_{\mu\nu}\,, \tag{4.7}$$

for coupling parameter $\frac{g}{\Lambda^2}$. Note here that the common usage in the literature is to define the coupling parameter as g [400], distinct from the Standard Model $SU(2)\times U(1)$ coupling parameters g and g' in eqs. (4.2)-(4.3) and (4.5)-(4.6). These Lagrangian terms have been developed extensively in the literature, applying direct, indirect and collider constraints often favouring masses of only a few GeV [391–404, 411, 418, 419, 534, 535].

4.2.1 Scattering cross sections of electromagnetic dipole dark matter

We now arrive at the derivation of the analytical expressions of the differential cross sections for each of our three models of electromagnetic dipole dark matter scattering from nuclei in the Sun. We follow a methodology which considers the electromagnetic current due to the dipole instead of calculating traces of Dirac matrices [400]. To begin, we start with the Golden Rule for the scattering cross section:

$$d\sigma = \frac{2\pi}{v}\delta\left(E_{p_N} + E_{p_\chi} - E_{k_N} - E_{k_\chi}\right)\overline{|\mathscr{M}|^2}\frac{d^3\vec{k}}{(2\pi)^3}\,, \tag{4.8}$$

where v is the velocity of the dark matter particle in the lab frame of the nucleus, $\vec{k}_\chi$ and $\vec{k}_N$ are the incoming four-momenta of the dark matter and nucleus respectively, $\vec{p}_\chi$ and $\vec{p}_N$ are the outgoing four-momenta of the dark matter and nucleus respectively, E is the energy of each of the four-momenta above, that is, the first component of the four-momenta and δ is the Dirac delta function. Expanding into spherical coordinates, the Golden Rule becomes:

$$d\sigma = \frac{2\pi}{v}\frac{d|\vec{k}|}{2\pi}\frac{d\Omega_{\rm CM}}{(2\pi)^2}|\vec{k}|^2\delta\left(E_{p_N} + E_{p_\chi} - E_{k_N} - E_{k_\chi}\right)\overline{|\mathscr{M}|^2}\,, \tag{4.9}$$

where we have expanded in terms of the solid angle in the centre of mass frame $\Omega_{\rm CM}$. Note that the velocity here is still in the lab frame of the target nucleus. Here, we utilise the identity:

$$d|\vec{k}|\delta\left(E_{p_N}+E_{p_\chi}-E_{k_N}-E_{k_\chi}\right)=\left(\frac{|\vec{k}|}{m_\chi}+\frac{|\vec{k}|}{m_N}\right)^{-1}=\frac{M_{\chi,N}}{|\vec{k}|}\,, \tag{4.10}$$

where m_χ and m_N are the masses of the dark matter particle and nucleus respectively, and $M_{\chi,N}$ is the reduced mass of the system of the dark matter particle and nucleus together. The differential cross section then simplifies to give:

$$\frac{d\sigma}{d\Omega_{\rm CM}}\frac{|\vec{k}|M_{\chi,N}}{4\pi^2 v}\,. \tag{4.11}$$

For a non-relativistic pair of particles in the centre of mass frame, the magnitude of the momentum $|\vec{k}|$ is given by $|\vec{k}|=vM_{\chi,N}$ where v is the incoming velocity in the frame where the nucleus is at rest. Thus the differential cross section simplifies further:

$$\frac{d\sigma}{d\Omega_{\rm CM}}=\frac{M_{\chi,N}^2}{4\pi^2}\overline{|\mathscr{M}|^2}\,. \tag{4.12}$$

For elastic scattering, it is common to express the differential cross section in terms of the nuclear recoil energy E_R, which is the amount of energy transferred from the dark matter particle to the nucleus. The three-momentum transferred is given as $|\vec{q}|$. The recoil energy is thus given by:

$$E_R=\frac{|\vec{q}|^2}{2m_N}=\frac{|\vec{k}|^2(1-\cos\theta_{\rm CM})}{m_N}=\frac{M_{\chi,N}^2v^2(1-\cos\theta_{\rm CM})}{m_N}\,. \tag{4.13}$$

where $\theta_{\rm CM}$ is the scattering angle in the centre of mass frame. Differentiating, the nuclear recoil gives:

$$dE_R=-\frac{|\vec{k}|^2}{m_N d(\cos\theta_{\rm CM})}\,, \tag{4.14}$$

with the solid angle differential giving, for a cylindrically symmetric scattering,

$$d\Omega_{\rm CM}=-2\pi d(\cos\theta_{\rm CM})\,. \tag{4.15}$$

The scattering cross section with respect to the recoil energy is then given by:

$$\frac{d\sigma}{dE_R}=\frac{m_N}{2\pi v^2}\overline{|\mathscr{M}|^2}\,. \tag{4.16}$$

The challenge therefore, is to compute the scattering amplitude $\overline{|\mathscr{M}|^2}$ for each of our three models scattering from a Standard Model nucleus.

The squared scattering amplitude is averaged and summed over the initial and final spin polarisations of each particles. Further, we can define the transition matrix iT from a state with initial spins s_χ and s_N for the dark matter particle and nucleus respectively to a state with final spins s'_χ and s'_N for the dark matter particle and nucleus respectively as:

$$\langle\vec{p},s'_\chi,s'_N|\,iT\,|\vec{k},s_\chi,s_N\rangle=i\mathscr{M}(2\pi)^4\delta\left(p_\chi+p_N-k_\chi-k_N\right)\,. \tag{4.17}$$

Such a transition matrix is related to the interacting component of the Lagrangian $\mathcal{L}_{\rm int}$ as:

$$iT=\mathrm{Texp}\left\{-i\int d^4x\mathcal{L}_{\rm int}\right\}\,, \tag{4.18}$$

where the right hand side represents the action of the interaction. Our goal is to write the interaction Lagrangian in the form:

$$\mathcal{L}_{\text{int}} = j_\mu A^\mu \,, \tag{4.19}$$

for some operator j_μ. Here, A^μ represents the electromagnetic interaction component of the Lagrangian, while j_μ represents the four-current due to the dipole. Such a decomposition allows us to rewrite the transition matrix at the leading order in the exponential as:

$$\langle \vec{p}, s'_\chi, s'_N | \, iT \, | \vec{k}, s_\chi, s_N \rangle = -i \int d^4x \, \langle \vec{p}, s'_\chi, s'_N | \, j_\mu(x) A^\mu(x) \, | \vec{k}, s_\chi, s_N \rangle \ . \tag{4.20}$$

We note here that the terms accompanying A^μ are always accompanied by a derivative component due to the field strength tensor $F_{\mu\nu}$ which appears in each of the Lagrangians eq. (4.1), (4.4) and (4.7). To deal with the derivative, we seek to transition from position-space to momentum space. Therefore, we expect that the derivative operator acting on A^μ will be replaced by its eigenvalue:

$$i\partial^\mu \to q^\mu \equiv k^\mu_\chi - p^\mu_\chi \,, \tag{4.21}$$

where q^μ is the four-momentum of the off-shell photon A^μ. Similarly, the spinors undergo a similar transformation:

$$\chi(x) \to e^{-ik_\chi \cdot x} \chi(k_\chi) \,. \tag{4.22}$$

We can now fully decompose the transition matrix into two, separate components for j_μ and A^μ, as the former is only dependent on the dark matter particle and the outer is only dependent on the photon and nucleus. The transition matrix becomes:

$$\langle \vec{p}, s'_\chi, s'_N | \, iT \, | \vec{k}, s_\chi, s_N \rangle = -i \, \langle \vec{p}, s'_\chi | \, j_\mu(q) \, | \vec{k}, s_\chi \rangle \int d^4x e^{-iq\cdot x} \, \langle s'_N | \, A^\mu(x) \, | s_N \rangle \ . \tag{4.23}$$

The current component is now independent on the position x, and so has been brought out of the integral, while the gauge field remains inside the integral. Such an integral now represents a four-dimensional Fourier transformation of the photon field $A(x) \to A(q)$, fully decomposing the transition matrix into two clear components:

$$\langle \vec{p}, s'_\chi, s'_N | \, iT \, | \vec{k}, s_\chi, s_N \rangle = -i \, \langle \vec{p}, s'_\chi | \, j_\mu(q) \, | \vec{k}, s_\chi \rangle \, \langle s'_N | \, A^\mu(q) \, | s_N \rangle \ . \tag{4.24}$$

The transition matrix now contains components which are dependent on the current due to the electromagnetic dipole and the coupling between the photon and the nucleus. Such terms can be evaluated separately and independently; brought back together to produce the scattering amplitudes.

4.2.2 Nucleus electromagnetic current and form factors

First, consider the photon-nucleus component $\langle s'_N | \, A^\mu(q) \, | s_N \rangle$. To evaluate this matrix element, we need to use the equation of motion for a photon in the Lorenz gauge $\partial_\mu A^\mu(x) = 0$:

$$\partial^2 A^\mu(x) = eJ^\mu \,. \tag{4.25}$$

where e is the electromagnetic coupling constant and J^μ is the electromagnetic current generated by the nucleus. We need to transform the equation to momentum space using eq. (4.21):

$$A^\mu(q) = -\frac{eJ^\mu}{q^2} \,. \tag{4.26}$$

Here, we note that both $|s_N\rangle$ and $|s'_N\rangle$ are energy eigenstates with eigenvalues E_{k_N} and E_{p_N} respectively, giving an overall δ function to the matrix element, which becomes:

$$\langle s'_N|\, A^\mu(q)\,|s_N\rangle = \frac{e\,\langle s'_N|\, J^\mu(q)\,|s_N\rangle}{|\vec{q}|^2}\,, \tag{4.27}$$

where we expand the four-momentum $q^2 = -|\vec{q}|^2$ for a massless photon.

Next, we need to find an expression for the electromagnetic current inside a nucleus J^μ. Such a current cannot be described using analytical functions, so we shall seek to express such quantities using electromagnetic form factors. Such form factors are well-studied properties of the nucleons as calibrated by deep inelastic scattering [536]. In order to compute the form factors, we consider the laboratory frame whereby the nucleus is at rest. By convention, the momentum exchange is defined to be in the z direction. Such a frame is spanned by a set of four-dimensional orthogonal basis vectors: the energy of the nucleus $k_N^\mu = (m_N, 0)$, the three-momentum transfer $Q^\mu = q^\mu - \frac{k_N^\nu q_\nu}{m_N^2} k_N^\mu = (0, \vec{q}_{\rm lab})$ and two unit vectors $e_x^\mu = (0, \hat{e}_x)$ and $e_y^\mu = (0, \hat{e}_y)$ where m_N is the mass of the nucleus. In this basis, the electromagnetic current decomposes as:

$$J^\mu = \frac{(J\cdot k_N)k_N^\mu}{k_N^2} + \frac{(J\cdot Q)Q^\mu}{Q^2} + (J\cdot\hat{e}_x)\hat{e}_x^\mu + (J\cdot\hat{e}_y)\hat{e}_y^\mu\,. \tag{4.28}$$

Here, we note that the electromagnetic current J^μ must satisfy the continuity equation $q_\mu J^\mu = 0$, allowing us to simplify slightly, utilising the fact that we are in the rest frame of the nucleus

$$J^\mu = \frac{\rho_{\rm lab}}{m_N} k_N^\mu + \frac{\rho_{\rm lab}}{m_N}\frac{(k_N\cdot q)}{|\vec{q}_{\rm lab}|^2} Q^\mu + J_x\hat{e}_x^\mu + J_y\hat{e}_y^\mu\,, \tag{4.29}$$

where we have defined $J_i = J\cdot\hat{e}_i$ and identified that $J^0 = \rho_{\rm lab}$ is the charge density in the lab frame. Now, we take the non-relativistic limit, which allows us to identify $q^2 = -|q_{\rm lab}|^2$ and $Q^\mu = q^\mu + \mathcal{O}(v^3)$, so

$$J^\mu = \frac{\rho_{\rm lab}}{m_N}\left(k_N^\mu - \frac{(k_N\cdot q)}{q^2} q^\mu\right) + J_x\hat{e}_x^\mu + J_y\hat{e}_y^\mu + \mathcal{O}(v^3)\,. \tag{4.30}$$

Lastly, we can expand $q^\mu = p_N^\mu - k_N^\mu$ to give an alternate expression for the term in the brackets as:

$$k_N^\mu - \frac{(k_N\cdot q)}{q^2} q^\mu = \frac{1}{2}\left(k_N^\mu + p_N^\mu\right)\,. \tag{4.31}$$

Now, where we are in the non-relativistic limit, we have an expression for the current of the nucleus in terms of lab frame components, which are much easier to measure and quantify:

$$\rho_{s_N s'_N}(\vec{q}) = \rho^{\rm lab}_{s_N s'_N}(\vec{q}) + \mathcal{O}(v^2)\,; \tag{4.32}$$

$$\vec{J}_{s_N s'_N}(\vec{q}) = \rho^{\rm lab}_{s_N s'_N}(\vec{q})\frac{\vec{k}_N + \vec{p}_N}{2m_N} + \vec{J}^{T,{\rm lab}}_{s_N s'_N}(\vec{q}) + \mathcal{O}(v^2)\,, \tag{4.33}$$

where we have defined $\vec{J}^{T,{\rm lab}}_{s_N s'_N}(\vec{q})$ as the component of $\vec{J}$ which is transverse to $\vec{q}$.

To calculate these quantities, we seek to express each as an electromagnetic form factor. Such form factors are approximations to the structure of the nucleus are more important for increasing momentum transfer. For low momentum transfer, the nucleus can be well approximated by a point particle. Examples include the scattering involved in the energy transport within the Sun. However, for larger momentum transfer the internal structure of the nucleus becomes a relevant quantity. In the case that particles are being captured from the galactic halo, the larger momenta involved means that the choice of approximation for the form factors becomes important [537]. The form factor for electromagnetic interactions is typically described in terms of an electric form factor F_E and a magnetic form factor F_M. Naturally, such quantities

describe the charge density ρ via electric interactions and the current density $\vec{J}$ via magnetic interactions respectively. However, it is possible to describe the form factors in an alternative basis, typically in terms of transverse and longitudinal components F_T and F_L respectively. Such quantities have a ready definition in terms of the lab frame quantities we have derived in eqs. (4.32)-(4.33). In momentum space such quantities are given as [536, 538, 539]:

$$4\pi|F_L(\vec{q})|^2 = \frac{1}{2I_N+1}\sum_{s_N}\sum_{s'_N}\rho^{\text{lab}}_{s_N s'_N}(\vec{q})\rho^{\text{lab},*}_{s_N s'_N}(\vec{q})\,; \tag{4.34}$$

$$2\pi|F_T(\vec{q})|^2 = \frac{1}{2I_N+1}\sum_{s_N}\sum_{s'_N}\vec{J}^{T,\text{lab}}_{s_N s'_N}(\vec{q})\cdot\vec{J}^{T,\text{lab},*}_{s_N s'_N}(\vec{q})\,. \tag{4.35}$$

where I_N is the spin of the nucleus and where we have summed over the initial and final spin polarisations. The factors of 4π and 2π are conventions which respectively arise from the multiple expansion of the form factors [536]. The form factors are listed as squared as such terms arise in scattering calculations when the scattering amplitude is sum-squared. Any crossover terms that arise in the squaring of the scattering amplitude vanish as the transverse and longitudinal components are orthogonal, that is,

$$\sum_{s_N}\sum_{s'_N}\left(\vec{J}^{T,\text{lab}}_{s_N s'_N}\right)_i(\vec{q})\rho^{\text{lab},*}_{s_N s'_N}(\vec{q}) = 0\,. \tag{4.36}$$

As the longitudinal form factor describes the charge distribution, it is directly related to the electric form factor with a factor of the total charge of the nucleus Z, given as:

$$|F_E(\vec{q})|^2 = \frac{4\pi}{Z^2}|F_L(\vec{q})|^2\,. \tag{4.37}$$

The magnetic form factor can be described in terms of the longitudinal form factor, with the coefficient describing the behaviour of the form factor as the momentum transfer approaches zero [539]:

$$|F_M(\vec{q})|^2 = \left[\left(\frac{I_N+1}{3I_N}\right)\left(\frac{q}{2m_N}\right)^2\left(\frac{\mu_N}{\frac{e}{2m_p}}\right)^2\right]^{-1}|F_T(\vec{q})|^2\,. \tag{4.38}$$

where I_N, m_N and μ_N are the spin, mass and magnetic dipole moment of the nucleus. Note here that a spin 0 nucleus the magnetic dipole moment is exactly zero, therefore there can be no interaction with the magnetic form factor. A key example is the ^{4}He atoms prevalent in the Sun, which are spin 0 bosons.

The approximations for the form factors F_E and F_M are typically described as analytic functions with parameters determined by matching to experimental results. The simplest approximation is a Dirac delta function, equivalent to approximating the nuclei as a point particle. Such an approximation here is not accurate enough to properly ascertain the capture rate [537]. The next approximation is to assume that the charge and current densities are spherically symmetric with the radial distribution assumed to be Gaussian [226, 540]. For example,

$$\rho(\vec{x}) = \rho_0 e^{-\frac{\vec{x}^2}{4b^2}}\,, \tag{4.39}$$

for arbitrary parameters ρ_0 and b which determine the size and shape of the distribution. The momentum space form factor is then determined using a Fourier transformation:

$$F_E(\vec{q}) = \frac{\rho_0}{Ze}\int d^3x e^{-i\vec{q}\cdot\vec{x}}e^{-\frac{\vec{x}^2}{4b^2}}\,. \tag{4.40}$$

Computing the integrals with the Gaussian functions, we obtain the expression:

$$F_E(\vec{q}) = \frac{1}{Ze}\frac{(2\pi)^{\frac{3}{2}}}{b^3}\rho_0 e^{-\frac{\vec{q}^2}{b^2}}\,. \tag{4.41}$$

To satisfy the normalisation conditions as the momentum transfer approaches zero, the initial charge density ρ_0 must be given by $\rho_0 = \frac{Zeb^3}{(2\pi)^{\frac{3}{2}}}$. The shape of the form factor is dependent on the factor b. The choice of b is determined by the physical size of the nucleus. Empirically, b is given by [246, 327, 356, 495, 541, 542]:

$$b^2 = \frac{3}{R^2}\,, \tag{4.42}$$

where R is the average nuclear radius. Experientially, R can be well approximated by [543]:

$$R = \left(0.3 + 0.89A^{\frac{1}{3}}\right)\,, \tag{4.43}$$

for a nucleus with baryon number A. The form factor is then given as:

$$F_E(\vec{q}) = e^{-3\frac{\vec{q}^2}{R^2}} = e^{-\frac{E_R}{E_0}}\,. \tag{4.44}$$

It is often convenient to express the form factor in terms of the nuclear recoil energy $E_R = \frac{\vec{q}^2}{2m_N}$:

$$F_E(E_R) = e^{-\frac{E_R}{E_0}}\,, \tag{4.45}$$

where $E_0 = \frac{1}{2m_N b^2} = \frac{3}{2m_N R^2}$.

The so-called Gaussian form factor in eq. (4.45) fits the data well where $\frac{E_R}{E_0} = \frac{q^2}{b^2} \lesssim 2$, with an approximate error in the calculation of $\lesssim 10\%$ [246]. Such a form factor is also often used to represent the mass distribution within a nucleus, which also provides a first order approximation to the magnetic form factor F_M. Indeed, here we shall use the approximation $F_E \simeq F_M$ [392]. It is possible to write more accurate form factors, such as a convolution of a uniform charge distribution and the Gaussian charge distribution [544]. However, the improved accuracy of such a form factor at the expense of mathematical complexity is not expected to have a significant effect on the capture rate of dark matter, especially as we will later show that the capture rate reaches a fundamental maximum in the regimes where the electromagnetic dipole interactions are relevant to solar energy transport.

4.2.3 Scattering of electric dipole dark matter

Now that we have an expression for the nuclear and photon components of eq. (4.24), we can consider the current due to the dipolar dark matter components $\langle \vec{p}, s'_\chi |\, j_\mu(q)\, | \vec{k}, s_\chi \rangle$. To solve this term, we must write the Lagrangian in eq. (4.1) in the form of eq. (4.19). Consider expanding the field strength tensor $F_{\mu\nu}$:

$$\mathcal{L}_{\text{ED}} = -\frac{i}{2}\mathcal{D}\overline{\chi}\sigma_{\mu\nu}\gamma^5\chi\left(\partial^\mu A^\nu - \partial^\nu A^\mu\right)\,. \tag{4.46}$$

We may integrate eq. (4.46) by parts (noting the integration of the Lagrangian in the action in eq. (4.18)), and invoke the antisymmetry of $\sigma^{\mu\nu}$ to obtain an expression:

$$\mathcal{L}_{\text{ED}} = i\mathcal{D}\partial^\mu\left(\overline{\chi}\sigma_{\mu\nu}\chi\right)A^\nu\,, \tag{4.47}$$

which allows us to identify the current due to the electromagnetic dipole as:

$$j_\nu(x) = \left(\rho(x), \vec{j}(x)\right) = i\mathcal{D}\partial^\mu\left(\overline{\chi}\sigma_{\mu\nu}\chi\right)\,. \tag{4.48}$$

We can transform to an momentum space current by replacing the derivative operator by the momentum transfer as for eq. (4.21) giving a current of:

$$j_\nu(q) = \left(\rho(q), \vec{j}(q)\right) = \mathcal{D}q^\mu\left(\overline{\chi}\sigma_{\mu\nu}\chi\right)\,. \tag{4.49}$$

We can now seek to evaluate the bilinear by expanding and evaluating the spinors and σ matrices. Here, we expand the Dirac spinor χ in the Dirac representation as:

$$\chi_{ks} = \begin{pmatrix} 1 \\ \frac{\vec{\sigma}\cdot\vec{k}}{E+m} \end{pmatrix} \xi_s \,, \tag{4.50}$$

for some two-component spinor ξ_s, where the spin of the spinor is s and the momentum is $\vec{k}$. Here, we are using $\vec{\sigma} = (\sigma_1, \sigma_2, \sigma_3)$ as a vector consisting of the Pauli matrices. We are considering interactions in the non relativistic limit, so $E \simeq m$ and the spinors are normalised such that $\chi^\dagger\chi = \xi^\dagger\xi = 1$. We evaluate the spatial and temporal components separately. In the Dirac representation, the σ-matrix becomes:

$$\sigma^{i0} = -i \begin{pmatrix} 0 & \sigma^i \\ \sigma^i & 0 \end{pmatrix} \,, \tag{4.51}$$

where the axial γ^5 matrix in the Dirac representation is:

$$\gamma^5 = \begin{pmatrix} 0 & 1 \\ 1 & 0 \end{pmatrix} \,, \tag{4.52}$$

with the conjugate Dirac spinor given by $\overline{\chi} = \chi^\dagger\gamma^0$ where the γ^0 is given in the Dirac representation as:

$$\gamma^0 = \begin{pmatrix} 1 & 0 \\ 0 & -1 \end{pmatrix} \,. \tag{4.53}$$

We can now expand the temporal components of the electromagnetic dipole current as:

$$\overline{\chi}_{p_\chi s'_\chi}\sigma^{i0}\gamma^5\chi_{k_\chi s'_\chi} = -i \begin{pmatrix} \xi^\dagger_{s'_\chi} & \xi^\dagger_{s'_\chi}\left(\frac{\vec{\sigma}\cdot\vec{p}_\chi}{2m_\chi}\right)^\dagger \end{pmatrix} \begin{pmatrix} 1 & 0 \\ 0 & -1 \end{pmatrix} \begin{pmatrix} 0 & \sigma^i \\ \sigma^i & 0 \end{pmatrix} \begin{pmatrix} 0 & 1 \\ 1 & 0 \end{pmatrix} \begin{pmatrix} \xi_{s_\chi} \\ \left(\frac{\vec{\sigma}\cdot\vec{k}_\chi}{2m_\chi}\right)\xi_{s_\chi} \end{pmatrix} \,. \tag{4.54}$$

Expanding out, we reduce to:

$$\overline{\chi}_{p_\chi s'_\chi}\sigma^{i0}\gamma^5\chi_{k_\chi s'_\chi} = -i\xi^\dagger_{s'_\chi}\sigma^i\xi_{s_\chi} + i\xi^\dagger_{s'_\chi}\left(\frac{(\vec{\sigma}\cdot\vec{p}_\chi)\sigma^i(\vec{\sigma}\cdot\vec{k}_\chi)}{4m_\chi^2}\right)\xi_{s_\chi} \,. \tag{4.55}$$

In the non-relativistic limit, the second term is $\mathcal{O}(v^2)$, compared to the first term which is $\mathcal{O}(1)$ so can be ignored. For the first term, we can define the quantity:

$$\vec{s} = \xi^\dagger_{s'_\chi}\vec{\sigma}\xi_{s_\chi} \,. \tag{4.56}$$

The non-relativistic approximation is then:

$$\overline{\chi}_{p_\chi s'_\chi}\sigma^{i0}\gamma^5\chi_{k_\chi s'_\chi} = -is^i \,. \tag{4.57}$$

We then obtain an expression for the charge density due to the electromagnetic dipole from eq. (4.49) as:

$$\rho_{s_\chi s'_\chi}(q) = -i\mathcal{D}\vec{q}\cdot\vec{s}. \tag{4.58}$$

We see that the charge density is maximised where the momentum transfer and spin are parallel as we would expect for an electric dipole. For the spatial components, we use the fact that in the Dirac representation, the spatial components of the σ matrices are given by:

$$\sigma^{ij} = \epsilon^{ijk}\begin{pmatrix} \sigma_k & 0 \\ 0 & \sigma_k \end{pmatrix} \,. \tag{4.59}$$

We then can expand the temporal components as:

$$\overline{\chi}_{p_\chi s'_\chi}\sigma^{ij}\gamma^5\chi_{k_\chi s_\chi} = \epsilon^{ijk}\begin{pmatrix}\xi^\dagger_{s'_\chi} & \xi^\dagger_{s'_\chi}\left(\frac{\vec{\sigma}\cdot\vec{p}_\chi}{2m_\chi}\right)^\dagger\end{pmatrix}\begin{pmatrix}1 & 0\\ 0 & -1\end{pmatrix}\begin{pmatrix}\sigma_k & 0\\ 0 & \sigma_k\end{pmatrix}\begin{pmatrix}0 & 1\\ 1 & 0\end{pmatrix}\begin{pmatrix}\xi_{s_\chi}\\ \left(\frac{\vec{\sigma}\cdot\vec{k}_\chi}{2m_\chi}\right)\xi_{s_\chi}\end{pmatrix}, \tag{4.60}$$

which expands to:

$$\overline{\chi}_{p_\chi s'_\chi}\sigma^{ij}\gamma^5\chi_{k_\chi s_\chi} = \epsilon^{ijk}\frac{1}{2m_\chi}\xi^\dagger_{s'_\chi}\left[\sigma_k\sigma_l k^l_\chi - \sigma_l p^l_\chi\sigma_k\right]\xi_{s_\chi}\,. \tag{4.61}$$

We can simplify with the identity $\sigma_i\sigma_j = \delta_{ij} + i\epsilon_{ijk}\sigma^k$ such that:

$$\overline{\chi}_{p_\chi s'_\chi}\sigma^{ij}\gamma^5\chi_{k_\chi s_\chi} = \epsilon^{ijk}\frac{1}{2m_\chi}\xi^\dagger_{s'_\chi}\left[q_k + i\epsilon_{klm}\left(k^l_\chi + p^l_\chi\right)\sigma^m\right]\xi_{s_\chi}\,, \tag{4.62}$$

since $\vec{q} = \vec{k}_\chi - \vec{p}_\chi$. We therefore obtain an expression for the current due to the electromagentic dipole from eq. (4.49) as:

$$\vec{j}_{s_\chi s'_\chi} = i\mathcal{D}\frac{1}{2m_\chi}\left[\vec{q}\cdot\left(\vec{k}_\chi + \vec{p}_\chi\right)\vec{s} - (\vec{q}\cdot\vec{s})\left(\vec{k}_\chi + \vec{p}_\chi\right)\right]. \tag{4.63}$$

Here, the first term vanishes for elastic scattering since $\vec{q}\cdot\left(\vec{k}_\chi + \vec{p}_\chi\right) = \left(\vec{k}_\chi - \vec{p}_\chi\right)\left(\vec{k}_\chi + \vec{p}_\chi\right) = 0$. The current density is then given by:

$$\vec{j}_{s_\chi s'_\chi} = -i\mathcal{D}\frac{1}{2m_\chi}(\vec{q}\cdot\vec{s})\left(\vec{k}_\chi + \vec{p}_\chi\right). \tag{4.64}$$

Here, we see that the the electromagnetic current is directly proportional to the charge density in eq. (4.58), which is as expected. The direction of the current is an average of the incoming and outgoing momenta.

We now have constructed all of the charge and current elements for both the nucleus and the electromagnetic dipole. We can now combine each of these elements into the scattering amplitude $\mathscr{M}$ using eqs. (4.17) and (4.24). In terms of the charges and currents, the four-vector product gives the scattering amplitude as:

$$\mathscr{M} = -i\frac{e}{|\vec{q}|^2}\left(\rho_{s_\chi s'_\chi}\rho_{s_N s'_N} - \vec{j}_{s_\chi s'_\chi}\cdot\vec{J}_{s_N s'_N}\right), \tag{4.65}$$

where the coefficient has arisen due to the equation of motion of the photon propagator in eq. (4.26). Inserting our expressions for the charge and current elements, we obtain the amplitude as:

$$\mathscr{M} = -e\mathcal{D}\left(\rho^{\text{lab}}_{s_N s'_N}\frac{\vec{q}\cdot\vec{s}}{|\vec{q}|^2} - \frac{\vec{q}\cdot\vec{s}}{2m_\chi|\vec{q}|^2}\left(\vec{k}_\chi + \vec{p}_\chi\right)\cdot\vec{J}^{T,\text{lab}}_{s_N s'_N}(\vec{q})\right). \tag{4.66}$$

In order to calculate the interaction cross section, we need to consider the squared scattering amplitude, summed and averaged over the spins of the initial and final states. For the nucleus, such sums and averages are naturally incorporated into the form factors derived in section 4.2.2. For the dark matter states, these must be computed explicitly. In terms of the longitudinal and transverse form factors, the squared scattering amplitude is therefore given by:

$$\overline{|\mathscr{M}|^2} = e^2\mathcal{D}^2\left(\frac{\overline{s_i q^i s^*_j q^j}}{|\vec{q}|^4}4\pi\left|F_L(\vec{q})\right|^2 + \frac{s_i q^i s^*_j q^j}{4m^2_\chi|\vec{q}|^4}\left(\vec{k}_\chi + \vec{p}_\chi\right)^2 2\pi\left|F_T(\vec{q})\right|^2.\right) \tag{4.67}$$

The average over the initial and final states of the vector $\vec{s}$ can be calculated from the definition as:

$$\overline{s_i s^*_j} = \frac{1}{2}\sum_{s_\chi s'_\chi}\left(\xi^\dagger_{s'_\chi}\sigma_i\xi_{s_\chi}\right)\left(\xi^\dagger_{s'_\chi}\sigma_j\xi_{s_\chi}\right)^* = \sum_{s_\chi s'_\chi}\xi^z_{s'_\chi}\,\dagger\,\sigma_i\xi^\dagger_{s_\chi}\sigma_j\xi_{s'_\chi} = \frac{1}{2}\,\text{Tr}\left[\sigma_i\sigma_j\right] = \delta_{ij}\,, \tag{4.68}$$

where we have expanded the sums in to the trace using the completeness relation for the two-component spinors. The scattering amplitude for the electric dipole dark matter then becomes:

$$\overline{|\mathscr{M}|^2} = \frac{4\pi e^2 \mathcal{D}^2}{|\vec{q}|^2} \left(|F_L(\vec{q})|^2 + \frac{\left(\vec{k}_\chi + \vec{p}_\chi\right)^2}{8m_\chi^2} |F_T(\vec{q})|^2 \right) . \tag{4.69}$$

In the non-relativistic limit, the component $\frac{\left(\vec{k}_\chi+\vec{p}_\chi\right)^2}{8m_\chi^2} \sim \mathcal{O}(v^2)$ with the transverse form factor only contributing additional positive powers of the velocity. By contrast, the longitudinal form factor contains no additional powers of v, so the second term is negligible. We can also expand the longitudinal form factor as the electric form factor in eq. (4.37), giving the amplitude squared as:

$$\overline{|\mathscr{M}|^2} = \frac{Z^2 e^2 \mathcal{D}^2}{|\vec{q}|^2} |F_E(\vec{q})|^2 . \tag{4.70}$$

We are now ready to compute the differential cross section in eq. (4.16). For electric dipole dark matter, the scattering cross section is:

$$\left(\frac{d\sigma}{dE_R}\right)_{\text{EDM}} = \frac{Z^2 e^2 \mathcal{D}^2}{4\pi E_R v^2} |F_E(E_R)|^2 , \tag{4.71}$$

where we have substituted $|\vec{q}|$ for E_R using the definition of the recoil energy in eq. (4.13). As expected, the scattering cross section is directly proportional to the strength of the electromagnetic couplings for each particle, namely the charge Ze of the nucleus and the electric dipole moment $\mathcal{D}$ of the dark matter particle. We shall use the cross section in eq. (4.71) to compute the capture rate of dark matter by the Sun.

To compute the energy transport rate, we require the thermally averaged cross section $\langle\sigma_{\text{EDM}}\rangle$. The thermally averaged cross section is computed by integrating the cross section with a velocity distribution:

$$\langle\sigma_{\text{EDM}}\rangle = \int d^3\vec{v} F(v) \int_{-1}^{1} d\cos\theta_{\text{CM}} \frac{d\sigma}{d\cos\theta_{\text{CM}}} , \tag{4.72}$$

where the Boltzmann distribution $F(v)$ is here defined as:

$$F(v) = \left(\pi(1+\mu)v_T^2\right)^{-\frac{3}{2}} e^{-\frac{v^2}{(1+\mu)v_T^2}} , \tag{4.73}$$

where μ is the mass ratio $\mu = \frac{m_N}{m_\chi}$ and v_T is the thermal velocity defined by:

$$v_T(r) = \sqrt{\frac{2k_B T(r)}{m_\chi}} , \tag{4.74}$$

where k_B is the Boltzmann constant and $T(r)$ is the temperature of the Sun at radius r. The $(1+\mu)$ component accounts for the transformation of the lab frame velocity v to the centre of mass frame in the collision.

Firstly, we transform the differential cross section with respect to recoil energy in eq. (4.71) to a differential cross section with respect to scattering angle using eq. (4.13):

$$\left(\frac{d\sigma}{d\cos\theta_{\text{CM}}}\right)_{\text{ED}} = \frac{M_{\chi,N}^2}{2\pi} \frac{Z^2 e^2 \mathcal{D}^2}{|\vec{q}|^2} |F_E(\vec{q})|^2 . \tag{4.75}$$

Here, we digress slightly to note an important correspondence. The equation above can be written in the functional form:

$$\frac{d\sigma}{d\cos\theta_{\rm CM}} = \sigma_0 \left(\frac{q_0}{q}\right)^2 , \tag{4.76}$$

with the definitions $\sigma_0 = Z^2 e^2 \mathcal{D}^2$ and $q_0^2 = \frac{m_\chi^2}{\pi}(1+\mu)^{-2} = \frac{M_{\chi,N}^2}{\pi}$. Such a functional form, that is $\sigma \sim q^{-2}$, is a momentum dependent cross section that was shown by ref. [532] to have an appreciable effect on the thermal transport of dark matter in the Sun to alleviate the solar abundance problem outlined in the introduction to this chapter. We therefore expect that the electric dipole model will also have a similar effect on the solar abundance problem.

To compute eq. (4.72), we must make the dependence of the momentum transfer on the scattering angle and velocity explicit using:

$$|\vec{q}|^2 = 2M_{\chi,N}^2, v^2(1-\cos\theta_{\rm CM}) , \tag{4.77}$$

such that:

$$\left(\frac{d\sigma}{d\cos\theta_{\rm CM}}\right)_{\rm ED} = \frac{Z^2 e^2 \mathcal{D}^2}{4\pi v^2}(1-\cos\theta_{\rm CM})^{-1} \left|F_E(\vec{q})\right|^2 . \tag{4.78}$$

However, the above expression is problematic: it possesses an infrared divergence as $\cos\theta_{\rm CM} \to 1$. However, such scenarios correspond to forward scattering where there is little to no transfer of energy. To regulate such a divergence, we adopt a technique from plasma physics [545, 546] and consider the momentum transfer cross section σ_T defined as:

$$\sigma_T = (1-\cos\theta_{\rm CM})\sigma . \tag{4.79}$$

Furthermore, as the interactions we are considering are at typically low energies, it is sufficient to consider an approximation to the form factor $|F_E(\vec{q})|^2 = 1$, that is, the nuclei being scattered from appear to the dark matter particles as point particles. Therefore, we compute the total momentum transfer cross section as:

$$\sigma_{T,\rm ED}(v) = \int_{-1}^{1} d\cos\theta_{\rm CM}(1-\cos\theta_{\rm CM}) \left(\frac{d\sigma}{d\cos\theta_{\rm CM}}\right)_{\rm ED} = \frac{Z^2 e^2 \mathcal{D}^2}{2\pi v^2} , \tag{4.80}$$

leading to the thermally averaged cross section as:

$$\langle\sigma_{\rm ED}\rangle = \int d^3\vec{v} F(v)\sigma_{T,\rm ED}(v) = Z^2 e^2 \mathcal{D}^2 \pi^{-\frac{5}{2}}(1+\mu)^{-\frac{3}{2}} v_T^{-3} \frac{1}{2}\int d^3\vec{v}\frac{1}{v^2} e^{-\frac{v^2}{(1+\mu)v_T^2}} . \tag{4.81}$$

Computing the integral:

$$\langle\sigma_{\rm ED}\rangle = Z^2 e^2 \mathcal{D}^2 \pi^{-1}(1+\mu)^{-1} v_T^{-2} , \tag{4.82}$$

in agreement with ref. [532].

We have now constructed the relevant quantities for considering the dynamics of electric dipole dark matter in the Sun. Importantly, we have shown that the electric dipole model corresponds to the q^{-2} case in ref. [532]. We can now move on to the magnetic dipole and anapole models, which will follow a similar treatment to the electric dipole model.

4.2.4 Scattering of magnetic dipole dark matter

Next, we seek to derive the scattering cross section for magnetic dipole dark matter. As for the electric dipole, we seek to write down a current density j_μ in the form of eq. (4.19). Again, we modify the magnetic dipole Lagrangians in eq. (4.4) by expanding the field strength tensor and performing integration by parts. The difference between the magnetic dipole and electric dipole cases is that the magnetic dipole has a tensor component instead of a psuedotensor component with a γ^5 component. After we transform into

momentum space with the transformation $i\partial^\mu \to q^\mu$, the current is given by:

$$j^\mu(q) = \left(\rho(q), \vec{j}(q)\right) = i\mu_\chi q_n u\left(\overline{\chi}\sigma^{\nu\mu}\chi\right) , \tag{4.83}$$

where μ_χ is the magnetic dipole moment of the dark matter particle. As before, we expand the Dirac spinor in terms of a non-relativistic two-component spinor ξ_s as per eq. (4.50). We expand the bilinear component $\overline{\chi}_{p_\chi s'_\chi}\sigma_{\nu\mu}\chi_{k_\chi s_\chi}$ in terms of temporal and spatial components. For the temporal component, using the definition of σ^{i0} in the Dirac representation in eq. (4.51) as:

$$\overline{\chi}_{p_\chi s'_\chi}\sigma_{i0}\chi_{k_\chi s_\chi} = -i\begin{pmatrix}\xi^\dagger_{s'_\chi} & \xi^\dagger_{s'_\chi}\left(\frac{\vec{\sigma}\cdot\vec{p}_\chi}{2m_\chi}\right)^\dagger\end{pmatrix}\begin{pmatrix}1 & 0\\ 0 & -1\end{pmatrix}\begin{pmatrix}0 & \sigma^i\\ \sigma^i & 0\end{pmatrix}\begin{pmatrix}\xi_{s_\chi}\\ \left(\frac{\vec{\sigma}\cdot\vec{k}_\chi}{2m_\chi}\right)\xi_{s_\chi}\end{pmatrix} , \tag{4.84}$$

which expands to give:

$$\overline{\chi}_{p_\chi s'_\chi}\sigma^{i0}\chi_{k_\chi s_\chi} = -i - \frac{i}{2m_\chi}\left(\xi^\dagger_{s'_\chi}\sigma^i\sigma^j k_{\chi_j}\xi_{s_\chi} - \xi^\dagger_{s'_\chi}\sigma^j p_{\chi_j}\sigma^i\xi_{s_\chi}\right) . \tag{4.85}$$

Here, unlike the electric dipole case where the γ^5 prevented the positive energy and negative energy solutions from combining which resulted in a momentum and velocity independent bilinear at non-relativistic velocities, the magnetic dipole case combines the positive and negative energy solutions, which results in two terms which are both dependent to a linear power in the incoming and outgoing momenta. Both terms are therefore at $\mathcal{O}(v)$. We simplify the combinations of the Pauli matrices again using the identity $\sigma^i\sigma^j = \delta^{ij} + i\epsilon^{ijk}\sigma_k$ and the definition of the momentum transfer as $\vec{q} = \vec{p}_\chi - \vec{k}_\chi$ to obtain:

$$\overline{\chi}_{p_\chi s'_\chi}\sigma^{i0}\chi_{k_\chi s_\chi} = -i - \frac{i}{2m_\chi}\left(-q^i\xi^\dagger_{s'_\chi}\xi_{s_\chi} + i\epsilon^{ijk}\left(k_{\chi j} + p_{\chi j}\right)s_k\right) , \tag{4.86}$$

where we have implemented $\vec{s}$ from eq. (4.56). We can therefore evaluate the charge density of the magnetic dipole moment using eq. (4.83) as:

$$\rho_{s_\chi s'_\chi} = \frac{\mu_\chi}{2m_\chi}|\vec{q}|^2\xi^\dagger_{s'_\chi}\xi_{s_\chi} + i\frac{\mu_\chi}{2m_\chi}\vec{q}\cdot\left[\left(\vec{k}_\chi + \vec{p}_\chi\right)\times\vec{s}\right] . \tag{4.87}$$

Whereas for the electric dipole where the charge density was maximised where the momentum and spin were parallel, here the charge density is maximised where the average momentum and spin are perpendicular. Meanwhile, for the spatial components, we obtain using eq. (4.59):

$$\overline{\chi}_{p_\chi s'_\chi}\sigma^{ij}\chi_{k_\chi s_\chi} = \epsilon^{ijk}\begin{pmatrix}\xi^\dagger_{s'_\chi} & \xi^\dagger_{s'_\chi}\left(\frac{\vec{\sigma}\cdot\vec{p}_\chi}{2m_\chi}\right)^\dagger\end{pmatrix}\begin{pmatrix}1 & 0\\ 0 & -1\end{pmatrix}\begin{pmatrix}\sigma_k & 0\\ 0 & \sigma_k\end{pmatrix}\begin{pmatrix}\xi_{s_\chi}\\ \left(\frac{\vec{\sigma}\cdot\vec{k}_\chi}{2m_\chi}\right)\xi_{s_\chi}\end{pmatrix} , \tag{4.88}$$

which expands to:

$$\overline{\chi}_{p_\chi s'_\chi}\sigma^{ij}\chi_{k_\chi s_\chi} = \epsilon^{ijk}\xi_{s'^\dagger_\chi}\left[\sigma_k - \frac{(\vec{\sigma}\cdot\vec{p}_\chi)\sigma_k(\vec{\sigma}\cdot\vec{k}_\chi)}{4m_\chi^2}\right]\xi_{s_\chi} . \tag{4.89}$$

Where the spatial component of the electric dipole mixed the positive and negative energy solutions, the magnetic dipole prevents these from mixing resulting in a velocity and momentum independent term and a term which is negligible in the non-relativistic limit as $p_\chi k_\chi \ll m_\chi^2$ giving a current density for the magnetic dipole as:

$$\vec{j}_{s_\chi s'_\chi} = i\mu_\chi\left(\vec{s}\times\vec{q}\right) . \tag{4.90}$$

The current density maintains a familiar form perpendicular to the spin and momentum transfer. We now are ready to compute the scattering amplitude $\mathscr{M}$ using eq. (4.65) as:

$$\mathscr{M} = -i\frac{e\mu_\chi}{|\vec{q}|^2}\left(-\frac{|\vec{q}|^2}{2m_\chi}\xi^\dagger_{s'_\chi}\xi_{s_\chi}\rho_{s_N s'_N} + \frac{i}{2m_\chi}\vec{q}\cdot\left[\left(\vec{k}_\chi + \vec{p}_\chi\right)\times\vec{s}\right]\rho_{s_N s'_N} - i\left(\vec{s}\times\vec{q}\right)\cdot\vec{J}_{s_N s'_N}\right), \tag{4.91}$$

or in terms of the lab frame nuclear variables in eqs. (4.32)-(4.33):

$$\mathscr{M} = \frac{e\mu_\chi}{|\vec{q}|^2}\left(\frac{i|\vec{q}|^2}{2m_\chi}\xi^\dagger_{s'_\chi}\xi_{s_\chi}\rho^{\text{lab}}_{s_N s'_N} + \left(\vec{s}\times\vec{q}\right)\cdot\vec{V}_T\rho^{\text{lab}}_{s_N s'_N} - \left(\vec{s}\times\vec{q}\right)\cdot\vec{J}^{T,\text{lab}}_{s_N s'_N}\right), \tag{4.92}$$

where we have used the circular shifting property of the scalar triple product $\vec{a}\cdot(\vec{b}\times\vec{c}) = \vec{c}\cdot(\vec{b}\times\vec{a})$ and defined the transverse velocity $\vec{V}_T$ as:

$$\vec{V}_T = \frac{\vec{k}_\chi + \vec{p}_\chi}{2m_\chi} - \frac{\vec{k}_N + \vec{p}_N}{2m_N}\,. \tag{4.93}$$

Note that $\vec{V}_T$ satisfies the transversality condition $\vec{V}_t\cdot\vec{q} = 0$ for $\vec{q} = \vec{p}_\chi - \vec{k}_\chi = \vec{k}_N - \vec{p}_N$. The transverse velocity can be expressed in terms of the lab frame velocity $\vec{v} = \frac{\vec{k}_\chi}{m_\chi} - \frac{\vec{k}_N}{m_N}$ and the momentum transfer as:

$$\vec{V}_T = \frac{\vec{k}_\chi}{m_\chi} - \frac{\vec{k}_N}{m_N} - \frac{\vec{q}}{2m_\chi} - \frac{\vec{q}}{2m_N} = \vec{v} - \frac{\vec{q}}{2M_{\chi,N}}\,, \tag{4.94}$$

for reduced mass of the dark matter particle and nucleus $M_{\chi,N}$. The squared expression is straightforward due to the transversality condition :

$$|\vec{v}|^2 = |\vec{V}_T|^2 + \frac{|\vec{q}|^2}{4M^2_{\chi,N}}\,. \tag{4.95}$$

We can now construct the spin averaged squared amplitude required for the scattering cross section, using the longitudinal and transverse form factors in eq. (4.34) and (4.35):

$$\begin{aligned}\overline{|\mathscr{M}|^2} = \frac{e^2\mu_\chi^2}{|\vec{q}|^4}\frac{1}{2}\sum_{s_\chi s'_\chi}\Bigg[&\overline{\left(\frac{i|\vec{q}|^2}{2m_\chi}\xi^\dagger_{s'_\chi}\xi_{s_\chi} + \epsilon_{ijk}s^i q^i V_T^k\right)\left(-\frac{i|\vec{q}|^2}{2m_\chi}\xi^\dagger_{s_\chi}\xi_{s'_\chi} + \epsilon_{lmn}s^{*l}q^m V_T^n\right)}4\pi|F_L(\vec{q})|^2 \\ &+ \overline{\epsilon_{ijk}s^j q^k\epsilon^{ilm}s^*_l q_m}2\pi|F_T(\vec{q})|^2\Bigg]\,.\end{aligned} \tag{4.96}$$

To compute the spin averages we use the expression:

$$\frac{1}{2}\sum_{s_\chi s'_\chi}\xi^\dagger_{s'_\chi}\xi_{s_\chi}\xi^\dagger_{s_\chi}\xi_{s'_\chi} = \frac{1}{2}\,\text{Tr}[1] = 1\,, \tag{4.97}$$

which follows from the completeness relations for ξ_{s_χ} alongside the similar equation in eq. (4.68). Note that the cross terms in the expansion of the coefficient of the longitudinal component vanish as the Pauli matrices are traceless. The squared scattering amplitude is then:

$$\overline{|\mathscr{M}|^2} = \frac{e^2}{\mu_\chi^2}|\vec{q}|^2\left[\left(\frac{|\vec{q}|^2}{4m_\chi^2} + |\vec{V}_T|^2\right)4\pi|F_L(\vec{q})|^2 + 4\pi|F_T(\vec{q})|^2\right], \tag{4.98}$$

where we have also used the transversality condition for the transverse velocity.

We can now write an expression for the differential cross section with respect to the nuclear recoil energy from eq. (4.16):

$$\left(\frac{d\sigma}{dE_R}\right)_{\text{MD}} = \frac{e^2\mu_\chi^2}{4\pi v^2}\left[Z^2\left(\frac{v^2}{E_R} - \frac{1}{2m_N} - \frac{1}{m_\chi}\right)|F_E(E_R)|^2 + \frac{I_N+1}{3I_N}\frac{\mu_N^2}{\mu_p^2}\frac{m_N}{m_p^2}|F_M(E_R)|^2\right], \tag{4.99}$$

for nuclear recoil energy $E_R = \frac{|\vec{q}|^2}{2m_N}$, nucleus spin I_N, nuclear magnetic moment μ_N in units of the proton magnetic moment μ_p and proton mass m_p, where we have used the expressions for the electric and magnetic form factors in eqs. (4.37) and (4.38). Like the electric dipole moment, this expression is used to calculate the capture rate of dark matter by the Sun. One component of eq. (4.99) couples the magnetic dipole moment to the charge density of the nucleus, the natural magnetic field generated by the motion of the charge distribution relative to the motion of the incoming dark matter particle. The other component couples to the intrinsic magnetic dipole of the nucleus where the nucleus has non-zero spin and hence a non-zero magnetic dipole moment.

We also need to compute the thermally averaged cross section like eq. (4.72) in order to calculate the energy transported by the dark matter in the Sun. We transform to the differential cross section with respect to the scattering angle as:

$$\left(\frac{d\sigma}{d\cos\theta_{\rm CM}}\right)_{\rm MD} = \frac{e^2\mu_\chi^2}{4\pi}\left[Z^2\left(\frac{2M_{\chi,N}^2v^2}{q^2}+\frac{1}{(1+\mu)^2}-\frac{1}{2}\right)|F_E(\vec{q})|^2 + \frac{I_N+1}{3I_N}\frac{M_{\chi,N}^2}{m_p^2}\frac{\mu_N^2}{\mu_p^2}|F_M(\vec{q})|^2\right], \tag{4.100}$$

where the mass ratio μ is defined as $\mu = \frac{m_\chi}{m_N}$. The functional form of the differential cross section is:

$$\frac{d\sigma}{d\cos\theta_{\rm CM}} = \sigma_0\left(\left(\frac{v}{v_0}\right)^2\left(\frac{q_0}{q}\right)^2 + K\right). \tag{4.101}$$

The exact version of the functional form $\sigma \sim const + \frac{v^2}{q^2}$ has not previously been investigated in the context of solar dark matter, although it is fairly similar the canonical momentum and velocity independent models. Indeed, the evaluation of the $\frac{v^2}{q^2}$ reveals only a dependence on the scattering angle, which should average out as the thermalised particles are not biased with respect to any particular direction. Indeed, after identifying $q^2 = 2M_{\chi,N}^2v^2(1-\cos\theta_{\rm CM})$ and setting the form factors to the simplified case $F_E = F_M \simeq 1$ for low momentum scattering, the differential cross section becomes:

$$\left(\frac{d\sigma}{d\cos\theta_{\rm CM}}\right)_{\rm MD} = \frac{e^2\mu_\chi^2}{4\pi}\left[Z^2\left(\frac{1}{1-\cos\theta_{\rm CM}}+\frac{1}{(1+\mu)^2}-\frac{1}{2}\right)+\frac{I_N+1}{3I_N}\frac{M_{\chi,N}^2}{m_p^2}\frac{\mu_N^2}{\mu_p^2}\right], \tag{4.102}$$

which again contains an infrared divergence for the forward scattering case. The divergence is again solved by considering the momentum transfer cross section in eq. (4.79):

$$\begin{aligned}\sigma_{T,\rm MD} &= \int_{-1}^{1} d\cos\theta_{\rm CM}(1-\cos\theta_{\rm CM})\left(\frac{d\sigma}{d\cos\theta_{\rm CM}}\right)_{\rm MD}\\ &= \frac{e^2\mu_\chi^2}{2\pi}\left[Z^2\left(1+\frac{1}{(1+\mu)^2}\right)+\frac{I_N+1}{3I_N}\frac{M_{\chi,N}^2}{m_p^2}\frac{\mu_N^2}{\mu_p^2}\right]\\ &= \langle\sigma_{T,\rm MD}\rangle\,,\end{aligned} \tag{4.103}$$

where the total cross section is exactly equal to the thermally averaged cross section because the total cross section is not dependent on the velocity of the interaction. The only way that the magnetic dipole moment will be different to the vanilla spin-independent cross section for the purposes of thermally averaged energy transport is that the the magnetic dipole moment also contains a spin dependent component.

4.2.5 Scattering of anapole dark matter

Finally, we turn to the cross section for scattering of a dark matter particle from a nucleus via an anapole moment. The methodology will be very similar to the electric and magnetic dipole, and mirrors a similar derivation in ref. [400]. Once again, we seek to write the Lagrangian for the interaction in eq. (4.7) in the form eq. (4.19). To accomplish the task, we must integrate by parts twice as there is an additional derivative on the field strength tensor:

$$\mathcal{L}_{\rm AN} = \frac{1}{2}\frac{g}{\Lambda^2}\left(g^{\mu\sigma}\partial^2 - \partial^\sigma\partial^\mu\right)\overline{\chi}\gamma_\sigma\gamma^5\chi A_\mu\,, \tag{4.104}$$

which enables us to define the electromagentic current in position space for the anapole as:

$$j^\mu(x) = \left(\rho(x), \vec{j}(x)\right) = \frac{1}{2}\frac{g}{\Lambda^2}\left(g^{\mu\sigma}\partial^2 - \partial^\sigma\partial^\mu\right)\overline{\chi}\gamma_\sigma\gamma^5\chi\,, \tag{4.105}$$

which may then be transformed into momentum space using eq. (4.21):

$$j^\mu(q) = \left(\rho(q), \vec{j}(q)\right) = -\frac{1}{2}\frac{g}{\Lambda^2}q^2\left(g^{\mu\nu} - \frac{q^\mu q^\nu}{q^2}\right)\overline{\chi}\gamma_\nu\gamma^5\chi\,. \tag{4.106}$$

Once again, we expand in terms of the spatial and temporal components, however, here we only need consider the regular γ_μ matrices and not the antisymmetric $\sigma_{\mu\nu}$ matrices, so we will not need to consider a convolution of Pauli matrices. Instead, we identify that in the Dirac representation:

$$\gamma_i\gamma^5 = \begin{pmatrix}\sigma_i & 0\\ 0 & -\sigma_i\end{pmatrix} \tag{4.107}$$

$$\gamma^0\gamma^5 = \begin{pmatrix}0 & 1\\ -1 & 0\end{pmatrix}. \tag{4.108}$$

Inserting the Dirac spinor in eq. (4.50) is now straightforward, giving in the non-relativistic limit

$$\overline{\chi}_{p_\chi s'_\chi}\gamma_0\gamma^5\chi_{k_\chi s_\chi} = \frac{\vec{k}_\chi + \vec{p}_\chi}{2m_\chi}\cdot\vec{s}\,; \tag{4.109}$$

$$\overline{\chi}_{p_\chi s'_\chi}\gamma_o\gamma^5\chi_{k_\chi s_\chi} = -s_i\,. \tag{4.110}$$

using $\vec{s}$ defined in eq. (4.56). The spin component in the temporal component arises from the combination of positive and negative energy spinors, whereas the spin component in the spatial component arises from the Pauli matrices that form the components of the γ_i matrices. It therefore becomes straightforward to write down the current and charge densities due to the anapole moment in momentum space as:

$$\rho_{s_\chi s'_\chi} = |\vec{q}|^2\frac{g}{\Lambda^2}\vec{s}\cdot\frac{\vec{k}_\chi + \vec{p}_\chi}{2m_\chi}\,; \tag{4.111}$$

$$\vec{j}_{s_\chi s'_\chi} = |\vec{q}|^2\frac{g}{\Lambda^2}\vec{s}_T\,, \tag{4.112}$$

where $\vec{s}_T$ is defined as:

$$\vec{s}_T = \vec{s} - \frac{(\vec{s}\cdot\vec{q})\vec{q}}{\vec{q}^2}\,, \tag{4.113}$$

being the component of $\vec{s}$ transverse to the momentum exchange $\vec{q}$, assuming the collision is elastic. The expression for the current illuminates the unique feature of the anapole coupling as only coupling to the component of the spin wihch is transverse to the momentum transfer, rather than directly along the momentum transfer as the other two electromagentic moments. Now, inserting into the equation for the

amplitude $\mathscr{M}$ gives:

$$\mathscr{M} = \frac{eg}{\Lambda^2}\vec{s}_T \cdot \left(\frac{\vec{k}_\chi + \vec{p}_\chi}{2m_\chi}\rho_{s_N s'_N} - \vec{J}_{s_N s'_N} \right) , \tag{4.114}$$

where we have substituted $\vec{s}$ for $\vec{s}_T$ since $\vec{q}\cdot(\vec{k}_\chi + \vec{p}_\chi) = 0$. In terms of the lab frame charge and current densities used to define the form factors in eqs. (4.32)-and (4.33), the amplitude becomes:

$$\mathscr{M} = \frac{eg}{\Lambda^2}\vec{s}_T \cdot \left[\left(\frac{\vec{k}_\chi + \vec{p}_\chi}{2m_\chi} - \frac{\vec{k}_N + \vec{p}_N}{2m_N} \right) \rho^{\rm lab}_{s_N s'_N} = \vec{J}^{T,{\rm lab}}_{s_N s'_N} \right] , \tag{4.115}$$

which can be simplified using the definition of the transverse velocity in eq. (4.93) to be:

$$\mathscr{M} = \frac{eg}{\Lambda^2}\vec{s}_T \cdot \left(\vec{V}_T \rho^{\rm lab}_{s_N s'_N} - \vec{J}^{T,{\rm lab}}_{s_N s'_N} \right) . \tag{4.116}$$

Like before, we calculate the squared amplitude by using the sums and averages of the spins in the scattering amplitude, which allows substitution of the longitudinal and transverse form factors in eq. (4.35) and (4.34):

$$\overline{|\mathscr{M}|^2} = \frac{e^2 g^2}{\Lambda^2}\left(\overline{(\vec{s}_T \cdot \vec{V}_T)(\vec{s}^*_T \cdot \vec{V}_T)} 4\pi |F_L(\vec{q})|^2 + \overline{\vec{s}_T \cdot \vec{s}^*_T} 2\pi |F_T(\vec{q})|^2 \right) . \tag{4.117}$$

The averages over the spin may be solved using eq. (4.68) to note that:

$$\overline{\vec{s}_{T,i}\vec{s}^*_{T,j}} = \overline{(s_i - s_k \hat{q}_k \hat{q}_i)(s_j - s_l \hat{q}_l \hat{q}_j)^*} = \delta_{ij} - \hat{q}_i \hat{q}_j , \tag{4.118}$$

where $\hat{q}$ is a unit vector in the direction of $\vec{q}$ and we have used the transversality condition $\vec{s}_T \cdot \vec{q} = 0$. The transversality condition $\vec{V}_T \cdot \vec{q} = 0$ for the transverse velocity then gives the squared amplitude as:

$$\overline{|\mathscr{M}|^2} = \frac{4\pi e^2 g^2}{\Lambda^4}\left(|\vec{V}_T|^2 |F_L(\vec{q})|^2 + |F_T(\vec{q})|^2 \right) , \tag{4.119}$$

giving us a differential cross section with respect to the recoil energy from eq. (4.16): as

$$\left(\frac{d\sigma}{dE_R} \right)_{\rm AN} = \frac{e^2 g^2 m_N}{2\pi v^2 \Lambda^4}\left[Z^2 \left(v^2 - E_R \frac{m_N}{2M^2_{\chi,N}} \right) |F_E(E_R)|^2 + E_R \frac{I_N + 1}{3I_N}\frac{\mu_N^2}{\mu_p^2}\frac{m_N}{m_p^2}|F_M(E_R)|^2 \right] , \tag{4.120}$$

where the E_R terms have arisen from the definition of the transverse velocity in eq. (4.93), and we have substituted the longitudinal and transverse form factors for the electric and magnetic form factors in eqs. (4.37) and (4.38). Once again, the form of the cross section above is required for calculating the capture rate of dark matter by the Sun.

To compute the thermally averaged cross section, we transform eq. (4.120) into the differential cross section with respect to the scattering angle, giving:

$$\left(\frac{d\sigma}{d\cos\theta_{\rm CM}} \right)_{\rm AN} = \frac{M^2_{\chi,N}}{2\pi}\frac{e^2 g^2}{\Lambda^4}\left[Z^2 \left(v^2 - \frac{q^2}{4M^2_{\chi,N}} \right) + \frac{I_N + 1}{3I_N}\frac{q^2}{2m_N^2}\frac{\mu_N^2}{\mu_p^2}\frac{m_N^2}{m_p^2} \right] , \tag{4.121}$$

where we have set the electromagnetic form factors to unity for low momentum scattering. Here, we see the rather unique functional form of the cross section to be:

$$\frac{d\sigma}{d\cos\theta_{\rm CM}} = \sigma_0 \left[\frac{1}{2}\left(\frac{v}{v_0} \right)^2 + \left(\frac{q}{q_0} \right)^2 \right] , \tag{4.122}$$

where $\sigma_0 = \frac{M^2_{\chi,N}}{2\pi}\frac{e^2 g^2}{\Lambda^4}$, $v_0 = \frac{1}{Z}$ and $q_0 = \left(-\frac{Z^2}{M^2_{\chi,N}} + \frac{1}{2m_N^2}\frac{\mu_N^2}{\mu_p^2}\frac{m_N^2}{m_p^2} \right)^{-\frac{1}{2}}$. Such a functional form is a linear combination of two of the functional forms considered in ref. [532], namely $\sigma \sim v^2 + q^2$. Such a combination

is unique and has not been previously considered in the literature in regard to solar models, making the implementation here novel.

For the thermally averaged cross section, we expand $q^2 = 2M_{\chi,N}^2 v^2(1-\cos\theta_{\rm CM}$. As we do not have any infrared divergences here, we can directly calculate the total velocity dependent cross section to be:

$$\sigma_{\rm AN}(v) = \frac{M_{\chi,N}^2}{2\pi}\frac{e^2 g^2}{\Lambda^4}\left[Z^2 v^2 + \frac{I_N+1}{3I_N}\frac{2M_{\chi,N}^2 v^2}{m_N^2}\frac{\mu_N^2}{\mu_p^2}\frac{m_N^2}{m_p^2}\right]. \tag{4.123}$$

The thermally averaged cross section is then calculated using the distribution in eq. (4.73) to be:

$$\begin{aligned}\langle\sigma_{\rm AN}\rangle &= \frac{M_{\chi,N}^2}{2\pi}\frac{e^2 g^2}{\Lambda^4}\left[\pi(1+\mu)v_T^2\right]^{-\frac{3}{2}}\int d^3 v e^{-\frac{v^2}{(1+\mu)v_T^2}}\left[Z^2 v^2 + \frac{I_N+1}{3I_N}\frac{2M_{\chi,N}^2 v^2}{m_N^2}\frac{\mu_N^2}{\mu_p^2}\frac{m_N^2}{m_p^2}\right] \\ &= \frac{3M_{\chi,N}^2}{4\pi}\frac{e^2 g^2}{\Lambda^4}(1+\mu)v_T^2\left(Z^2 + \frac{I_N+1}{I_N}\frac{2M_{\chi,N}^2}{m_N^2}\frac{\mu_N^2}{\mu_p^2}\frac{m_N^2}{m_p^2}\right),\end{aligned} \tag{4.124}$$

where v_T is the thermal velocity in eq. (4.74) and the mass ratio μ is defined as $\mu = \frac{m_\chi}{m_N}$.

To recap, we have derived the differential cross sections for electric dipole, magnetic dipole and anapole dark matter scattering from a nucleus. We parametrised the scattering amplitude in each case in terms of electromagnetic charge and current densities j_μ generated by each operator as well as the nucleus J^μ, with the equation of motion for the photon forming the propagator between the two. In the latter case, we approximated the charge and current densities inside the atomic nucleus with electromagnetic form factors which are calibrated using techniques like deep inelastic scattering. However, for low momentum as is the case for energy transport inside the Sun, these form factors can be well approximated by a Dirac delta function in position space - unity in momentum space, that is, a single point particle. For the higher momentum collisions such as capture of the particle from the galactic halo, we considered approximating the form factors by a Gaussian form factor. We then computed the thermally averaged cross sections, utilising the momentum transfer cross section to regulate infrared divergences. Along the way, we discovered the functional form for the differential cross sections: the electric dipole cross section is proportional to q^{-2}, the magnetic dipole cross section is proportional to $\frac{v^2}{q^2} + const.$ and the anapole cross section is proportional to $v^2 + q^2$. Of these three functional forms, the first and last are of the velocity and momentum dependent types that may alleviate the problems with the sound speed profile in the Sun, the latter never having been investigated before. The remaining form has previously been investigated in ref. [547], but did not consider the correct formalisms juxtaposing Knusden and local thermal equilibrium transport that we will develop shortly.

4.3 Population of dark matter particles in the Sun

As we have now developed the theoretical understanding of the electromagnetic dipole models and their interactions with the nuclei that are abundant in the Sun, we now turn to quantifying the effects of such interactions on the mechanisms of the Sun on a global scale. We seek to construct the theoretical formalisms required to describe the relevant physics and any observables that can be used to distinguish and promote different models of dark matter. There will be two key quantities to consider. The first is the total population of dark matter particles within the Sun. Increasing the mass of particles in the solar halo will increase the scale of any changes to the solar structure itself by multiplying any other processes. The second quantity is the energy transport within the Sun due to the dark matter particles. The energy transport can alter the temperature of the different regions of the Sun in a manner that can be readily observed using helioseismology and other related techniques. Models which degrade the helioseismology

measurements can be considered unfavourable, while models which improve the helioseismology fits can perhaps provide a clue towards the true nature of dark matter.

First, consider the total population of dark matter in the Sun, an important first step in determining whether observable physical effects may exist. The number of dark matter particles N in the Sun is determined by the rate equation:

$$\frac{dN}{dt} = C(t) - A(t) - E(t)\,, \tag{4.125}$$

where $C(t)$ is the rate at which the Sun captures dark matter from the galactic halo by scattering the particles to velocities lower than the escape velocity of the Sun, $A(t)$ is the rate at which dark matter particles in the Sun collide with other dark matter particles within the Sun and annihilate, and $E(t)$ is the rate at which dark matter particles already in the Sun scatter to velocities higher than the escape velocity and evaporate [495]. The capture rate $C(t)$ is the most important of these three processes: it is the only way for dark matter particles to build up their quantity inside the Sun as no Standard Model processes at temperatures present in the Sun are expected to spontaneously produce dark matter. Particles in the galactic halo moving in some velocity distribution are gravitationally attracted towards the Sun, but an energy-depleting collision with a stellar nucleus is required to kick the particle into the solar halo. The process therefore is highly dependent on the scattering dynamics of the dark matter.

The annihilation processes within the Sun are a key way of reducing the quantity of dark matter particles present, reducing the impact of the dark matter particles on the solar physics. For example, any Majorana particle present will undergo self-annihilations, as will any combined presence of Dirac dark matter and its antiparticle. As the electric and magnetic dipoles are not present for Majorana fermions as discussed in section 2.5.1, the complications arising from self-annihilations are automatically resolved. For a Majorana anapole dark matter, some annihilation may exist, but we assume that the rate is small compared to the capture rate. The full consideration of Majorana anapole dark matter annihilations are beyond the scope of this work. For Dirac dark matter, we assume that the dark matter is asymmetric, that is, it is present in the universe in only its matter form much like the Standard Model [494,495,533,548–550]. Limits on the levels of asymmetry of dark matter suggest that the fraction of matter to antimatter may be as low as 10^{-10} in order to ensure a stable proportion of dark matter relative to the Standard Model in the universe [551]. Such asymmetry suppresses the annihilation rate relative to the capture rate such that $A(t) \simeq 0$. Even if a small proportion of the dark matter antiparticle is present, if it has a different interaction cross section then the symmetric component may still be captured alone in large quantities [550].

The final process affecting the population of dark matter particles is evaporation, which depletes dark matter by scattering dark matter particles to velocities greater than the local escape velocity. Evaporation events are relatively rare due to the large momentum transfer that is required between the solar nuclei and the dark matter particle [327, 479]. Typical velocities for dark matter particles in the Sun are ~ 100 km s^{-1}, while the local escape velocity can be up to ~ 1400 km s^{-1}. For dark matter particles which are significantly heavier than the majority of the population of nuclei in the Sun like hydrogen and helium, large momentum transfer is required, whereas light dark matter is more susceptible to evaporation. For dark matter above the so-called evaporation mass, the rate of evaporation can essentially be ignored [552], unless there is a very close match between the dark matter mass and one of the heavy nuclei in the Sun [327]. Estimates suggest that the evaporation mass occurs at approximately 4 GeV, roughly the mass of the helium in the Sun. Below the threshold, evaporation is considered to be a significant component of the rate equation in eq. (4.125). In the present work, we include dark matter masses down to $m_\chi = 3$ GeV, and note that such models should be treated with care. Meanwhile, we can safely ignore the evaporation effects for all higher mass models.

We turn to calculating the capture rate $C(t)$ of dark matter particles by the Sun, the dominant component of eq. (4.125). The description of the capture rate follows refs. [328, 553], which we generalise to allow for dark matter interacting via an electromagnetic dipole moment with momentum and velocity dependent cross sections following refs. [494, 495].

Consider a dark matter particle moving through the galactic halo with some velocity u. The distribution of velocities of all dark matter particle velocities in the halo is described by a Maxwell-Boltzmann distribution. In the galactic rest frame, the distribution is unbiased with some velocity dispersion u_0 typically taken as $u_0 = 270$ km s^{-1}. However, we need to consider the motion of the Sun with respect to the galactic rest frame. In the solar rest frame, which moves with a velocity $u_\odot = 220$ km s^{-1} with respect to the galactic rest frame, the distribution of velocities is given by a modified Maxwell-Boltzmann distribution as [554]:

$$f(u) = \left(\frac{3}{2}\right)^{\frac{3}{2}} \frac{4}{\sqrt{\pi}} \frac{\rho_\chi}{m_\chi} \frac{u^2}{u_0^3} \exp\left(-\frac{3(u_\odot^2 + u^2)}{2u_0^2}\right) \frac{\sinh\left(3uu_\odot/u_0^2\right)}{3uu_\odot/u_0^2} \,. \tag{4.126}$$

Now consider such particles passing through a spherical shell centred around the Sun with radius R, with values typically much larger than the solar radius $R_\odot$ so that the effect of gravitational attraction is negligible. The particles are assumed to have a uniform angular distribution. The local flux $d\mathscr{F}_a$ of halo dark matter particles passing through a surface element da is given by:

$$d\mathscr{F}_a = u \cos\theta da \, dn \,. \tag{4.127}$$

where θ is the direction of travel of each particle and dn is the local number density of dark matter particles travelling in the direction $\theta + d\theta$, given by:

$$dn = \frac{1}{2} f(u) du \, d(\cos\theta) \,, \tag{4.128}$$

where $f(u)$ is the velocity distribution of halo particles, where the factor of $\frac{1}{2}$ arises as the flux is azimuthally symmetric. Integrating over the surface area of the entire shell $\int_a da = 2\pi R^2$ gives the differential flux passing through the entire shell $d\mathscr{F}_s$ as:

$$d\mathscr{F}_s = 2\pi R^2 f(u) u \cos\theta \, du \, d(\cos\theta) \,. \tag{4.129}$$

Given the rate at which the particles pass through the shell, there is some probability dP that the particle will scatter in the shell to a velocity less than the escape velocity of the Sun $v_{\rm esc}$. The particle passing through the shell will fall into the gravitational well of the Sun, giving it a velocity w of:

$$w(r) = \sqrt{u^2 + v_{\rm esc}(r)^2} \,, \tag{4.130}$$

where u is the initial halo velocity of the particle before it has entered the gravitational well. Note here that we do not consider the accelerated velocity w when considering the flux $\mathscr{F}$ as in the latter case we are considering the number that have arrived from the halo itself, whereas now we are considering the rate at which those particles are being scattered. Let $\Omega(w, r)$ be the rate at which the particles scatter from a velocity w to a velocity less than the escape velocity $v_{\rm esc}$ at a radius r. The probability that a particle will in a second shell contained within the Sun with thickness dl will be captured is then given by:

$$dP = \Omega(w, r) \frac{dl}{w} \,, \tag{4.131}$$

since $\frac{dl}{w}$ is the time spent by the particle in the shell. The distance travelled in the shell is determined by the angle ϕ at which the angle passes through the shell by:

$$dr = \cos\phi dl\,, \tag{4.132}$$

for a shell with radius between r and $r + dr$. The two angles here, ϕ and θ are related as the angle before and after gravitational acceleration and are related by conservation of angular momentum as:

$$Ru\sin\theta = rw\sin\phi\,, \tag{4.133}$$

or in terms of $\cos\phi$ as:

$$\cos\phi = \sqrt{1 - \frac{R^2u^2\sin^2\theta}{r^2w^2}}\,. \tag{4.134}$$

The probability of capturing a particle in the shell is then given by:

$$dP = \frac{\Omega(w,r)}{w}\left[1 - \frac{R^2u^2\sin^2\theta}{r^2w^2}\right]^{-\frac{1}{2}} dr\,. \tag{4.135}$$

Now, the capture rate dC is determined as the rate at which particles passing through the shell with flux $d\mathscr{F}_s$ are captured by the material in the shell, dP, namely:

$$dC = d\mathscr{F}_s\, dP\,, \tag{4.136}$$

that is,

$$dC = 2\pi R^2 f(u)u\frac{\Omega(w,r)}{w}\left[1 - \frac{R^2u^2\sin^2\theta}{r^2w^2}\right]^{-\frac{1}{2}} dr\, du\, d(\cos\theta)\,. \tag{4.137}$$

The total capture rate is then integrated over these variables to give:

$$C = 2\pi R^2\int_0^{R_\odot}\int_0^\infty du\int_{-1}^1 d\cos\theta f(u)u\frac{\Omega(w,r)}{w}\cos\theta\left[1 - \frac{R^2u^2\sin^2\theta}{r^2w^2}\right]^{-\frac{1}{2}}\,, \tag{4.138}$$

where $R_\odot$ is the radius of the Sun. Performing the integration with respect to $\cos\theta$ removes the dependence on the outer shell, giving the expression from ref. [327]:

$$C = 4\pi\int_0^{R_\odot} r^2dr\int_0^\infty du\frac{f(u)}{u}w(r)\Omega(w,r)\,. \tag{4.139}$$

The relevant particle physics are encapsulated by the rate of particle capture $\Omega(w,r)$, which is the total rate of scattering subject to the kinematic constraints that the velocity must drop from w to less than the escape velocity $v_{\rm esc}$. The minimum required loss in kinetic energy is therefore given by:

$$E_R \geq \frac{1}{2}m_\chi w^2 - \frac{1}{2}m_\chi v_{\rm esc}^2 = \frac{1}{2}m_\chi u^2\,, \tag{4.140}$$

using the definition for w in eq. (4.130), where E_R is equivalently the nucleus recoil energy by the conservation of energy. The maximum possible recoil energy occurs where the nucleus initially has zero kinetic energy. The bound on the recoil energy is then given by:

$$E_R \leq \frac{1}{2}m_\chi w^2 - \frac{1}{2}m_\chi w_f^2\,, \tag{4.141}$$

where w_f is the velocity of the particle after the collision with a zero-velocity nucleus, determined kinematically to be $w_f = \frac{m_\chi - m_N}{m_\chi + m_N} w$, which provides an upper bound as:

$$E_R \leq \frac{2m_\chi^2 m_N}{(m_\chi + m_N)^2} w^2 = \frac{1}{2} m_\chi w^2 \frac{\mu}{\mu_+}\,, \tag{4.142}$$

using the standard notation [328] $\mu = \frac{m_\chi}{m_N}$ and $\mu_\pm = \frac{\mu \pm 1}{2}$. The bounds in eqs. (4.140) and (4.142) provide the required limits on the total cross section for scattering to kinematically capture particles. We therefore can construct the rate of particle capture $\Omega(w, r)$ as:

$$\Omega(w, r) = w(r) \sum_i n_i(r, t) \int_{\frac{m_\chi u^2}{2}}^{\frac{m_\chi w^2 \mu}{2\mu_+^2}} \frac{d\sigma_i}{dE_R} dE_R\,, \tag{4.143}$$

where we have summed over the nuclear species i, and where $n_i(r, t)$ is the number density of nuclear species i at some location a radius r from the centre of the Sun. The number density is time dependent as the production and transfer of nuclear species via fusion throughout the evolution of the Sun changes the composition of the different nuclear species. Therefore, the overall rate is also time-dependent during the evolution of the Sun. For each dark matter model, we compute the integral of the cross section in eq. (4.143) numerically using our expressions for the scattering cross sections in eqs. (4.71), (4.99) and (4.120). We shall compare our results to another model with a spin-independent interaction with cross section.

Additionally, there exists a fundamental limit to the capture rate; whereby the total cross section is equal to the total cross section of the Sun $\sigma = \pi R_\odot^2$. Here, every particle that collides with the Sun from the halo will be captured making the Sun opaque to dark matter, the so-called solar vacuum cleaner [495]. The capture rate is said to be saturated. The result is an analytic expression for the maximum capture rate:

$$C_{\max} = \frac{1}{3}\pi \frac{\rho_\chi}{m_\chi} R_\odot^2(t) \left(e^{-\frac{3}{2}\frac{u_\odot^2}{u_0^2}} \sqrt{\frac{6}{\pi}} u_0 + \frac{6G_N M_\odot + R_\odot(u_0^2 + 3u_\odot^2)}{R_\odot u_\odot} \operatorname{erf}\left[\sqrt{\frac{3}{2}} \frac{u_\odot}{u_0} \right] \right)\,. \tag{4.144}$$

The total capture rate is then the lesser of eqs. (4.139) and (4.144).

To calculate the capture rate for each model, we must consider the number density of each element as a function of the radius of the Sun. To compare capture rates here, we use the present day solar model AGSS09ph [491, 492]. When we later perform full simulations of the Sun, we can consider using the solar model generated at each time step of the simulation to compute the capture rate, although for the vast majority of cases we consider, we are at the maximum capture rate imposed from the saturation case in eq. (4.144).

We compute the capture rate for modern day solar physics for each of the three electromagnetic dipole models as well as a constant cross section, spin independent model in figure 4.2. Areas of the parameter space which produce large capture rates are shown in red or black. Areas with a reduced capture rate are shown in yellow and white. For each mass value, we compute the saturation limit as a function of the interaction strength, shown as a blue line on each graph. Above the saturation limit, the capture rate is constant, with a slight increase for smaller dark matter masses. Here, there is no dependence on the strength of the interaction as almost all particles are being captured regardless of their strength. Below the saturation cross section, the capture rate decreases by the square of the interaction strength as expected due to the dependence on the cross section on the interaction strength. The amounts of dark matter captured in these regimes are diminishingly small. We expect that the total effect on the solar observables will be greatly reduced in regimes where the capture rate is not saturated. By way of comparison, the total amount of mass of dark matter captured by the Sun per year when the capture is

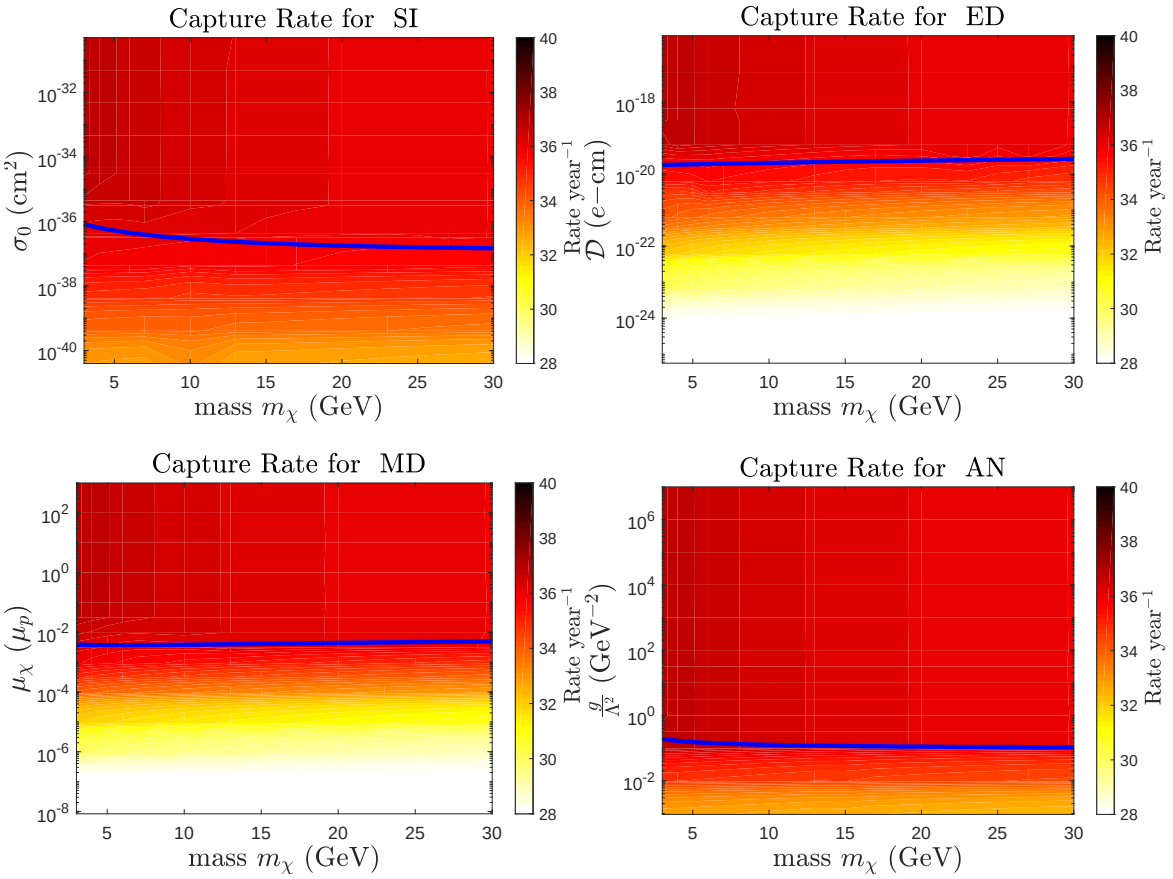

Figure 4.2: Capture rate for spin independent dark matter (top left), electric dipole dark matter (top right), magnetic dipole dark matter (bottom left) and anapole dark matter (bottom right). The colour axis shows the base-10 logarithm of the capture rate in units of year^{-1}. The point at which saturation first occurs is shown as a blue line.

saturated is roughly the same as the mass lost by the Sun due to fusion reactions every second. The total mass of dark matter in the Sun is roughly the same as the mass of a dwarf planet or large asteroid [555]. Although these quantities are not large enough to significantly alter the main solar observables such as mass and luminosity, we shall see that there is a sufficient effect on the helioseismology of the Sun.

4.4 Energy transport

We now turn to the calculation of the energy transported by dark matter throughout the internal structures of the Sun. The total transported energy is described by two quantities, the distribution of dark matter within the Sun and the local luminosity of energy transported. To calculate these quantities, we follow the procedure of refs. [480, 532, 533]. The equation of motion of the phase space distribution $F(\vec{v}, \vec{r}, t)$ of dark matter is described by a Boltzmann collision equation:

$$DF = l_\chi^{-1} CF \,, \tag{4.145}$$

where D is a differential operator describing the flow in phase space due to the motion of the particles, l_χ is the mean free path of a dark matter particle and C is the collision operator. The mean free path is given as:

$$l_\chi(\vec{r}) = \left[\sum_i \sigma_i n_i(\vec{r}) \right]^{-1} , \tag{4.146}$$

for total cross section σ_i of scattering between the dark matter particles and an atomic nucleus species i with abundance n_i. The collision operator is determined in a regime known as the dilute gas approximation, whereby the expected collision rate between the dark matter and the nuclei is considered to be much larger than the self-collision rate of dark matter [480]. Here the collision operator is given as:

$$CF = \int d^3v C_{\text{in}}(\vec{u}, \vec{v}, \vec{r}, t) F(\vec{v}, \vec{r}, t) - C_{\text{out}}(\vec{u}, \vec{r}, t) = F(\vec{u}, \vec{r}, t)\,, \tag{4.147}$$

where C_{in} is the rate at which particles scatter from velocity $\vec{v}$ to a specific velocity $\vec{u}$ and C_{out} is the rate at which particles scatter from velocity $\vec{u}$ to any other velocity. The method for solving eq. (4.145) is to consider a decomposition of the phase space into spherical harmonics $Y^{jm}(\hat{r})$ and expanding perturbatively as $F = F_0 + \epsilon F_1 + \mathcal{O}(\epsilon^2)$. The typical notation defines F_ν^{jm}, corresponding to the jm spherical harmonic and order ν in ϵ in the perturbative expansion. Here, the expansion parameter is defined as $\epsilon = l_\chi(r)|\nabla \ln T(r)|$ for a temperature T. ϵ is required to be small so that the mean free path is much less than the change in the temperature gradient. The first order approximation, corresponding to the case where the dark matter is in local thermal equilibrium with the solar material is then:

$$DF_0^{jm} = \frac{\epsilon}{l_\chi} CF_1 jm\,. \tag{4.148}$$

From here, it is also typical to normalise the distributions to remove the dependence on the amount of dark matter from the scale of flow in phase space:

$$f_\nu^{jm}(\vec{x}, \vec{r}) dx = \frac{1}{n_\chi(\vec{r})} F_\nu^{jm}(\vec{v}, \vec{r}) dv\,, \tag{4.149}$$

where n_χ is the local number density of dark matter particles, and the normalised velocities $\vec{x}$ and $\vec{y}$ are defined as $\vec{x} = \frac{\vec{v}}{v_T}$ and $\vec{y} = \frac{\vec{u}}{v_T}$ for v_T the thermal velocity defined in eq. (4.74).

The dynamics of the energy transport can now be parametrised into two dimensionless parameters: the thermal diffusivity α and the thermal conductivity κ [480, 532, 533]. The thermal diffusivity describes the spread of dark matter throughout the solar dark matter halo due to thermal pressure. The thermal conductivity parametrises the efficiency of the dark matter at transporting dark matter within the Sun. The diffusivity is defined as:

$$\alpha = \frac{\langle y |\, C^{-1}\, | y^3 f_0^{00} \rangle}{\langle y |\, C^{-1}\, | f_0^{00} \rangle}\,, \tag{4.150}$$

for inverse collision operator C^{-1}, where the Dirac bra-ket notation is here defined as:

$$\langle g |\, Q\, | f \rangle = \int dy dx\, g(y) Q(y, x) f(x)\,. \tag{4.151}$$

The thermal conductivity is also defined as:

$$\kappa = \frac{\sqrt{2}}{3} \int dy\, y^3 f_1^{10}\,. \tag{4.152}$$

The first order term in phase space f_1^{10} is calculated using the thermal diffusivity and the zero-th order term f_0^{00} by ref. [532]:

$$\alpha y - y^3 f_0^{00}(y) = \int dx\, C(y, x, r) f_1^{10}(x)\,. \tag{4.153}$$

The full details of the derivations of α and κ can be found in ref. [480]. The thermal diffusivity and conductivity are dependent on the cross sections from the different nuclear species and are generalised

from species specific diffusivity and conductivity as:

$$\alpha(r,t) = l_\chi(r,t,) \sum_i \sigma_i n_i(r,t) \alpha_i(\mu)\,, \tag{4.154}$$

and

$$\kappa(r,t) = \left[l_\chi(r,t) \sim_i \frac{\sigma_i n_i(r,t)}{\kappa_i(\mu)} \right]^{-1}\,, \tag{4.155}$$

where α and κ are now only dependent on the mass ratio $\mu = \frac{m_\chi}{m_N}$ and can be calculated as a parameter independently for each dark matter model.

Using these expressions, it is possible to show that the density profile $n_\chi(r)$ can be given by [532, 533]:

$$n_\chi(r) = n_\chi(0) \left[\frac{T(r)}{T(0)}\right]^{-\frac{3}{2}} \exp\left[-\int_0^r dr' \frac{k_B \alpha(r') \frac{dT(r')}{dr'} + m_\chi \frac{d\phi(r')}{dr'}}{k_B T(r')} \right]\,, \tag{4.156}$$

where k_B is the Boltzmann constant, $T(r)$ is the temperature of the Sun and $\phi(r)$ is the gravitational potential within the Star. The factors of $n_\chi(0)$ and $T(0)$ normalise the total expression given the total number of dark matter particles in the Sun and the core temperature of the Sun. The two terms in the integral describe the physical process which affect the distribution of the dark matter. The $\frac{d\phi}{dr}$ term captures the gravitational pull of the Sun on the dark matter, while the $\frac{dT}{dr}$ describes the conduction of dark matter due to interactions with the Sun.

Further, the luminosity carried by the dark matter is given by:

$$L_\chi(r) = 4\pi r^2 \kappa(r) n_\chi(r) l_\chi(r) \left[\frac{k_B T(r)}{m_\chi}\right]^{\frac{1}{2}} k_B \frac{dT}{dr}\,. \tag{4.157}$$

Here, the thermal conductivity κ describes the efficiency of transport, while the mean free path l_χ describes the distance over which the energy can be transported. The expression for the luminosity transported in ref. [532], which generalised the derivations for momentum and velocity dependent cross sections, is incorrect by a factor of ζ^{2n}, which was remedied by ref. [533]. The correction of the error modified the improvement in the sound speed profile, now favouring high powers of momentum transfer in the functional form of the cross section.

In eqs. (4.156) and (4.157), we have the required components for calculating the transport due to dark matter in the Sun, parametrised by α_i and κ_i. We will need to compute α_i and κ_i for each of our models, however, first we consider the case where approximation in eq. (4.148) breaks down.

4.4.1 Knusden vs. LTE transport

Where the mean free path of the dark matter particle is sufficiently large, the physical distance between two interactions of the dark matter and the solar nuclei overcomes the temperature gradient and the assumption of local thermal equilibrium no longer applies. Ref. [480] estimates that the breakdown of these assumptions occurs when the mean free path exceeds $l_\chi \gg r_\chi$ where the scale height r_χ is defined as:

$$r_\chi = \left(\frac{3 k_B T_c}{2\pi G_N \rho_c m_\chi} \right)^{\frac{1}{2}}\,, \tag{4.158}$$

where T_c and ρ_c are the temperature and physical matter densities at the core of the Sun, and G_N is the Newtonian gravitational constant. Beyond this limit, the energy transfer is in the so-called Knusden regime, whereby the dark matter may travel for long distances between interactions, hence allowing for long distance energy transport. The downside to the Knusden regime is that the strength of the interaction

is usually quite weak, so the amount of energy transported will decrease. Conversely, if the interaction is well within the local thermal equilibrium regime, the mean free path will be too short and although interactions are plentiful, the distance that energy is transported is relatively small.

The effects of the Knusden regime are accounted for by empirical corrections [480, 481, 528, 554, 556]. The corrected luminosity is given by:

$$L_\chi(r) = \mathfrak{f}(K)\mathfrak{h}(r,t)L_{\chi,\mathrm{LTE}}(r)\,, \tag{4.159}$$

for L_χ defined in eq. (4.157). The corrected number density of dark matter is also given by:

$$n_\chi(r) = \mathfrak{f}(K)n_{\chi,\mathrm{LTE}}(r) + [1-\mathfrak{f}(K)]\,n_{\chi,\mathrm{iso}}\,, \tag{4.160}$$

for $n_{\chi,\mathrm{LTE}}(r)$ given by eq. (4.156) and where $n_{\chi,\mathrm{iso}}$ is the number density of an collisionless halo of dark matter, given by:

$$n_{\chi,\mathrm{iso}} = N(t)\frac{e^{-\frac{r^2}{r_\chi^2}}}{\pi^{\frac{3}{2}}r_\chi^3}\,, \tag{4.161}$$

for $N(t)$ as the total number of dark matter particles. The empirical parameters $\mathfrak{f}(K)$ and $\mathfrak{h}(r)$ are defined as:

$$\mathfrak{f}(K) = \frac{1}{1+\left(\frac{K}{K_0}\right)^{\frac{1}{\tau}}}\,; \tag{4.162}$$

and

$$\mathfrak{h}(r) = \left(\frac{r-r_\chi}{r_\chi}\right)^3 + 1\,. \tag{4.163}$$

where $K = \frac{l_\chi}{r_\chi}$ and the constants K_0 and τ are emperically determined to be $K_0 = 0.4$ and $\tau = 0.5$ [481].

We now have all of the components required for computing the energy transport due to dark matter. We may now begin considering the specific parameters of each model in turn.

4.4.2 Energy transport due to electric dipole dark matter

The calculation of the thermal parameters is dependent on the particular model of dark matter. α and κ are dependent on a number of particulars, namely the mass ratio $\mu = \frac{m_\chi}{m_N}$, the functional form of the cross section and the total cross section, the latter at least for the species independent parameters. Before the calculation of the total cross section, the thermal parameters can be tabulated for the various values of μ.

As we have already discovered in eq. (4.75), the electric dipole moment possesses a q^{-2} dependent cross section. The thermal coefficients for q^{-2} dependent cross sections have already been calculated and tabulated by ref. [532]. We use these tabulations with the identification of $\sigma_0 = Z^2e^2\mathcal{D}^2$ and $q_0^2 = \frac{m_\chi^2}{\pi}(1+\mu)^{-2} = \frac{M_{\chi,N}^2}{\pi}$. Although the thermal conductivity and diffusivity coefficients will be the same as ref. [532], the overall results will be slightly different due to the cross section dependence of q_0 on the mass of the dark matter particle. We can therefore use the exact expression for the outbound collision operator C_{out} from ref. [532], namely:

$$C_{\mathrm{out}}(y) = \mu^{-\frac{1}{2}}w^{-1}\,\mathrm{erf}(w)\,, \tag{4.164}$$

where $w = \frac{y}{\sqrt{\mu}}$ and erf is the Gauss error function.

4.4.3 Energy transport due to magnetic dipole dark matter

Unlike the electric dipole case, the thermal conductivity and diffusivity have not previously been calculated for the functional form of the magnetic dipole. As we discovered in eq. (4.101), the functional form for the magnetic dipole cross section is $\sim const + \frac{v^2}{q^2}$. Indeed, no linear or non-linear combinations of velocity and momentum dependent cross section dark matter had previously had their conductivity and diffusivity calculated. The combination of the velocity and momentum dependence cancels out the velocity component, leaving only an angular dependence on the cross section. We should therefore expect the conductivity and diffusivity parameters to be similar to a canonical spin-independent non-momentum or velocity dependent cross section.

Calculating the conductivity coefficient is not a trivial task as eq. (4.150) requires a calculation of the inverse of the collision operator C^{-1}. To achieve the goal, we first need to further develop our expressions for the collision operator in eq. (4.147). Of the two components of eq. (4.147), $C_{\rm out}$ is calculated in a straightforward manner:

$$C_{\rm out} = \int d^3z\, |\vec{x} - \vec{z}|\, \hat{\sigma}_{\rm tot}(v_T|\vec{x} - \vec{z}|) F_{\rm nuc}\,, \tag{4.165}$$

where the thermal velocity distribution of the nuclei is given as:

$$F_{\rm nuc}(\vec{z}) = (\pi\mu)^{-\frac{3}{2}} e^{-\frac{|\vec{z}|^2}{\mu}}\,, \tag{4.166}$$

where $\vec{x} = \frac{\vec{v}}{v_T}$ and $\vec{z} = \frac{\vec{v}_{\rm nuc}}{v_T}$ are dimensionless velocities relative to the thermal velocity v_T, and $\hat{\sigma}_{\rm tot}$ is the total dimensionless cross section defined such that $\hat{\sigma}_{\rm tot}(v_T) = 1$. For the magnetic dipole, $\hat{\sigma}$ can be determined easily from eq. (4.103). The presence of the integral in the expression for $C_{\rm int}$ in eq. (4.147) is more difficult due to the presence of the integral with respect to the incoming particle velocities. Ref. [480] calculated an expression for $C_{\rm in}$ as:

$$\begin{aligned} C^j_{\rm in}(y,x,r) = (1+\mu)^4 \frac{y}{x} \int_0^\infty da \int_0^\infty db F_{\rm nuc}(\vec{z}) 2\pi b \langle P_j \hat{\sigma}\rangle \\ \times \Theta(y - |a-b|)\Theta(a+b-y)\Theta(x-|a-b|)\Theta(a+b-x)\,, \end{aligned} \tag{4.167}$$

where Θ is a Heaviside step function and $\langle Pj\hat{\sigma}\rangle$ is the angle-averaged product fo the normalised differential cross section and the j-th Legendre polynomial, expanded around the transverse scattering angles in the lab frame [532]. The angle averaged product here is where the expressions for α and κ will differ form the spin-independent model. Calculating to the first order in the collision equation in eq. (4.145), the Legendre polynomial is expanded to first order as:

$$\langle P_j \hat{\sigma}\rangle = \langle P_1 \hat{\sigma}\rangle = \frac{1}{2\pi}\int_0^{2\pi} d\phi \left(G + B\frac{b^2}{xy}\cos\phi\right) \hat{\sigma}\left[(1+\mu)bv_T, A + B\cos\phi\right]\,, \tag{4.168}$$

where:

$$A = \frac{(x^2 - a^2 - b^2)(y^2 - a^2 - b^2)}{4a^2b^2}\,; \tag{4.169}$$

$$G = \frac{(x^2 + a^2 - b^2)(y^2 + a^2 - b^2)}{4a^2xy}\,; \tag{4.170}$$

$$B^2 = 1 - \frac{A^2}{G^2} - G^2 + A^2\,, \tag{4.171}$$

and the cross section is evaluated at $v_{\rm rel} = (1+\mu)bv_T$ and $\cos\theta = A + B\cos\phi$ [532].

To compute eq. (4.168), we first rewrite eq. (4.100) in the form eq. (4.101), Although there are multiple degenerate choices here, we choose the parameters σ_0, v_0 q_0 and K such that the maintain the correct dimensions. Thus we choose $\sigma_0 = \frac{Z^2e^2\mu_\chi^2}{4\pi}$, $q_0 = \sqrt{2}M^2_{\chi,N}$, $v_0 = 1$ and $K = \frac{1}{2}\left(\frac{1}{(1+\mu)^2} - 1\right) + S$ where the

parameter S is defined as:

$$S = \frac{1}{Z^2}\frac{I_N+1}{3I_N}\frac{M_{\chi,N}^2}{m_p^2}\frac{\mu_N^2}{\mu_p^2}\,. \tag{4.172}$$

Starting from the form in eq. (4.101), we further decompose the momentum in terms of the angular and velocity components such that $q^2 = 2b^2\zeta_q^2 q_0^2(1-\cos\theta_{\rm CM})$ where b is defined as the velocity of the incoming dark matter particle and $\theta_{\rm CM}$ is the scattering angle in the centre of mass frame. The dimensionless coefficients ζ_q and ζ_v are defined as $\zeta_q = \frac{q_0}{m_\chi v_T}$ and $\zeta_V = \frac{v_0}{v_T}$. The cross section then becomes:

$$\frac{d}{\cos\theta_{\rm CM}} = \sigma_0\left(\frac{(1+\mu)^2}{\zeta_v^2\zeta_q^{-2}(1+\cos\theta_{\rm CM})} + K\right), \tag{4.173}$$

where we have transformed the velocity from the lab frame ot the centre of mass frame. As we have previously noted, the expression for the cross section possesses an infrared divergence where $\theta_{\rm CM}\to 0$. Once again, we use the momentum transfer cross section, giving the total cross section as:

$$\sigma_{T,\rm tot} = \int_{-1}^{1} d\cos\theta_{\rm CM}\,(1-\cos\theta_{\rm CM})\frac{d\sigma}{d\cos\theta_{\rm CM}} = \sigma_0\left(\frac{(1+\mu)^2}{\zeta_v^2\zeta_q^{-2}} + 2K\right). \tag{4.174}$$

Here, we note that the total cross section is independent of the velocity and the scattering angle. The normalised total cross section is therefore constant and therefore equal to unity. The expression for $C_{\rm out}$ in eq. (4.165) may now be calculated explicitly as:

$$C_{\rm out} = \mu^{\frac{1}{2}}\left[\left(w+\frac{1}{2w}\right)\mathrm{erf}(w) + \frac{1}{\sqrt{\pi}}e^{-w^2}\right], \tag{4.175}$$

where $w = \frac{y}{\sqrt{\mu}}$ [532].

We now normalise the differential cross section to the form required for eq. (4.168) to calculate the incoming collision rate $C_{\rm in}$. Here, the cross section is defined to be equal to unity where $v_T = 1$, but as there is no velocity dependence, we simply normalise the differential cross section to be:

$$\hat{\sigma} = \frac{(1+\mu)^2 + 2(1-\cos\theta_{\rm CM})\zeta_v^2\zeta_q^{-2}K}{2(1+\mu)^2 + 4\zeta_v^2\zeta_q^{-2}K}\,. \tag{4.176}$$

We can now insert the expression into eq. (4.168). There is no velocity dependence, but we do insert $A + B\cos\phi$ for $\cos\theta_{\rm CM}$ obtaining:

$$\langle P_q\hat{\sigma}\rangle = \frac{1}{2\pi}\int_0^{2\pi} d\phi\left(G + B\frac{b^2}{xy}\right)\frac{(1+\mu)^2 + 2(1-A-B\cos\phi)\zeta_v^2\zeta_q^{-2}K)}{2(1+\mu)^2 + 4\zeta_v^2\zeta_q^{-2}K}\,. \tag{4.177}$$

We now perform the integral to give an expression for the angle averaged Legendre polynomial as

$$\langle P_1\hat{\sigma}\rangle = G\frac{(1+\mu)^2 + 2(1-A)\zeta_v^2\zeta_q^{-2}K}{2(1+\mu)^2 + 4\zeta_v^2\zeta_q^{-2}K} - \frac{B^2\frac{b^2}{xy}\zeta_v^2\zeta_q^{-2}K}{2(1+\mu)^2 + 4\zeta_v^2\zeta_q^{-2}K}\,, \tag{4.178}$$

which simplifies slightly to give:

$$\langle P_1\hat{\sigma}\rangle = \frac{G}{2} - \frac{2GA\zeta_v^2\zeta_q^{-2}K + B^2\frac{b^2}{xy}\zeta_v^2\zeta_q^{-2}K}{2(1+\mu)^2 + 4\zeta_v^2\zeta_q^{-2}K}\,. \tag{4.179}$$

Notice here that all of the parameters that are specific to the magnetic dipole model are incorporated in the expression $\zeta_v^2\zeta_q^{-2}K$. Using our definitions for ζ_v, ζ_q, v_0 and q_0, we note that

$$\zeta_q^2 = \frac{q_0^2}{m_\chi^2 v_T^2} = \frac{2}{(1+\mu)^2 v_T^2}\,, \tag{4.180}$$

and

$$\zeta_v^2 = \frac{1}{v_T^2}\,, \tag{4.181}$$

which gives a combined expression for the dipole parameters as:

$$\zeta_v^2\zeta_q^{-2}K = \frac{(1+\mu)^2}{2}\frac{1}{2}\left(\frac{1}{(1+\mu)^2} - 1 + 2S\right) = \frac{1}{4}\left(1 + (2S-1)(1+\mu)^2\right)\,, \tag{4.182}$$

which gives a new expression for the angle averaged Legendre polynomial as:

$$\langle P_q\hat{\sigma}\rangle = \frac{G}{2} - \frac{\left(2GA + B^2\frac{b^2}{xy}\right)\left(1 + (2S-1)(1+\mu)^2\right)}{4(2S+1)(1+\mu)^2 + 4}\,. \tag{4.183}$$

We have now reduced the expression for the angle averaged Legendre polynomial two input parameters μ and S as well as the remaining velocity parameters. The expression for S in eq. (4.172) is only non-zero if the relevant nucleus has a non-zero nuclear magnetic moment. It may be computed explicitly for each nuclei present in the Sun and relevant to the simulations as a function of μ as:

Hydrogen-1: $$S_{\mathrm{H}^1} = 2.79285\frac{\mu^2}{(1+\mu)^2}\,. \tag{4.184a}$$

Nitrogen-14: $$S_{\mathrm{N}^{14}} = 1.076696\frac{\mu^2}{(1+\mu)^2}\,. \tag{4.184b}$$

Sodium-23: $$S_{\mathrm{Na}^{23}} = 5.385992\frac{\mu^2}{(1+\mu)^2}\,. \tag{4.184c}$$

Aluminium-27: $$S_{\mathrm{Al}^{27}} = 7.330418\frac{\mu^2}{(1+\mu)^2}\,. \tag{4.184d}$$

We have taken the magnetic dipoles and masses from the collated experimental results from ref. [557]. We now have all of the required elements to compute the inward collision rate C_{in} and the outward collision rate C_{out}, and hence the thermal conductivity and diffusivity.

4.4.4 Energy transport due to anapole dark matter

As for the magnetic dipole, the functional forms for anapole dark matter have not previously been analysed for the purpose of the thermal conductivity and diffusivity. Of the three models, the functional form for the anapole is perhaps the most interesting as it is a linear combination of momentum and velocity dependent cross sections, namely $\sigma_0 \sim q^2 + v^2$ from eq. (4.121). As before, we need to calculate the operators C_{out} and C_{in}. For the former, we need the total cross section then to be integrated via eq. (4.165), while for the latter we need to calculate the angle averaged Legendre polynomial in eq. (4.168). Again to begin we consider the generalised form of the cross section in eq. (4.122). We select $v_0 = 1$, $\sigma_0 = \frac{M_{\chi,N}^2}{2\pi}\frac{Z^2e^2g^2}{\Lambda^4}$ and

$$q_0 = \left[-\frac{1}{4M_{\chi,N}^2} + \frac{1}{Z^2}\frac{I_N+1}{3I_N}\frac{1}{2m_p^2}\frac{\mu_N^2}{\mu_p^2}\right]^{-\frac{1}{2}}\,. \tag{4.185}$$

Using the definitions of the dimensionless parameters $\zeta_v = \frac{v_0}{v_T}$ and $\zeta_q = \frac{q_0}{m_\chi v_T}$ gives an expression for the generalised cross section in eq. (4.122) expanding the momentum in terms of the incoming velocity and scattering angle as:

$$\frac{d\sigma}{d\cos\theta_{\mathrm{CM}}} = \sigma_0\left[(1+\mu)^2b^2\zeta_v^{-2} + 2b^2\zeta_q^{-2}(1-\cos\theta_{\mathrm{CM}})\right]\,, \tag{4.186}$$

where the dimensionless velocity b is defined as $b = \frac{v}{v_T}$. The total cross section is calculated by integrating with respect to $\cos\theta_{\rm CM}$ such that:

$$\sigma_{\rm tot} = \int_{-1}^{1} d\cos\theta_{\rm CM}\, \frac{d\sigma}{d\cos\theta_{\rm CM}} = 2\sigma_0 b^2 \left[(1+\mu)^2\zeta_v^{-2} + 2\zeta_q^{-2}\right] . \tag{4.187}$$

To calculate $C_{\rm out}$, we need to normalise the cross section such that $\hat{\sigma}(v_T) = 1$, noting that we need to transform the velocity to the centre of mass frame we get:

$$\hat{\sigma}_{T,\rm tot} = \frac{b^2\left[(1+\mu)^2 + 2\zeta_v^2\zeta_q^{-2}\right]}{\left[1 + 2(1+\mu)^{-2}\zeta_v^2\zeta_q^{-2}\right]} , \tag{4.188}$$

here, we note the combination of ζ_v and ζ_q can be evaluated along with our definition for q_0 to be:

$$\zeta_v^2\zeta_q^{-2} = \frac{m_\chi}{q_0^2} = \frac{1}{2}(2S-1)(1+\mu)^2 , \tag{4.189}$$

for S defined as eq. (4.172). We can therefore greatly simplify eq. (4.188) such that:

$$\hat{\sigma}_{T,\rm tot} = b^2(1+\mu)^2 . \tag{4.190}$$

Such a total cross section is a linear combination of momentum and velocity dependent total cross sections investigated by ref. [532], so we can fully calculate the integrals required for $C_{\rm out}$ such that:

$$C_{\rm out}(y) = \mu^{\frac{3}{2}}\left[\frac{3+12w^2+4w^4}{4w}\,\mathrm{erf}(w) + \frac{5+2w^2}{2\sqrt{\pi}}e^{-w^2}\right] , \tag{4.191}$$

for $w = \frac{y}{\sqrt{\mu}}$.

Meanwhile, for the inward collision operator $C_{\rm in}$ we need to calculate the angle averaged Legendre polynomial. The normalised differential cross section, from eq. (4.186) is given by:

$$\hat{\sigma} = \frac{b^2\left((1+\mu)^2\zeta_v^{-2} + 2\zeta_q^{-2}(1-\cos\theta_{\rm CM})\right)}{2\zeta_v^{-2} + 4(1+\mu)^{-2}\zeta_q^{-2}} . \tag{4.192}$$

We insert the differential cross section into the expression for eq. (4.168) with the substitutions $b \to (1+\mu)b$ and $\cos\theta_{\rm CM} \to A + B\cos\phi$ such that

$$\langle P_1\hat{\sigma}\rangle = \frac{1}{2\pi}\int_0^{2\pi} d\phi\, \left(G + B\frac{b^2}{xy}\cos\phi\right)\frac{b^2\left[(1+\mu)^2\zeta_v^{-2} + 2\zeta_q^{-2}(1-A-B\cos\phi)\right]}{4\zeta_v^{-2} + 2(1+\mu)^{-2}\zeta_q^{-2}} . \tag{4.193}$$

Integrating out the angles and simplifying, we obtain:

$$\langle P_1\hat{\sigma}\rangle = \frac{b^2G}{2}(1+\mu)^2 - \frac{b^2}{2}(1+\mu)^2 - \frac{b^2}{2}(1+\mu)^2\frac{2GA + 2B^2\frac{b^2}{2xy}}{(1+\mu)^2\zeta_v^{-2}\zeta_q^2 + 2} . \tag{4.194}$$

We can modify this expression to give:

$$\langle P_1\hat{\sigma}\rangle = \frac{\frac{b^2G}{2}(1+\mu)^2}{1 + 2\zeta_q^{-2}\zeta_v^2(1+\mu)^{-2}} + \frac{\frac{1}{2}b^2(1+\mu)^2\left[G(1-A) - \frac{b^2B^2}{2xy}\right]}{\frac{1}{2}(1+\mu)^2\zeta_v^{-2}\zeta_q^2 + 1} . \tag{4.195}$$

However, we note two results for ref. [532] for the momentum and velocity dependent cross sections:

$$\langle P_1\hat{\sigma}_{v^2}\rangle = \frac{1}{2}b^2G(1+\mu)^2 ; \tag{4.196}$$

and,

$$\langle P_1\hat{\sigma}_{q^2}\rangle = \frac{1}{2}b^2(1+\mu)^2\left[G(1-A) - \frac{b^2B^2}{2xy}\right], \tag{4.197}$$

which illuminates the angle averaged Legendre polynomial of a cross section, which is a linear combination of momentum and velocity dependent components, is itself a linear combination of angle averaged Legendre polynomials of cross sections that are momentum and velocity dependent, that is:

$$\langle P_1\hat{\sigma}\rangle = \frac{\langle P_1\hat{\sigma}_{v^2}\rangle}{1+2\zeta_q^{-2}\zeta_v^2(1+\mu)^{-2}} + \frac{\langle P_1\hat{\sigma}_{q^2}\rangle}{\frac{1}{2}(1+\mu)^2\zeta_v^{-2}\zeta_q^2+1}\,. \tag{4.198}$$

Utilising the expression in eq. (4.192), we can parameterise the linear combination in terms of a single parameter S:

$$\langle P_1\hat{\sigma}\rangle = \frac{\langle P_1\hat{\sigma}_{v^2}\rangle}{1+\frac{1}{2}(2S-1)} + \frac{\langle P_1\hat{\sigma}_{q^2}\rangle}{2(2S-1)^{-1}+1}\,. \tag{4.199}$$

As the S parameter is μ dependent, and takes on four different coefficients depending on the nuclear species, we essentially obtain five different linear combinations of the angle averaged Legendre polynomials, including the case where the nuclear spin and hence magnetic dipole is zero. Here, we now have all of the components for the full tabulation α and κ for all models with the various values of S for the magnetic dipole and anapole models.

4.4.5 Tabulation of diffusivity and conductivity coefficients

We are now ready to compute and tabulate the thermal diffusivity α and conductivity κ using the mathematics developed above. Following ref. [532], we construct a discrete distribution of the lowest order spherical harmonics of the phase space f_0^{00}, defined in eq. (4.149), into a 500 element vector. We normalise the velocity distribution with respect to the thermal velocity v_T and consider a range of velocities from $y = 0$ to $y = 5$, where the $y = 5$ case forms the upper limit to the integral over the velocities as it corresponds to particles with a velocity five times the thermal average. We then use the expressions for $C_{\rm out}$ in eqs. (4.164), (4.175) and (4.191), the expressions for $\langle P_1\hat{\sigma}\rangle$ in eqs. (4.183) and (4.199) with the relation between the angle averaged Legendre polynomial and the inbound collision operator $C_{\rm in}$ in eq. (4.167) to compute the collision operator itself as C, a 500×500 element matrix acting upon the discretised phase space vector. Indeed, we compute a different C for each of our models, as well as the different choices of S as defined by eq. (4.172) We then are able to perform a matrix inversion on C to find the inverted operator C^{-1} as required to compute α in eq. (4.150). From here, we compute the first order spherical harmonics of the phase space distribution f_1^{10} using eq. (4.153), which allows us to compute the thermal conductivity κ using eq. (4.152) These raw values are then tabulated, though in order to utilise them in calculation, we must re-insert the cross section and elemental abundance dependencies using eqs. (4.154) and (4.155). We compute the different values of C for a range of values of the mass ratio $\mu = \frac{m_\chi}{m_N}$ from 10^{-2} to 10^2. The tabulated diffusivity and conductivity coefficients for each model are plotted in figure 4.3. We segregate the nuclei with non-zero spin and show these results separately alongside the zero spin calculations.

We compare the results for the thermal diffusivity α and conductivity κ for each of the electromagentic dipole models with a model representing a constant, momentum and velocity dependent spin independent model, listed in figure 4.3 as SI. For the electric dipole moment models, the diffusivity is enhanced relative to the spin-independent case for small μ, that is, the dark matter mass is much smaller than the nucleon mass, but the conductivity is enhanced for large μ. For larger masses, where the momentum transfer relative to the size fo the dark matter particle is smaller, the q^{-2} cross section means that there will be

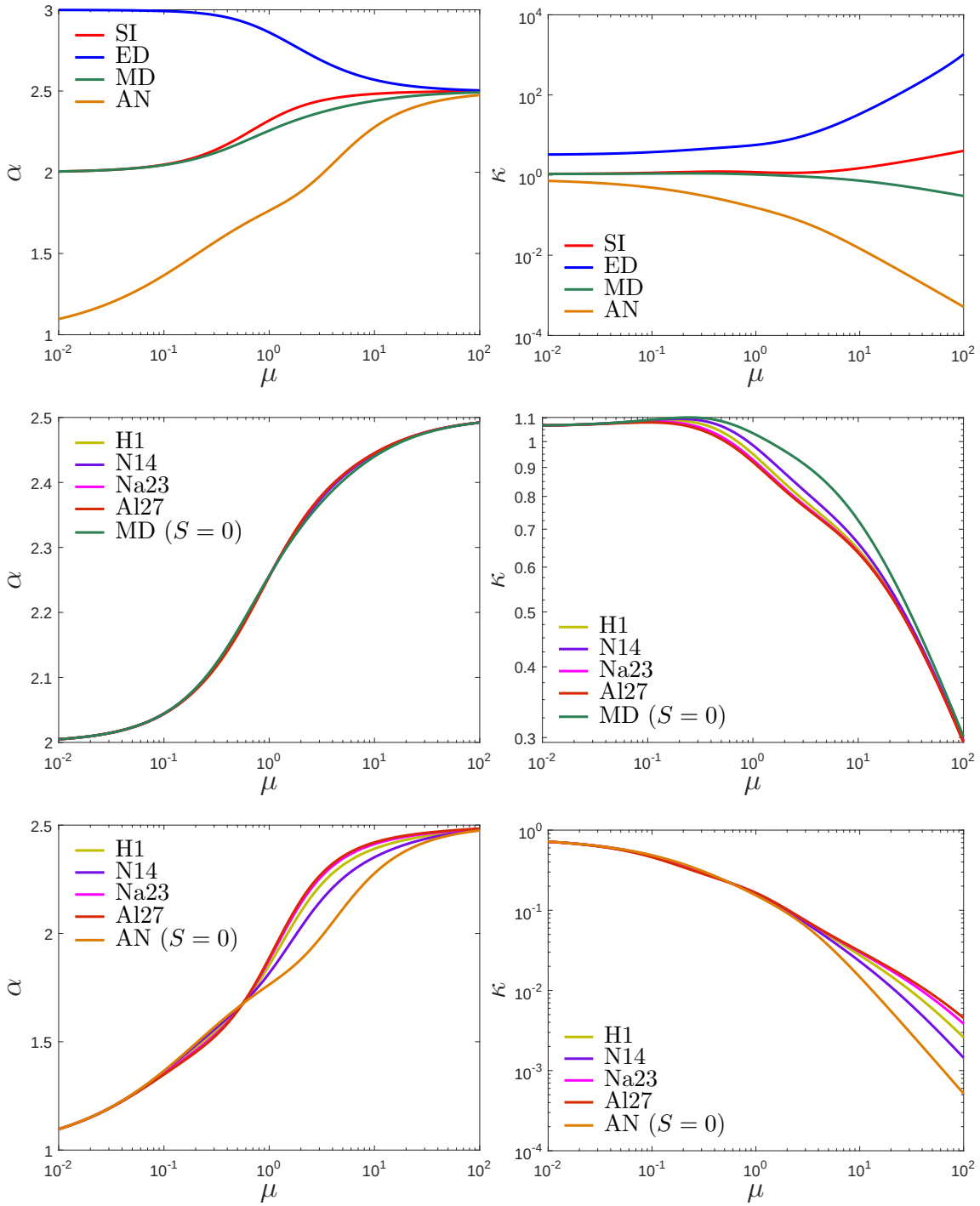

Figure 4.3: Dimensionless thermal diffusivity α (left) and conductivity κ (right) as a function of mass ratio μ. The plots at the top compare values for spin-independent (SI), electric dipole moment (ED), magnetic dipole moment (MD), and anapole moment (AN), with $S = 0$ for the latter two. The middle and bottom graphs compare the α (left) and κ (right) for non-zero values of S for the magnetic dipole (middle) and anapole (bottom) respectively (see Eqs. (4.183) and (4.199)).

on average more interactions capable of transferring energy. The q^{-2} interaction arises as the force carrier here is the photon, rather than a heavy weak boson, making the momentum transfer more efficient.

The diffusivity and conductivity coefficients for the magnetic dipole model follow closely to the constant cross section spin independent model. The result is expected since we have already discovered that the momentum and velocity dependencies of the magnetic dipole moment cancel out leaving only an angular dependence on the cross section. For larger values of μ the conductivity decreases slightly relative to the spin independent model. Here, there second term in eq. (4.183) becomes significant, resulting in a cancellation which reduces the total inbound rate of scattering C_{in}. As the scattering is angular dependent, there are angles of scattering which result in a reduced cross section. Where the dark matter particle is significantly smaller larger than the nucleus, the relative contributions from the nuclear spin that generate the angular dependence are more important. The angular dependence for heavy dark matter is due to the requirement that the dark matter particle should have a component of its spin, which generates the magnetic dipole, oriented parallel to the incoming nucleus to maximise the interaction strength. For light masses, the cross section is dominated by the electric field induced by the changing magnetic field which lacks the angular dependence.

The anapole model produces the most significant diversion from the standard spin independent cross section of the three models. For small masses, the anapole produces a much more compact halo as it is less able to diffuse, while for large masses, the anapole diffuses more easily but cannot as easily conduct energy transfer. The anapole cross section follows the behaviour of the q^2 and v^2 models of [532], where the momentum dependence means that heavy mass particles are more likely to undergo interactions producing some level of energy transfer. The result is that low mass anapole models produce compact halos with smaller outwards diffusivity along the temperature gradient. The larger masses diffuse more easily but there increased interactions mean that the distanced travelled between interactions is smaller, reducing the long distance energy transport.

The models considering the interaction between the magnetic dipole and anapole models with the non zero spin nuclei which produce a non zero value for S in eq. (4.172) are shown in the middle and bottom panels in figure 4.3. Here, we consider the interaction between the four nuclei in the sun with non zero spin with a non-negligible abundance, namely ^{1}H, ^{14}N ^{23}Na, ^{27}Al. Of these nuclei, the hydrogen is by far the most prominent in the Sun. For the magnetic dipole, there is very little modification to the thermal diffusivity. For the remaining models, there is a minor modification to the diffusivity and conductivity coefficients provided the dark matter mass is greater than the nucleus mass. For the anapole, the added spin components slightly increase the thermal conductivity, since the new terms reduce the size of the momentum dependant terms that cause the conduction to be inefficient. Meanwhile the magnetic dipole decreases the thermal conductivity as the new spin terms make the momentum dependent components larger.

4.4.6 Effectiveness of energy transport

As we have now developed all of the relevant theory for analysing the effect of electromagnetic dipole dark matter on the solar interior, we can analyse each of the models to see which are more or less efficient in providing a mechanism for energy transport inside the Sun. The models which are particularly efficient are the most likely to be a viable solution to the solar abundance problem.

To begin, we define the total energy transported per unit mass at a given radius r from the centre of the Sun as:

$$\epsilon_\chi(r) = \frac{1}{4\pi r^2 \rho(r)} \frac{dL_\chi(r)}{dr}\,, \tag{4.200}$$

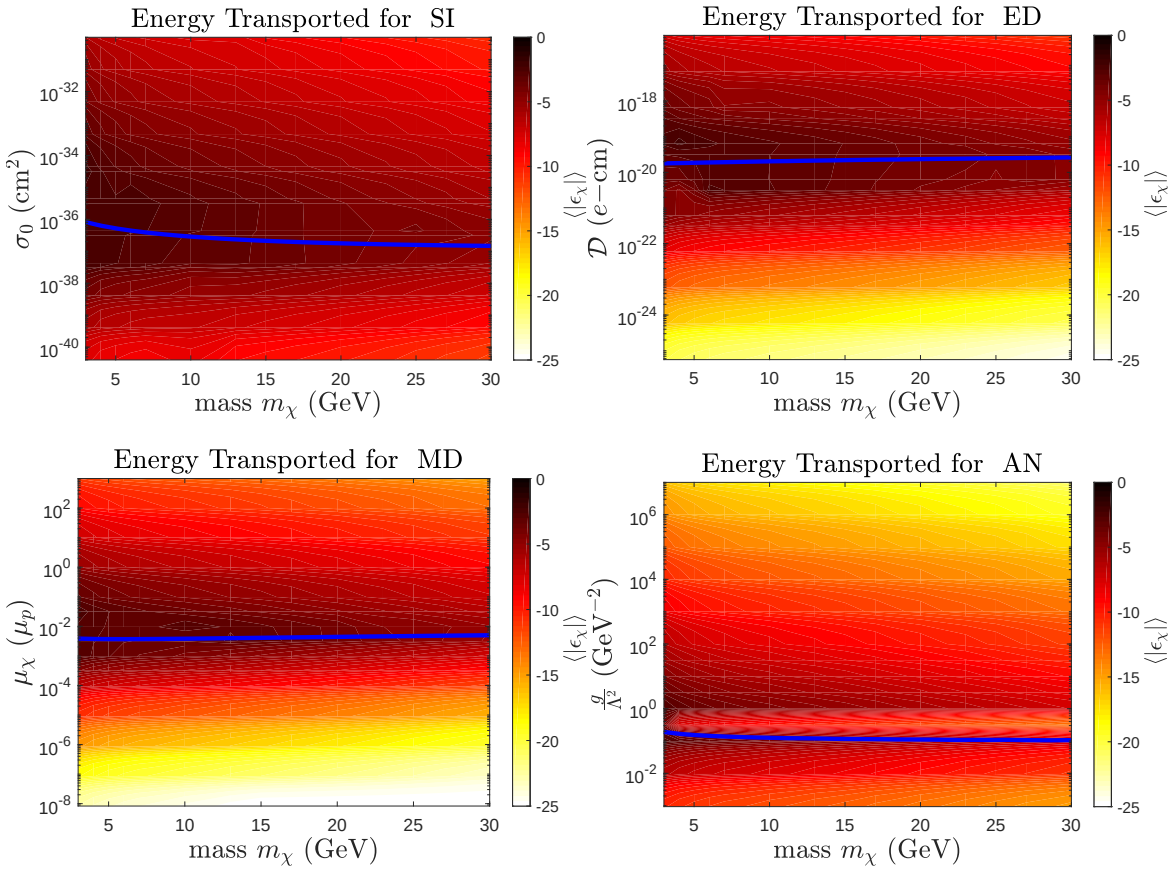

Figure 4.4: Average absolute value of the rate of energy transfer $|\epsilon|$ for spin independent dark matter (top left), electric dipole dark matter (top right), magnetic dipole dark matter (bottom left) and anapole dark matter (bottom right). The blue line illustrates the saturation capture rate, above which the population of dark matter within the star is roughly constant. The colour scale is measured in units of $\log_{10}\left(\epsilon\ [\ \mathrm{erg\ g^{-1}\ s^{-1}}]\right)$.

where $\rho(r)$ is the density profile of the nucleus matter of the Sun, and $L_\chi(r)$ is the luminosity transported as defined in eq. (4.157). For a spherically symmetric star, the average rate of energy transport is then given by:

$$\langle|\epsilon_\chi|\rangle = \frac{\int_0^{R_\odot} r^2 |\epsilon_\chi(r)| dr}{\int_0^{R_\odot} r^2 dr}\,, \tag{4.201}$$

for a star of radius $R_\odot$. By averaging the energy transported in this way, we obtain a rough approximation for the magnitude of the changes to the solar structure due to the additional energy transport. It does not necessarily indicate that the additional energy transport causes changes to the solar structure in a way that reduces the tension in the sound speed profile. The averaged energy transported for each of our models is presented in figure 4.4 for a star with an age of 4.59 Gyr based on the AGSS09ph model [491].

There are multiple physical processes that are affecting the total energy transported by the dark matter inside the Sun. Firstly, the total energy transported is dependent on the sum total of dark matter particles in the Sun as determined by the capture rates in section 4.3. We show the level at which the capture rate is saturated as a blue line in figure 4.4. Where the model exists below the saturation threshold, the total number of particles decreases with the square of the interaction strength, which reduces the overall population and hence luminosity as L_χ is linearly dependent on n_χ in eq. (4.157). For each of the models under consideration here, the saturation point occurs at or near the models where the energy transport is maximised. Models which saturate the cross section are much more likely to produce a solution to the solar abundance problem.

For each of the models, there is a balance between the local thermal equilibrium solution and the Knusden transport regime. Between these two regimes, there is a band where the energy transport is maximised. Where the model is in the local equilibrium regime, decreasing the interaction strength increases the total energy transported. Here, the stronger interactions interact more frequently, meaning that the dark matter is more readily thermalised with the local solar environment and cannot transport energy over any significant distance. Where the model is in the Knusden regime [481], the mean free path is long, allowing energy to be transported long distances. However, the small interaction strength reduces the amount of energy that can be transported. Such a regime is also likely to be below the saturation cut off as it becomes possible for the dark matter particle to perform one or more orbits between interactions. The result is the energy transported is maximised at the transition point between the local thermal equlibrium and Knusden regimes, that is, where the mean free path is approximately equal to the scale factor in eq. (4.158).

Finally, there is a dependence of the energy transported on the mass of the dark matter particle, although we do not consider as wide a range of masses as in section 4.4.5. In general, the energy transported is stronger for smaller masses as for most of the models, the thermal conductivity is greater for smaller mass particles. The exception is for the electric dipole model, where the conductivity is much greater for high mass particles. Thus for the electric dipole, the energy transported does not decrease with mass over the range we consider here.

We have now developed and understood all of the elements required to simulate the effect of electromagnetic dipole dark matter within the Sun. We have computed the total number of particles in the Sun by considering the capture rate of each of our models, which was dependent on the cross section of dark matter scattering from a nuclei. We have discovered the fundamental limit of saturation on the capture rate, and noted that models which saturate are significantly more likely to produce a large amount of energy transport. Further, we have introduced two mechanisms for energy transport, the local thermal equilibrium and Knusden transport and developed the required calculations for both. The total energy transport is maximised at the nexus between these to regimes, where the mean free path of the particle is equal to the scale factor r_χ. We have encapsulated the physics of the local thermal equilibrium model in terms of two dimensionless parameters, namely the thermal diffusivity α and conductivity κ and produced tabulations for each. We now have all of the necessary ingredients to perform full simulations of the Sun to predict the effect of dark matter on the physical observables.

Chapter 5

Simulating dark matter in the Sun

Having developed the relevant theory to describe the interactions of dark matter within the Sun, we now consider implementing the solar theory into simulations of the Sun to make predictions about solar observables, in particular the sound speed profile. We perform simulations of the Sun in the presence of dark matter using the modified `DarkStec` code [494, 495, 533]. The `DarkStec` code combines the stellar evolution features of the `GARSTEC` Garching Stellar Evolution Code and the dark matter capture and transport features from the `DarkStars` code. `GARSTEC` has been developed over many authors and versions originating from the legendary Kippenhahn stellar evolution code [526, 558–563]. It provides a convenient and effective method of tracking the solar abundances in the standard solar models. The `DarkStars` code is evolved from the `STARS` stellar evolution code [564–567] with the implementation incorporated to include dark matter physics from `DarkSUSY` [554, 556, 568–571].

`DarkStec` takes, as an input, a protostellar model which, when evolved, gives a star with similar characteristics to the Sun. It then calculates a number of physical parameters, namely the age ($\tau_\odot = 4.57$ Gyr), the solar luminosity $L_\odot = 3.8418 \times 10^{33}$ erg s^{-1}, the solar radius $R_\odot = 6.9598 \times 10^{10}$ cm and the metal to hydrogen fraction $(Z/X)_\odot = 0.0181$ [491]. These quantities discriminate whether the output model is to be accepted as a description for the Sun. If not, then input parameters of the protostellar model must be varied. The parameters considered are the mixing length parameter, conventionally labelled $\alpha_{\rm MLT}$, and the initial helium and metal mass fractions $Y_{\rm ini}$ and $Z_{\rm ini}$ respectively. The code then follows a Newton-Raphson iteration scheme to calculate the best-fit parameters [495]. We terminate the iteration regime when the constraints are satisfied to better than a part in 10^4. We consider adjusting several input parameters to the model to calibrate the iteration scheme, namely, the initial helium abundance ($Y_{\rm ini}$) and metallicity ($Z_{\rm ini}$) of the models and the mixing length parameter $\alpha_{\rm MLT}$, associated with the efficiency of convection.

There is no guarantee that the iteration scheme converges for one of two reasons. First, the iteration may not converge to an acceptable stellar model due to the vagaries of the root finding algorithm. Second, the iteration may be aborted midway due to unexpected behaviour in the stellar evolution. These problems can arise in models where dark matter may be transporting energy in an unusual or unexpected manner. For example, if dark matter carries too much energy out of the core, the temperature of the core may become significantly lower than its surroundings. The result is an unusual distributions of nuclear fusion within the star, possibly resulting in a density inversion. The code is not designed to handle such physics and may fail. Regions of the parameter space which do not converge are identified in all plots in grey. Whilst a solution may exist for at least some points which do not converge, the surrounding parameter points are often in very strong disagreement with observations. For the plots in this section, regions around the non-converging regions may show discontinuities in the contours due to difficulties in the interpolating procedures.

The impact of electromagnetic dipolar dark matter physics on the stellar evolution outlined in section 4 required some modification to the original `DarkStec` code. The capture rate evaluation was rewritten to be able to handle more complicated momentum and velocity-dependent cross sections, which may be passed into the program analytically or numerically. Previously, the code could only accept analytic expressions of the cross section. Whilst acceptable for constant cross section or generalised momentum or velocity-dependent dark matter, it was not suitable for the more involved expressions for the magnetic and anapole moments. The new routine is also more adaptable to more accurate electromagnetic form factors within the capture rate [537]. Contrastingly, the calculation of thermal conduction due to electromagnetic dipolar dark matter needed only the insertion of the recalculated tables for the parameters α and κ outlined in section 4.4.

We perform solar calculations for five different categories of models, and numerous point of parameter spaces therein. Each electromagnetic dipole moment from section 4.2 contributes one category. Additionally, we consider a model of dark matter with a constant spin-independent cross section determined by a arbitrary parameter σ_0, which has previously been the orthodox implementation of dark matter within the Sun. Finally, we consider a solar model without any dark matter at all, corresponding to the baseline interpretation of the standard solar model. For the four categories with dark matter, we simulate a solar model on a grid of points in a parameter space covering the dark matter mass m_χ and the electromagnetic or spin independent coupling parameter, represented by $\mathcal{D}$, μ_χ, $\frac{g}{\Lambda^2}$ or σ_0 as appropriate. We consider a range of masses from 3 GeV and 30 GeV. The lower bound is determined by the limits of evaporation on low mass dark matter, with models with masses below ~ 4 GeV subject to strong evaporation rates and so should be treated with caution [552]. The upper limit is chosen as an order of magnitude above the most common nuclear masses in the Sun, beyond which the effects of solar transport are muted. The ranges for the coupling strengths are selected based on the direct detection constraints, the interaction strength at which the capture rate is saturated, and the nexus point between the local thermal equilibrium and Knusden transport. Where regions showed substantial deviation from the case of no dark matter, the grid of the parameter space is calculated to a higher resolution. Where no points in the parameter space showed any results of interest, the bounds of the parameter space were widened.

For each point in our parameter space grids, we compute a number of outputs that can be compared to well-measured solar observables. Using these outputs, we can compute a goodness of fit for each of the simulations. In this chapter, we consider a number of solar observables available which show moderate to severe discrepancies from the Standard Solar Model [495, 526, 533]. Note that the choice of observables are not necessarily independent, nor provide a complete description of the defects in our understanding of the Sun. We now consider each of these solar observables in turn, including the solar neutrino fluxes in section 5.1, helioseismology and the sound speed profile in section 5.2, the frequency separation ratios in section 5.3, the convection zone depth in section 5.4 and surface helium abundance in section 5.5. Finally we compute a total likelihood for all observations in section 5.6.

5.1 Solar neutrino fluxes

The first constraints that we consider provide tight bounds on the behaviour of the models in the inner core of the Sun, namely, the observed solar neutrino fluxes due to ^{7}Be and ^{8}B. The vast majority of neutrinos emitted from the Sun arise from the nuclear fusion of photons into deuterium via the process $p + p \to d + e^+ + \nu_e$. However, a small number of neutrinos are emitted from higher order processes, due to the nuclear fusion of a number of composite nucleons. The key processes that we consider are the fusion processes of boron and beryllium, in particular, $^7\mathrm{Be} + e^- \to {}^7\mathrm{Li} + \nu_\mathrm{e}$ and $^8\mathrm{B} \to {}^8\mathrm{Be} + \mathrm{e}^+ + \nu_\mathrm{e}$. Due to the higher energies involved in such fusion interactions, the neutrinos produced by these interactions follow a different energy spectrum, and may be distinguished in neutrino detection experiments from the

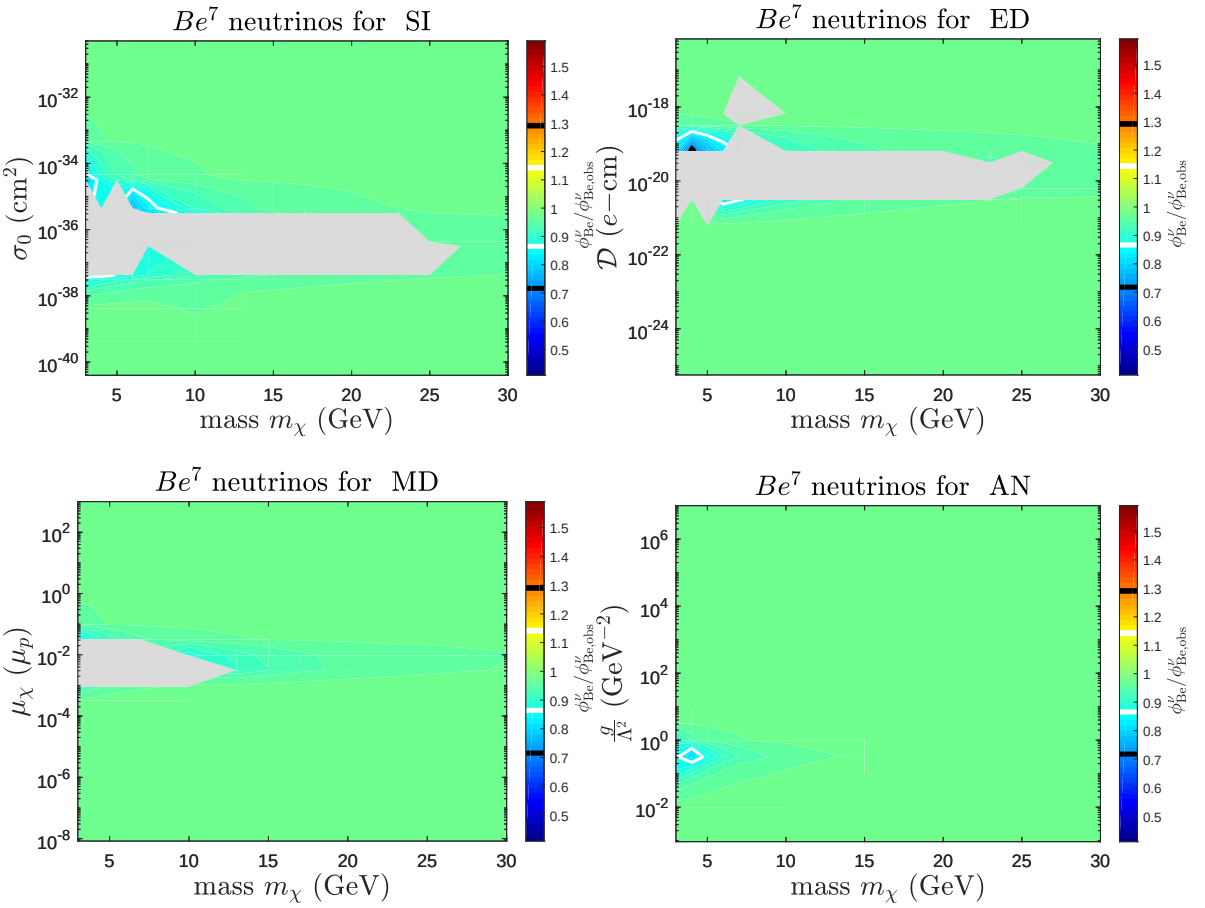

Figure 5.1: Ratio of predicted ^{7}Be neutrino flux to the measured value $\phi_{Be,\rm obs} = 4.82 \times 10^9$ cm^{-2} s^{-1} for spin independent dark matter (top left), electric dipole dark matter (top right), magnetic dipole dark matter (bottom left) and anapole dark matter (bottom right). The expected value is 1. The white contours show the regions where the flux is 1σ above/below the expected value . Simulations in the grey regions did not converge.

proton fusion neutrinos. Such neutrinos also have a sufficiently high flux when they reach Earth to be precisely measured without large uncertainties. The aggregated results give values for the flux of neutrinos from ^{8}B decays as $\phi_{B,\rm obs} = 5.16 \times 10^6$ cm^{-2} s^{-1} and the flux of neutrinos from electron capture of ^{7}Be as $\phi_{Be,\rm obs} = 4.80 \times 10^9$ cm^{-2} s^{-1} [572, 573]. The observational errors on the fluxes are estimated at 5% and the additional error due to modelling effects are estimated to be $\sim 14\%$ and $\sim 7\%$ respectively [495, 533].

The relative flux of the ^{7}Be and ^{8}B neutrinos is highly dependent on the core temperature of the Sun. If the core temperature heats or cools, the rate of fusion of these elements changes substantially due to the amount of energy available, which in turn alters the neutrino fluxes. Analytical approximates suggest that the dependence on the ratio of neutrino fluxes on the core temperature models as $\frac{\phi_B}{\phi_{Be}} \sim T_c^{13.5}$ where T_c is the core temperature [574, 575]. We therefore treat the neutrino fluxes as a very sensitive test of the impact of introducing dark matter on the core temperature of the Sun, a feature that is difficult to probe using the sound speed profile due to the low order oscillations required. Since the proposal of introducing dark matter into the Sun is to provide mechanisms for energy transport out of the core into the radiative zone, such bounds on the core are an important test of whether the dark matter thermal transport has irrevocably cooled the core to unacceptable levels.

We show the simulated neutrino flux across our parameter spaces as a ratio with the measured neutrino fluxes in figures 5.1 and 5.2 for neutrinos from ^{7}Be and ^{8}B respectively. Models without any dark matter or where the introduction of dark matter has a minimal impact provide an excellent fit to the observed models. Such regions are shown in figures 5.1 and 5.2 in green. Where the dark matter is introduced to

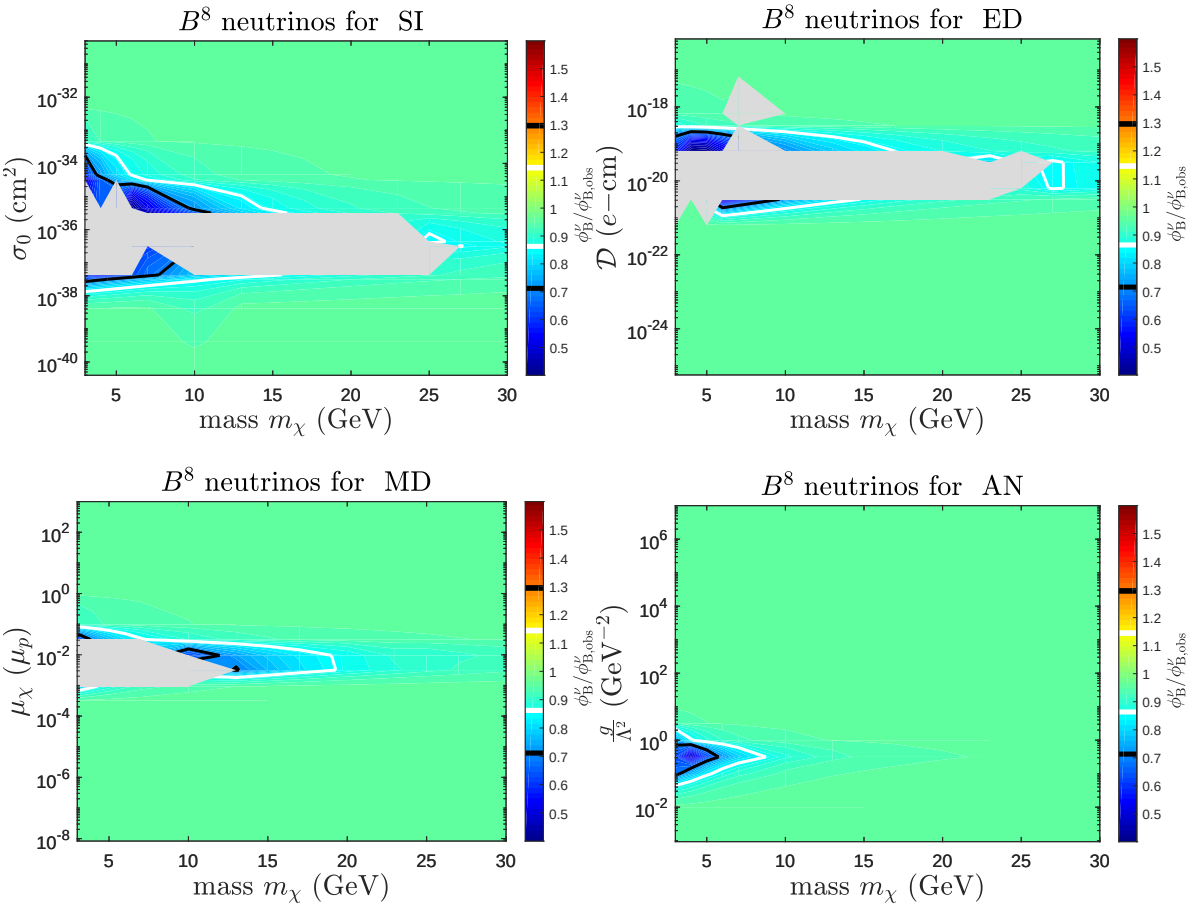

Figure 5.2: Ratio of predicted ^{8}B neutrino flux to the measured value $\phi_{B,\rm obs} = 5.00 \times 10^6$ cm^{-2} s^{-1} for spin independent dark matter (top left), electric dipole dark matter (top right), magnetic dipole dark matter (bottom left) and anapole dark matter (bottom right). The expected value is 1. The white and black contours show the regions where the flux is 1σ and 2σ above/below the expected value respectively. Simulations in the grey regions did not converge.

the Sun and has a small to moderate impact, the overall effect is a broad worsening of the fit. For each of these models, the reduction on the fit can be more than 2σ, shown as black contours, beyond which the models fail to converge as they can not replicate the observed physics of the Sun. The bands which correspond to the reduction in core temperatures neatly corresponds to the regions with significant energy transport from figure 4.4. For each of the models, there is a regime near to the bands on non-convergence which only corresponds to a 1σ depreciation in the fit, shown as a white contour. Such models are still broadly acceptable as a viable measurement of the Sun. The band where dark matter has a substantial impact on the Sun is shown in blue and is truncated for the magnetic dipole and anapole models above $m_\chi > 15$ GeV and $m_\chi > 5$ GeV respectively. The band in each case corresponds to a reduced core temperature. The reduction in neutrino flux for the ^{8}B neutrinos is more pronounced as the ^{8}B neutrino flux is more sensitive to the core temperature. The neutrino fluxes provide an important discriminating feature on our dark matter models.

5.2 Helioseismology

One of the best probes of the structure of Sun is helioseismology, specifically the sound-speed profile. To recap, helioseismology is the measurement of surface oscillations of the Sun with Doppler radar, which indicate the propagation of pressure waves throughout the Sun. Such propagation is presented as a

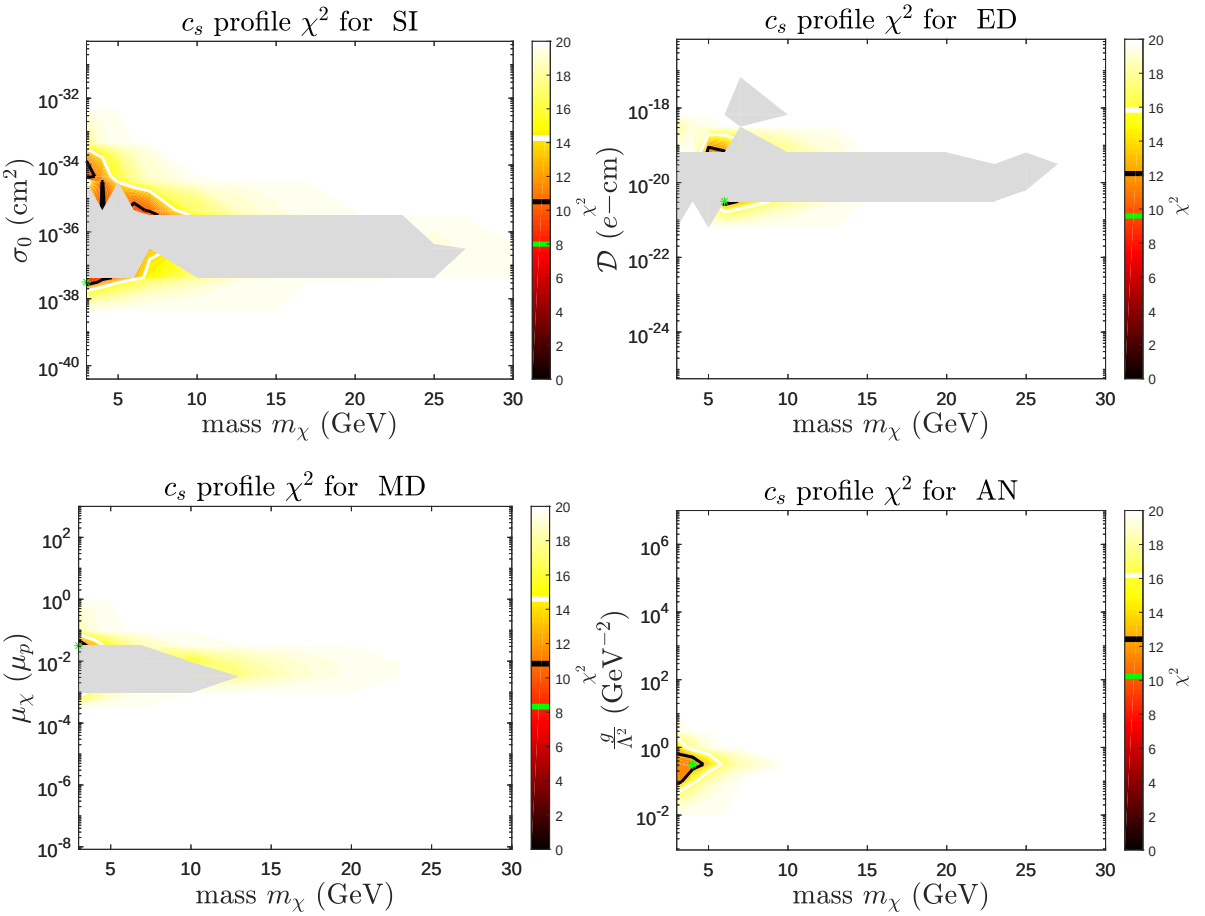

Figure 5.3: Combined likelihood χ^2 of the sound-speed profile defined in eq. (5.1) for spin independent dark matter (top left), electric dipole dark matter (top right), magnetic dipole dark matter (bottom left) and anapole dark matter (bottom right). The green star shows the best-fit χ^2 and the black and white contours show the preferred regions at 1 and 2σ respectively, corresponding to $\Delta\chi^2 = 2.3$ and 6.18 respectively. Simulations in the grey regions did not converge.

function of the radius of the Sun via the sound speed profile, as determined from inversions from the oscillation modes. The sound speed profile is predicted from the standard solar model via the measurement of the temperature T and mean molecular weight μ at a given radius in the Sun, which is approximated by $c^2 \sim \sqrt{\frac{T}{\mu}}$.

The standard solar models with the updated surface composition [491, 492, 526] are not generally compatible with helioseismology observations. At the core, $R \sim 0.2R_\odot$, the models predict a sound speed larger than observed, while in the radiation zone, that is $0.2 \lesssim R \lesssim 0.7$, the models predict a sound speed smaller than observed. However, in the convective zone, defined by $R \gtrsim 0.7R_\odot$, there is good agreement as expected since the temperature gradient is by definition adiabatic. Provided the AGSS09ph abundances [491, 492, 526] are appropriate throughout the Sun, there is strong evidence for some mechanism for transporting energy from the core to the radiative zone to match the results to the observations. The goal of introducing dark matter is to provide a modification to the temperature profile due to an additional energy transport mechanism, plus minor changes to μ such that it can satisfy the standard solar models.

We compare the sound speed profile simulated by `DarkStec` to the helioseismological inversions calculated by ref. [576]. There are two main contributions to the errors in these measurement. The first is the error due to the uncertainties in modelling, which we take from ref. [495]. The second is the error due to the helioseismological inversion, which are taken from ref. [577]. We add both errors together in

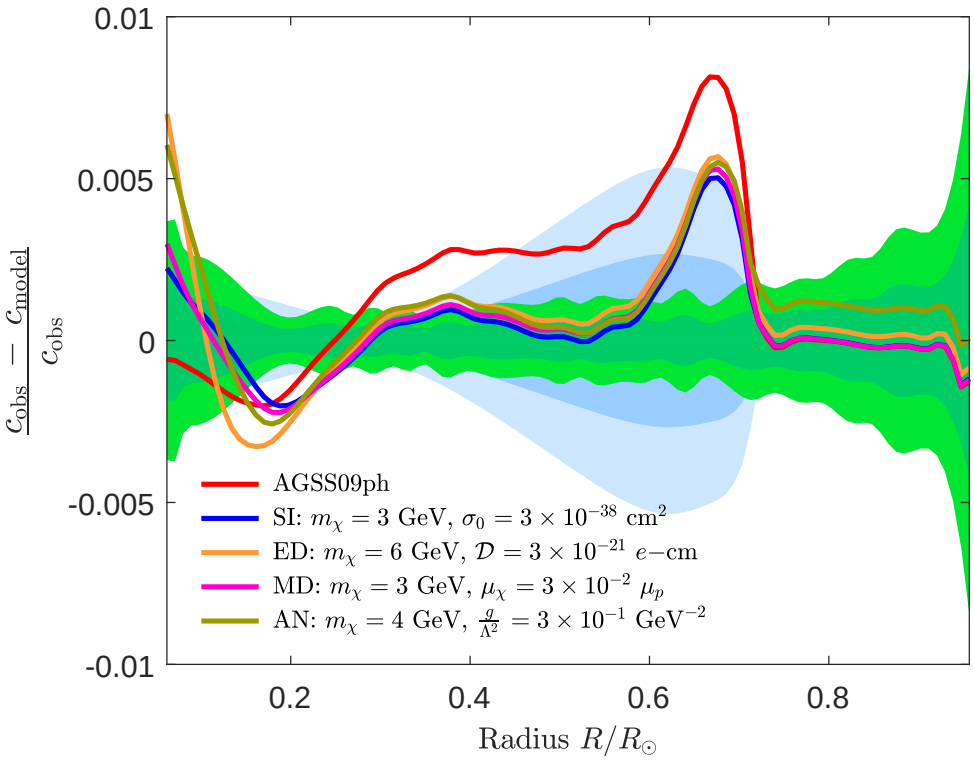

Figure 5.4: Best fit profile of the sound speed for spin independent dark matter (SI), electric dipole dark matter (ED), magnetic dipole dark matter (MD) and anapole dark matter (AN). The light blue regions are the 1σ and 2σ errors from modelling. The green regions are the 1σ and 2σ errors from inversions. The red profile is the AGSS09ph [491] without dark matter.

quadrature. From here, we define an effective χ^2 value following ref. [495]:

$$\chi^2_{c_s} = \sum_{r_i} \frac{(c_{s,\rm model}(r_i) - c_{s,\rm hel}(r_i))^2}{\sigma^2_{c_s,\rm hel}(r_i)} \,. \tag{5.1}$$

We sample the data for the calculation of the χ^2 value from 5 equally spaced radii r_i between $R = 0.1R_\odot$ and $R = 0.67R_\odot$, the upper limit chosen as the boundary of the radiative and convective zones, while the lower limit is chosen near but not at the core in order to maintain statistical independence from the neutrino measurement. The measured helioseismological values in the core have large uncertainties, while the measured helioseismological values in the convection zone are all in good agreement with the models. Note that the sound speed profile and the frequency separation ratios both derive from helioseismology observations and so are not statistically independent and can not be combined in a χ^2 fit.

We compute the sound speed profile for each point in the parameter spaces, and the χ^2 likelihood fit by eq. (5.1) and present the χ^2 fits in figure 5.3. The darker red regions in figure 5.3 correspond to better fits to the sound speed profile. The regions which show an improvement to the sound speed profile correspond to the same regions which show the decreases to the fits to the neutrino fluxes in figures 5.1 and 5.2, since in general the increased energy transport that reduces the sound speed profile reduces the core temperature of the Sun. Many of the models remove too much heat from the very inner core of the Sun, or don't deposit it efficiently into the radiative zone. The result is a modelled sound speed in the inner core $R < 0.1R_\odot$ well over 4σ from observations, similar to the exclusion from the observations of the neutrino flux.

We now compare the parameter points for each model which produce the best fit to the sound speed profile to the sound speed profile in models without any dark matter. The best fit sound speed profiles are shown in figure 5.4. All of the best fits occur at light dark matter masses, which we note corresponds

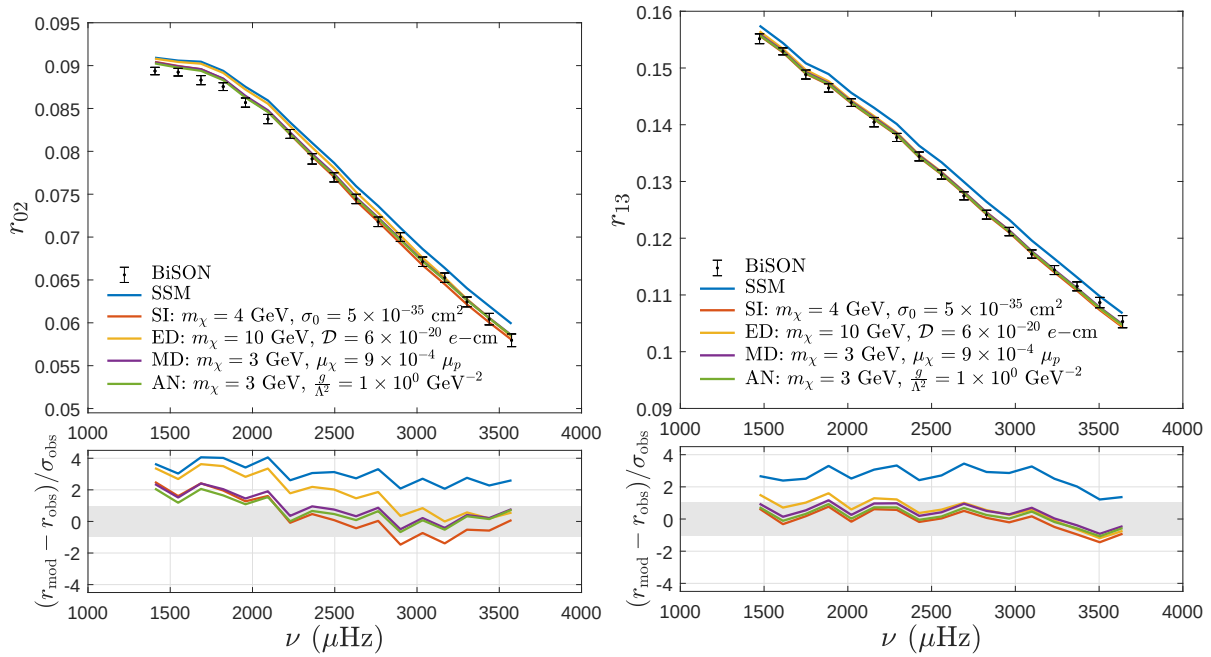

Figure 5.5: Small frequency separations r_{02} (left) and r_{13} (right) for the best-fit models to helioseismological observations. Data is compared to the Standard Solar Model (SSM) and BiSON experiment [578]. The error bars correspond to observational and modelling error [495]. Below each figure are the residuals with respect to BiSON data, in units of the total error.

to the regime where evaporation effects are significant. The best fit model for all models provide a remediation of the tension at the base of the convective zone, $R \sim 0.6 R_\odot$ to well within the standard error. However, all models increase the speed of sound near the core of the Sun; the best fit models for the momentum-dependent electric dipole and anapole most egregiously. Here, the results are best constrained by the neutrino flux. Such best fit models correspond to decreases in the neutrino flux of up to 35%. The sound speed profile of the magnetic dipole closely follows that of the spin indepednent model, since both have approximately equal thermal conductivities κ for low mass ratios. Meanwhile, the anapole at these mass regimes has a more tightly packed distribution due to the thermal diffusivity α, partially explaining the change in distribution in the core. Our models improve the fits from other works on spin independent dark matter [493, 547] due to the improved description of energy transport we follow from refs. [495, 533].

5.3 Frequency separation ratios

Another related probe that relates the inner structure of the Sun to helioseismology measurments are the so-called frequency separation ratios. Since the ratios do not rely on the inversion of the oscillation modes and are not as dependent on the solar surface composition [579], they are sensitive to the core structure of the Sun whilst minimising systematic errors [578, 580]. The frequency separation ratios are defined by the relative sizes of the differences of adjacent frequencies of solar oscillations, in particular the low frequencies, namely:

$$r_{02}(n) = \frac{d_{02}(n)}{\Delta_1(n)}, \quad r_{13}(n) = \frac{d_{13}(n)}{\Delta_0(n+1)}, \tag{5.2}$$

where

$$d_{l,l+2}(n) \equiv \nu_{n,l} - \nu_{n-1,l+2} \simeq -(4l+6)\frac{\Delta_l(n)}{4\pi^2 \nu_{n,l}} \int_0^{R_\odot} \frac{dc_s}{dr}\frac{dr}{r}, \tag{5.3}$$

and $\Delta_l(n) = \nu_{n,l} - \nu_{n-1,l}$ for

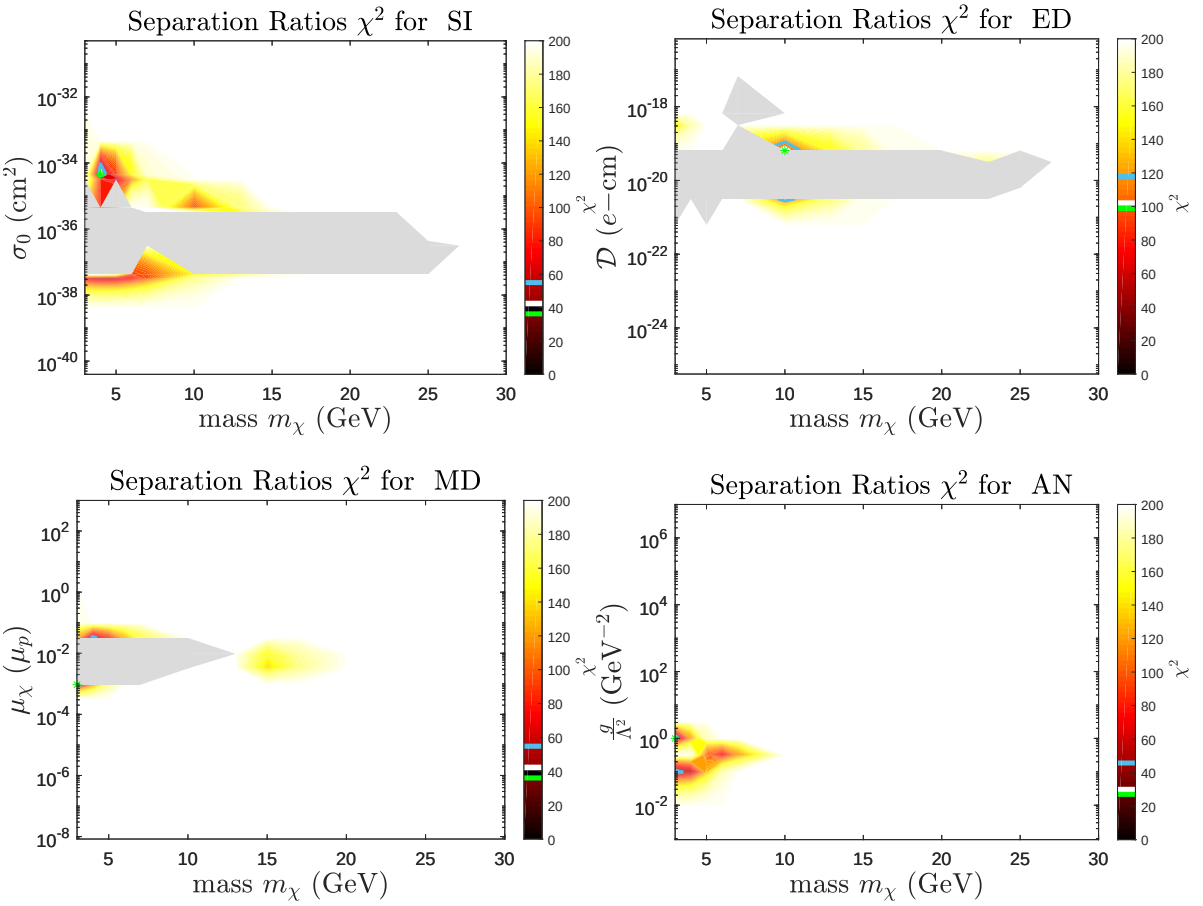

Figure 5.6: Combined likelihood χ^2 of the small frequency separation ratios defined in eq. (5.4) for spin independent dark matter (top left), electric dipole dark matter (top right), magnetic dipole dark matter (bottom left) and anapole dark matter (bottom right). The green star shows the best-fit χ^2 and the black, white and cyan contours show the preferred regions at 1, 2 and 4σ respectively, corresponding to $\Delta\chi^2 = 2.3$, 6.18 and 19.33 respectively. Simulations in the grey regions did not converge.

We define a combined χ^2 statistic for the frequency separation modes for a range of radial modes n for each of the separation ratios r_{02} and r_{13} such that:

$$\chi^2_{r_{l,l+1}} = \sum_n \frac{[r_{l,l+2,\text{th.}}(n) - r_{l,l+2,\text{obs.}}(n)]^2}{\sigma^2_{\text{obs.}}(n) + \sigma^2_{\text{th.}}(n)} \,. \tag{5.4}$$

We present the parameters space points which show the best fit to the frequency separation ratios r_{02} and r_{13} as measured by the BiSON experiment [578, 580] for each of the dark matter models in figure 5.5. Dipole moment dark matter improves the error in the frequency separation modes from approximately $3-4\sigma$ to within approximately 2σ, with the exception of the electric dipole model at low frequencies, due to the q^{-2} dependence of the electric dipole cross section. The overall χ^2 for both models, namely $\chi^2_{r_{02}} + \chi^2_{r_{13}}$ fits for the entire parameter space are shown in figure 5.6. Not all of the regions which show the best fit to the sound speed profile, as the frequency separation ratios are more sensitive to changes in the solar core, and so provide a better overall fit to the energy profile throughout the Sun.

5.4 Depth of the convection zone

We now move out from measurements dependent on the inner, nuclear fusing core of the Sun to parameters that are found in the outer regions, which are less related to the helioseismology observations. The first

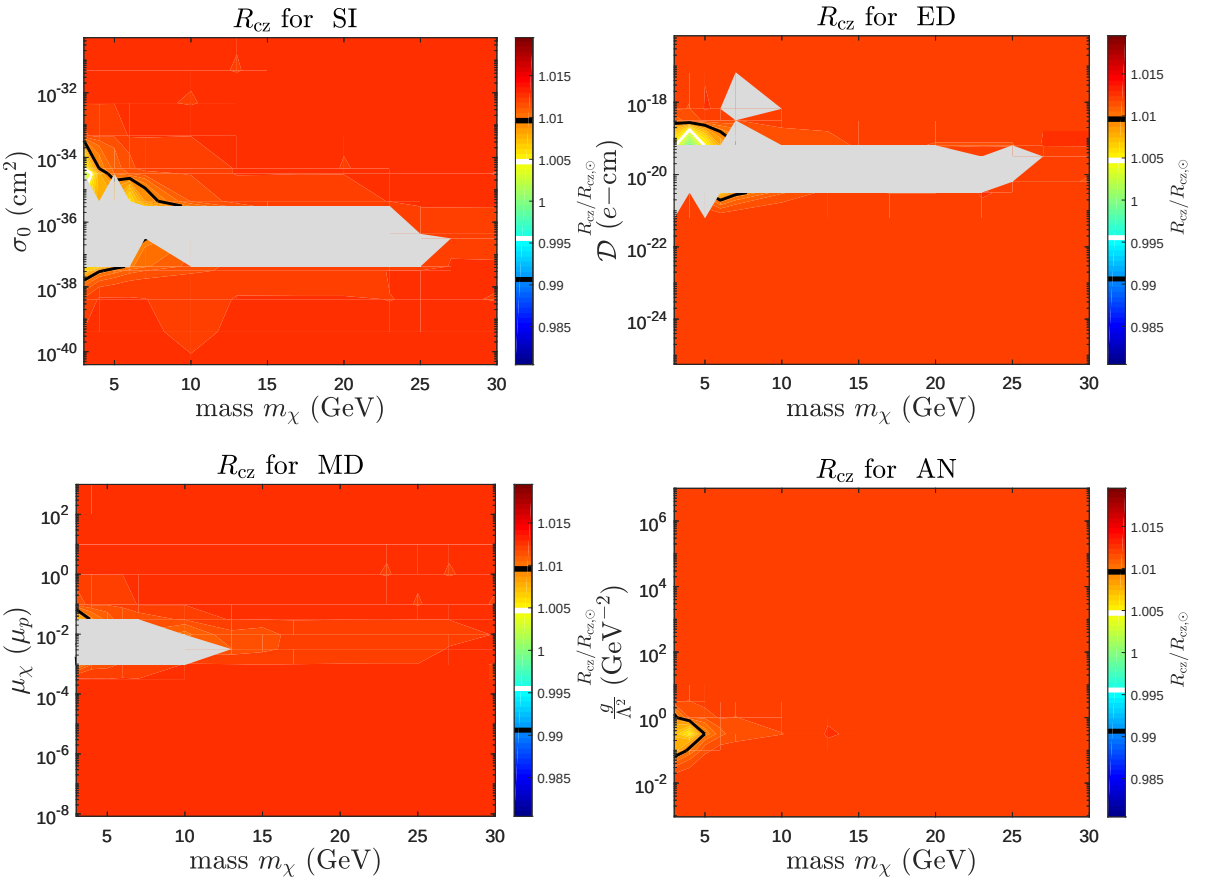

Figure 5.7: Ratio of predicted convective zone depth to the measured value $R_{\rm cz} = 0.713 R_\odot$ for spin independent dark matter (top left), electric dipole dark matter (top right), magnetic dipole dark matter (bottom left) and anapole dark matter (bottom right). The expected value is therefore 1. The white and black contours show the regions where the $R_{\rm cz}$ is 1σ and 2σ above/below the expected value respectively. Simulations in the grey regions did not converge.

such observation we consider is the depth of the convection zone $R_{\rm cz}$. Also known as the tachocline, it denotes the boundary between the radiative zone, where major heat transfer mechanism is radiation by high energy photons, and the convection zone, where convection patterns are the main heat transfer mechanism and the matter exists in local thermal equilibrium. Nuclei in the convection zone are transported from the tachocline to the surface via the convection mechanisms, while nuclei in the radiative zone are typically confined locally subject to the pressure and temperature gradients [581, 582]. The homogenous nature of the convection zone means that the elemental composition is well known throughout based on surface measurements. The convection zone depth is measured from the higher frequency modes of helieoseismology, since the propogation of pressure waves undergoes a step change at the boundary between the two zones, as their is a discontinuity in the derivative of the temperature gradient.

The value for $R_{\rm cz}$ is determined by calculating the discontinuity of the temperature gradient from the sound speed profile, making the measurement of the convection zone radius not statistically independent form the sound speed profile. The measured values of the convection zone radius is calculated from observations to be $R_{\rm cz} = (0.713 \pm 0.001) R_\odot$ [521, 582–584] which is approximately 3σ above the value predicted by standard solar models without any dark matter, a significant tension.

We present the ratio of the predicted to measured convection zone radius for each point in our parameter spaces for each of our models in figure 5.7. The models which do not modify the convection zone radius are shown as red in figure 5.7, indicating that they are in significant tension with the observed model. The better fits are indicated in yellow or green, in regions that correspond to the better fits to the

sound speed profile in figure 5.3. Indeed, the key feature of the best fits to the sound speed profile in figure 5.4 is an improvement to the major discrepancy at around $0.65R_\odot$, just inside the convection zone radius. Such models have provided sufficient energy transport into the radiative zone which increases the temperature gradient, exceeding the adiabatic gradient at a lower depth. However, such energy transport tends to correspond to the regions with poorer fits to the neutrino fluxes. The tension between the cooling of the inner core and heating of the convection zone is at the heart of the solar abundance problem.

5.5 Surface helium abundance

The best way of measuring the impact of the new models of dark matter on the convection zone, which runs all the way from the convection zone radius $R_{\rm cz}$ to the surface of the Sun is by measuring the surface helium abundance. Convective heat transfer means that the temperature and compositional profile at the surface is deterministic of the properties of the entire convection zone at time scales of months, rather than the thousands of years for the changes of structure in the remainder of the Sun. At the outer surface of the Sun is the solar convective envelope, where a second ionization of helium occurs in a region around $R = 0.98R_\odot$ [527], which causes a sharp depression in the adiabatic index, defined as $\Gamma_1 = \left.\frac{\partial \log P}{\partial \log \rho}\right|_{\rm ad}$. The depression affects the propogation of the pressure waves through the Sun and hence the high frequency helioseismology modes. The magnitude and position of the depression is determined by the proportion of helium to other nuclei, mainly hydrogen, in the convection zone. Due to the chemical mixing in the convection zone, the surface helium abundance can be measured independently from helioseismology through photospheric observations. Both are well in agreement. The best measurements for the surface helium abundance are $Y_{\rm surf} = 0.2485 \pm 0.0034$ [527].

Since the introduction of dark matter is to effect the energy transport in the Sun, it is expected that there will be a reduction in temperature in the solar core, where nuclear energy is released through fusion reactions. Such a reduction in temperature for any given star would be expected to reduce the total energy produced through nuclear fusion, and hence both the temperature throughout the star and the abundance of nuclear fusion by products would be reduced. However, in iterating our initial conditions to produce an overall luminosity that matches the observed solar luminosity $L_\odot$, we have marginally adjusted the initial hydrogen and helium abundances from the standard solar models in order for the resultant start to match the present day Sun. The resultant reduction in helium abundance is propagated through to the solar surface in a number of models we consider, though at most the reduction is $1 - 2\%$, approximately 1σ of the overall error budget.

For the vast majority of parameter points we consider, however, the effect on the surface helium abundance is negligible. We do not show the contour plots for the surface helium abundances as there is not a sufficiently significant variation for any but the most extreme cases. Most changes in the convection zone are convectively mixed, reducing the overall impact on any one observable at a single layer. The results are included in our overall consideration of the likelihoods.

5.6 Total likelihood

We have now considered the impact of introducing dark matter into the Sun on a range of helioseismological observables at all layers of the Sun. The temperature of the inner core is represented by the ^{8}B and ^{7}Be neutrino fluxes, the outer core and inner radiation zone is measured by the frequency separation ratios, the size of the outer radiation zone and temperature gradient is determined by the convection zone radius, and the properties of the convection zone are determined by the surface helium abundance. We can now construct a combined total likelihood by combining the χ^2 measurements from each of these observables

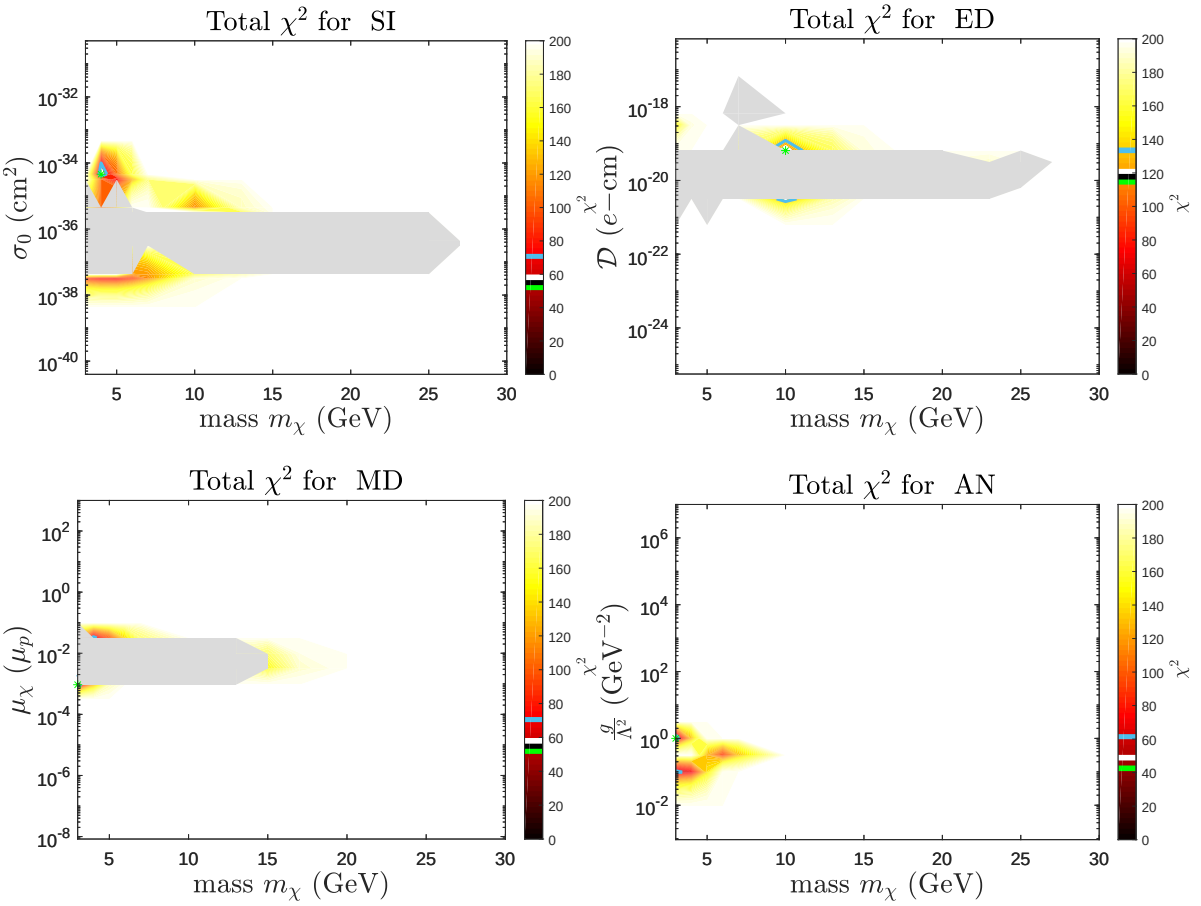

Figure 5.8: Combined χ^2 of neutrino fluxes, convective zone radius, surface helium abundance and frequency separation ratios matching observed values as given by eq. (5.5) for spin independent dark matter (top left), electric dipole dark matter (top right), magnetic dipole dark matter (bottom left) and anapole dark matter (bottom right). The green star shows the best-fit χ^2 and the black, white and cyan contours show the preferred regions at 1, 2 and 4σ respectively, corresponding to $\Delta\chi^2 = 2.3$, 6.18 and 19.33 respectively. Simulations in the grey regions did not converge.

as an overall χ^2 as:

$$\chi^2 = \frac{(\phi_B - \phi_{B,\text{obs}})^2}{\sigma_B^2} + \frac{(\phi_{Be} - \phi_{Be,\text{obs}})^2}{\sigma_{Be}^2} + \frac{(R_{\text{cz}} - R_{\text{cz,obs}})^2}{\sigma_{R_{\text{cz}}}^2} + \frac{(Y_{\text{surf}} - Y_{\text{surf,obs}})^2}{\sigma_{Y_{\text{surf}}}^2} + \chi_{r_{02}}^2 + \chi_{r_{13}}^2 \,. \quad (5.5)$$

taking the measurements from uncertainties from each of the observables independently. We do not include the sound speed profile as it is directly correlated with the frequency separation ratios and convection zone radius, and partially correlated with the surface helium abundance. We plot the total χ^2 likelihood for each point in parameter space in figure 5.8. We further present the points of parameter space which producess the best fit overall χ^2 likelihood in table 5.1. The best fit models overall roughly correspond to the best fit models for the sound speed profile and small frequency separations from figures 5.4 and 5.5 respectively, there being minor variations in the masses or coupling strengths.

On the whole, the introduction of any mechanism for energy transport due to dark matter improves the fit of the standard solar model to the selected observables compared to the case without any dark matter at all. In particular, the introduction of the electric dipole, magnetic dipole and anapole models perform better than the canonical spin independent dark matter at explaining the relevant observables. The reduced fit in the neutrino fluxes from the core of the Sun is at least partially offset by the improved measurements of the frequency separation ratios. The electric dipole and magnetic dipole interactions perform particularly well at mitigating the helioseismology tension without causing too much tension to

Runtype	m_χ	Coupling Strength	ν_{Be^7}	ν_{B^8}	R_{cz}	Y_s	χ^2_{total}
no DM	-	-	4.71	4.95	0.722	0.236	1000.0
SI	5	$\sigma_0 = 10^{-37.5}$ cm^2	4.366	3.714	0.720	0.234	72.6
ED	3	$\mathcal{D} = 10^{-9.5}$ $e-$cm	4.422	4.153	0.719	0.233	42.6
MD	3	$\mu_\chi = 10^{-3.0}$ μ_p	4.418	3.961	0.720	0.234	50.6
AN	3	$\frac{g}{\Lambda^2} = 10^{3.0}$ GeV^{-2}	4.280	3.640	0.718	0.233	36.3

Table 5.1: Table of parameters for best fit models. The run types are: Spin Independent (SI), Electric Dipole (ED), Magnetic Dipole (MD), Anapole (AN). The mass is in units of GeV. The beryllium-7 neutrino flux is in units 10^{-6}cm^{-2}s^{-1}, the boron-8 neutrino flux is in units 10^{-9}cm^{-2}s^{-1} and the convective zone radius is in units $R_\odot$.

the neutrino fluxes. Caution needs to be considered, however, due to the mass of the best fit particles. Each of the masses that generates the best fit is the lowest in the parameter space that we can consider before the effects of evaporation become dominant [552].

5.7 Discussion

Introducing dark matter into the Sun is an appealing, though not conclusive, mechanism for alleviating the tension between the standard solar models and the helioseismology observations. It has also provides a possible hint at the nature of dark matter if no other solution to the solar abundance problem can be found. Potentially favoured models include dark matter interacting through an anapole with an anapole moment of 1 GeV^{-2} and mass 3 GeV or an electric dipole moment with mass 3 GeV and dipole moment of 10^{-10} e - cm, though the viable models cover a non trivial part of the parameter space. All dark matter models have the ability to trigger some improvement to the helioseismological parameters beyond the standard solar model without any dark matter.

There is, however, a major problem with these findings. All of the favoured points in the parameter space for each of these models is well within the exclusion regions for direct detection, beam dump and collider constraints on electromagnetic dipole dakr matter [394, 400, 402]. The anapole moment and magentic dipole bounds are bounded above $\sim 10^{-4}$ GeV^{-2} and $10^{-4}\mu_p$ respectively for the given dark matter mass that produces the best fit. These bounds are more than an order of magnitude below the required best fit models for the Sun. Without a theoretical novelty to explain away the lack of direct detection of these models of dark matter, it is almost impossible to reconcile these models of dark matter existing in the Sun.

Despite the fact that the models are excluded by other experiments, the concept of introducing dark matter into the Sun does provide an example solution for the types of physics may be able to solve the solar abundance problem. Even then, that the inclusion of dark matter in general worsens the fit for the neutrino fluxes and surface helium abundance, hints that other mechanisms may be required, even if it replicates the same mechanics of energy transport. We have also made liberal assumptions about the number of dark matter particles in the Sun. By assuming that the annihilation and evaporation processes are negligible compared to the capture process, we have generated the best case scenario for the overall population of dark matter. However, since the evaporation effects are not negligible for dark matter masses less than ~ 4 GeV. It is precisely this regime which corresponds to our best fit results, casting further doubt on their veracity. What we have instead shown here is that improvement for the solar abundance problem is possible, either through a lighter or alternative dark matter process or some alternative astrophysical process.

The effect of magnetic dipole dark matter in the Sun had been previously analysed by ref. [547] which provided helioseismology bounds on the magnetic dipole moment. Here, we use the updated formalism for

energy transport in the Sun provided by ref [495], rather than the now outdated formalism of ref. [467]. The new formalism correctly accounts for the angular dependence in the differential cross section for magnetic dipole dark matter. By accounting for the angular dependence in the calculation of the thermal diffusivity α and thermal conductivity κ, our method produces a different energy transport mechanism. The electric dipole moment is equivalent to the q^{-2} dependent dark matter models that have been previously considered by refs. [495, 533], and we attain similar results, but reinterpret them in terms of the electric dipole moment of the dark matter particle. Anapole moment dark matter, with its unique $q^2 + v^2$ dependent cross section, has never before been considered in the Sun, making our results here completely novel.

In general, our models either improve the fits to the standard solar model or provide no change to the parameter space. As a result, we can not impose new exclusion bounds on the parameter space for each of our models of dark matter. The presence of other factors, such as evaporation or unknown features of solar physics makes such bounds difficult to enforce with statistical rigour. The few parameter space points which do result in a worsening of the solar physics bounds are too small to make generalised statements of the viability of such exclusion bounds.

There are several possible steps to improve on the shortcomings of our methodology to provide more precision, accuracy and tests of viability on dark matter models in the Sun. First, a full examination on the evaporation rates of momentum and velocity dependent dark matter now exists for light masses [552], though is not implemented her. Similarly, the calculation of the annihilation rates of dark matter in the Sun not only reduces the uncertainty in the dark matter population, but also direct detection of the by products of such dark matter annihilation, albeit from a location with significant amounts of background from other Standard Model fusion processes. Other modifications to the capture rate have been suggested where it is not already saturated, including modifications to the nuclear form factor we consider here [537] and enhancements to the capture rate for self interacting dark matter [585, 586], the latter of which is due to scattering of halo dark matter from dark matter which has already been captured by the Sun. There are also a number of astrophysical uncertainties due to the dependence on the capture rate on velocity distribution of dark matter in the galactic halo [328, 587]. Indeed, such uncertainties apply for most observations on dark matter including the direct and indirect detection rates. Attempts have been made to write descriptions of dark matter in a manner independent from halo measurements. In particular, refs. [400, 588] suggest that halo independent measurements of anapole and magnetic dipole dark matter could, albeit under tension, reconcile the required interaction strengths with the negative direct detection experiments.

We have now fully explored the effect of dark matter with dimension 5 electromagnetic dipole operators on the Sun, as well as a single dimension 6 operator. We have examined the mathematical and physical formalisms for introducing electric dipole, magnetic dipole and anapole moments in the Sun, coupling to the electric field, magnetic field and electromagnetic current respectively. We have developed the requirements for the capture rate and energy transport mechanisms due to these models of dark matter. Such mechanisms describe the quantity and distribution of the dark matter in the Sun and the changes to the temperature and molecular distributions of the Standard Model particles in the Sun itself. We have simulated the evolution of the Sun under these conditions with the `DarkStec` code, and have shown it is possible to alleviate problems with the sound speed profile, small frequency separations and convection zone radius, at the expense of increased tension with the rare fusion neutrino fluxes. Overall, such models improve the discrepancies of the solar abundance problem, but the required strengths of the dipole moments are excluded by direct detection experiments [391–396, 398–401, 403, 404, 411]. The result suggests that the discrepancies between solar models and helioseismology cannot be solved by dipole moment dark matter alone without some modification to the direct detection constraints.

Part III

Conclusion

Chapter 6

Discussion

We have now introduced and analysed dark matter which interacts through effective field theory operators through several different lenses. Our motivation for introducing such operators was to fully realise the possible viable parameter space of dark matter interacting at or around the weak scale with a model independent description in light of the persistent negative results from direct detection searches and failure to-date of the Large Hadron Collider to show any signals of supersymmetry. Overall, the evidence suggests that weak scale dark matter does remain viable, though future experiments will likely cover the last outposts of the parameter space. Due to the negative results from mainstream conventional dark matter detection experiments, we have also investigated a novel method of indirectly testing dark matter parameters, namely, the search for dark matter particles interacting via an electromagnetic dipole moment in the Sun. Although our results do suggest an improvement to the observable parameters in the Sun, the required coupling strengths and poor alterations to the dynamics of the inner core suggest that such models are not the precise solution to the solar abundance problem.

The most straightforward explanations of astronomical and cosmological observations of dark matter suggest that dark matter in the Universe exists as a fundamental or composite particle existing beyond the Standard Model. Colliding galaxy clusters indicate that dark matter cannot easily be explained by modifications to gravitational theories, and the anisotropies in the cosmic microwave background radiation and the levels of big bang nucleosynthesis both indicate that dark matter exists as a non-baryonic particle or collection of particles. Large scale structure formation suggests that the vast majority of such particles are not relativistic. Together, these observations narrow down a mass range for fermionic dark matter to no less than a few keV. In this work, we have consistently assumed that the dark matter is fermionic; a common assumption motivated by the observation that long-lived massive particles in the Standard Model are also fermionic. In principle, dark matter may be bosonic or fermionic with a spin greater than $\frac{1}{2}$. We have not considered such examples as they are generally motivated by alternate theoretical anomalies, for instance the axion. Our goal, rather, is to explore the limits of the parameter space of spin $\frac{1}{2}$ fermions, which posses most of their theoretical motivations at the weak scale.

We have described fermionic dark matter existing in the Universe in terms of its multiplet structure under the action of the $SU(2)$ weak interaction gauge groups. Our scope narrowed further by looking at three multiplets in particular, namely the singlet, doublet and triplet. These multiplets correspond to the trivial, fundamental and adjoint representations of the gauge group. Such representations give natural analogies to the neutralino particles in supersymmetric models, namely the bino, higgsino and wino respectively. Although there is a neat mapping from our models to supersymmetry, we stress that our models are not inherently supersymmetric: they may be any such fermion multiplets added to the Standard Model, regardless of the higher order theory. By considering effective field theory operators, we can approximate all of the higher order effects that would be caused by other supersymmetric particles in a

supersymmetric theory. Indeed, we have not even specifically stated whether our particles are fundamental or composite. Instead, the key limitation we have made on our models is that we have not considered higher order multiplets. In principle, such fermions may instead live in representations of dimension 4 or higher. However, we do not expect such multiplets to have a major impact on the physics behind our results. Of the two broad categories of dimension 5 operators we have constructed, the physical principles behind the electromagnetic dipole moments are relatively independent of the gauge structure of the multiplet. Indeed, in order to write down gauge invariant quantities for such theories would require decomposing the reducible representations of the higher orders into subrepresentations which include the adjoint representation, where the electroweak particles live. Similarly, the interactions which involve coupling a dark matter particle to the Higgs boson would require decomposing the reducible representations of the multiplets into the fundamental representation in order to construct a gauge invariant Lagrangian.

Here, we have considered only effective field theory operators up to dimension 5. The exception is the anapole, which lives at dimension 6, which we have included here as it is often considered in the literature as a direct companion to the electric dipole and magnetic dipole operators. Indeed, the anapole is also motivated as the only electromagnetic dipole moment for Majorana mass particles in CPT-invariant theories. Other higher order operators are generally considered to be suppressed by powers of the cut-off parameter Λ, although operators of up to dimension 7 are also thought to approximate the mass splitting between neutral and charged winos at the two loop level [406]. Considering dimension 6 operators would unlock a suite of operators which describe four-point interactions between dark matter and Standard Model fermions, or even between two different classes of dark matter particles. The latter would be constrained by the limits on self interacting dark matter from colliding galaxy clusters and the cusp-core problem, while the former would be expected to correspond to loop effects in scattering and annihilation to Standard Model fermions as observed by direct and indirect detection experiments respectively. However, the number of operators and hence independent parameters at dimension 6 is prohibitively large for a study such as the present one, as it is straightforward to construct gauge invariant quantities through the simple multiplication of two bilinears of gauge objects, especially as we strive to be model independent in our descriptions of such particles.

Additionally, at dimension 6 we would also unlock variations of the dimension 5 operators which now posses a derivative coupling to the boson operators, which includes the anapole as an derivative coupled interaction to the Standard Model electromagnetic field strength tensor. Such interactions naturally produce interactions with strong momentum dependence, which motivates them for scenarios where momentum dependence is required to evade other detection constraints. An example of a requirement for momentum dependence is a reconciliation between direct detection experiments which experience an annual modulation - which typically use lower mass nuclei - to those that do not - which typically use higher mass nuclei. However, it is the suggestion that dark matter which possess a momentum-dependent cross section could be a solution to the solar abundance problem by ref. [494] that motivated our analysis of electromagnetic dipole operators in the Sun.

We have used the thermal relic abundance of the dark matter as a guiding principle for evaluating the viability of any model. In particular, we have sought models which correctly account for density of dark matter in the Universe. We have investigated two mechanisms for expanding the region of masses which correspond to the observed relic density. For each of the operators, the direct annihilation through the dimension 5 operator is able to reduce the density of parameter points where are otherwise overabundant. The result is in general an increase of the viable thermal relic dark matter mass. However, the coupling strength required in such models are generally relatively large, with the particle masses close to and often exceeding the UV cut-off for the theory. In general, the effect is stronger for the electromagnetic dipole operators rather than the Higgs boson operators, as the annihilation by-products for the former are the somewhat lighter on-shell gauge bosons which fall out of thermal equilibrium at a slightly later epoch.

Nonetheless, our results show that the range of particle masses an order of magnitude above the TeV scale cannot be ignored. Such large mass particles are difficult to detect in direct detection experiments where the nuclear recoil targets have typical masses at the GeV scale, especially where the scattering processes involves the exchange of for example a Higgs boson.

The second regime which can produce viable thermal relics is where the masses of the particles are significantly modified by operators which carry interactions with the Higgs boson, and become mass terms after spontaneous symmetry breaking. In particular, where there is a mass cancellation between the mass parameter in the theory and dimension 5 operator the neutral particles lose their degeneracy with the charged particles in the theory. The result is a strong reduction in the rates of co-annihilation, which are some of the more dominant annihilation modes present. The reduction in the overall annihilation rate lifts otherwise under-abundant models back to the observed relic abundance. We have already discussed that such a cancellation does not necessarily correspond to a strong fine-tuning of the model; we are not seeking a complete reduction in the annihilation rate to reproduce the observed Universe. The result is viable thermal relics on the order of 100 GeV, particles with masses much less reach experimental constraints from the invisible width of the Z boson. However, we have only considered introducing the operators to the theory one at a time, and even then only for real coupling parameters. In reality, one might expect multiple operators to exist simultaneously with differing interaction strengths. Nonetheless, the overall principle remains the same, even if the combination of operators which produce the cancellation is different from that presented here. Indeed, the addition of extra operators only shifts the interaction strengths for which the cancellation occurs.

It is worth noting that modifications to the mass matrix in, for example, supersymmetric higgsinos in the manner we have demonstrated here are common in supersymmetric theories, corresponding to the one-loop interactions with higher order supersymmetric particles. In many supersymmetric models, the mass splittings are a small fraction of that which we consider here since the off-shell particles in the loop corrections are typically at the GUT scale. As we do not limit ourselves to supersymmetry models, and permit the inclusion of complex higher order physics or a composite particle as dark matter, we are not subject to the same limitations. Overall, the lighter masses in these dark matter models compared to their canonical values need to be considered seriously as the potential mass regime, and are within range of future indirect detection experiments.

In addition to the common catalogue of dark matter detection experiments, we have additionally considered alternate observations that may be used to measure dark matter interacting via our dimension 5 operators. The interactions coupled to a pair of Higgs bosons or the heavy electroweak bosons are necessarily short range, and scattering processes from the Standard Model are necessarily limited to the types of interactions that can be detected in direct detection experiments. However, the interaction via an electromagnetic dipole opens a new category of scattering processes, namely long range interactions via photons. Astrophysical processes that may be influenced by these interactions that may be detectable necessarily require a large concentration of dark matter spatially coincident with a large concentration of Standard Model particles. The dynamics of the latter must be reasonably well understood and precisely measured in order for the effects of the dark matter to be significant above any modelling or observational uncertainties. The Sun therefore becomes an appealing laboratory, with highly precise observations arising from helioseismology and a statistical tension with hints towards a resolution with dark matter. In particular, it has been previously suggested that momentum or velocity-dependent dark matter is a particularly appealing theory, precisely corresponding to electromagnetic dipole dark matter.

We have explored the full theory of introducing dark matter into the Sun and measuring its effect on energy transport, albeit subject to a number of key assumptions. For instance, we have made favourable assumptions with regards to the population of dark matter in the Sun. In reality, the annihilation processes may be a significant component of the Boltzmann equation, especially as the strength of the interaction

increases. Indeed, various experiment have proposed indirect detection from annihilation within the Sun producing neutrinos as a means for constraining dark matter [331]. Additionally, evaporation rates of dark matter from the Sun are predicted to become significant for light dark matter masses [552], precisely where we our models suggest the effect on the energy transport is strongest. We have also made minor assumptions about the transition to Knusden transport by assuming that the same values for the Knusden parameters are valid for momentum and velocity dependent and independent dark matter. A full analysis of dark matter in the Sun should include a correct calculation of all of these phenomenon. Such an inclusion would weaken the effect on energy transport. However, because the scales of interaction required are excluded by the direct detection rates, it would not be a worthwhile endeavour to pursue such accuracy, at least for the models of electromagnetic dipole dark matter.

The prospect of resolving the solar abundance problem with dark matter is not removed by our results, however it further demonstrates the difficulty involved in threading the needle between dark matter which resolves the tension in helioseismology observations and direct detection experiments. Low mass particles are an option as they can scatter resonantly with the hydrogen in the Sun while avoiding the lower thresholds of direct detection, but are susceptible to evaporation. Higher masses are both more readily excluded by direct detection and less able to efficiently provide energy transport. Finally, the possibility of other unknown systematics affecting the modelling or measurements prohibits any conclusive observations about the nature of dark matter.

Overall, there are still considerable prospects for discovering dark matter as a weakly interacting fermion, even when considering the lack of detection signal from direct or indirect detection experiments and the to-date failure of the Large Hadron Collider to provide reliable evidence of physics beyond the Standard Model. To rule out such models requires a full consideration of the available parameter space, from the order of tens of GeV through to the hundreds of TeV, not just at the masses which reliably produce thermal relics at dimension 4. In particular, the regions of parameter space with masses less than the canonical value are well within the possible detection regimes of current or near-future technology, though the heavier mass models are more difficult for searches. In particular, the detection of a particle in the lower mass regime would provide significant clues to the underlying nature and interactions of such particles. The effective field theory approach has provided a simple model to describe such interactions, independent of the vagaries of the higher scale physics, and is a key step between the eventual detection of dark matter and the description of the true underlying theory.

References

[1] B. Geytenbeek and B. Gripiaos, *Effective field theory analysis of composite higgsino-like and wino-like thermal relic dark matter*, *Journal of Cosmology and Astroparticle Physics* **05** (2021) 060, [arXiv:2011.06025].

[2] B. Geytenbeek, S. Rao, P. Scott, A. Serenelli, A. C. Vincent, M. White et al., *Effect of electromagnetic dipole dark matter on energy transport in the solar interior*, *Journal of Cosmology and Astroparticle Physics* **03** (2017) 029, [arXiv:1610.06737].

[3] F. Zwicky, *Die Rotverschiebung von extragalaktischen Nebeln (the redshift of extragalactic nebulae)*, *Heletica Physica Acta* **6** (1933) 110–127.

[4] F. Zwicky, *Nebulae as gravitational lenses*, *Physical Review* **51** (1937) 290.

[5] A. Einstein, *Lens-like action of a star by the deviation of light in the gravitational field*, *Science* **84** (1936) 506.

[6] F. Zwicky, *On the probability of detecting nebulae which act as gravitational lenses*, *Physical Review* **51** (1937) 679.

[7] E. Boldt, F. B. McDonald, G. Rigler and P. Serlemitsos, *Extended source of energetic cosmic X rays*, *Physical Review Letters* **17** (1966) 447.

[8] J. E. Felten, R. J. Gould, W. A. Stein and N. J. Woolf, *X-rays from the Coma Cluster of galaxies*, *The Astrophysical Journal* **146** (1966) 955.

[9] S. M. Lea, J. Silk, E. Kellogg and S. Murray, *Thermal-bremsstrahlung interpretation of cluster X-ray sources*, *The Astrophysical Journal* **184** (1973) L105.

[10] E. Kellogg and S. Murray, *Studies of cluster X-ray sources: Size measurements*, *The Astrophysical Journal* **193** (1974) L57.

[11] J. H. Oort, *The force exerted by the stellar system in the direction perpendicular to the galactic plane and some related problems*, *Bulletin of the Astronomical Institutes of the Netherlands* **238** (1932) 249.

[12] F. Zwicky, *On the masses of nebulae and clusters of nebulae*, *The Astrophysical Journal* **86** (1937) 217.

[13] V. C. Rubin and W. K. Ford, Jnr, *Rotation of the Andromeda nebula from a spectroscopic survey of emission regions*, *The Astrophysical Journal* **159** (1970) 379.

[14] H. C. van de Hulst, E. Raimond and H. van Woerden, *Rotation and density distribution of the Andromeda nebula derived from observations of the 21-cm line*, *Bulletin of the Astronomical Institutes of the Netherlands* **14** (1957) 1.

[15] V. C. Rubin, W. K. Ford, Jnr and N. Thonnard, *Rotational properties of 21 Sc galaxies with a large range of luminosities and radii, from NGC 4605 ($r = 4$ kpc) to UGC 2885 ($r = 122$ kpc)*, *The Astrophysical Journal* **238** (1980) 471.

[16] T. S. van Albada, J. N. Bahcall, K. Begeman and R. Sanscisi, *Distribution of dark matter in the spiral galaxy NGC 3198*, *The Astrophysical Journal* **295** (1985) 305.

[17] M. Fich, L. Blitz and A. A. Stark, *The rotation curve of the Milky Way to $2R_\odot$*, *The Astrophysical Journal* **342** (1989) 272.

[18] W. B. Burton and M. A. Gordon, *Carbon Monoxide in the galaxy. III. The overall nature of its distribution in the equatorial plane*, *Astronomy and Astrophysics* **63** (1978) 7.

[19] F. Pont, M. Mayor and G. Burki, *New radial velocities for classical cepheids. Local galactic rotation revisited*, *Astronomy and Astrophysics* **285** (1994) 415.

[20] S. Casertano and J. H. van Gorkom, *Declining rotation curves: The end of a conspiracy?*, *The Astronomical Journal* **101** (1991) 1231.

[21] J. P. Ostriker, P. J. E. Peebles and A. Yahil, *The size and mass of galaxies and the mass of the universe*, *The Astrophysical Journal* **193** (1974) L1.

[22] J. Einasto, A. Kaasik and E. Saar, *Dynamic evidence on massive coronas of galaxies*, *Nature* **250** (1974) 309.

[23] R. A. Flores and J. R. Primack, *Observational and theoretical constraints on singular dark matter halos*, *The Astrophysical Journal* **427** (1994) L1, [arXiv:astro-ph/9402004].

[24] A. Burkert, *The structure of dark matter halos in dwarf galaxies*, *The Astrophysical Journal* **447** (1995) L25, [arXiv:astro-ph/9504041].

[25] J. Dubinski and R. G. Carlberg, *The structure of cold dark matter halos*, *The Astrophysical Journal* **378** (1991) 496.

[26] L. Hernquist, *An analytical model for spherical galaxies and bulges*, *The Astrophysical Journal* **356** (1990) 359.

[27] J. F. Navarro, C. S. Frenk and S. D. M. White, *The structure of cold dark matter halos*, *The Astrophysical Journal* **462** (1996) 563, [arXiv:astro-ph/9508025].

[28] A. Borriello and P. Salucci, *The dark matter distribution in disc galaxies*, *Monthly Notices of the Royal Astronomical Society* **323** (2001) 285, [arXiv:astro-ph/0001082].

[29] B. Moore, F. Governato, T. Quinn, J. Stadel and G. Lake, *Resolving the structure of cold dark matter halos*, *The Astrophysical Journal* **310** (1998) L1147, [arXiv:astro-ph/9709051].

[30] B. Moore, T. Quinn, F. Governato, J. Stadel and G. Lake, *Cold collapse and the core catastrophe*, *Monthly Notices of the Royal Astronomical Society* **310** (1999) 1147, [arXiv:astro-ph/9903164].

[31] R. Jimenez, L. Verde and S. P. Oh, *Dark halo properties from rotation curves*, *Monthly Notices of the Royal Astronomical Society* **339** (2003) 243, [arXiv:astro-ph/0201352].

[32] J. F. Navarro, A. Ludlow, V. Springel, J. Wang, M. Vogelsberger, S. D. M. White et al., *The diversity and similarity of simulated cold dark matter haloes*, *Monthly Notices of the Royal Astronomical Society* **402** (2010) 21, [arXiv:0810.1522].

[33] A. Genina, A. Benítez-Llambay, C. S. Frenk, S. Cole, A. Fattahi, J. F. Navarro et al., *The core-cusp problem: a matter of perspective*, *Monthly Notices of the Royal Astronomical Society* **474** (2018) 1398, [arXiv:1707.06303].

[34] A. Pontzen and F. Governato, *How supernova feedback turns dark matter cusps into cores*, *Monthly Notices of the Royal Astronomical Society* **421** (2012) 3464, [arXiv:1106.0499].

[35] A. M. Brooks and A. Zolotov, *Why baryons matter: The kinematics of dwarf spheroidal satellites*, *The Astrophysical Journal* **786** (2014) 87, [arXiv:1207.2468].

[36] A. El-Zant, I. Shlosman and Y. Hoffman, *Dark halos: The flattening of the density cusp by dynamical friction*, *The Astrophysical Journal* **560** (2001) 636, [arXiv:astro-ph/0103386].

[37] F. J. Sánchez-Salcedo, J. Reyes-Iturbide and X. Hernandez, *An extensive study of dynamical friction in dwarf galaxies: the role of stars, dark matter, halo profiles and MOND*, *Monthly Notices of the Royal Astronomical Society* **370** (2006) 1829, [arXiv:astro-ph/0601490].

[38] S. Mashchenko, J. Wadsley and H. M. P. Couchman, *Stellar feedback in dwarf galaxy formation*, *Science* **319** (2007) 174, [arXiv:0711.4803].

[39] A. Del Popolo and P. Kroupa, *Density profiles of dark matter haloes on galactic and cluster scales*, *Astronomy and Astrophysics* **502** (2009) 733, [arXiv:0906.1146].

[40] D. R. Cole, W. Dehnen and M. I. Wilkinson, *Weakening dark matter cusps by clumpy baryonic infall*, *Monthly Notices of the Royal Astronomical Society* **416** (2011) 1118, [arXiv:1105.4050].

[41] D. N. Spergel and P. J. Steinhardt, *Observational evidence for self-interacting cold dark matter*, *Physical Review Letters* **84** (2000) 3760, [arXiv:astro-ph/9909386].

[42] A. Burkert, *The structure and evolution of weakly self-interacting cold dark matter halos*, *The Astrophysical Journal Letters* **534** (2000) 143, [arXiv:astro-ph/0002409].

[43] N. Yoshida, V. Springel, S. D. M. White and G. Tormen, *Weakly self-interacting dark matter and the structure of dark halos*, *The Astrophysical Journal Letters* **544** (2000) 87, [arXiv:astro-ph/0006134].

[44] R. Davé, D. N. Spergel, P. J. Steinhardt and B. D. Wandelt, *Halo properties in cosmological simulations of self-interacting cold dark matter*, *The Astrophysical Journal* **547** (2001) 574, [arXiv:astro-ph/0006218].

[45] B. Moore, S. Gelato, A. Jenkins, F. R. Pearce and V. Quilis, *Collisional versus collisionless dark matter*, *The Astrophysical Journal Letters* **535** (2000) 21, [arXiv:astro-ph/0002308].

[46] N. Yoshida, V. Springel, S. D. M. White and G. Tormen, *Collisional dark matter and the structure of dark halos*, *The Astrophysical Journal Letters* **535** (2000) 103, [arXiv:astro-ph/0002362].

[47] C. S. Kochanek and M. White, *A quantitative study of interacting dark matter in halos*, *The Astrophysical Journals* **543** (2000) 514, [arXiv:astro-ph/0003483].

[48] O. Y. Gnedin and J. P. Ostriker, *Limits on collisional dark matter from elliptical galaxies in clusters*, *The Astrophysical Journal* **561** (2001) 61, [arXiv:astro-ph/0010436].

[49] J. Miralda-Escude, *A test of the collisional dark matter hypothesis from cluster lensing*, *The Astrophysical Journal* **564** (2002) 60, [arXiv:astro-ph/0002050].

[50] A. H. G. Peter, M. Rocha, J. S. Bullock and M. Kaplinghat, *Cosmological simulations with self-interacting dark matter - II. Halo shapes versus observations*, *Monthly Notices of the Royal Astronomical Society* **430** (2013) 105, [arXiv:1208.3026].

[51] M. Rocha, A. H. G. Peter, J. S. Bullock, M. Kaplinghat, S. Garrison-Kimmel, J. Oñorbe et al., *Cosmological simulations with self-interacting dark matter - I. Constant-density cores and substructure*, *Monthly Notices of the Royal Astronomical Society* **430** (2013) 81, [arXiv:1208.3025].

[52] M. Vogelsberger, J. Zavala and A. Loeb, *Subahloes in self-interacting galactic dark matter haloes*, *Monthly Notices of the Royal Astronomical Society* **423** (2012) 3740, [arXiv:1201.5892].

[53] A. Loeb and N. Weiner, *Cores in dwarf galaxies from dark matter with a Yukawa potential*, *Physical Review Letters* **106** (2011) 171302, [arXiv:1011.6374].

[54] J. Zavala, M. Vogelsberger and M. G. Walker, *Constraining self-interacting dark matter with the Milky Way's dwarf spheroidals*, *Monthly Notices of the Royal Astronomical Society: Letters* **431** (2013) L20, [arXiv:1211.6426].

[55] S. Tulin and H.-B. Yu, *Dark matter self-interactions and small scale structure*, *Physics Reports* **730** (2018) 1, [arXiv:1705.02358].

[56] B. Paczyński, *Gravitational microlensing by the galactic halo*, *The Astrophysical Journal* **304** (1986) 1.

[57] K. Griest, *Galactic microlensing as a method of detecting massive compact halo objects*, *The Astrophysical Journal* **366** (1991) 412.

[58] MACHO Collaboration, *Gravitational microlensing as a method of detecting disk dark matter and faint disk stars*, *The Astrophysical Journal* **372** (1991) L79.

[59] MACHO Collaboration, *The MACHO project: Microlensing results from 5.7 years of Large Magellanic Cloud observations*, *The Astrophysical Journal* **542** (2000) 281, [arXiv:astro-ph/0001272].

[60] EROS-2 Collaboration, *Limits on the MACHO content of the Galactic Halo from the EROS-2 survey of the Magellanic Clouds*, *Astronomy and Astrophysics* **469** (2007) 387, [arXiv:astro-ph/0607207].

[61] Y. B. Zel'dovich and I. D. Novikov, *The hypothesis of cores retarded during expansion and the hot cosmological model*, *Soviet Astronomy* **10** (1966) 602.

[62] S. W. Hawking, *Black hole explosions?*, *Nature* **248** (1974) 30.

[63] B. Carr, F. Kühnel and M. Sandstad, *Primordial black holes as dark matter*, *Physical Review D* **94** (2016) 083504, [arXiv:1607.06077].

[64] R. Lynds and V. Petrosian, *Giant luminous arcs in galaxy clusters*, *Bulletin of the American Astronomical Society* **18** (1986) 1014.

[65] G. Soucail, Y. Mellier, B. Fort, G. Mathez and M. Cailloux, *The giant arc in A370: spectroscopic evidence for gravitational lensing from a source at $z = 0.724$*, *Astronomy and Astrophysics Letters* **191** (1988) 19.

[66] J. A. Tyson, F. Valdes and R. A. Wenk, *Detection of systematic gravitational lens galaxy images alignments: Mapping dark matter in galaxy clusters*, *The Astrophysical Journal* **349** (1990) L1.

[67] N. Kasier and G. Squires, *Mapping the dark matter with weak gravitational lensing*, *The Astrophysical Journal* **404** (1993) 441.

[68] G. Fahlman, N. Kaiser, G. Squires and D. Woods, *Dark matter in MS 1224 from distortion of background galaxies*, *The Astrophysical Journal* **437** (1994) 56.

[69] G. Squires, N. Kaiser, G. Fahlmna, A. Babul and D. Woods, *A weak gravitational lensing analysis of Abell 2390*, *The Astrophysical Journal* **469** (1996) 73, [arXiv:astro-ph/9602105].

[70] D. Clowe, A. Luppino, N. Kaiser, J. P. Henry and I. M. Giola, *Weak lensing by two $z \sim 0.8$ clusters of galaxies*, *The Astrophysical Journal* **497** (1998) L61, [arXiv:astro-ph/9801208].

[71] R. Barrena, A. Biviano, M. Ramella, E. E. Falco and S. Seitz, *The dynamical status of the cluster of galaxies 1E0657-56*, *Astronomy and Astrophysics* **386** (2002) 816, [arXiv:astro-ph/0202323].

[72] D. Clowe, A. Gonzalez and M. Markevitch, *Weak-lensing mass reconstruction of the interacting cluster 1E 0657-558: Direct evidence for the existence of dark matter*, *The Astrophysical Journal* **604** (2004) 596–603, [arXiv:astro-ph/0312273].

[73] D. Clowe, M. Bradač, A. H. Gonzalez, M. Markevitch, S. W. Randall, C. Jones et al., *A direct empirical proof of the existence of dark matter*, *The Astrophysical Journal* **648** (2006) 109, [arXiv:astro-ph/0608407].

[74] M. Bradač, D. Clowe, A. H. Gonzalez, P. Marshall, W. Forman, C. Jones et al., *Strong and weak lensing united. III. Measuring the mass distribution of the merging galaxy cluster 1ES 0657-558*, *The Astrophysical Journal* **652** (2006) 937, [arXiv:astro-ph/0608408].

[75] M. Markevitch, A. H. Gonzalez, D. Clowe, A. Vikhlinin, W. Forman, C. Jones et al., *Direct constraints on the dark matter self-interaction cross section from the merging galaxy cluster 1E 0657-56*, *The Astrophysical Journal* **606** (2004) 819, [arXiv:astro-ph/0309303].

[76] F. Kahlhoefer, K. Schmidt-Hoberg, M. T. Frandsen and S. Sarkar, *Colliding clusters and dark matter self-interactions*, *Monthly Notices of the Royal Astronomical Society* **437** (2013) 2865, [arXiv:1308.3419].

[77] W. A. Dawson, D. Wittman, M. J. Jee, P. Gee, J. P. Hughes, J. A. Tyson et al., *Discovery of a dissociative galaxy cluster merger with large physical separation*, *The Astrophysical Journal Letters* **747** (2012) L42, [arXiv:1110.4391].

[78] F. Gastaldello, M. Limousin, G. Foëx, R. P. Munñoz, T. Verdugo, V. Motta et al., *Dark matter-baryons separation at the lowest mass scale: the Bullet Group*, *Monthly Notices of the Royal Astronomical Society Letters* **442** (2014) L76.

[79] H. Dahle, C. L. Sarazin, L. A. Lopez, C. Kouveliotou, S. K. Patel, E. Rol et al., *The Burst Cluster: Dark matter in a cluster merger associated with the short gamma-ray burst GRB 050509B*, *The Astrophysical Journal* **772** (2013) 23, [arXiv:1305.4660].

[80] A. Mahdavi, H. Hoekstra, A. Babul, D. D. Balam and P. L. Capak, *A dark core in Abell 520*, *The Astrophysical Journal* **668** (2007) 806, [arXiv:0706.3048].

[81] D. Clowe, M. Markevitch, M. Bradač, A. H. Gonzalez, S. M. Chung, R. Massey et al., *On dark peaks and missing mass: A weak-lensing mass reconstruction of the merging cluster system A520*, *The Astrophysical Journal* **758** (2012) 128, [arXiv:1209.2143].

[82] M. J. Jee, A. Mahdavi, H. Hoekstra, A. Babul, J. J. Dalcanton, P. Carroll et al., *A study of the dark core in A520 with the Hubble Space Telescope: The mystery deepens*, *The Astrophysical Journal* **747** (2012) 96, [arXiv:1202.6368].

[83] J. Merten, D. Coe, R. Dupke, R. Massey, A. Zitrin, E. S. Cypriano et al., *Creation of cosmic structure in the complex galaxy cluster merger Abell 2744*, *Monthly Notices of the Royal Astronomical Society* **417** (2011) 333, [arXiv:1103.2772].

[84] M. Bradač, S. W. Allen, T. Treu, H. Ebeling, R. Massey, R. G. Morris et al., *Revealing the properties of dark matter in the merging cluster MACS J0025.4-1222*, *The Astrophysical Journal* **687** (2008) 959, [arXiv:0806.2320].

[85] LIGO Scientific Collaboration and Virgo Collaboration, Fermi Gamma-ray Burst Monitor and INTEGRAL, *Gravitational waves and gamma-rays from a binary neutron star merger: GW170817 and GRB 170817A*, *The Astrophysical Journal Letters* **848** (2017) L13, [arXiv:1710.05834].

[86] A. Goldstein, P. Veres, E. Burns, M. S. Briggs, R. Hamburg, D. Kocevski et al., *An ordinary gamma-ray burst with extraordinary implications: Fermi-GBM detection of GRB 170817A*, *The Astrophysical Journal Letters* **848** (2017) L14, [arXiv:1710.05446].

[87] LIGO Scientific Collaboration and Virgo Collaboration, Fermi GBM, INTEGRAL, IceCube Collaboration, AstroSat Cadmium Zinc Telluride Imager Team, IPN Collaboration et al., *Multi-messenger observations of a binary neutron star merger*, *The Astrophysical Journal Letters* **848** (2017) L12, [arXiv:1710.05833].

[88] E. O. Kahya and R. P. Woodard, *A generic test of modified gravity models which emulate dark matter*, *Physics Letters B* **652** (2007) 213, [arXiv:0705.0153].

[89] S. Boran, S. Desai, E. O. Kahya and R. P. Woodard, *GW170817 falsifies dark matter emulators*, *Physical Review D* **97** (2018) 041501, [arXiv:1710.06168].

[90] S. Seager, D. D. Sasselov and D. Scott, *How exactly did the universe become neutral?*, *The Astrophysical Journal Supplement Series* **128** (2000) 407, [arXiv:astro-ph/9912182].

[91] J. Dunkley, E. Komatso, M. R. Nolta, D. N. Spergel, D. Larson, G. Hinshaw et al., *Five-year Wilkinson Microwave Anisotropy Probe observations: Likelihoods and parameters from the WMAP data*, *The Astrophysical Journal Supplement Series* **180** (2009) 306, [arXiv:0803.0586].

[92] R. A. Alpher and R. Herman, *Evolution of the universe*, *Nature* **162** (1948) 774.

[93] A. A. Penzias and R. W. Wilson, *A measurement of excess antenna temprature at 4080 Mc/s*, *The Astrophysical Journal* **142** (1965) 419.

[94] D. J. FIxsen, *The temperature of the cosmic microwave background*, *The Astrophysical Journal* **707** (2009) 916, [arXiv:0911.1955].

[95] G. F. Smoot, M. V. Gorenstein and R. A. Muller, *Detection of anisotropy in the cosmic blackbody radiation*, *Physical Review Letters* **39** (1977) 898.

[96] Y. Hoffman, H. M. Courtois and R. B. Tully, *Cosmic bulk flow and the local motion from cosmicflows-2*, *Monthly Notices of the Royal Astronomical Society* **449** (2015) 4494, [arXiv:1503.05422].

[97] G. F. Smoot, C. L. Bennett, A. Kogut, E. L. Wright, J. Aymon, N. W. Boggess et al., *Structure in the COBE differential microwave radiometer first-year maps*, *The Astrophysical Journal* (1992) L1.

[98] A. Friedman, *Über die krümmung des raumes*, *Zeitschrift für Physik* **10** (1922) 377.

[99] L. Verde, H. V. Peiris, D. N. Spergel, M. R. Nolta, C. L. Bennett, M. Halpern et al., *First-year Wilkinson Microwave Anisotropy Probe (WMAP) observations: Parameter estimation methodology*, *The Astrophysical Journal Supplement Series* **148** (2003) 195, [arXiv:astro-ph/0302218].

[100] E. Hubble, *A relation between distance and radial velocity among extra-galactic nebulae*, *Proceedings of the National Academy of Sciences of the United States of America* **15** (1929) 168.

[101] W. L. Freedman, B. F. Madore, B. K. Gibson, L. Ferrarese, D. D. Kelson, S. Sakai et al., *Final results from the Hubble Space Telescope key project to measure the Hubble constant*, *The Astrophysical Journal* **553** (2001) 47, [arXiv:astro-ph/0012376].

[102] D. N. Spergel, L. Verde, H. V. Peiris, E. Komatsu, M. R. Nolta, C. L. Bennett et al., *First-year Wilkinson Microwave Anisotropy Probe (WMAP) observations: Determination of cosmological parameters*, *The Astrophysical Journal Supplement Series* **148** (2003) 175, [arXiv:astro-ph/0302209].

[103] D. N. Spergel, R. Bean, O. Doré, M. R. Nolta, C. L. Bennett, J. Dunkley et al., *Three-year Wilkinson Microwave Anisotropy Probe (WMAP) observations: Implications for cosmology*, *The Astrophysical Journal Supplement Series* **170** (2007) 377, [arXiv:astro-ph/0603449].

[104] G. Hinshaw, J. L. Weiland, R. S. Hill, N. Odegard, D. Larson, C. L. Bennett et al., *Five-year Wilkinson Microwave Anisotropy Probe observations: Data processing, sky maps, and basic results*, *The Astrophysical Journal Supplement Series* **180** (2009) 225, [arXiv:0803.0732].

[105] E. Komatsu, K. M. Smith, J. Dunkley, C. L. Bennett, B. Gold, G. Hinshaw et al., *Seven-year Wilkinson Microwave Anisotropy Probe (WMAP) observations: Cosmological interpretation*, *The Astrophysical Journal Supplement Series* **192** (2011) 18, [arXiv:1001.4538].

[106] G. Hinshaw, D. Larson, E. Komatsu, D. N. Spergel, C. L. Bennett, J. Dunkley et al., *Nine-year Wilkinson Microwave Anisotropy Probe (WMAP) observations: Cosmological paramter results*, *The Astrophysical Journal Supplement Series* **208** (2013) 19, [arXiv:1212.5226].

[107] Planck Collaboration, *Planck 2013 results. XVI. Cosmological paramters*, *Astronomy and Astrophysics* **571** (2014) A16, [arXiv:1303.5076].

[108] Planck Collaboration, *Planck 2015 results. XIII. Cosmological parameters*, *Astonomy and Astrophysics* **594** (2016) A13, [arXiv:1502.01589].

[109] Planck Collaboration, *Planck 2018 results. VI. Cosmological paramters*, *preprint* (2018) , [arXiv:1807.06209].

[110] A. M. Boesgaard and G. Steigman, *Big bang nucleosynthesis: Theories and observations*, *Annual Review of Astronomy and Astrophysics* **23** (1985) 319.

[111] S. Burles and D. Tytler, *The deuterium abundance towards Q1937-1009*, *The Astrophysical Journal* **499** (1998) 699, [arXiv:astro-ph/9712108].

[112] S. Burles and D. Tytler, *The deuterium abundance towards Q1009+2956*, *The Astrophysical Journal* **507** (1998) 732, [arXiv:astro-ph/9712109].

[113] P. M. Garnavich, R. P. Kirshner, P. Challis, J. Tonry, R. L. Gilliland, R. C. Smith et al., *Constraints on cosmological models from Hubble Space Telescope observations of high-z supernovae*, *The Astrophysical Journal* **493** (1998) L53, [arXiv:astro-ph/9710123].

[114] B. P. Schmidt, N. B. Suntzeff, M. M. Phillips, R. A. Schommer, A. Clocchiatti, R. P. Kirshner et al., *The high-z supernova search: Measuring cosmic decleration and global curvature of the universe using Type Ia supernoave*, *The Astrophysical Journal* **507** (1998) 46, [arXiv:astro-ph/9805200].

[115] A. G. Riess, A. V. Filippenko, P. Challis, A. Clocchiatti, A. Diercks, P. M. Garnavich et al., *Observational evidence from supernovae for an accelerating universe and a cosmological constant*, *The Astronomical Journal* **116** (1998) 1009, [arXiv:astro-ph/9805201].

[116] P. M. Garnavich, S. Jha, P. Challis, A. Clocchiatti, A. Diercks, A. V. Filippenkp et al., *Supernova limits on the cosmic equation of state*, *The Astrophysical Journal* **509** (1998) 74, [arXiv:astro-ph/9806396].

[117] J. H. Jeans, *The stability of a spherical nebula*, *Philosophical Transactions of the Royal Society A* **199** (1902) 1.

[118] J. R. Bond, A. S. Szalay and M. S. Turner, *Formation of galaxies in a gravitino-dominated universe*, *Physical Review Letters* **48** (1982) 1636.

[119] J. R. Bond and A. S. Szalay, *The collisionless damping of density fluctuations in an expanding universe*, *The Astrophysical Journal* **274** (1983) 443.

[120] G. R. Blumenthal, H. Pagels and J. R. Primack, *Galaxy formation by dissipationless particles heavier than neutrinos*, *Nature* **299** (1982) 37.

[121] A. G. Doroshkevich, M. Y. Khlopov, R. A. Sunyaev, A. S. Szalay and Y. B. Zeldovich, *Cosmological impact of the neutrino rest mass*, *Annals of the New York Academy of Sciences* **375** (1981) 32.

[122] P. J. E. Peebles, *Large-scale background temperature and mass fluctuations due to scale-invariant primeval perturbations*, *The Astrophysical Journal* **263** (1982) L1.

[123] S. Davidson, B. Campbell and D. Bailey, *Limits on particles of small electric charge*, *Physical Review D* **43** (1991) 2314.

[124] S. Davidson, S. Hannestad and G. Raffelt, *Updated bounds on milli-charged particles*, *Journal of High Energy Physics* **05** (2000) 003, [arXiv:hep-ph/0001179].

[125] W. Hu, R. Barkana and A. Gruzinov, *Fuzzy cold dark matter: The wave properties of ultralight particles*, *Physical Review Letters* **85** (2000) 1158, [arXiv:astro-ph/0003365].

[126] B. W. Lee and S. Weinberg, *Cosmological lower bound on heavy-neutrino masses*, *Physical Review Letters* **39** (1977) 165.

[127] P. Hut, *Limits on masses and number of neutral weakly interacting particles*, *Physics Letters B* **69B** (1977) 85.

[128] G. Steigman, *Cosmology confronts particle physics*, *Annual Review of Nuclear and Particle Science* **29** (1979) 313.

[129] J. L. Feng, A. Rajaraman and F. Takayama, *Superweakly interacting massive particles*, *Physical Review Letters* **91** (2003) 011302, [arXiv:hep-ph/0302215].

[130] J. L. Feng, A. Rajaraman and F. Takayama, *Superweakly interacting massive particle dark matter signals from the early universe*, *Physical Review D* **68** (2003) 063504, [arXiv:hep-ph/0305024].

[131] M. Bolz, A. Brandenburg and W. Buchmüller, *Thermal production of gravitinos*, *Nuclear Physics B* **606** (2001) 518, [arXiv:hep-ph/0012052].

[132] W. Buchmuller, K. Hamaguchi, M. Ratz and T. Yanagida, *Supergravity at colliders*, *Physics Letters B* **588** (2004) 90, [arXiv:hep-ph/0402179].

[133] J. Ellis, K. A. Olive, Y. Santoso and V. Spanos, *Gravitino dark matter in the CMSSM*, *Physics Letters B* **588** (2004) 7, [arXiv:hep-ph/0312262].

[134] F. Wang and J. M. Yang, *SuperWIMP dark matter scenario in light of WMAP*, *European Physical Journal C* **38** (2004) 129, [arxiv:hep-ph/0405186].

[135] L. Roszkowski, R. Ruiz de Austri and K.-Y. Choi, *Gravitino dark matter in the CMSSM and implications for leptogenesis and the LHC*, *Journal of High Energy Physics* **08** (2005) 080, [arXiv:hep-ph/0408227].

[136] K. Rajagopal, M. S. Turner and F. Wilczek, *Cosmological implications of axinos*, *Nuclear Physics B* **358** (1991) 447.

[137] L. Covi, J. E. Kim and L. Roszkowski, *Axinos as cold dark matter*, *Physical Review Letters* **82** (1999) 4180, [arXiv:hep-ph/9905212].

[138] L. Covi, H. B. Kim, J. E. Kim and L. Roszkowski, *Axinos as dark matter*, *Journal of High Energy Physics* **05** (2001) 033, [arXiv:hep-ph/0101009].

[139] K.-Y. Choi, L. Covi, J. E. Kim and L. Roszkowski, *Axino cold dark matter revisited*, *Journal of High Energy Physics* **04** (2012) 106, [arXiv:1108.2282].

[140] H. Baer and A. D. Box, *Fine-tuning favors mixed axion/axino cold dark matter over neutralinos in the minimal supergravity model*, *European Physical Journal C* **68** (2010) 523, [arXiv:0910.0333].

[141] R. D. Peccei and H. R. Quinn, *CP conservation in the presence of psuedoparticles*, *Physical Review Letters* **38** (1977) 1440.

[142] S. Weinberg, *A new light boson?*, *Physical Review Letters* **40** (1978) 223.

[143] F. Wilczek, *Problem of strong P and T invariance in the presence of instantons*, *Physical Review Letters* **40** (1978) 279.

[144] R. J. Crewther, P. Di Vecchia, G. Veneziano and E. Witten, *Chiral estimate of the electric dipole moment in quantum chromodynamics*, *Physics Letters* **88B** (1979) 123.

[145] J. M. Pendlebury, S. Afach, N. J. Ayers, C. A. Baker, G. Ban, G. Bison et al., *Revised experimental upper limit on the electric dipole moment of the neutron*, *Physical Review D* **92** (2015) 092003, [arXiv:1509.04411].

[146] S. J. Asztalos, L. J. Rosenberg, K. van Bibber, P. Sikivie and K. Zioutas, *Searches for astrophysical and cosmological axions*, *Annual Reviews of Nuclear and Particle Science* **56** (2006) 293.

[147] J. E. Kim, *Weak-interaction singlet and strong cp invariance*, *Physical Review Letters* **43** (1979) 103.

[148] M. A. Shifman, A. I. Vainshtien and V. I. Zakharov, *Can confinement ensure natural cp invariance of strong interactions*, *Nuclear Physics B* **166** (1980) 493.

[149] A. R. Zhitnitsky, *On posisble suppression of the axion hadron interactions*, *Soviet Journal of Nuclear Physics* **31** (1980) 260.

[150] M. Dine, W. Fischler and M. Srednicki, *A simple solution to the strong cp problem with a harmless axion*, *Physics Letters B* **104** (1981) 199.

[151] W. Keil, H.-T. Janka, D. N. Schramm, G. Sigl, M. S. Turner and J. Ellis, *Fresh look at axions and SN 1987A*, *Physical Review D* **56** (1997) 2419, [arXiv:astro-ph/9612222].

[152] K. J. Bae, J.-H. Huh and K. E. Kim, *Updating the axion cold dark matter energy density*, *Journal of Cosmology and Astroparticle Physics* **09** (2008) 005, [arXiv:0806.0497].

[153] S. Chang, C. Hagmann and P. Sikivie, *Studies of the motion and decay of axion walls bounded by strings*, *Physical Review D* **59** (1998) 023505, [arXiv:hep-ph/9807374].

[154] ADMX Collaboration, *Extended search for the invisible axion with the Axion Dark Matter Experiment*, *Physical Review Letters* **124** (2020) 101303, [arXiv:1910.08638].

[155] Super-Kamiokande Collaboration, *Evidence for oscillation in atmospheric neutrinos*, *Physical Review Letters* **81** (1998) 1562, [arXiv:hep-ex/9807003].

[156] SNO Collaboration, *Direct evidence for neutrino flavor transformation from neutral-current interactions in the Sudbury Neutrino Observatory*, *Physical Review Letters* **89** (2002) 011301, [arXiv:nucl-ex/0204008].

[157] A. Manohar, *Statistical mechancis of noninteracting particles*, *Physics Letters B* **186** (1987) 370.

[158] S. Dodelson and L. M. Widrow, *Sterile neutrinos as dark matter*, *Physical Review Letters* **72** (1994) 17, [arXiv:hep-ph/9303287].

[159] K. Abazajian and S. M. Koushiappas, *Constriants on sterile neutrino dark matter*, *Physical Review D* **74** (2006) 023527, [arXiv:astro-ph/0605271].

[160] A. Kusenko, *Sterile neutrinos, dark matter, and the pulsar velocities in models with a higgs singlet*, *Physics Review Letters* **97** (2006) 241301, [arXiv:hep-ph/0609081].

[161] P. B. Pal and L. Wolfenstein, *Radiative decays of massive neutrinos*, *Physical Review D* **25** (1982) 766.

[162] E. Bulbul, M. Markevitch, A. Foster, R. K. Smith, M. Loewenstein and S. W. Randall, *Detection of an unidentified emission line in the stacked X-ray spectrum of galaxy clusters*, *The Astrophysical Journal* **789** (2014) 13, [arXiv:1402.2301].

[163] A. Boyarsky, O. Ruchayskiy, D. Iakubovskyi and J. Franse, *Unidentified line in X-ray spectra of the Andromeda galaxy and Perseus galaxy cluster*, *Physical Review Letters* **113** (2014) 251301, [arXiv:1402.4119].

[164] D. Malyshev, A. Neronov and D. Eckert, *Constraints on 3.55 kev line emission from stacked observations of dwarf spheroidal galaxies*, *Physical Review D* **90** (2014) 103506, [arXiv:1408.3531].

[165] T. Jeltema and S. Profumo, *Deep XMM observations of Draco rule out at the 99 per cent confidence level a dark matter decay origin for the 3.5 kev line*, *Monthly Notices of the Royal Astronomical Society* **458** (2016) 3592, [arXiv:1512.01239].

[166] Z. G. Berezhiani, A. D. Dolgov and R. N. Mohapatra, *Asymmetric inflationary reaheating and the nature of mirror universe*, *Physics Letters B* **375** (1996) 26, [arXiv:hep-ph/9511221].

[167] J. Y. Kobzarev, L. B. Okun and I. Y. Pomeranchuk, *On the possibility of experimental observations of mirror particles*, *Soviet Journal of Nuclear Physics* **6** (1966) 837.

[168] Y. Kahn, G. Krnjaic, S. Mishra-Sharma and T. M. P. Tait, *Light weakly coupled axial forces: models, constraints and projections*, *Journal of High Energy Physics* **05** (2017) 002, [arXiv:1609.09072].

[169] P. F. Smith and J. D. Lewin, *Dark matter detection*, *Physics Reports* **187** (1990) 203.

[170] R. Bernabei, *Researches on dark matter*, *La Rivista del Nuovo Cimento* **18** (1995) 5.

[171] C. Bacci, P. Belli, R. Bernabei, D. Changjiang, D. Linkai, E. Gaillard et al., *WIMPs search with low activity NaI crystals. Preliminary results*, *Physics Letters B* **293** (1992) 460.

[172] N. J. C. Spooner, G. J. Davies, J. D. Davies, G. J. Pyle, T. D. Bucknell, G. T. A. Squier et al., *The scintillation efficiency of sodium and iodine recoils in a NaI(Tl) detector for dark matter searches*, *Physics Letters B* **321** (1994) 156.

[173] K. Fushimi, H. Ejiri, H. Kudomi, K. Kume, K. Nagata, H. Ohsumi et al., *Application of a large-volume NaI scintillator to search for dark matter*, *Physical Review C* **47** (1993) R425.

[174] T. Shutt, B. Ellman, P. D. Barnes Jnr, A. Cummings, A. Da Silva, J. Emes et al., *Measurement of ionization and phonon production by nuclear recoils in a 60 g crystak of germanium at 25 mK*, *Physical Review Letters* **69** (1992) 3425.

[175] T. Shutt, N. Wang, B. Ellman, Y. Giraud-Héraud, C. Stubbs, P. D. Barnes Jnr et al., *Simultaneous high resolution measurement of phonons and ionization created by particle interaction in a 60 g germanium crystal at 25 mK*, *Physical Review Letters* **69** (1992) 3531.

[176] M. L. Sarsa, F. T. Avignone, R. L. Brodzinski, E. Cerezo, J. I. Collar, E. García et al., *Dark matter searches at the Canfranc tunnel*, *Nuclear Physics B - Proceedings Supplements* **35** (1994) 154.

[177] F. Iachello, L. M. Krauss and G. Maino, *Spin-dependent scattering of weakly interacting massive particles in heavy nuclei*, *Physics Letters B* **254** (1991) 220.

[178] R. Bernabei, P. Belli, V. Landoni, F. Montecchia, W. Di Noclantonio, A. Incicchitti et al., *New limits on WIMP search with large-mass low-radioactivity NaI(TI) set-up at Gran Sasso*, *Physics Letters B* **389** (1996) 757.

[179] CDMS Collaboration, *Exclusion limits on the WIMP-nucleon cross section from the Cryogenic Dark Matter Search*, *Physical Review Letters* **84** (2000) 5699, [arXiv:astro-ph/0002471].

[180] R. Bernabei, P. Belli, F. Montecchia, W. Di Nicolantonio, A. Incicchitti, D. Prosperi et al., *Searching for WIMPs by the annual modulation signature*, *Physics Letters B* **424** (1998) 195.

[181] A. K. Drukier, K. Freese and D. N. Spergel, *Detecting cold dark-matter candidates*, *Physical Review D* **33** (1986) 3495.

[182] R. Bernabei, P. Belli, F. Montecchia, W. Di Nicolantonio, G. Ignesti, A. Incicchitti et al., *On a further search for a yearly modulation of hte rate in particle dark matter direct search*, *Physics Letters B* **450** (1999) 448.

[183] R. Bernabei, P. Belli, R. Cerulli, F. Montecchia, M. Amato, G. Ignesti et al., *Search for WIMP annual modulation signature: results from DAMA/NaI-3 and DAMA/NaI-4 and the global combined analysis*, *Physics Letters B* **480** (2000) 23.

[184] R. Bernabei, P. Belli, F. Cappella, R. Cerulli, C. J. Dai, A. d'Angelo et al., *First results from DAMA/LIBRA and the combined results with DAMA/NaI*, *European Physical Journal C* **56** (2008) 333, [arXiv:0804.2741].

[185] R. Bernabei, P. Belli, F. Cappella, R. Cerulli, C. J. Dai, A. d'Angelo et al., *New results from DAMA/LIBRA*, *European Physical Journal C* **67** (2010) 39, [arXiv:1002.1028].

[186] R. Bernabei, P. Belli, F. Capella, V. Caracciolo, S. Castellano, R. Cerulli et al., *Final model independent result of DAMA/LIBRA-phase 1*, *European Physical Journal C* **73** (2013) 2648, [arXiv:1308.5109].

[187] CDMS Collaboration, *Exclusion limits on the WIMP-nucleon cross section from the Cryogenic Dark Matter Search*, *Physical Review D* **66** (2002) 122003, [arXiv:astro-ph/0203500].

[188] CDMS Collaboration, *New results from the Cryogenic Dark Matter Search experiment*, *Physical Review D* **68** (2003) 082002.

[189] CDMS Collaboration, *First results from the Cryogenic Dark Matter Search in the Soudan Underground Laboratory*, *Physical Review Letters* **93** (2004) 211301, [arXiv:astro-ph/0405033].

[190] CDMS Collaboration, *Exclusion limits on the WIMP-nucleon cross section from the first run of the Cryogenic Dark Matter Search in the Soudan Underground Laboratory*, *Physical Review D* **72** (2005) 052009, [arXiv:astro-ph/0507190].

[191] CDMS Collaboration, *Limits on spin-independent interactions of Weakly Interacting Massive Particles with nucleons form the two-tower run of the Cryogenic Dark Matter Search*, *Physical Review Letters* **96** (2006) 011302, [arXiv:astro-ph/0509259].

[192] CDMS Collaboration, *Limits on spin-dependent WIMP-nucleon interactions from the Cryogenic Dark Matter Search*, *Physical Review D* **73** (2006) 011102, [arXiv:astro-ph/0509269].

[193] CDMS Collaboration, *Search for weakly interacting massive particles with the first five-tower data from the Cryogenic Dark Matter Search at the Soudan Underground Laboratory*, *Physical Review Letters* **102** (2009) 011301.

[194] CDMS-II Collaboration, *Dark matter search results from the CDMS II experiment*, *Science* **327** (2010) 1619.

[195] CDMS Collaboration and EDELWEISS Collaboration, *Combined limits on WIMPs from the CDMS and EDELWEISS experiments*, *Physical Review D* **84** (2011) 011102, [arXiv:1105.3377].

[196] CDMS Collaboration, *Silicion detector results from the first five-tower run of CDMS II*, *Physical Review D* **88** (2013) 031104, [arXiv:1304.3706].

[197] CDMS Collaboration, *Silicon detector dark matter results from the final exposure of CDMS II*, *Physical Review Letters* **111** (2013) 251301, [arXiv:1304.4279].

[198] SuperCDMS Collaboration, *Results from the Super Cryogenic Dark Matter Search experiment at Soudan*, *Physical Review Letters* **120** (2018) 061802, [arXiv:1708.08869].

[199] SuperCDMS Collaboration, *Seach for low-mass weakly interacting massive particles with SuperCDMS*, *Physical Review Letters* **112** (2014) 241302, [arXiv:1402.7137].

[200] SuperCDMS Collaboration, *New results from the search for low-mass weakly interacting massive particles with the CDMS low ionization threshold experiment*, *Physical Review Letters* **116** (2016) 071301, [arXiv:1509.02448].

[201] SuperCDMS Collaboration, *Low-mass dark matter search with CDMSlite*, *Physical Review D* **97** (2018) 022002, [arXiv:1707.01632].

[202] D. Speller, *A Background-subtracted search for annual modulation in CDMS II*. PhD thesis, University of California, Berkeley, 2017.

[203] CDMS Collaboration, *Search for annual modulation in low-energy CDMS-II data*, *arXiv:1203.1309* (2012) , [arXiv:1203.1309].

[204] C. Savage, G. Gelmini, P. Gondolo and K. Freese, *Compatibility of DAMA/LIBRA dark matter detection with other searches*, *Journal of Cosmology and Astroparticle Physics* **04** (2009) 010, [arXiv:0808.3607].

[205] COSINE-100 Collaboration, *An experiment to search for dark-matter interactions using sodium iodide detectors*, *Nature* **564** (2018) 83, [arXiv:1906.01791].

[206] M. Antonello, E. Barberio, T. Baroncelli, J. Benziger, L. J. Bignell, I. Bolognino et al., *The SABRE project and the SABRE proof-of-principle*, *European Journal of Physics C* **79** (2019) 363, [arXiv:1806.09340].

[207] R. Bernabei, M. Amato, P. Belli, R. Cerulli, C. J. Dai, H. L. He et al., *Investigating the DAMA annual modulation data in a mixed coupling framework*, *Physics Letters B* **509** (2001) 197.

[208] R. Bernabei, P. Belli, R. Cerullia, F. Montecchia, M. Amato, A. Incicchitti et al., *Investigating the DAMA annual modulation data in the framework of inelastic dark matter*, *European Physical Journal C* **23** (2002) 61.

[209] R. Bernabei, P. Belli, F. Montecchia, F. Nozzoli, F. Cappella, A. Incicchitti et al., *Investigating electron interacting dark matter*, *Physical Review D* **77** (2008) 023506, [arXiv:0712.0562].

[210] R. Bernabei, P. Belli, F. Cappella, R. Cerulli, C. J. Dai, H. L. He et al., *Investigation on light dark matter*, *Modern Physics Letters A* **23** (2008) 2125, [arXiv:0802.4336].

[211] UK Dark Matter Collaboration, *First limits on nuclear recoil events fro the ZEPLIN I galactic dark matter detector*, *Astroparticle Physics* **23** (2005) 444.

[212] XENON Collaboration, *First results from the XENON10 dark matter experiment at the Gran Sasso National Laboratory*, *Physical Review Letters* **100** (2008) 021303, [arXiv:0706.0039].

[213] G. J. Alner, H. M. Araújo, A. Bewick, C. Bungau, B. Camanzi, M. J. Carson et al., *First limits on WIMP nuclear recoil signals in ZEPLIN-II: A two-phase xenon detector for dark matter detection*, *Astroparticle Physics* **28** (2007) 287, [arXiv:astro-ph/0701858].

[214] D. Y. Akimov, H. M. Araújo, E. J. Barnes, V. A. Belov, A. Bewick, A. A. Burnekov et al., *WIMP-nucleon cross-section results from the second science run of ZEPLIN-III*, *Physics Letters B* **709** (2012) 14, [arXiv:1110.4769].

[215] LUX Collaboration, *First results from the LUX dark matter experiment at the Sanford Underground Research Facility*, *Physical Review Letters* **112** (2014) 091303, [arXiv:1310.8214].

[216] LUX Collaboration, *Results from a search for dark matter in the complete LUX exposure*, *Physical Review Letters* **118** (2017) 021303, [arXiv:1608.07648].

[217] PandaX Collaboration, *First dark matter search results from the PandaX-I experiment*, *Science China Physics* **57** (2014) 2024, [arXiv:1408.5114].

[218] PandaX-II Collaboration, *Dark matter results from the first 98.7-day data of PandaX-II experiment*, *Physical Review Letters* **117** (2016) 121303, [arXiv:1607.07400v3].

[219] PandaX-II Collaboration, *Dark matter results fom the 54-ton-day exposure of PandaX-II experiment*, *Physical Review Letters* **119** (2017) 181302, [arXiv:1708.06917].

[220] XENON100 Collaboration, *Dark matter results from 100 live days of XENON100 data*, *Physical Review Letters* **107** (2011) 131302, [arXiv:1104.2549].

[221] XENON100 Collaboration, *Dark matter results from 255 live days of XENON100 data*, *Physical Review Letters* **109** (2012) 181301, [arXiv:1207.5988].

[222] XENON Collaboration, *XENON100 dark matter results from a combination of 477 live days*, *Physical Review D* **94** (2016) 122001, [arXiv:1609.06154].

[223] XENON Collaboration, *First dark matter search results from the XENON1T experiment*, *Physical Review Letters* **119** (2017) 181301, [arXiv:1705.06655].

[224] XENON Collaboration, *Dark matter search results from a one ton-year exposure of XENON1T*, *Physical Review Letters* **121** (2018) 11302, [arXiv:1805.12562].

[225] LUX-ZEPLIN Collaboration, *Projected WIMP sensitivity of the LUX-ZEPLIN (LZ) dark matter experiment*, arXiv:1802.06039.

[226] D. Z. Freedman, *Coherent effects of a weak neutral current*, *Physical Review D* **9** (1974) 1389.

[227] J. D. Vergados and H. Ejiri, *Can solar neutrinos be a serious background in direct dark matter searches?*, *Nuclear Physics B* **804** (2008) 144, [arXiv:0805.2583].

[228] T. K. Gaisser and M. Honda, *Flux of atmospheric neutrinos*, *Annual Review of Nuclear and Particle Science* **52** (2002) 153, [arXiv:hep-ph/0203272].

[229] K. Hirata, T. Kajita, M. Koshiba, M. Nakahata, Y. Oyama, N. Sato et al., *Observation of a neutrino burst from the supernova SN1987A*, *Physical Review Letters* **58** (1987) 1490.

[230] R. M. Bionta, G. Blewitt, C. B. Bratton, D. Casper, A. Ciocio, R. Claus et al., *Observation of a neutrino burst in coincidence with Supernova 1987A in the Large Magellanic Cloud*, *Physical Review Letters* **58** (1987) 1494.

[231] L. E. Strigari, *Neutrino coherent scattering rates at direct dark matter detectors*, *New Journal of Physics* **11** (2009) 105011, [arXiv:0903.3630].

[232] J. Billard, E. Figueroa-Feliciano and L. Strigari, *Implication of neutrino backgrounds on the reach of next generation dark matter direct detection experiments*, *Physical Review D* **89** (2014) 023524, [arXiv:1307.5458].

[233] COHERENT Collaboration, *Observation of coherent elastic neutrino-nucleus scattering*, *Science* **357** (2017) 1123, [arXiv:1708.01294].

[234] C. Bœhm, D. G. Cerdeño, P. A. N. Machado, A. Olivares-Del Campo, E. Perdomo and E. Reid, *How high is the neutrino floor*, *Journal of Cosmology and Astroparticle Physics* **01** (2019) 043, [arXiv:1809.06385].

[235] J. H. Davis, *Dark matter vs. neutrinos: the effect of astrophysical uncertainties and timing information on the neutrino floor*, *Journal of Cosmology and Astroparticle Physics* **03** (2015) 012, [arXiv:1412.1475].

[236] P. Grothaus, M. Fairbairn and J. Monroe, *Directional dark matter detection beyond the neutrino bound*, *Physical Review D* **90** (2014) 055018, [arXiv:1406.5047].

[237] C. A. J. O'Hare, A. M. Green, J. Billard, E. Figueroa-Feliciano and L. E. Strigari, *Readout strategies for directional dark matter detection beyond the neutrino background*, *Physical Review D* **92** (2015) 063518, [arXiv:1505.08061].

[238] F. Ruppin, J. Billard, E. Figueroa-Feliciano and L. Strigari, *Complementarity of dark matter detectors in the light of the neutrino background*, *Physical Review D* **90** (2014) 083510, [arXiv:1408.3581].

[239] J. B. Dent, B. Dutta, J. L. Newstead and L. E. Strigari, *Effective field theory treatment of the neutrino background in direct dark matter detection*, *Physical Review D* **93** (2016) 075018, [arXiv:1602.05300].

[240] SuperCDMS Collaboration, *Search for low-mass dark matter with CDMSlite using a profile likelihood fit*, *Physical Review D* **99** (2019) 062001, [arXiv:1808.09098].

[241] CRESST Collaboration, *First results from the CRESST-III low-mass dark matter program*, *Physical Review D* **100** (2019) 102002, [arXiv:1904.00498].

[242] DARWIN Collaboration, *DARWIN: towards the ultimate dark matter detector*, *Journal of Cosmology and Astroparticle Physics* **11** (2016) 017, [arXiv:1606.07001].

[243] ZEPLIN-II Collaboration, *Limits on spin-dependent WIMP-nucleon cross sections from the first ZEPLIN-II data*, *Physics Letters B* **653** (2007) 161, [arXiv:0708.1883].

[244] LUX Collaboration, *Limits on spin-dependent WIMP-nucleon cross section obtained from the complete LUX exposure*, *Physical Review Letters* **118** (2017) 251302, [arXiv:1705.03380].

[245] PandaX-II Collaboration, *Spin-dependent weakly-interacting-massive-particle-nucleon cross section limits from first data of PandaX-II experiment*, *Physical Review Letters* **118** (2017) 071301, [arXiv:1611.06553].

[246] J. Ellis and R. A. Flores, *Elastic supersymmtric relic-nucleus scattering revisited*, *Physics Letters B* **263** (1991) 259.

[247] M. Barnabé-Heider, M. Di Marco, P. Doane, M.-H. Genest, R. Gornea, R. Guénette et al., *Improved spin-dependent limits from the PICASSO dark matter search experiment*, *Physics Letters B* **624** (2005) 186, [arXiv:hep-ex/0502028].

[248] COUPP Collaboration, *First dark matter search results from a 4-kg CF_3I bubble chamber operated in a deep underground site*, *Physical Review D* **86** (2012) 052001, [arXiv:1204.3094].

[249] PICO Collaboration, *Dark matter search results form the complete exposure of the PICO-60 c_3f_8 bubble chamber*, *Physical Review D* **100** (2019) 022001, [arXiv:1902.04031].

[250] T. A. Girard and F. Giuliani, *On the direct search for spin-dependent WIMP interactions*, *Physical Review D* **75** (2007) 043512, [arXiv:hep-ex/0511044].

[251] UK Dark Matter Collaboration, *Limits on WIMP cross-sections from the NAIAD experiment at the Boulby Underground Laboratory*, *Physics Letters B* **616** (2005) 17, [arXiv:hep-ex/0504031].

[252] KIMS collaboration, *Limits on interactions between weakly interacting massive particles and nucleons obtained with NaI(Tl) crystal detectors*, *Journal of High Energy Physics* **03** (2019) 194, [arXiv:1806.06499].

[253] KIMS Collaboration, *Limits on interactions between weakly interacting massive particles and nucleons obtained with CsI(Tl) crystal detectors*, *Physical Review Letters* **99** (2007) 091301, [arXiv:1204.2646].

[254] CRESST Collaboration, *First results on sub-GeV spin-dependent dark matter interactions with ^7Li*, *European Physical Journal C* **79** (2019) 630, [arXiv:1902.07587].

[255] C. Savage, P. Gondolo and K. Freese, *Can WIMP spin dependent couplings explain DAMA data, in light of null results from other experiments?*, *Physical Review D* **70** (2004) 123513, [arXiv:astro-ph/0408346].

[256] S. Scopel and K.-H. Yoon, *Inelastic dark matter with spin-dependent couplings to protons and large modulation fractions in DAMA*, *Journal of Cosmology and Astroparticle Physics* **02** (2016) 050, [arXiv:1512.00593].

[257] S. Baum, K. Freese and C. Kelso, *Dark matter implicaitons of DAMA/LIBRA-phase2 results*, *Physics Letters B* **789** (2019) 262, [arXiv:1804.01231].

[258] L. Bergström and H. Snellman, *Observable monochromatic photons from cosmic photino annihilation*, *Physical Review D* **37** (1988) 3737.

[259] L. Bergstrom, *Radiative processes in dark matter photino annihilation*, *Physics Letters B* **225** (1989) 372.

[260] L. Bergström, T. Bringmann, M. Eriksson and M. Gustafsson, *Gamma rays from heavy neutralino dark matter*, *Physical Review Letters* **95** (2005) 241301.

[261] M. Srednicki, S. Theisen and J. Silk, *Cosmic quarkonium: A probe of dark matter*, *Physical Review Letters* **56** (1986) 263.

[262] M. Gustafsson, E. Lundström, L. Bergström and J. Edjö, *Significant gamma lines from inert Higgs dark matter*, *Physical Review Letters* **99** (2007) 041301, [arXiv:astro-ph/0703512].

[263] T. Bringmann, L. Bergström and J. Edsjö, *New gamma-ray contributions to supersymmetric dark matter annihilation*, *Journal of High Energy Physics* **01** (2008) 049, [arXiv:0710.3169].

[264] M. Cirelli, N. Fornengo, T. Montaruli, I. Sokalski, A. Strumia and F. Vissani, *Spectra of neutrinos from dark matter annihilations*, *Nuclear Physics B* **727** (2005) 99, [arXiv:hep-ph/0506298].

[265] V. Barger, W.-Y. Keunga, G. Shaughnessy and A. Tregre, *High energy neutrinos from neutralino annihilations in the Sun*, *Physical Review D* **76** (2007) 095008, [arXiv:0708.1325].

[266] HESS Collaboration, *Search for dark matter annihilations towards the inner galactic halo from 10 years of observations with H.E.S.S.*, *Physical Review Letters* **117** (2016) 111301, [arXiv:1607.08142].

[267] HESS Collaboration, *Constraints on an annihilation signal from a core of constant dark matter density around the Milky Way centre with H.E.S.S.*, *Physical Review Letters* **114** (2015) 081301, [arXiv:1502.03244].

[268] D. Hooper and L. Goodenough, *Dark matter annihilation in the Galactic Center as seen by the Fermi gamma ray space telescope*, *Physics Letters B* **697** (2011) 412, [arXiv:1010.2752].

[269] C. Gordon and O. Macías, *Dark matter and pulsar model constraints from Galactic Center Fermi-LAT gamma-ray observations*, *Physical Review D* **88** (2013) 083521, [arXiv:1306.5725].

[270] K. N. Abazajian and M. Kaplinghat, *Detection of a gamma-ray source in the Galactic Center consistent with extended emission from dark matter annihilation and concentrated astrophysical emission*, *Physical Review D* **86** (2012) 083511, [arXiv:1207.6047].

[271] P. Scott, J. Conrad, J. Edsjö, L. Bergström, C. Farnier and Y. Akrami, *Direct constraints on minimal supersymmetry from Fermi-LAT observations of the dwarf galaxy Segue 1*, *Journal of Cosmology and Astroparticle Physics* **01** (2010) 031, [arXiv:0909.3300].

[272] A. A. Abdo, M. Ackermann, M. Ajello, W. B. Atwood, L. Baldini, J. Ballet et al., *Observations of Milky Way dwarf spheroidal galaxies with the Fermi-Large Area Telescope detector and constraints on dark matter models*, *The Astrophysical Journal* **712** (2010) 147, [arXiv:1001.4531].

[273] M. Wood, G. Blaylock, S. M. Bradbury, J. H. Buckley, K. L. Bryum, Y. C. K. Chow et al., *A search for dark matter annihilation with the Whipple 10 m telescope*, *The Astrophysical Journal* **678** (2008) 594, [arXiv:0801.1708].

[274] F. Aharonian, A. G. Akhperjanian, A. R. Bazer-Bachi, M. Beilicke, W. Benbow, D. Berge et al., *Observations of the Sagittarius dwarf galaxy by the HESS experiment and search for a dark matter signal*, *Astroparticle Physics* **29** (2008) 55, [arXiv:0711.2369].

[275] F. Aharonian, A. G. Akhperjanian, A. R. Bazer-Bachi, M. Beilicke, W. Benbow, D. Berge et al., *Erratum to "Observations of the Sagittarius dwarf galaxy by the HESS experiment and search for a dark matter signal" [Astroparticle Physics 29(1) (2008) 55-62]*, *Astroparticle Physics* **33** (2010) 274, [arXiv:0711.2369].

[276] J. Albert, E. Aliu, H. Anderhub, P. Antoranz, M. Backes, C. Baixeras et al., *Upper limit for γ-ray emission above 140 GeV from the dwarf spheroidal galaxy Draco*, *The Astrophysical Journal* **679** (2008) 421, [arXiv:0711.2574].

[277] F. Aharonian, A. G. Akhperjanian, U. Barres de Almeida, A. R. Bazer-Bachi, B. Beher, W. Benbow et al., *A search for a dark matter annihilation signal toward the Canis Major overdensity with H.E.S.S.*, *The Astrophysical Journal* **691** (2009) 175, [arXiv:0809.3894].

[278] V. Acciari, T. Arlen, T. Aune, M. Beilicke, W. Benbow, D. Boltuch et al., *VERITAS search for VHE gamma-ray emission from dwarf spheroidal galaxies*, *The Astrophysical Journal* **720** (2010) 1174, [arXiv:1006.5955].

[279] S. M. Faber and D. N. C. Lin, *Is there nonluminous matter in dwarf spheriodal galaxies?*, *The Astrophysical Journal* **266** (1983) L17.

[280] E. Brinks and U. Klein, *Dark matter in the dwarf galaxie II Zwicky 40*, *Monthly Notices of the Royal Astronomical Society* **231** (1988) 63P.

[281] S. Côté, C. Carignan and K. C. Freeman, *The various kinematics of dward irregular galaxies in neraby groups and their dark matter distributions*, *The Astronomical Journal* **120** (2000) 3027.

[282] S. S. McGaugh, *The baryonic Tully-Fisher relation of galaxies with extended rotation curves and the stellar mass of rotating galaxies*, *The Astrophysical Journal* **632** (2005) 859, [arXiv:astro-ph/0506750].

[283] E. Storm, T. E. Jeltema, S. Profumo and L. Rudnick, *Constraints on dark matter annihilation in clusters of galaxies from diffuse radio emission*, *The Astrophysical Journal* **768** (2013) 106, [arXiv:1210.0872].

[284] M. Ackermann, M. Ajello, A. Allanfort, L. Baldini, J. Ballet, G. Barbiellini et al., *Constraints on dark matter annihilation in clusters of galaxies with the Fermi large area telescope*, *Journal of Cosmology and Astroparticle Physics* **05** (2010) 025, [arXiv:1002.2239].

[285] L. Dugger, T. E. Jeltema and S. Profumo, *Constraints on decaying dark matter from Fermi observations of nearby galaxies and clusters*, *Journal of Cosmology and Astroparticle Physics* **12** (2010) 015, [arXiv:1009.5988].

[286] S. Ando and D. Nagai, *Fermi-LAT constraints on dark matter annihilation cross section from observations of the Fornax cluster*, *Journal of Cosmology and Astroparticle Physics* **07** (2012) 017, [arXiv:1201.0753].

[287] X. Huang and G. V. nd Cristoph Weniger, *Probing dark matter decay and annihilation with Fermi LAT observations of nearby galaxy clusters*, *Journal of Cosmology and Astroparticle Physics* **01** (2012) 042, [arXiv:1110.1529].

[288] E. Nezri, R. White, C. Combet, J. A. Hinton, D. Maurin and E. Pointecouteau, *γ-rays from annihilating dark matter in galaxy clusters: stacking versus single source analysis*, *Monthly Notices of the Royal Astronomical Society* **425** (2012) 477, [arXiv:1203.1165].

[289] J. Han, C. S. Frenk, V. R. Eke, L. Gao, S. D. M. White, A. Boyarsky et al., *Constraining extended gamma-ray emission from galaxy clusters*, *Monthly Notices of the Royal Astornomical Society* **427** (2012) 1651, [arXiv:1201.1003].

[290] HESS Collaboration, *Search for dark matter annihilation signals from the Fornax galaxy clsuter with H.E.S.S.*, *The Astrophysical Journal* **750** (2012) 123, [arXiv:1202.5494].

[291] MAGIC Collaboration, *MAGIC gamma-ray telescope observation of the Perseus cluster of galaxies: Implications for cosmic rays, dark matter and NGC 1275*, arXiv:0909.3267.

[292] Fermi LAT Collaboration, *Anisotropies in the diffuse gamma-ray background measured by the Fermi LAT*, *Physical Review D* **85** (2012) 083007, [arXiv:1202.2856].

[293] S. Camera, M. Fornasa, N. Fornengo and M. Regis, *A novel approach in the weakly interacting massive particle quest: Cross-correlation of gamma-ray anisotropies and cosmic shear*, *The Astrophysical Journal Letters* **771** (2013) L5, [arXiv:1212.5018].

[294] M. Ackermann, M. Ajello, W. B. Atwood, L. Baldini, G. Barbiellini, D. Bastieri et al., *Constraints on the galactic halo dark matter from Fermi-LAT diffuse measurements*, *The Astrophysical Journal* **761** (2012) 761, [arXiv:1205/6474].

[295] A. A. Abdo, M. Ackermann, M. Ajello, L. BAldini, J. Ballet, G. Barbiellini et al., *Constraints on cosmological dark matter annihilation from the Fermi-LAT isotropic diffuse gamma-ray measurement*, *Journal of Cosmology and Astroparticle Physics* **04** (2010) 014, [arXiv:1002.4415].

[296] K. N. Abazajian, S. Blanchet and J. P. Harding, *Current and future constraints on dark matter from prompt and inverse-Compton photon emission in the isotropic diffuse gamma-ray background*, *Physical Review D* **85** (2012) 043509, [arXiv:1011.5090].

[297] T. Bringmann, F. Calore, M. Di Mauro and F. Donato, *Constraining dark matter annihilation with the isotropic γ-ray background: Updated limits and future potential*, *Physical Review D* **89** (2014) 023012, [arXiv:1303.3284].

[298] D. Hooper, A. V. Belikov, T. E. Jeltema, T. Linden, S. Profumo and T. R. Slatyer, *The isotropic radio background and annihilating dark matter*, *Physical Review D* **86** (2012) 103003, [arXiv:1203.3547].

[299] J. A. Hinton, *The status of the HESS project*, *New Astronomy Reviews* **48** (2004) 331, [astro-ph/0403052].

[300] C. Baixeras, *The MAGIC telescope*, *Nuclear Physics B Proceedings Supplements* **114** (2003) 247.

[301] J. Holder, R. W. Atkins, H. M. Badran, G. Blaylock, S. M. Bradbury, J. H. Buckley et al., *The first VERITAS telescope*, *Astroparticle Physics* **25** (2006) 391, [astro-ph/0604119].

[302] W. B. Atwood, R. Bagagli, L. Baldini, R. Bellazzini, G. Barbiellini, F. Belli et al., *Design and initial tests of the Tracker-converter of the Gamma-ray Large Area Space Telescope*, *Astroparticle Physics* **28** (2007) 422.

[303] H.E.S.S. Collaboration, *Search for photon linelike signatures from dark matter annihilations with H.E.S.S.*, *Physical Review Letters* **110** (2013) 041301, [arXiv:1301.1173].

[304] H.E.S.S. Collaboration, *H.E.S.S. limits on linelike dark matter signatures in the 100 GeV to 2 TeV energy range close to the galactic centre*, *Physical Review Letters* **117** (2016) 151302, [arXiv:1609.08091].

[305] H.E.S.S. Collaboration, *Search for γ-ray line signals from dark matter annihilations in the inner galactic halo from 10 years of observations with H.E.S.S.*, *Physical Review Letters* **120** (2018) 201101.

[306] M. Ackermann, M. Ajello, A. Albert, B. Anderson, W. B. Atwood, L. Baldini et al., *Updated search for spectral lines from Galactic dark matter interactions with pass 8 data from the Fermi Large Area Telescope*, *Physical Review D* **91** (2015) 122002, [arXiv:1506.00013].

[307] Fermi-LAT Collaboration, *Seach for gamma-ray spectral lines with the Fermi Large Area Telescope and dark matter implications*, *Physical Review D* **88** (2013) 082002, [arXiv:1305.5597].

[308] Fermi LAT Collaboration, *The Fermi Galactic Center GeV excess and implications for dark matter*, *The Astrophysical Journal* **43** (2017) 840, [arXiv:1704.03910].

[309] H.E.S.S. Collaboration, *Search for a dark matter annihilation signal from the Galactic Center halo with H.E.S.S.*, *Physical Review Letters* **106** (2011) 161301, [arXiv:1103.3266].

[310] M. Fornasa, A. Cuoco, J. Zavala, J. M. Gaskins, M. A. Sánchez-Conde, G. Gomez-Vargas et al., *Angular power spectrum of the diffuse gamma-ray emission as measured by the Fermi Large Area Telescope and constraints on its dark matter interpretation*, *Physical Review D* **94** (2016) 123005, [arXiv:1608.07289].

[311] Fermi LAT Collaboration, *Limits on dark matter annihilation signals from the Fermi LAT 4-year measurement of the isotropic gamma-ray background*, *Journal of Cosmology and Astroparticle Physics* **09** (2015) 008, [1501.05464].

[312] Fermi-LAT, *Fermi LAT search for dark matter in gamma-ray lines and the inclusive photon spectrum*, *Physical Review D* **86** (2012) 022002, [arXiv:1205.2739].

[313] HESS Collaboration, *HESS observations of the Galactic Center region and their possible dark matter interpretation*, *Physical Review Letters* **97** (2006) 221102, [astro-ph/0610509].

[314] MAGIC Collaboration, *Searches for dark matter annihilation signatures in the Segue 1 satellite galaxy with the MAGIC-I telescope*, *Journal of Cosmology and Astroparticle Physics* **06** (2011) 035, [arXiv:1103.0477].

[315] H.E.S.S. Collaboration, *H.E.S.S. constraints on dark matter annihilations towards the scupltor and carina dwarf galaxies*, *Astroparticle Physics* **34** (2011) 608, [arXiv:1012.5602].

[316] H.E.S.S. Collaboration, *Search for dark matter annihilation signatures in H.E.S.S. observations of dwarf spheroidal galaxies*, *Physical Review D* **90** (2014) 112012, [arXiv:1410.2589].

[317] Fermi-LAT Collaboration and DES Collaboration, *Searching for dark matter annihilation in recently discovered Milky Way satellites with fermi-LAT*, *The Astrophysical Journal* **834** (2017) 110, [arXiv:1611.03184].

[318] Fermi-LAT Collaboration, *Searching for dark matter annihilation from Milky Way dwarf spheriodal galaxies with six years of Fermi Large Area Telescope data*, *Physical Review Letters* **115** (2015) 231301, [arXiv:1503.02641].

[319] Fermi-LAT Collaboration, *Dark matter constraints from observations of 25 Milky Way satellite galaxies with the Fermi Large Area Telescope*, *Physical Review D* **89** (2014) 042001, [arXiv:1310.0828].

[320] Fermi-LAT Collaboration, *Constraining dark matter models from a combined analysis of Milky Way satellites with the Fermi Large Area Telescope*, *Physical Review Letters* **107** (2011) 241302, [arXiv:1108.3546].

[321] VERITAS Collaboration, *Dark matter constraints from a joint analysis of dwarf Spheriodal galaxy observations with VERITAS*, *Physical Review D* **95** (2017) 082001, [arXiv:1703.04937].

[322] MAGIC Collaboration, J. Aleksić, M. Wood, B. Anderson, E. D. Bloom, J. Cohen-Tanugi et al., *Limits to dark matter annihilation cross-section from a combined analysis of MAGIC and Fermi-LAT observations of dwarf satellite galaxies*, *Journal of Cosmology and Astroparticle Physics* **02** (2016) 039, [arXiv:1601.06590].

[323] MAGIC Collaboration, *Indirect dark matter searches in the dwarf satellite galaxy Ursa Major II with the MAGIC telescopes*, *Journal of Cosmology and Astroparticle Physics* **03** (2018) 009, [arXiv:1712.03095].

[324] H.E.S.S. Collaboration, M. Cirelli, P. Panci, F. Sala, J. Silk and M. Taoso, *Searches for gamma-ray lines and 'pure WIMP' spectra from dark matter annihilations in dwarf galaxies with H.E.S.S.*, *Journal of Cosmology and Astroparticle Physics* **11** (2018) 037, [arXiv:1810.00995].

[325] HESS Collaboration, *H.E.S.S. observations of the globular clusters NGC 6388 and M15 and search for a dark matter signal*, *The Astrophysical Journal* **735** (2011) 12, [arXiv:1104.2548].

[326] T. Arlen, T. Aune, M. Beilicke, W. Benbow, A. Bouvier, J. H. Buckley et al., *Constraints on cosmic rays, magnetic fields, and dark matter from gamma-ray observations of the Coma cluster of galaxies with VERITAS and fermi*, *The Astrophysical Journal* **757** (2012) 123, [arXiv:1208.0676].

[327] A. Gould, *Weakly interacting massive particle distribution in and evaporation from the Sun*, *The Astrophysical Journal* **321** (1987) 560.

[328] A. Gould, *Resonant enhancements in weakly interacting massive particle capture by the Earth*, *The Astrophysical Journal* **321** (1987) 571.

[329] A. R. Zentner, *High-energy neutrinos from dark matter particle self-capture within the Sun*, *Physical Review D* **80** (2009) 063501, [arXiv:0907.3448].

[330] A. Cuoco, P. De La Torre Luque, F. Gargano, M. Gustafsson, F. Loparco, M. N. Mazziotta et al., *Search for dark matter cosmic-ray electrons and positrons from the Sun with the Fermi Large Area Telescope*, *Physical Review D* **101** (2020) 022002, [arXiv:1912.09373].

[331] ANTARES Collaboration, *First results on dark matter annihilation in the Sun using the ANTARES neutrino telescope*, *Journal of Cosmology and Astroparticle Physics* **11** (2013) 032, [arXiv:1302.6516].

[332] S. Adrián-Martínez, A. Albert, M. André, G. Anton, M. Ardid, J.-J. Aubert et al., *Limits on dark matter annihilation in the Sun using the ANTARES neutrino telescope*, *Physics Letters B* **759** (2016) 69, [arXiv:1603.02228].

[333] IceCube Collaboration, *Improved limits on dark matter annihilation in the Sun with the 79-string IceCube detector and implications for supersymmetry*, *Journal of Cosmology and Astroparticle Physics* **04** (2016) 022, [arXiv:1601.00653].

[334] IceCube Collaboration, *Searching for annihilating dark matter in the Sun with 3 years of IceCube data*, *European Physical Journal C* **77** (2017) 146, [arXiv:1612.05949].

[335] C.-S. Chen, F.-F. Lee, G.-L. Lin and Y.-H. Lin, *Probing dark matter self-interaction in the Sun with IceCube-PINGU*, *Journal of Cosmology and Astroparticle Physics* **10** (2014) 049, [arXiv:1408.5471].

[336] IceCube Collaboration, *First search for dark matter annihilations in the Earth with the IceCube detector*, *European Physical Journal C* **77** (2017) 82, [arXiv:1609.01492].

[337] A. Albert, M. André, M. Anghinolfi, G. Anton, M. Ardid, J.-J. Aubert et al., *Search for dark matter annihilation in the earth using the ANTARES neutrino telescope*, *Physics of the Dark Universe* **16** (2017) 41, [arXiv:1612.06792].

[338] ANTARES Collaboration, *Search of dark matter annihilation in the galactic centre using the ANTARES neutrino telescope*, *Journal of Cosmology and Astroparticle Physics* **10** (2015) 068, [1505.04866].

[339] A. Albert, M. André, M. Anghinolfi, G. Anton, M. Ardid, J.-J. Aubert et al., *Results from the search for dark matter in the Milky Way with 9 years of data of the ANTARES neutrino telescope*, *Physics Letters B* **769** (2017) 249, [arXiv:1612.04595].

[340] IceCube Collaboration, *Search for dark matter annihilation in the Galactic Center with IceCube-79*, *European Physical Journal C* **75** (2015) 492, [arXiv:1505.07259].

[341] IceCube Collaboration, *IceCube search for dark matter annihilation in nearby galaxies and galaxy clusters*, *Physical Review D* **88** (2013) 122001, [arXiv:1307.3473].

[342] IceCube Collaboration, *Search for neutrinos from decaying dark matter with IceCube*, *European Physical Journal C* **78** (2018) 831, [arXiv:1804.03848].

[343] J.-L. Gervais and B. Sakita, *Field theory interpretation of supergauges in dual models*, *Nuclear Physics B* **34** (1971) 632.

[344] R. Haag, J. T. Łuposzański and M. Sohnius, *All possible generators of supersymmetries of the S-matrix*, *Nuclear Physics B* **88** (1975) 257.

[345] S. Coleman and J. Mandula, *All possible symmetries of the S matrix*, *Physical Review* **159** (1967) 1251.

[346] ATLAS Collaboration, *Observation of a new particle in the search for the Standard Model Higgs boson with the ATLAS detector at the LHC*, *Physics Letters B* **716** (2012) 1, [arXiv:1207.7214].

[347] CMS Collaboration, *Observation of a new boson at a mass of 125 GeV with the CMS experiment at the LHC*, *Physics Letters B* **716** (2012) 30, [arXiv:1207.7235].

[348] L. Alvarez-Gaumé and E. Witten, *Gravitational anomalies*, *Nuclear Physics B* **234** (1983) 269.

[349] A. Djouadi, *The anatomy of electroweak symetry breaking Tome II: The Higgs bosons in the Minimal Supersymmetric Model*, *Physics Reports* **459** (2008) 1, [arXiv:hep-ph/0503173].

[350] S. Weinberg, *A model of leptons*, *Physical Review Letters* **19** (1967) 1264.

[351] J. Goldstone, *Field theories with superconductor solutions*, *Il Nuovo Cimento* **19** (1961) 154.

[352] G. Dvali, G. F. Giudice and A. Pomarol, *The μ-problem in theories with gauge-mediated supersymmetry breaking*, *Nuclear Physics B* **478** (1996) 31, [arXiv:hep-ph/9603238].

[353] J. S. Hagelin, G. L. Kane and S. Raby, *Perhaps scalar neutrinos are the lightest supersymmetric partners*, *Nuclear Physics B* **241** (1984) 638.

[354] L. E. Ibáñez, *The scalar neutrinos as the lightest supersymmetric particles and cosmology*, *Physics Letters B* **137** (1984) 160.

[355] D. E. López-Fogliani, A. D. Perez and R. Ruiz de Austri, *Dark matter candidates in the NMSSM with RH neutrino superfields*, *Journal of Cosmology and Astroparticle Physics* **04** (2021) 067, [arXiv:2102.08986].

[356] S. P. Ahlen, F. T. Avignone, III, R. L. Brodzinski, A. K. Drukier, G. Gelmini and D. N. Spergel, *Limits on cold dark matter candidates from an ultralow background germanium spectrometer*, *Physics Letters B* **195** (1987) 603.

[357] M. Beck, *The HEIDELBERG-MOSCOW experiment: Searching for dark matter*, *Nuclear Physics B - Proceedings Supplements* **35** (1994) 150.

[358] D. O. Caldwell, R. M. Eisberg, D. M. Grumm, M. S. Witherell, B. Sadoulet, F. S. Goulding et al., *Laboratory limits on galactic cold dark matter*, *Physical Review Letters* **61** (1988) 510.

[359] T. Falk, K. A. Olive and M. Srednicki, *Heavy sneutrinos as dark matter*, *Physics Letters B* **339** (1994) 248, [arXiv:hep-ph/9409270].

[360] L. D. Rose, S. Khalil, S. J. D. King, S. Kulkarni, C. Marzo, S. Moretti et al., *Sneutrino dark matter in the BLSSM*, *Journal of High Energy Physics* **07** (2018) 100, [arXiv:1712.05232].

[361] J. Ellis, J. S. Hagelin, D. V. Nanopoulos, K. Olive and M. Srednicki, *Supersymmetric relics from the big bang*, *Nuclear Physics B* **238** (1984) 453.

[362] J. Ellis, J. S. Hagelin, D. V. Nanopoulos and M. Srednicki, *Search for supersymmetry at the $\bar{p}p$ collider*, *Physics Letters B* **127** (1983) 233.

[363] P. Draper and H. Rzehak, *A review of higgs mass calculations in supersymmetric models*, *Physics Reports* **619** (2016) 1, [arXiv:1601.01890].

[364] G. Jungman, M. Kamionkowski and K. Griest, *Supersymmetric dark matter*, *Physics Reports* **267** (1996) 195.

[365] L. Roszkowski, E. M. Sessolo and S. Trojanowski, *WIMP dark matter candidates and searches-current status and future prospects*, *Reports on Progress in Physics* **81** (2018) 066201, [1707.06277].

[366] OPAL Collaboration, *Measurement of the Z^0 mass and width with the OPAL detector at LEP*, *Physics Letters B* **231** (1989) 530.

[367] J. L. Feng and M. J. Strassler, *Determination of fundamental supersymmetry paramters from chargino produciton at CERN LEP II*, *Physical Review D* **51** (1995) 4661, [arXiv:hep-ph/9408359].

[368] J. Hisano, S. Matsumoto, M. M. Nojiri and O. Saito, *Direct detection of the Wino and Higgsino-like neutralino dark matter at one-loop level*, *Physical Review D* **71** (2005) 015007, [arXiv:hep-ph/0407168].

[369] J. Hisano, S. Matsumoto, M. Nagai, O. Saito and M. Senami, *Non-perturbative effect on thermal relic abundance of dark amtter*, *Physics Letters B* **646** (2007) 34, [arXiv:hep-ph/0610249].

[370] A. Hryczuk, R. Iengo and P. Ullio, *Relic densities including Sommerfeld enhancements in the MSSM*, *Journal of High Energy Physics* **03** (2011) 69, [arXiv:1010.2172].

[371] M. Beneke, A. Bharucha, F. Dighera, C. Hellmann, A. Hryczuk, S. Recksiegel et al., *Relic density of wino-like dark matter in the MSSM*, *Journal of High Energy Physics* **03** (2016) 119, [arXiv:1601.04718].

[372] M. Beneke, C. Hellmann and P. Ruiz-Fermenía, *Non-relativistic pair annihilation of nearly mass degenerate neutralinos and charginos III. Computation of the Sommerfeld enhancements*, *Journal of High Energy Physics* **05** (2015) 115, [arXiv:1411.6924].

[373] N. Arkani-Hamed, A. Delgado and G. F. Giudice, *The well-tempered neutralino*, *Nuclear Physics B* **741** (2006) 108, [arXiv:hep-ph/0601041].

[374] S. Profumo and C. E. Yaguna, *Statisical analysis of supersymmetric dark matter in the minimal supersymmetric standard model after WMAP*, *Physical Review D* **70** (2004) 095004, [arXiv:hep-ph/0407036].

[375] H. Baer, A. Lessa, S. Rajagopalan and W. Sreethawong, *Mixed axion/neutralino cold dark matter in supersymmetric models*, *Journal of Cosmology and Astroparticle Physics* **06** (2011) 031, [arXiv:1103.5413].

[376] H. Baer, V. Barger and D. Mickelson, *Direct and indirect detection of higgsino-like WIMPs: Concluding the story of electroweak naturalness*, *Physics Letters B* **726** (2013) 330, [arXiv:1303.3816].

[377] K. J. Bae, H. Baer and V. Barger, *Supersymmetry with radiatvely-driven naturalness: Implications for WIMP and axion searches*, *Symmetry* **7** (2015) 788, [arXiv:1503.04137].

[378] J. Fan and M. Reece, *In wino veritas? Indirect searches shed light on neutralino dark matter*, *Journal of High Energy Physics* **10** (2013) 124, [arXiv:1307.4400].

[379] H. Baer, V. Barger, D. Sngupta and X. Tata, *Is natural higgsino-only dark matter excluded?*, *European Physical Journal C* **78** (2018) 838, [arXiv:1803.11210].

[380] A. Salam and J. Strathdee, *Supersymmetry and fermion-number conservation*, *Nuclear Physics B* **87** (1975) 85.

[381] Super-Kamiokande Collaboration, *Search for proton decay via $p \to e^+\pi^0$ and $p \to \mu^+\pi^0$ in a large water Cherenkov detector*, *Physical Review Letters* **102** (2009) 141801, [arXiv:0903.0676].

[382] G. R. Farrar and P. Fayet, *Phenomenology of the production, decay, and detection of new hadronic states associated with supersymmetry*, *Physics Letters B* **76** (1978) 575.

[383] G. R. Farrar and S. Weinberg, *Supersymmetry at ordinary energies. II. R invariance, Goldstone bosons, and gauge-fermion masses*, *Physical Review D* **27** (1983) 2732.

[384] J. R. Oppenheimer, *Note on the theory of the interaction of field and matter*, *Physical Review* **35** (1930) 461.

[385] H. A. Bethe, *The electromagnetic shift of energy levels*, *Physical Review* **72** (1947) 339.

[386] J. Schwinger, *On quantum-electrodynamics the magnetic moment of the electron*, *Physical Review* **73** (1948) 416.

[387] R. P. Feynman, *A relativistic cut-off for classical electrodynamics*, *Physical Review* **74** (1948) 939.

[388] S. Tomonaga, *On a relativistically invariant formulation of the quantum theory of wave fields*, *Progress of Theoretical Physics* **1** (1946) 27.

[389] K. G. Wilson and J. Kogut, *The renormalization group and the ϵ expansion*, *Physics Reports* **12** (1974) 75.

[390] T. Appelquist and J. Carazzone, *Infrared singularities and massive fields*, *Physical Review D* **11** (1975) 2856.

[391] M. Pospelov and T. ter Veldhuis, *Direct and indirect limits on the electromagnetic form factors of WIMPs*, *Physics Letters B* **480** (2000) 181, [arXiv:hep-ph/0003010].

[392] V. Barger, W.-Y. Keung and D. Marfatia, *Electromagnetic properties of dark matter: dipole moments and charge form factor*, *Physics Letters B* **696** (2011) 74, [arXiv:1007.4345].

[393] K. Sigurdson, M. Doran, A. Kurylov, R. R. Caldwell and M. Kamionkowsi, *Dark-matter electric and magnetic dipole moments*, *Physical Review D* **70** (2004) 083501, [arXiv:astro-ph/0406355].

[394] E. Massó, S. Mohanty and S. Rao, *Dipolar dark matter*, *Physical Review D* **80** (2009) 036009, [arXiv:0906.1979].

[395] A. L. Fitzpatrick and K. M. Zurek, *Dark moments and the DAMA-CoGeNT puzzle*, *Physical Review D* **82** (2010) 075004, [arXiv:1007.5325].

[396] J.-F. Fortin and T. M. P. Tait, *Collider constraints on dipole-interacting dark matter*, *Physical Review D* **85** (2012) 063506, [arXiv:1103.3289].

[397] J. H. Heo, *Minimal Dirac fermionic dark matter with nonzero magnetic dipole moment*, *Physics Letters B* **693** (2010) 255, [arXiv:0901.3815].

[398] J. H. Heo, *Electric dipole moment of Dirac fermionic dark matter*, *Physics Letters B* **702** (2011) 205, [arXiv:0902.2643].

[399] E. Del Nobile, C. Kouvaris, P. Panci, F. Sannino and J. Virkajärvi, *Light magnetic dark matter in direct detection searches*, *Journal of Cosmology and Astroparticle Physics* **2012** (2012) 010, [arXiv:1203.6652].

[400] E. Del Nobile, G. B. Gelmini, P. Gondolo and J.-H. Huh, *Direct detection of light anapole and magnetic dipole DM*, *Journal of Cosmology and Astroparticle Physics* **2014** (2014) 002, [arXiv:1401.4508].

[401] M. I. Gresham and K. M. Zurek, *Light dark matter anomalies after LUX*, *Physical Review D* **89** (2014) 016017, [arXiv:1311.2082].

[402] S. Mohanty and S. Rao, *Detecting dipolar dark matter in beam dump experiments*, arXiv:1506.06462.

[403] T. Banks, J.-F. Fortin and S. Thomas, *Direct detection of dark matter electromagnetic dipole moments*, arXiv:1007.5515.

[404] W. S. Cho, J.-H. Huh, I.-W. Kim, J. E. Kim and B. Kyae, *Constraining WIMP magnetic moment from CDMS II experiment*, *Physics Letters B* **687** (2010) 6, [arXiv:1001.0579].

[405] N. Nagata and S. Shirai, *Higgsino dark matter in high-scale supersymmetry*, *Journal of High Energy Physics* **2015** (2015) 29, [arXiv:1410.4549].

[406] M. Ibe, S. Matsumoto and R. Sato, *Mass splitting between charged and neutral winos at two-loop level*, *Physics Letters B* **721** (2013) 252, [arXiv:1212.5989].

[407] J. B. Munñoz and A. Loeb, *A small amount of min-charged dark matter could cool the baryons in the early Universe*, *Nature* **557** (2018) 685.

[408] M. Cirelli, N. Fornengo and A. Strumia, *Minimal dark matter*, *Nuclear Physics B* **753** (2006) 178, [arXiv:hep-ph/0512090].

[409] M. Fierz, *Zur Fermischen Theorie des β-Zerfalls*, *Zeitschrift für Physik* **104** (1937) 553.

[410] D. Smith and N. Weiner, *Inelastic dark matter*, *Physical Review D* **64** (2001) 043502, [arXiv:hep-ph/0101138].

[411] C. M. Ho and R. J. Scherrer, *Anapole dark matter*, *Physics Letters B* **722** (2013) 341, [arXiv:1211.0503].

[412] E. E. Radescu, *On the electromagnetic properties of Majorana fermions*, *Physical Review D* **32** (1985) 1266.

[413] S. Y. Choi, H. E. Haber, J. Kalinowski and P. M. Zerwas, *The neutralino sector in the $U(1)$-extended supersymmetric Standard Model*, *Nuclear Physics B* **778** (2007) 85, [arXiv:hep-ph/0612218].

[414] Y. B. Zel'dovich, *Electromagnetic interaction with parity violation*, *Soviet Physics Journal of Experimental and Theoretical Physics* **6** (1958) 1184.

[415] V. M. Dubovik and V. E. Kuznetsov, *The toroid moment of the neutrino*, *International Journal of Modern Physics A* **13** (1998) 5257, [arXiv:hep-ph/9606258].

[416] C. S. Wood, S. C. Bennett, D. Cho, B. P. Masterson, J. L. Roberts, C. E. Tanner et al., *Measurement of parity nonconservation and an anapole moment in cesium*, *Science* **275** (1997) 1759.

[417] C. Giunti and A. Studenikin, *Neutrino electromagnetic properties*, *Physics of Atomic Nuclei* **72** (2009) 2089, [arXiv:0812.3646].

[418] Y. Gao, C. M. Ho and R. J. Scherrer, *Anapole dark matter at the LHC*, *Physical Review D* **89** (2014) 045006, [arXiv:1311.5630].

[419] L. G. Cabral-Rosetti, M. Mondragón and E. Reyes Pérez, *Anapole moment of the lightest neutralino in the cMSSM*, *Nuclear Physics B* **907** (2016) 1, [arXiv:1504.01213].

[420] D. A. Dicus, E. W. Kolb, A. M. Gleeson, E. C. G. Sudarshan, V. L. Teplitz and M. Turner, *Primordial nucleosythensis including radiative, Coulomb, and finite-temperature corrections to weak rates*, *Physical Review D* **26** (1982) 2694.

[421] P. Binétruy, G. Girardi and P. Salati, *Constraints on a system of two neutral fermions from cosmology*, *Nuclear Physics B* **237** (1984) 285.

[422] K. Griest and D. Seckel, *Three exceptions in the calculation of relic abundances*, *Physical Review D* **43** (1991) 3191.

[423] J. L. Feng and J. Kumar, *Dark-matter particles without weak-scale masses or weak interactions*, *Physical Review Letters* **101** (2008) 231301, [arXiv:0803.4196].

[424] H. Baer, K.-Y. Choi, J. E. Kim and L. Roszkowski, *Dark matter production in the early universe: beyond the thermal WIMP paradigm*, *Physics Reports* **555** (2015) 1, [arXiv:1407.0017].

[425] T. Cohen, M. Lisanti, A. Pierce and T. R. Slatyer, *Wino dark matter under seige*, *Journal of Cosmology and Particle Physics* **10** (2013) 061, [1307.4082].

[426] M. Lisanti, *Chapter 7. lectures on dark matter physics*, in *New Frontiers in Fields and Strings* (J. Polchinski, P. Vieira and O. DeWolfe, eds.), Proceedings of the 2015 Theoretical Advanced Study Institute in Elementary Particle Physics, p. 399, TASI 2015, World Scientific, 2017. arXiv:1603.03797. DOI.

[427] P. Gondolo and G. Gelmini, *Cosmic abundances of stable particles: Improved analysis*, *Nuclear Physics B* **360** (1991) 145.

[428] P. S. B. Dev, A. Mazumdar and S. Qutub, *Constraining non-thermal and thermal properties of dark matter*, *Frontiers in Physics* **2** (2014) 1, [arXiv:1311.5297].

[429] J. Hisano, K. Ishiwata, N. Nagata and T. Takesako, *Direct detection of electroweak-interacting dark matter*, *Journal of High Energy Physics* **07** (2011) 005, [arXiv:1104.0228].

[430] R. J. Hill and M. P. Solon, *Universal behavior in the scattering of heavy, weakly interacting dark matter on nuclear targets*, *Physics Letters B* **707** (2012) 539, [arXiv:1111.0016].

[431] D. Tucker-Smith and N. Weiner, *Status of inelastic dark matter*, *Physical Review D* **72** (2005) 063509, [arXiv:hep-ph/0402065].

[432] P. Verkerk, G. Grynberg, B. Pichard, M. Spiro, S. Zylberajch, M. E. Goldberg et al., *Search for superheavy hydrogen in sea water*, *Physical Review Letters* **98** (1992) 1116.

[433] G. Bélanger, F. Boudjema, A. Pukhov and A. Semenov, *micrOMEGAs: A program for calculating the relic denisty in the MSSM*, *Computer Physics Communications* **129** (2002) 103, [arXiv:hep-ph/011278].

[434] G. Bélanger, F. Boudjema, A. Pukhov and A. Semenov, *micrOMEGAs: Version 1.3*, *Computer Physics Communications* **174** (2006) 577, [arXiv:hep-ph/0405253].

[435] D. Barducci, G. Bélanger, J. Bernon, F. Boudjema, J. Da Silva, S. Kraml et al., *Collider limits on new physics with micrOMEGAs_4.3*, *Computer Physics Communications* **222** (2018) 327, [arXiv:1606.03834].

[436] T. R. Slatyer, *The Sommerfeld enhancement for dark matter with an excited state*, *Journal of Cosmology and Astroparticle Physics* **02** (2010) 028, [0910.5713].

[437] J. L. Feng, M. Kaplinghat and H.-B. Yu, *Sommerfeld enhancements for thermal relic dark matter*, *Physical Review D* **82** (2010) 083525, [arXiv:1005:4678].

[438] S. Cassel, *Sommerfeld factor for arbitrary partial wave processes*, *Journal of Physics G: Nuclear and Particle Physics* **37** (2010) 105009.

[439] K. Griest, M. Kamionkowski and M. S. Turner, *Supersymmetric dark matter above the w mass*, *Physical Review D* **41** (1990) 3565.

[440] L3 Collaboration, *A determination of the properties of the neutral intermediate vector boson Z^0*, *Physics Letters B* **231** (1989) 509.

[441] ALEPH Collaboration, *Determination of the number of light neutrino species*, *Physics Letters B* **231** (1989) 519.

[442] DELPHI Collaboration, *Measurement of the mass and with of the Z^0-particle from multihadronic final states produced in e^+e^- annihilations*, *Physics Letters B* **231** (1989) 539.

[443] H. Baer, M. Drees and X. Tata, *Constraints on supersymmetric particles from the CERN LEP data on Z^0 decay properties*, *Physical Review D* **41** (1990) 3414.

[444] M. Drees, C. S. Kim and X. Tata, *Supersymmetry phenomenology and the nature of the lightest supersymmetric particle*, *Physical Review D* **37** (1988) 784.

[445] A. Sommerfeld, *Über die Beugung und Bremsung der Elektronen*, *Annalen der Physik* **403** (1931) 257.

[446] J. Hisano, S. Matsumoto and M. M. Nojiri, *Explosive dark matter annihilation*, *Physical Review Letters* **92** (2004) 031303, [arXiv:hep-ph/0307216].

[447] J. Hisano, S. Matsumoto, M. M. Nojiri and O. Saito, *Nonperturbative effect on dark matter annihilation and gamma ray signature from the galactic center*, *Physical Review D* **71** (2005) 063528, [arXiv:hep-ph/0412403].

[448] M. Cirelli, A. Strumia and M. Tamburini, *Cosmology and astrophysics of minimal dark matter*, *Nuclear Physics B* **787** (2007) 152, [arXiv0706.4071].

[449] N. Arkani-Hamed, D. P. Finkbeiner, T. R. Slatyer and N. Weiner, *A theory of dark matter*, *Physical Review D* **79** (2009) 015014, [arXiv:0810.0713].

[450] J. L. Feng, M. Kaplinghat and H.-B. Yu, *Halo-shape and relic-density exclusions of Sommerfeld-enhanced dark matter explanations of cosmic ray excesses*, *Physical Review Letters* **104** (2010) 151301, [arXiv:0911.0422].

[451] G. Wentzel, *Eine Verallgemeinerung der Quantenbedingungen für die Zwecke der Wellenmechanik*, *Zeitschrift für Physik* **38** (1926) 518.

[452] H. A. Kramers, *Wellenmechanik und halbzahlige Quantisierung*, *Zeitschrift für Physik* **39** (1926) 828.

[453] L. Brillouin, *La mécanique ondulatoire de schrödinger: une méthod générale de resolution par approximations successives*, *Comptes Rendus de l'Académie des Sciences* **183** (1926) 24.

[454] J. March-Russel and S. M. West, *WIMPonium and boost factors for indirect dark matter detection*, *Physics Letters B* **676** (2009) 133, [arXiv:0812.0559].

[455] J. B. Dent, S. Dutta and R. J. Scherrer, *Thermal relic abundances of particles with velocity-dependent interactions*, *Physics Letters B* **687** (2010) 275, [arXiv:0909.4128].

[456] J. Zavala, M. Vogelsberger and S. D. M. White, *Relic density and CMB constraints on dark matter annihilation with Sommerfeld enhancement*, *Physical Review D* **81** (2010) 083502, [arXiv:0910.5221].

[457] A. Belyaev, N. D. Christensen and A. Pukhov, *CalcHEP 3.4 for collider physics within and beyond the Standard Model*, *Computer Physics Communications* **184** (2013) 1729, [arXiv:1207.6082].

[458] A. V. Semenov, *LanHEP-a package for the automatic generation of Feynman rules in field theory. Version 3.0*, *Computer Physics Communications* **180** (2009) 431, [arXiv:0805.0555].

[459] J. McDonald, K. A. Olive and M. Srednicki, *Relic densities of neutralinos*, *Physics Letters B* **293** (1992) 80.

[460] S. Mizuta and M. Yamaguchi, *Coannihilation effects and relic abundance of higgsino-dominant LSPs*, *Physics Letters B* **298** (1993) 120, [arXiv:hep-ph/9208251].

[461] CoGeNT Collaboration, *Results from a search for light-mass dark matter with a p-type point contact germanium detector*, *Physical Review Letters* **106** (2011) 131301, [arXiv:1002.4703].

[462] G. Angloher, A. Bento, C. Bucci, L. Canonica, X. Defay, A. Erb et al., *Results on light dark matter particles with a low-threshold CRESST-II dark matter search*, *European Physical Journal C* **76** (2016) 25, [arXiv:1509.01515].

[463] XENON10 Collaboration, *Search for light dark matter in XENON10 data*, *Physical Review Letters* **107** (2011) 051301, [arXiv:1207.5988].

[464] SIMPLE Collaboration, *Final analysis and results of the phase II SIMPLE dark matter search*, *Physical Review Letters* **108** (2012) 201302, [arXiv:1106.3014].

[465] G. Steigman, C. L. Sarazin, H. Quintana and J. Faulkner, *Dynamical interactions and astrophysical effects of stable heavy neutrinos*, *The Astronomical Journal* **83** (1978) 1050.

[466] J. Faulkner and R. L. Gilliland, *Weakly interacting, massive particles and the solar neutrino flux*, *The Astrophysical Journal* **299** (1985) 994.

[467] D. N. Spergel and W. H. Press, *Effect of hypothetical, weakly interacting, massive particles on energy transport in the solar interior*, *The Astrophysical Journal* **294** (1985) 663.

[468] L. M. Krauss, K. Freese, D. N. Spergel and W. H. Press, *Cold dark matter candidates and the solar neutrino problem*, *The Astrophysical Journal* **299** (1985) 1001.

[469] L. M. Krauss, M. Srednicki and F. Wilczek, *Solar System constraints and signatures for dark-matter candidates*, *Physical Review D* **33** (1986) 2079.

[470] K. Griest and D. Seckel, *Cosmic asymmetry, neutrinos and the Sun*, *Nuclear Physics B* **283** (1987) 681.

[471] S. Raby and G. B. West, *A simple solution to the solar neutrino and missing mass problems*, *Nuclear Physics B* **292** (1987) 793.

[472] S. Raby and G. B. West, *A fourth generation neutrino with a standard Higgs scalar solves both the solar neutrino and dark matter problems*, *Physics Letters B* **202** (1988) 47.

[473] G. F. Giudice and E. Roulet, *A supersymmetric solution to the solar neutrino and dark matter problems*, *Physics Letters B* **219** (1989) 309.

[474] E. Roulet and G. Gelmini, *Cosmions, cosmic asymmetry and underground detection*, *Nuclear Physics B* **325** (1989) 733.

[475] R. Davis, Jnr, D. S. Harmer and K. C. Hoffman, *Search for neutrinos from the Sun*, *Physical Review Letters* **20** (1968) 1205.

[476] J. N. Bahcall and G. Shaviv, *Solar models and neutrino fluxes*, *The Astrophysical Journal* **153** (1968) 113.

[477] SNO Collaboration, *Measurement of the rate of $\nu_e + d \to p + p + e^-$ interactions produced by ^8B solar neutrinos at the Sudbury Neutrino Observaory*, *Physical Review Letters* **87** (2001) 071301, [arXiv:nucl-ex/0106015].

[478] J. E. Littleton, H. M. van Horn and H. L. Helfer, *Process of energy transport by longitudinal waves and the problem of solar neutrinos*, *The Astrophysical Journal* **173** (1972) 677.

[479] A. Gould, *Evaporation of WIMPs with arbitary cross sections*, *The Astrophysical Journal* **356** (1990) 302.

[480] A. Gould and G. Raffelt, *Thermal conduction by massive particles*, *The Astrophysical Journal* **352** (1990) 654.

[481] A. Gould and G. Raffelt, *Cosmion energy transfer in stars: the Knusden limit*, *The Astrophysical Journal* **352** (1990) 699.

[482] J. Silk, K. Olive and M. Srednicki, *The photino, the Sun and high-energy neutrinos*, *Physical Review Letters* **55** (1985) 257.

[483] R. B. Leighton, R. W. Noyes and G. W. Simon, *Velocity fields in the solar atmosphere. I. Preliminary report*, *The Astrophysical Journal* **135** (1962) 474.

[484] A. Claverie, G. R. Isaak, C. P. McLeod, H. B. van der Raay and T. Roca Cortes, *Solar structure from global studies of the 5-minute oscillation*, *Nature* **282** (1979) 591.

[485] F.-L. Deubner, *Observations of low wavenumber nonradial eigenmodes of the Sun*, *Astronomy and Astrophysics* **371** (1975) 44.

[486] T. L. Duvall, Jnr and J. W. Harvey, *Observations of solar oscillations of low and intermediate degree*, *Nature* **302** (1983) 24.

[487] A. G. Kosovichev, *Inversion methods in helioseismology and solar tomography*, *Journal of Computational and Applied Mathematics* **109** (1999) 1.

[488] J. Christensen-Dalsgaard, D. O. Gough and J. G. Morgan, *Dirty solar models*, *Astronomy and Astrophysics* **73** (1979) 121.

[489] J. Chrsitensen-Dalsgaard, T. L. Duvall, Jnr, D. O. Gough, J. W. Harvey and E. J. Rhodes, Jnr, *Speed of sound in the solar interior*, *Nature* **315** (1985) 378.

[490] N. Grevesse and A. J. Sauval, *Standard solar composition*, *Space Science Reviews* **85** (1998) 161.

[491] M. Asplund, N. Grevesse, A. Jacques Sauval and P. Scott, *The chemical composition of the Sun*, *Annu. Rev. Astronomy and Astrophysics* **47** (2009) 481, [arXiv:0909.0948].

[492] A. M. Serenelli, S. Basu, J. W. Ferguson and M. Asplund, *New solar composition: the problem with solar models revisited*, *The Astrophysical Journal* **705** (2009) L123, [arXiv:0909.2668].

[493] D. T. Cumberbatch, J. A. Guzik, J. Silk, L. S. Watson and S. M. West, *Light WIMPs in the Sun: Constraints from helioseismology*, *Physical Review D* **82** (2010) 103503, [arXiv:1005.5102].

[494] A. C. Vincent, P. Scott and A. Serenelli, *Possible indication of momentum-dependent asymmetric dark matter in the Sun*, *Physical Review Letters* **114** (2015) 081302, [arXiv:1411.6626].

[495] A. C. Vincent, A. Serenelli and P. Scott, *Generalised form factor dark matter in the Sun*, *Journal of Cosmology and Astroparticle Physics* **2015** (2015) 040, [arXiv:1504.04378].

[496] J. W. Harvey, F. Hill, R. P. Hubbard, J. R. Kennedy, J. W. Leibacher, J. A. Pintar et al., *The Global Oscillation Network Group (GONG) project*, *Science* **272** (1996) 1284.

[497] A. H. Gabriel, G. Grec, J. Charra, J.-M. Robillot, T. Roca Cortés, S. Turck-Chièze et al., *Global oscillations at low frequency from the SOHO mission (GOLF)*, *Solar Physics* **162** (1995) 61.

[498] D. O. Gough, A. G. Kosovichev, J. Toomre, E. Anderson, H. M. Antia, S. Basu et al., *The seismic structure of the Sun*, *Science* **272** (1996) 1296.

[499] L. Bertello, C. J. Henney, R. K. Ulrich, F. Varadi, A. G. Kosovichev, P. H. Scherrer et al., *Comparison of frequencies and rotational splittings of solar acoustic modes of low angular degree from simultaneous MDI and GOLF observations*, *The Astrophysical Journal* **535** (2000) 1066.

[500] L. Bertello, F. Varadi and R. K. Ulrich, *Identification of solar acoustic modes of low angular degree and low radial order*, *The Astrophysical Journal* **537** (2000) L143.

[501] R. A. García, C. Régulo, S. Turck-Chièze, L. Bertello, A. G. Kosovichev, A. S. Brun et al., *Low-degree low-order solar p-modes as seen by GOLF on board SOHO*, *Solar Physics* **200** (2001) 361.

[502] J. N. Bahcall and M. H. Pinsonneault, *What do we (not) know theoretically about solar neutrino fluxes?*, *Physical Review Letters* **92** (2004) 121301, [arXiv:astro-ph/0402114].

[503] J. N. Bahcall, A. M. Serenelli and S. Basu, *New solar opacities, abundances, helioseismology, and neutrino fluxes*, *The Astrophysical Journal* **621** (2005) L85, [arXiv:astro-ph/0412440].

[504] C. Allende Prieto, D. L. Lambert and M. Asplund, *The 'forbidden' abundance of oxygen in the Sun*, *The Astrophysical Journal* **556** (2001) L63, [arXiv:astro-ph/0106360].

[505] C. Allende Prieto, D. L. Lambert and M. Asplund, *A reappraisal of the solar photospheric C/O ratio*, *The Astrophysical Journal* **573** (2002) L137, [arXiv:astro-ph/0206089].

[506] M. Asplund, N. Grevesse, A. J. Sauval, C. Allende Prieto and D. Kiselman, *Line formulation in solar granulation. IV. OI and OH lines and the photospheric O abundance*, *Astronomy and Astrophysics* **417** (2004) 751, [arXiv:astro-ph/0312290].

[507] M. Asplund, N. Grevesse, A. J. Sauval, C. Allende Prieto and R. Blomme, *Line formation in solar granulation. IV. [C I], C I, CH and* C_2 *lines in the photospheric C abundance*, *Astronomy and Astrophysics* **431** (2005) 693, [arXiv:astro-ph/0410681].

[508] P. C. Scott, M. Asplund, N. Grevesse and A. J. Sauval, *Line formulation in solar granulation. VII. CO lines and the solar C and O isotopic abundances*, *Astronomy and Astrophysics* **456** (2006) 675, [arXiv:astro-ph/0605116].

[509] J. Meléndez and M. Asplund, *Another forbidden solar oxygen abundance: the [O I] 5577 a line*, *Astronomy and Astrophysics* **490** (2008) 817, [arXiv:0808.2796].

[510] P. Scott, M. Asplund, N. Grevesse and A. J. Sauval, *On the solar nickel and oxygen abundances*, *The Astrophysical Journal* **691** (2009) L119, [arXiv:0811.0815].

[511] P. Scott, N. Grevesse, M. Asplund, A. J. Sauval, K. Lind, Y. Takeda et al., *The elemental composition of the Sun. I. the intermediate mass elements Na to Ca*, *Astronomy and Astrophysics* **573** (2015) A25, [arXiv:1405.0279].

[512] P. Scott, M. Asplund, N. Grevesse, M. Bergemann and A. J. Sauval, *The elemental composition of the Sun. II. the iron group elements Sc to Ni*, *Astronomy and Astrophysics* **573** (2015) A26, [arXiv:1405.0287].

[513] N. Grevesse, P. Scott, M. Asplund and A. J. Sauval, *The elemental composition of the Sun. III. the heavy elements Cu to Th*, *Astronomy and Astrophysics* **573** (2015) A27, [arXiv:1405.0288].

[514] T. M. D. Pereira, M. Asplund and D. Kiselman, *Oxygen lines in solar granulation. II. Centre-to-limb variation, NLTE line formation, blends, and the solar oxygen abundance*, *Astronomy and Astrophysics* **508** (2009) 1403, [arXiv:0909.2310].

[515] K. Lind, M. Asplund, P. S. Barklem and A. K. Belyaev, *Non-LTE calculations for neutral Na in late-type stars using improved atomic data*, *Astronomy and Astrophysics* **528** (2011) A103, [arXiv:1102.2160].

[516] M. Bergemann, K. Lind, R. Collet, Z. Magic and M. Asplund, *Non-LTE line formation of fe in late-type stars - I. Standard stars with 1D and* $\langle 3D \rangle$ *model atmospheres*, *Monthly Notices of the Royal Astronomical Society* **427** (2012) 27, [arXiv:1207.2455].

[517] L. Mashonkina, A. Ryabtsev and A. Frebel, *Non-LTE effects on the lead and thorium abundance determinations for cool stars*, *Astronomy and Astrophysics* **540** (2012) A98, [arXiv:1202.2630].

[518] E. Caffau, H.-G. Ludwig, M. Steffen, B. Freytag and P. Bonifacio, *Solar chemical abundances determined with a CO5BOLD 3D model atmosphere*, *Solar Physics* **268** (2011) 255, [arXiv:1003.1190].

[519] R. von Steiger and T. H. Zurbuchen, *Solar metallicity derived from in situ solar wind composition*, *The Astrophysical Journal* **816** (2016) 13.

[520] A. Serenelli, P. Scott, F. L. Villante, A. C. Vincent, M. Asplund, S. Basu et al., *Implications of solar wind measurements for solar models and composition*, *Monthly Notices of the Royal Astronomical Society* **463** (2016) 2, [arXiv:1604.05318].

[521] S. Basu and H. M. Antia, *Constraining solar abundances using helioseismology*, *The Astrophysical Journal* **606** (2004) L85, [arXiv:astro-ph/0403485].

[522] J. N. Bahcall, S. Basu, M. Pinsonneualt and A. M. Serenelli, *Helioseismological implications of recent solar abundance determinations*, *The Astrophysical Journal* **618** (2005) 1049, [arXiv:astro-ph/0407060].

[523] J. N. Bahcall, A. M. Serenelli and S. Basu, *10,000 standard solar models: a Monte Carlo simulation*, *The Astrophysical Journal Supplement Series* **165** (2006) 400, [arXiv:astro-ph/0511337].

[524] W. M. Yang and S. L. Bi, *Solar models with revised abundances and opacities*, *The Astrophysical Journal* **658** (2007) L67, [arXiv:0805.3644].

[525] S. Basu and H. M. Antia, *Helioseismology and solar abundances*, *Physics Reports* **457** (2008) 217, [arXiv:0711.4590].

[526] A. M. Serenelli, W. C. Haxton and C. Peña-Garay, *Solar models with accretion. I. application to the solar abundance problem*, *The Astrophysical Journal* **743** (2011) 24, [arXiv:1104.1639].

[527] A. M. Serenelli and S. Basu, *Determining the initial helium abundance of the Sun*, *The Astrophysical Journal* **719** (2010) 865, [arXiv:1006.0244].

[528] A. Bottino, G. Fiorentini, N. Fornengo, B. Ricci, S. Copel and F. L. Villante, *Does solar physics provide constraints to weakly interacting massive particles*, *Physical Review D* **66** (2002) 053005, [arXiv:hep-ph/0206211].

[529] I. P. Lopes, J. Silk and S. H. Hansen, *Helioseismology as a new constraint on supersymmetric dark matter*, *Monthly Notices of the Royal Astronomical Society* **331** (2002) 361, [arXiv:astro-ph/0111530].

[530] I. P. Lopes, G. Bertone and J. Silk, *Solar seismic model as a new constraint on supersymmetric dark matter*, *Monthly Notices of the Royal Astronomical Society* **337** (2002) 1179, [arXiv:astro-ph/0205066].

[531] M. Taoso, F. Iocco, G. Meynet, G. Bertone and P. Eggenberger, *Effect of low mass dark matter particles on the Sun*, *Physical Review D* **82** (2010) 083509, [arXiv:1005.5711].

[532] A. C. Vincent and P. Scott, *Thermal conduction by dark matter with velocity and momentum-dependent cross sections*, *Journal of Cosmology and Astroparticle Physics* **2014** (2014) 019, [arXiv:1311.2074].

[533] A. C. Vincent, P. Scott and A. Serenelli, *Updated constraints on velocity and momentum-dependent asymetric dark matter*, *J. Cosmology. Astroparticle Physics* **2016** (2016) 007, [arXiv:1605.06502].

[534] V. Barger, W.-Y. Keung, D. Marfatia and P.-Y. Tseng, *Dipole moment dark matter at the LHC*, *Physics Letters B* **717** (2012) 219, [arXiv:1206.0640].

[535] L. G. Cabral-Rosetti, M. Mondragón and E. Reyes Pérez, *Toroidal dipole moment of the LSP in the cMSSM*, in *PASCOS 2012 – 18th International Symposium on Particle Strings and Cosmology, Journal of Physics: Conference Series*, vol. 485, p. 012019, 2014. arXiv:1206.5052. DOI.

[536] T. de Forest, Jnr and J. D. Walecka, *Electron scattering and nuclear strucutre*, *Advances in Physics* **15** (1966) 1.

[537] R. Catena and B. Schwabe, *Form factors for dark matter capture by the Sun in effective theories*, *Journal of Cosmology and Astroparticle Physics* **2015** (2015) 042, [arXiv:1501.03729].

[538] T. W. Donnelly and J. D. Walecka, *Electron scattering and nuclear structure*, *Annual Review of Nuclear Science* **25** (1975) 329.

[539] T. W. Donnelly and I. Sick, *Elastic magnetic electron scattering from nuclei*, *Reviews of Modern Physics* **56** (1984) 461.

[540] R. Herman and R. Hofstadter, *High-Energy Electron Scattering Tables*. Stanford University Press, Stanford, CA, 1960.

[541] K. Freese, J. Frieman and A. Gould, *Signal modulation in cold dark matter detection*, *Physical Review D* **37** (1988) 3388.

[542] Y.-Z. Chen, Y.-A. Luo, L. LI, H. Shen and X.-Q. Li, *Determining nuclear form factor for detection of dark matter in relativistic mean field theory*, *Communications in Theoretical Physics* **55** (2011) 1059, [arXiv:1101.3049].

[543] G. Eder, *Nuclear Forces: Introduction to Theoretical Nuclear Physics*. M.I.T. Press, Cambridge, Massachusetts, 1968.

[544] R. H. Helm, *Inelastic and elastic scattering of 187-MeV electrons from selected even-even nuclei*, *Physical Review* **104** (1956) 1466.

[545] P. S. Krstić and D. R. Schultz, *Consistent definitions for, and relationships among, cross sections for elastic scattering of hydrogen ions, atoms, and molecules*, *Physical Review A* **60** (1999) 2118.

[546] S. Tulin, H.-B. Yu and K. M. Zurek, *Beyond collisionless dark matter: Particle physics dynamics for dark matter halo structure*, *Physical Review D* **87** (2013) 115007, [arXiv:1302.3898].

[547] I. Lopes, K. Kadota and J. Silk, *Constraint on light dipole dark matter from helioseismology*, *The Astrophysical Journal Letters* **780** (2014) 15, [arXiv:1310.0673].

[548] D. E. Kaplan, M. A. Luty and K. M. Zurek, *Asymmetric dark matter*, *Physical Review D* **79** (2009) 115016, [arXiv:0901.4117].

[549] K. Petraki and R. R. Volkas, *Review of asymmetric dark matter*, *International Journal of Modern Physics A* **28** (2013) 1330028, [arXiv:1305.4939].

[550] M. Blennow and S. Clementz, *Asymmetric capture of Dirac dark matter by the Sun*, *Journal of Cosmology and Astroparticle Physics* **2015** (2015) 036, [arXiv:1504.05813].

[551] I. Lopes and J. Silk, *Solar constraints on asymmetric dark matter*, *The Astrophysical Journal* **757** (2012) 130, [arXiv:1209.3631].

[552] G. Busoni, A. De Simone, P. Scott and A. C. Vincent, *Evaporation and scattering of momentum- and velocity-dependent dark matter in the Sun*, *Journal of Cosmology and Astroparticle Physics* **2017** (2017) 037, [arXiv:1703.07784].

[553] W. H. Press and D. N. Spergel, *Capture by the Sun of a galactic population of weakly interacting, massive particles*, *The Astrophysical Journal* **296** (1985) 679.

[554] P. Scott, M. Fairbairn and J. Edsjö, *Dark stars at the galactic centre - the main sequence*, *Monthly Notices of the Royal Astronomical Society* **394** (2009) 82, [arXiv:0809.1871].

[555] C. T. Russell, C. A. Raymond, A. Coradini, H. Y. McSween, M. T. Zuber, A. Nathues et al., *Dawn at Vesta: Testing the protoplanetary paradigm*, *Science* **336** (2012) 684.

[556] P. Scott, J. Edjsö and M. Fairbairn, *The DarkStars code: A publicly available dark stellar evolution package*, in *Dark Matter in Astrophysics and Particle Physics*, p. 320, 2009. arXiv:0904.2395. DOI.

[557] N. J. Stone, *Table of nuclear magnetic dipole and electric quadrupole moments*, *Atomic Data and Nuclear Data Tables Nucl. Data Tables* **90** (2005) 75.

[558] R. Kippenhahn, A. Weigert and E. Hofmeister, *Methods for calculating stellar evolution*, *Methods of Computational Physics* **7** (1967) 129.

[559] H.-C. Thomas, *Sternentwicklung VIII. Der Helium-Flash bei einem Stern von 1.3 Sonnenmassen*, *Zeitschrit für Astrophysik* **67** (1967) 420.

[560] A. Weiss, *The progenitor of SN 1987A: Uncertain evolution of a* 20 $M_\odot$ *star*, *The Astrophysical Journal* **339** (1989) 365.

[561] J. Wagenhuber and A. Weiss, *Numerical methods for AGB evolution*, *Astronomy and Astrophysics* **286** (1994) 121.

[562] A. Weiss and H. Schlattl, *Age-luminosity relations for low-mass metal-poor stars*, *Astronomy and Astrophysics Suppl. Ser.* **144** (2000) 487.

[563] A. Weiss and H. Schlattl, *GARSTEC - the Garching Stellar Evolution code*, *Astrophysics and Space Science* **316** (2008) 99.

[564] P. P. Eggleton, *The evolution of low mass stars*, *Monthly Notices of the Royal Astronomical Society* **151** (1971) 351.

[565] P. P. Eggleton, *Composition changes during stellar evolution*, *Monthly Notices of the Royal Astronomical Society* **156** (1972) 361.

[566] O. R. Pols, C. A. Tout, P. P. Eggleton and Z. Han, *Approximate input physics for stellar modelling*, *Monthly Notices of the Royal Astronomical Society* **274** (1995) 964, [arXiv:astro-ph/9504025].

[567] B. Paxton, *EZ to evolve ZAMS stars: A program derived from Eggleton's stellar evolution code*, *Publications of the Astronomical Society of the Pacific* **116** (2004) 699, [arXiv:astro-ph/0405130].

[568] P. Gondolo, J. Edsjö, P. Ullio, L. Bergström, M. Schelke and E. A. Baltz, *DarkSUSY: computing supersymmetric dark matter properties numerically*, *Journal of Cosmology and Astroparticle Physics* **2004** (2004) 008, [arXiv:astro-ph/0406204].

[569] M. Fairbairn, P. Scott and J. Edsjö, *The zero age main sequence of WIMP burners*, *Physical Review D* **77** (2008) 047301, [arXiv:0710.3396].

[570] P. Scott, M. Fairbairn and J. Edsjö, *Impacts of WIMP dark matter upon stellar evolution: main-sequence stars*, in *Proceedings of the Identification of Dark matter Conference*, p. 1, 2008. arXiv:0810.5560.

[571] P. C. Scott, J. Edsjó and M. Fairbairn, *Low mass stellar evolution with WIMP capture and annihilation*, in *Dark Matter in Astrophysics and Particle Physics*, p. 387, 2008. arXiv:0711.0991.

[572] V. Antonelli, L. Miramonti, C. Peña-Garay and A. Serenelli, *Solar neutrinos*, *Advances in High Energy Physics* **2013** (2013) 351926, [arXiv:1208.1356].

[573] J. Bergström, M. C. Gonzalez-Garcia, M. Maltoni, C. Peña-Garay, A. M. Serenelli and N. Song, *Updated determination of the solar neutrino fluxes from solar neutrino data*, *Journal of High Energy Physics* **3** (2016) 132, [arXiv:1601.00972].

[574] V. Castellani, S. Degl'Innocenti and G. Fiorentini, *The pp reaction in the Sun and solar neutrinos*, *Physics Letters B* **303** (1993) 68, [arXiv:1212.2985].

[575] V. Castellani, S. Degl'Innocenti, G. Fiorentini, M. Lissia and B. Ricci, *Neutrinos from the Sun: Experimental results confronted with solar models*, *Physical Review D* **50** (1994) 4749, [arXiv:astro-ph/9405064].

[576] S. Basu, W. J. Chaplin, Y. Elsworth, R. New and A. M. Serenelli, *Fresh insights on the structure of the solar core*, *The Astrophysical Journal* **699** (2009) 1403, [arXiv:0905.0651].

[577] S. Degl'Innoccenti, W. A. Dziembowski, G. Fiorentini and B. Ricci, *Helioseismology and standard solar models*, *Astroparticle Physics* **3** (1997) 77.

[578] S. Basu, W. J. Chaplin, Y. Elsworth, R. New, A. M. Serenelli and G. A. Verner, *Solar abundances and helioseismology: Fine-structure spacings and separation ratios of low-degree p-modes*, *The Astrophysical Journal* **655** (2007) 660, [arXiv:astro-ph/0610052].

[579] I. W. Roxburgh and S. V. Vorontsov, *The ratio of small to large separations of acoustic oscillations as a diagnostic of the interior of solar-like stars*, *Astronomy and Astrophysics* **411** (2003) 215.

[580] W. J. Chaplin, A. M. Serenelli, S. Basu, Y. Elsworth, R. New and G. A. Verner, *Solar heavy element abundance: constraints from frequency separation ratios of low-degree p modes*, *The Astrophysical Journal* **670** (2007) 872, [arXiv:0705.3154].

[581] E. A. Spiegel and J.-P. Zahn, *The solar tachocline*, *Astronomy and Astrophysics* **265** (1992) 106.

[582] J. Christensen-Dalsgaard, D. O. Gough and M. J. Thompson, *The depth of the solar convection zone*, *The Astrophysical Journal* **378** (1991) 413.

[583] S. Basu and H. M. Antia, *Seismic measurement of the depth of the solar convection zone*, *Monthly Notices of the Royal Astronomical Society* **287** (1997) 189.

[584] S. Basu, *Effects of errors in the solar radius on helioseismic inferences*, *Monthly Notices of the Royal Astronomical Society* **298** (1998) 719, [arXiv:astro-ph/9712133].

[585] M. T. Frandsen and S. Sarkar, *Asymmetric dark matter and the Sun*, *Physical Review Letters* **105** (2010) 011301, [arXiv:1003.4505].

[586] R. Catena and A. Widmark, *WIMP capture by the Sun in the effective theory of dark matter self-interactions*, *Journal of Cosmology and Astroparticle Physics* **12** (2016) 016, [arXiv:1609.04825].

[587] K. Choi, C. Rott and Y. Itow, *Impact of the dark matter velocity distribution on capture rates in the Sun*, *Journal of Cosmology and Astroparticle Physics* **2014** (2014) 049, [arXiv:1312.0273].

[588] E. Del Nobile, G. Gelmini, P. Gondolo and J.-H. Huh, *Generalized halo independent comparison of direct dark matter detection data*, *Journal of Cosmology and Astroparticle Physics* **2013** (2013) 048, [arXiv:1306.5273].